Accurate Crystal Structure Studies at High Pressure

Thesis submitted by
Malcolm Iain McMahon

For the Degree of
Doctor of Philosophy

Department of Physics
University of Edinburgh
October 1990

Acknowledgements

I would like to record my thanks to all those who have helped me in the course of this work. In particular, the following:

Prof. R.J. Nelmes for his guidance, assistance and encouragement, and for introducing me to the field of high-pressure diffraction.

Dr. P.D. Hatton for his encouragement when the going got tough, and for his unflagging interest.

Dr. J.S. Loveday with whom the x-ray diffraction experiments were done, and Dr. R.O.Piltz for his help and companionship in the wee small hours during experiments conducted at the Institut Laue Langevin.

Dr. H. Ahsbahs for providing access to his sapphire-anvil cell, to Dr. W.F Kuhs for his expertise and patient tuition in the art of accurate neutron-diffraction studies, and to R. Dorwarth for developing the variable-temperature apparatus for the Ahsbahs cell.

To Dr. G.J. McIntyre for his crystallographic expertise, sense of humour, and considerable help in making the neutron-diffraction studies.

To the technical staff at the University of Edinburgh, the Institut Laue Langevin, and at the Rutherford-Appleton Laboratory,

To the S.E.R.C. for financial support.

To E.J.P. Fraser for many things

and to my parents, for their unfailing encouragement and support throughout, and to whom this thesis is dedicated.

Contents

Chapter 1

Introduction

1.1 Pressure as a Thermodynamic Variable

Hydrostatic pressure is a powerful but sadly underutilised variable in the study of crystalline materials. Despite being one of the fundamental thermodynamic variables, comparatively little work has been done using pressure compared to work using the other well known thermodynamic variable, temperature. However, pressure is, in many ways, a more powerful and 'cleaner' variable, enabling the changing of interatomic distances and atomic potentials at constant thermal energy and without changing the chemical environment. These changes in atomic distances are considerably larger than those obtainable using temperature alone; for example, the change in the lattice parameter of Si as a function of pressure is 5% in 100kbars compared to a change of only 1.5% on cooling from 1700K (the melting temperature) to 0K. This ability to dramatically alter the interatomic distances within a material can lead to a great number of phase changes and, when coupled with variable temperature, the phase diagrams of even the simplest materials and elements assume great complexity. (Pistorius (1976))

Hydrostatic pressure can also lead to a wide range of interesting physical phenomena in these different phases. For example, the simple molecular solid I_2 undergoes a gradual phase change at pressures up to 160kbar from an insulating phase to a metallic phase (Lynch and Drickamer (1966)). A similar phase

transition has been claimed for H_2O at very high pressures (Vereschagin *et al.* (1975)), while theory predicts metallisation of even H_2 at extreme, but by no means unobtainable, pressures (LeSar (1989)). The experimental confirmation of the latter is considered by many as the 'Holy Grail' of experimental high-pressure physics.

Pressure may also lead to dramatic changes in the nature of phase transitions known to occur at atmospheric pressure. The hydrogen-ordering phase transition in KH_2PO_4, for example, occurs at T_c=122K at atmospheric pressure. This temperature decreases with applied pressure until $T_c \rightarrow 0$K at 17.1kbars (Samara (1971)). Pressure was also found to change the superconducting transition temperature in the new oxide superconductors (Griessen (1987)) and was instrumental in the substitution of smaller Y atoms for La atoms to use 'chemical pressure' to increase the transition temperature from $\sim$35K in $La_{1.85}Ba_{0.15}CuO_4$ to 92K in $YBa_2Cu_3O_{7-x}$. A final example of the use of high pressure has been the study of materials that are gases at ambient conditions but which can be studied as single crystals at room temperature under high pressures. Examples include He, H_2, N_2, O_2, CO and Ar (Holzapfel (1989)).

In view of this richness of the different phase diagrams and the interesting changes in physical properties that occur at high pressures, it is surprising that little structural work has been done above ambient pressure with virtually none at high pressure and non-ambient temperatures. (The terms structural work, structural study and structure determination used in this thesis refer to the refinement of the full crystal structure, that is, the refinement of atomic co-ordinates and thermal parameters for each atom in the structure. The terms should not be confused with the determination simply of the lattice parameters or spacegroup.) Indeed many of the phases discovered at high pressure have been found using techniques other than diffraction – Raman spectroscopy for example – and the lattice type, let alone spacegroup, of the large majority of them is completely unknown. The number of phases in which the full structure is known is even more limited.

It is also surprising that despite the fact that powder-diffraction studies have been performed at pressures close to 3Mbars (Vohra and Ruoff (1990)), no full structural study has been made using neutron-diffraction techniques above

40kbars (or just over 1% of the present upper pressure limit), and no full structural studies using x-ray diffraction techniques have been made at pressures greater than 200kbars. The structural studies that have been made to date at high pressures have mostly been performed by mineralogists concerned with the pressure dependence of the structure of minerals and crystalline gases, with application to the study of the cores of the Earth and Jovian planets respectively. However, these studies have mostly been of limited accuracy, with the subtle structural changes with pressure being, on the whole, poorly determined. The determination of the pressure dependence of the thermal motion of atoms has mostly been ignored and the thermal parameters, if refined, have mostly been treated as an error dump. However, in order to fully understand the nature and reason for changes in physical properties as a function of some structural variable, it is essential to accurately determine any structural changes that accompany these changes, rather than assuming or ignoring them. An accurate determination of the crystal structure, including an accurate determination of the thermal parameters is, therefore, essential at high pressures in order to fully understand the pressure dependence of physical properties. It is this problem of poor structure determination at high pressures that concerns the present work.

1.2 Present Work and Thesis Outline

In October 1987, a major new research project was started by the Condensed Matter Group at the University of Edinburgh on the accurate determination of crystal structures at high pressure. This project was built on the extensive, and unique, program of high-pressure single-crystal neutron-diffraction studies of H-ordering systems undertaken by members of the group since the late 1970's (for example Nelmes *et al.* (1982), Meyer *et al.* (1980), Tun *et al.* (1987)), and on more recent work using single-crystal x-ray diffraction techniques (Katrusiak and Nelmes (1986a,b)). However, the project was not confined to the use of these two techniques alone, but was planned to encompass all methods of structure determination at high pressure, including the use of the new generation of spallation-neutron and synchrotron x-ray sources and the use of powder-based techniques.

The specific aim of the new project was to allow the determination of crystal structures under high pressure with unprecedented accuracy and precision through improvements in the established methods and techniques, or by developing new techniques and equipment. This aim was prompted both by the desire to extend the scope of studies of materials whose structural dependence on pressure had already been the subject of investigation, but the results of which were uncertain or ambiguous due to data of insufficient quality, and, through the development of new techniques, to develop new areas of high-pressure science.

This thesis describes the author's scientific involvement in this wide-ranging project and, for completeness, some work not principally done by the author is included, although it is stressed that the author was closely connected with all the work described. Work included under this heading is the development of the Paris pressure cell described in Chapter 3, and the application of the newly developed single-crystal x-ray diffraction techniques to the study of the high-T_c superconductor $YBa_2Cu_4O_8$ in Chapter 4.

The thesis is organised as follows.

Chapter 2 introduces the essential details of high-pressure diffraction using x-rays and neutrons, single crystals and powders, and reviews the specialised equipment and techniques used in determining crystal structures at high pressures prior to the present work. A comparison is made of the accuracies available using the different techniques, and conclusions are drawn as to the state-of-the-art prior to this thesis.

Chapter 3 describes the present work in improving the accuracy and scope of high-pressure structural studies through the development of new techniques, and improvements to those already established. The majority of the work described is concerned with the development of single-crystal techniques using both x-rays and neutrons although accounts of preliminary work on new powder-diffraction techniques are also described.

Chapters 4 and 5 describe the application of the newly developed single-crystal techniques described in Chapter 3 to the study of two classes of materials – hydrogen-ordering (H-ordering) systems of the KH_2PO_4 type, and high-T_c superconductors.

The nature of the H-ordering phase transition in KH_2PO_4 type ferroelectrics has been the subject of a large number of theoretical and experimental studies since the discovery of ferroelectricity in the prototype material KH_2PO_4 (KDP) (Busch and Scherrer (1935)). These H-bonded materials undergo an H-ordering structural phase transition from a paraelectric to a ferroelectric or antiferroelectric phase on cooling through the transition temperature T_c, which is very sensitive to both deuteration and pressure: for example, T_c rises from 122K to 229K on deuterating KDP to KD_2PO_4 (DKDP) and T_c falls by $4.6Kkbar^{-1}$ in KDP (Samara (1987)). These changes in T_c with pressure and deuteration are presently explained using the tunnelling model of the transition (Blinc (1960)). However, previous high-pressure structural studies of KDP and DKDP using single-crystal neutron-diffraction (Nelmes *et al.* (1982), Tibballs *et al.* (1982a,b)), combined with high-pressure structural studies of another H-ordering material, $H_2C_4O_4$ (Squaric acid or $H_2SQ.$) (Tun *et al.* (1987)), have suggested that the changes in T_c on deuterating KDP to DKDP may be attributable to the accompanying changes in the H-bond geometry, the so-called Ubbelohde effect (Robertson and Ubbelohde (1939)), and similarly, that the differences in the H-bond geometry may account for the large difference in T_c between KDP (T_c=122K) and $H_2SQ.$ (T_c=374K). This relationship between T_c and the H-bond (or D-bond in deuterated materials) geometry is explored in Chapter 4, with high-pressure single-crystal neutron-diffraction studies of the H(D)-ordering materials $PbDPO_4$, CsD_2PO_4 and KH_2PO_4.

Since the early days of high-T_c oxide superconductors it has been known that applied pressure can have a strong effect on the superconducting transition temperature T_c (Griessen (1987)). The considerable differences in the pressure dependence of T_c has created much interest in determining any structural changes with pressure which occur in materials with a large value of dT_c/dP, but not in materials with a small value of dT_c/dP, and thus identifying a structural basis for the superconducting transition. Recently, it has been postulated that T_c in $YBa_2Cu_3O_{7-\infty}$ is coupled strongly to the valency of the Cu atom (Cava *et al.* (1988)) which, in turn, would seem to be strongly determined by the bondlength from the planar copper atom to the apical oxygen atom (Cava *et al.* (1990)). In the first high-pressure structural study of a high-T_c superconductor, Kaldis *et al.* (1989) have shown, using neutron powder-diffraction techniques, that the only notable structural change on compressing polycrystalline $YBa_2Cu_4O_8$ to 10kbars

was a very substantial decrease in the apical Cu-O bondlength. They associated this with the simultaneous increase in T_c. Since T_c has been measured in many oxide superconductors to pressures in excess of 100kbars (Griessen (1987)), it would be desirable to follow any structural changes as a function of pressure to much higher pressures than those obtained by Kaldis *et al.*. The relationship between T_c and the apical Cu-O bondlength is explored in Chapter 5 with structural studies of $YBa_2Cu_4O_8$ and $La_{1.85}Sr_{0.15}CuO_4$ using both neutron and x-ray diffraction techniques.

Finally, Chapter 6 draws conclusions from the present work and discusses possible future advances to be made in the determination of crystal structures at high pressure.

Chapter 2

A Review of Structure Determination at High Pressure

2.1 Introduction

Before trying to improve upon the quality of the structural information available at high pressure it was essential that the reasons for the present poor quality were first fully understood. In order to achieve this, it was felt necessary that a large, comprehensive and detailed search of the literature should be undertaken in order to determine the state-of-the-art methods and results of high-pressure structure determinations prior to the start of this thesis. It was felt that only after such a detailed study of the established methods and techniques could possible avenues for improvements in accuracy be found. This chapter contains a review of this extensive study and serves as a detailed introduction to the methods of crystal structure determination at high pressure.

It should be emphasised at this point that prior to this thesis only one review of structural studies at high pressure has been made and this was concerned primarily with single-crystal x-ray diffraction techniques (Ahsbahs (1987)). Although this subject will also be discussed here, the present review is aimed at encompassing all aspects of structure determination at high pressure using both x-rays and neutrons, single crystals and powders – topics not previously considered. The extensive nature of the review has resulted in a chapter of considerable length; however, the review is felt vital in laying the background against which

the present work is set and is therefore considered an integral part of the thesis.

The rest of this chapter is laid out as follows. Sections 2 and 3 consider the various techniques employed at both atmospheric pressure and high pressure to determine crystal structures, and discuss the criteria necessary for an accurate structural study. Section 4 discusses the basic principles of high-pressure diffraction and sections 5 and 6 contain a review of all aspects of high-pressure diffraction equipment and techniques respectively. Section 7 compares the quality of the results obtained in different high-pressure structural studies of two materials – α-Quartz and KH_2PO_4 – using different diffraction methods. Finally, section 8 draws conclusions as to the state-of-the-art prior to the start of the present work.

2.2 X-ray and Neutron Diffraction

In order to determine the crystal structure of a material it is necessary to measure the relative intensities of Bragg reflections, the necessary condition for which is given by Bragg's Law

$$\lambda = 2d\sin\Theta \tag{2.1}$$

where λ is the wavelength of the incident radiation, d is the spacing between the crystal planes that the radiation is diffracted from, and Θ is the angle of incidence of the radiation, or equivalently, half the diffraction angle. This equation allows two general methods of satisfying the diffraction condition.

In the first, λ is fixed and the data are collected in an angle–dispersive mode. This is the most commonly used method of determining crystal structures and all four possible combinations of x-rays and neutrons, powders and single crystals, have been used successfully to refine crystal structures at atmospheric pressure. Of the two possible sample types, single-crystal techniques usually give the most accurate and detailed structural information as each Bragg reflection is collected individually, generally without interference from other reflections. This is in contrast with powder methods where reflections at short d-spacing, or equivalently high Θ, are generally very numerous and overlap in the diffrac-

tion pattern. Although refinement of powder data generally follows the method of Rietveld (1969) and fits the entire diffraction pattern rather than individual peaks, the overlap of reflections leads to a significant loss of information at high Θ and subsequently makes high real-space resolution (high $\sin\Theta/\lambda$) studies very difficult, if not impossible.

Of the two possible choices of radiation, neutrons, in general, give more accurate results than x-rays and allow highly-detailed studies of structural disorder and thermal anharmonicity (for example McMahon *et al.* (1990a)). This is due to the isotropic nature of the nuclear form factor which does not decrease as a function of scattering angle in contrast to the atomic form factor (Figure 2.1). This reduction in intensity at high angles, in addition to the reduction due to thermal motion, limits the real-space resolution of x-ray data. Neutrons also allow the accurate determination of light atoms, for example hydrogen atoms, in crystals, as the nuclear scattering power does not depend on the number of electrons in the atom, as does the x-ray scattering power (Bacon (1975)). However, the absolute neutron scattering power of a nucleus is smaller than the x-ray scattering power of the equivalent atom (Figure 2.1), thus requiring that samples for neutron-diffraction studies be considerably larger than those used in x-ray studies.

The second method of satisfying Bragg's law is to fix Θ and vary λ – so-called λ-dispersive or energy-dispersive techniques. In this technique, the detector is fixed and the crystal planes select the appropriate wavelength from the polychromatic incident beam to diffract into the detector which contains some form of energy analysis in order to separate the intensity of individual reflections collected at different wavelengths. This technique has, until recently, been used rarely, but the development of spallation neutron sources and synchrotron x-ray sources, both of which produce the smooth, continuous spectrum of wavelengths necessary for such a technique, has lead to a recent increase in use. Of the four combinations of x-rays and neutrons, single crystals and neutrons, the most popular methods have used powders. However, energy-dispersive x-ray diffraction (or EDXRD) has been used very rarely for crystal structure refinement (for example Weir *et al.* (1989), Buras *et al.*(1979)) and the accuracy available is severely limited by the poor energy resolution of the semiconductor detectors employed resulting in large peakwidths and subsequently too many overlapping

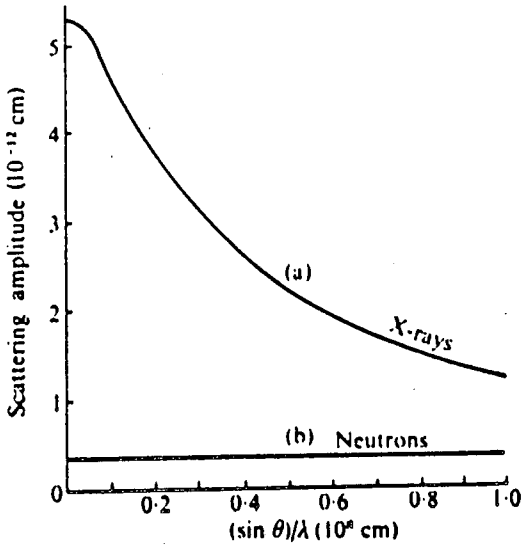

Figure 2.1: The x-ray and neutron scattering amplitudes for a potassium atom. (From Bacon (1975))

peaks for profile refinement. Therefore, despite the fact that the majority of x-ray diffraction studies at high pressure have employed this technique, for reasons described later, no further description of it is given here.

In contrast, λ-dispersive powder diffraction using neutrons has been widely used for structural studies. The pulsed structure of the neutrons provided by a spallation neutron source allows the time-of-flight (TOF) of a neutron from production to detection to be determined very accurately and then related to the wavelength through the de-Broglie equation. The peakwidths are also well determined and narrow, allowing full structure refinement with high-quality results (for example Jorgenson *et al.* (1987)).

The use of single-crystal studies using λ-dispersive techniques, the Laue method, has achieved much popularity recently in the protein crystallography community due to the ability to measure, on film, many thousands of Bragg peaks simultaneously in very short (less than 1 second) exposure times (for example Ritzkallah *et al.* (1990), Harding *et al.* (1988)). The quality of the structural data has been shown to be comparable with that obtained using standard angle-dispersive x-ray diffraction using single crystals (Gomez de Andrez *et al.* (1989)). The use of λ-dispersive single-crystal neutron diffraction, however, has

not yet been used extensively for structural studies although some success has been achieved (Alkire *et al.* (1984), Jauch *et al.* (1988)). Despite this, the use of very short wavelength neutrons from spallation sources opens up the possibility of very high resolution ($\sin\Theta/\lambda > 2.0\text{Å}^{-1}$) studies in the future.

Of these eight methods that have been used to refine the full crystal structure of materials at atmospheric pressure, only six have been used to determine crystal structures at high pressure. The other two, the Laue method using both x-rays and neutrons, have not yet been used although there are no technical reasons why this should be so. Indeed these techniques have several advantages over those currently employed and may permit future refinement of crystal structures to very high pressures (>500kbars). The future use of these techniques will be discussed in Chapter 6.

2.3 The Accurate Determination of Crystal Structures

The criteria necessary for the accurate determination of a crystal structure from diffraction data has attracted a large amount of attention and study (for example Ardnt and Mathieson (1969), Blessing (1987)) and it is not the author's intention to discuss the topic at length. However, some of these criteria are particularly relevant to the collection of diffraction data at high pressure and will be discussed briefly.

(1) The Bragg reflections measured in a single-crystal study should be distributed evenly throughout reciprocal space so as to avoid bias in the final refined structure. Ideally, all independent reflections out to the required Θ limit should be measured. For a powder, as full a diffraction pattern as possible should be measured.

(2) Single-crystal reflections should be on a smooth, flat and preferably low background in order to determine the integrated intensity of the reflection accurately and precisely. For powders, the background should also be low and flat, without any additional contaminating peaks from material other than the sample.

(3) The intensity of reflections should be corrected for absorption of the incident and diffracted beams.

(4) For powder studies, the sample should have a high degree of randomness in the orientation of the crystallites to avoid preferred orientation. This is usually realised by using as large a volume as possible of a finely-powdered sample.

The special relevance of these criteria to structural work at high pressures is discussed in the next section.

2.4 High-Pressure Diffraction

The generation and maintenance of hydrostatic pressure on a crystalline material follows the same basic principles whether one is using x-rays or neutrons, single crystals or powders: the sample is placed in a containment vessel and is surrounded by a fluid which, if hydrostatic pressures are required, should remain a liquid to the highest pressures used; force is then applied to the liquid which, being relatively incompressible, exerts pressure on the sample.

From the pioneering work of Bridgman in the 1930's (Bridgman (1971)) until the late 1960's, the methods of applying pressure to materials were very cumbersome and used large hydraulic rams. The invention of the diamond-anvil cell (hereafter DAC) at the NBS in the 1960's (Weir *et al.* (1965,1969)), however, revolutionised high-pressure science. The details of a DAC are shown in Figure 2.2.

The sample is mounted on the face, or culet, of the lower diamond anvil and a gasket of hardened metal with a small hole in it is placed around the sample. A pressure calibrant is then placed beside the sample and the gasket hole is filled with hydrostatic fluid. The upper diamond, which must be well aligned with respect to the bottom diamond, is then pressed onto the top of the gasket which extrudes around it, sealing the pressure chamber. The force needed to apply pressure to the sample is not great and can be applied in some cases by simply tightening screws with an Allen key.

In order to allow the incident and diffracted beams as wide an access as possible

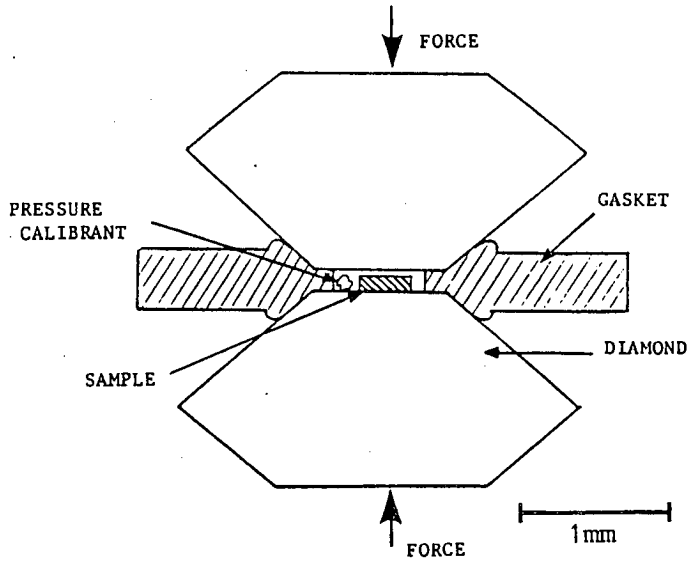

Figure 2.2: The basic principles of a diamond-anvil cell (DAC). Note the scale.

to the sample for single-crystal studies, and thus satisfy criterion (1) above, the diamonds are usually seated on beryllium (Be) backing plates. Be, although highly toxic, is both a very hard material and relatively transparent to x-rays, due to its low atomic number. However, the use of Be backing plates limits the upper pressure of the cell to that pressure at which the diamonds are pressed into, or break, the backing plates. Higher pressures can be obtained by the use of beveled diamonds (Mao and Bell (1978a)), by removing the Be plates, and by the use of smaller gasket holes and a smaller sample. However, in order to obtain higher pressures, the support given to the backs of the diamonds must also be increased, at the expense of angular access for the incident and diffracted beams to the sample. This can be overcome by the use of energy-dispersive techniques which do not require the wide angular access to the sample necessary for monochromatic methods, and explains the popular use of the EDXRD method for diffraction studies up to 3Mbars using a DAC.

The size of the pressure chamber in a DAC, even for modest pressures below 50kbars, is such that they can only be used for x-ray studies, the sample volume being far too small for the size of sample needed for neutron-diffraction studies. The pressure chamber in a DAC is also too small to contain a sufficient number of crystallites to give the degree of orientational averaging needed to give

reliable relative intensities when using monochromatic x-ray powder-diffraction techniques. This violates requirement (4) above, and explains the very limited number of structural studies made at high pressure using this technique.

The ease with which DACs allow high pressures to be achieved has prompted the use of suitably scaled up models for single-crystal neutron-diffraction studies (Ahsbahs (1984a)). The larger samples needed, of the order of 1mm in diameter and 0.5mm high, require a larger gasket hole and therefore larger anvils. This latter requirement has lead to sapphires being used as anvils due to cost, although a DAC for neutron-diffraction to 200kbars has been built with 4 carat (!) diamonds (Besedin *et al.* (1990)). This latter pressure cell, though, has a sample volume that is again too small to give a reliable powder average and the more usual type of pressure cell for both neutron powder and single-crystal studies is shown in Figure 2.3. This cell operates on the same general principle as the DAC – the containment of the fluid and the sample within a pressure chamber which in this case is usually sintered Al_2O_3 – but the size of the cell and the sample requires that the force on the pistons be applied with a hydraulic ram. The large volume of the pressure chamber and sample also reduces the upper pressure limit to approximately 40kbars. However, the large sample volume required when using neutron-diffraction techniques allows a sufficient degree of orientational averaging within the powder to enable the accurate determination of relative intensities.

Although the basic design configurations of the pressure cells used in structural studies explain the pressure limitations of the various techniques, in order to understand the reasons why high-pressure structural studies should be of poorer quality than those obtainable at ambient pressure, and to what extent the four criteria for accurate structural work listed previously are fulfilled, it is necessary to analyse the details of the diffraction process, and the collection of the diffraction data, more closely.

Figure 2.4 shows the path of the incident and diffracted x-ray beams for a single-crystal sample in a DAC. The incident beam, before illuminating the sample, must pass through one of the Be backing plates and one of the diamond (or sapphire) anvils. This will have two effects.

(1) The incident beam will be attenuated by absorption and this will depend

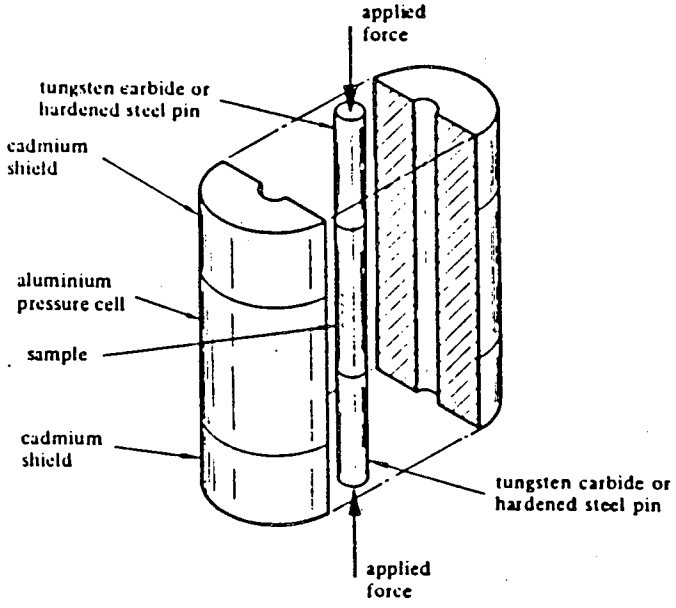

Figure 2.3: The basic principles of a pressure cell designed for neutron-diffraction studies. (From Carlile and Salter (1978)).

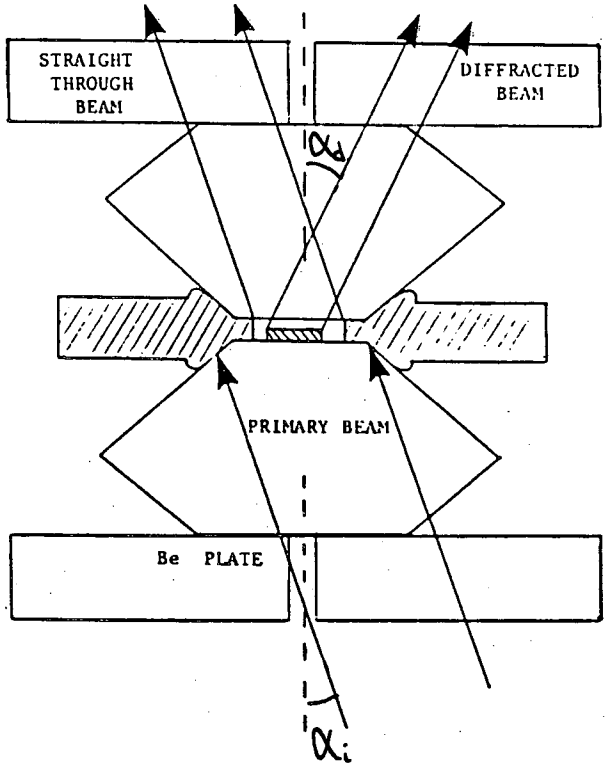

Figure 2.4: Details of the diffraction processes for a single-crystal sample in a DAC.

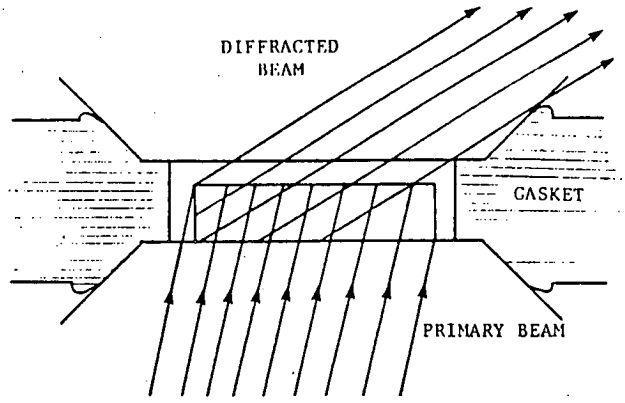

Figure 2.5: A detailed view of the gasket hole in a DAC. Only that part of the sample that is cross-hatched scatters into the detector, the rest being occluded by the highly absorbing gasket.

on the relative pathlengths through the Be and the diamond, ie. on α_i which is generally limited to a maximum of 40° by the steel housing of the cell.

(2) Parasitic scattering of the incident beam by the Be plates and the single-crystal anvils, will result in a structured background of powder lines and intense Bragg reflections.

After illuminating the sample, the main beam will continue on through the pressure cell, generating a second set of powder lines and Bragg reflections on passing through the second Be plate and diamond anvil as in (2) above. The diffracted beam will also produce a set of powder lines and Bragg peaks as it passes through the other side of the DAC, although the effects in this case will be much weaker than those produced by the main beam. The diffracted beam will also be attenuated because of absorption which will this time vary as a function of α_d, which is again usually limited to 40°.

Closer examination of the gasket hole (Figure 2.5) shows another effect that may reduce the intensity of a reflection. If either the incident or diffracted beam is occluded by the gasket, then the intensity of a reflection will be reduced. This effect may reduce the upper limits of α_i and α_d at which reflections may be safely measured below the 40° defined by the cell housing.

For single-crystal studies, the combined effect of these processes will be the production of a high, structured background which will make the accurate measurement of integrated intensities difficult. This high background, combined with the attenuation of the incident and diffracted beams, will result in a reduction in the signal-to-noise ratio for sample reflections, making the measurement of weak reflections especially difficult. The background will also contain very strong diamond, or sapphire, Bragg reflections which in the case of diamond will be few in number due to diamond's small lattice parameter and high-symmetry structure, while Bragg reflections from the sapphires will be far more numerous due to its low symmetry and large c-axis lattice parameter. All sample reflection intensities will have to be corrected for absorption of the incident and diffracted beams.

For x-ray powder-diffraction studies, the diffraction pattern may include, along with the peaks from the sample, diffraction peaks from the two Be plates (if used), peaks from the gasket, which is illuminated by the primary beam, and peaks from the steel housing of the cell if either α_i or α_d is close to 40°. Each of these individual diffraction patterns may be stronger than that from the sample itself, depending on the illuminated volume, and, combined, will seriously degrade the quality of the sample pattern.

The parasitic scatter from the pressure cell for neutron-diffraction studies (as in Figure 2.3), although not including any single-crystal Bragg peaks, will contain a large number of powder lines from the sintered Al_2O_3 pressure vessel. However, for neutron powder-diffraction, this problem can be cleverly avoided using λ-dispersive techniques on a spallation neutron source. Using a fixed detector at 2Θ=90°, and with suitable collimation of both the incident beam and the detector, only the sample will be both illuminated by the incident beam and viewed by the detector simultaneously (Figure 2.6), thus giving a powder pattern free from any parasitic lines. For the more commonly used angle-dispersive data collection methods, however, using both neutrons and x-rays, single crystals and powders, the combined effect of the high structured background, and the angular restrictions on the incident and diffracted beams, will be to limit the accuracy and precision with which individual reflections may be measured, through uncertainties in the background level, and to severely reduce the number of reflections which are accessible for measurement, leading to possible biasing or

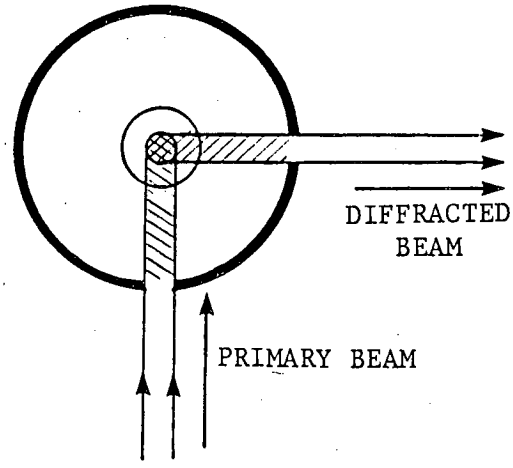

Figure 2.6: The 90° scattering geometry using time-of-flight neutron-diffraction techniques. Only the sample (cross shaded) is both illuminated by the primary beam and viewed by the detector simultaneously.

unrefineable parameters in the final analysis. Although many different designs of pressure cell and alternative data collection methods have been developed to minimise these problems and to reduce subsequent corrections that may still need to be applied, it is these inherent problems of low signal-to-noise, high structured background and reduced angular access that limit the quality of the structural data available at high pressure. The equipment and techniques that have been developed to deal with these problems are discussed in the next two sections.

2.5 High-Pressure Equipment

2.5.1 Pressure Cells

The number of pressure cells that have been developed specifically for structural studies is considerable and it is not possible to review each in great detail here. However, the specific design features of each cell, and their possible effect on the accuracy of the diffraction data collectable using that cell, will be described. Since the large majority of structural studies to date have been made using

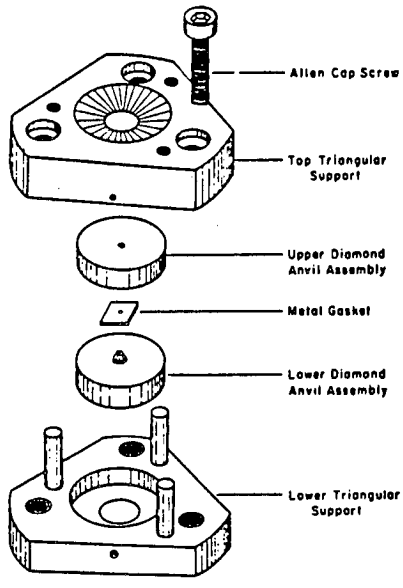

Figure 2.7: An exploded view of the Merrill-Bassett (1974) DAC, as modified by Hazen and Finger (1977). (From Hazen and Finger (1977)).

single-crystal x-ray diffraction techniques, the pressure cells used in these studies will be described first.

Single-crystal X-ray Diffraction

Almost all structural studies using this technique have been made using DACs of varying designs, and although single-crystal studies were made using the early design of DAC at the NBS (Weir *et al.* (1965)), and indeed some structural work was done using film techniques on modified precession cameras (Weir *et al.* (1969)), it was the introduction of the Merrill-Bassett pressure cell (Merrill and Bassett (1974)) that heralded the breakthrough in single-crystal structural studies. This cell was designed to be small enough, and light enough, to be mounted on unmodified x-ray equipment, specifically three or four-circle diffractometers, and can be treated in most cases as a standard crystal mounting. The cell is shown in Figure 2.7. Many of the design features incorporated into the original design of this pressure cell have been used in almost all subsequently designed DACs and it is worth examining the Merrill-Bassett (M-B) cell in some detail.

As mentioned above, the major criteria in the design of this cell were that it should be mountable on commercially available x-ray equipment while providing maximum access to reciprocal space. The fully assembled cell, without goniometer head, is 32mm in diameter and 16mm wide and possesses both mirror and cylindrical symmetry. This latter feature greatly simplifies the absorption correction for the cell by making the absorption dependent only on α_i and α_d (Figure 2.4). The Be backing plates are mounted in stainless-steel housings which have a conical opening of half-angle 50°, allowing wide angular access for the incident and diffracted beams. Each Be plate has a 1mm diameter hole drilled through it to allow optical access to the pressure chamber along the cell axis. This simplifies initial alignment on the diffractometer and allows the ruby fluorescence method to be used for pressure measurement (Chapter 2.6.7). The diamonds have 0.8mm diameter culets and are slightly recessed into the Be plates to lend them additional support.

Pressure is applied to the cell by the uniform tightening of three screws situated symmetrically around the steel housings. Alignment of the two halves of the pressure cell while pressure is being applied is maintained by two guide pins.

The original M-B cell has no independent method of aligning the diamonds with respect to each other. In order to obtain high pressures, and to avoid fracture of the anvils, it is essential to accurately align the diamonds translationally and to have their culet faces parallel. While the authors claimed this lack of accurate alignment was not critical for pressures up to 25kbars, the upper pressure limit for the original design, nearly all later modifications of the original M-B cell have been prompted by the desire to obtain higher pressures, and their designs have usually incorporated means of obtaining better diamond alignment.

The modification of the original M-B cell by Hazen and Finger (1977) was prompted by their wish to obtain higher pressures in their study of minerals. The resulting pressure cell has effectively superceded the original M-B design and is widely used and commercially available.

To obtain better alignment of the diamonds while applying pressure, the two guide pins of the original M-B design are replaced by three, located symmetrically around the steel housings. The Be plates, which proved to be the weakest point in the original design, are strengthened by removing the well for position-

ing the diamonds and by reducing the diameter of the hole for optical access to 0.8mm. Greater support for the Be plates is provided by reducing the conical opening in the steel plates to a half-angle of 40°. This, however, reduces the number of reflections accessible for measurement. Larger diamonds with 1mm culets allow better diamond alignment and produce less deformation of the gasket at the higher pressures obtainable with this cell. This feature is desirable as deformation of the gasket may lead to increased gasket occlusion.

Partial alignment of the diamonds is possible as one of the Be plates is held in its housing by three positioning screws which allows one of the diamonds to be translated with respect to the other diamond. However, there is still no method of adjusting the diamond culets so that they are parallel to each other. The modifications made, though, allow a substantially higher pressure of 60kbars to be reached with both greater reliability and pressure stability.

A modification to the M-B cell which allows structural studies to even higher pressures was made by Mao and Bell (1980). Their cell, which was originally designed for the cryogenic loading of gases and their subsequent study as crystalline solids at high pressure, has been used in the highest pressure structural study to date at 190kbars (Hazen and Finger (1989)). Although of similar design to the original M-B cell, extensive modifications were necessary to enable its use at low temperatures. All steel parts of the cell are made of maraging steel due to its strength at low temperatures. The three guide pins and screws of the Hazen and Finger design are replaced by four of each, the screws being tightened alternately in pairs to maintain diamond alignment. One of the diamonds is again able to be translated with respect to the other, but there is no mechanism for aligning the culet faces. The angular apertures in the steel housing are reduced to a half-angle of 30° in order to provide additional support to the Be backing plates, again at the expense of limiting the number of reflections measurable. However, the pressure limit of the cell is greatly increased to 200kbars.

A very simple modification to the M-B cell by Takeuchi (1986) solved the problem of aligning the diamond culet faces by giving one of the Be backing plates a hemispherical shape. Mounted in a similarly shaped steel housing, this allows the Be plate to rotate until the diamond faces are parallel.

The DAC design of Keller and Holzapfel (1977) was again instigated to achieve

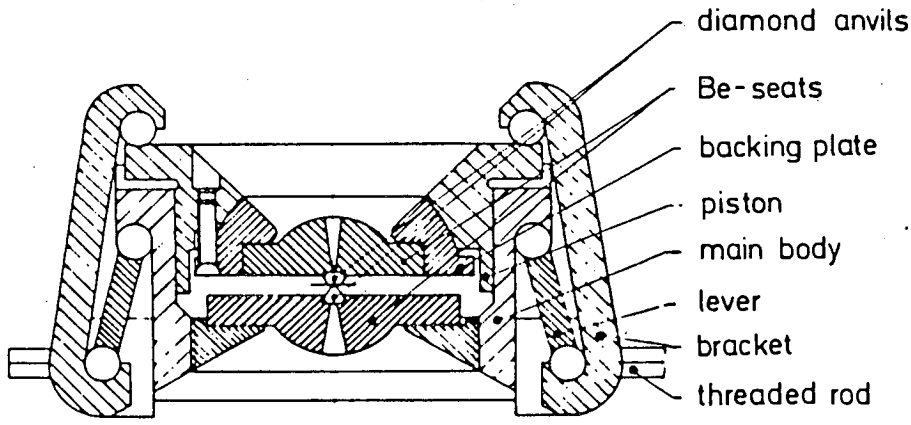

Figure 2.8: The single-crystal DAC of Keller and Holzapfel (1977). (From Keller and Holzapfel (1977).)

higher pressures than were possible using the M-B cell. The design of this cell, however, differed significantly from the previous cells designed for structural studies and, through better diamond alignment and a stronger cell structure, could achieve pressures of 100kbars.

The cell is basically a modification of a pressure cell designed for optical studies (Huber *et al.* (1977)) and is shown in Figure 2.8. Although the diamonds are again mounted on Be backing plates, the backing plate design is very different from those in the M-B cell. Each plate is shaped to allow the absorption of the incident and diffracted beams to be constant and independent of α_i and α_d. However, the drawbacks of increased absorption and background scatter from using such large Be backing plates are described in Chapter 2.8. The shape of the Be plates also gives them additional strength (indeed David Schiferl (1977b) has designed similar Be backing plates for the M-B cell which extend its upper pressure limit to 100kbars) and enables the upper plate to rotate in its semi-spherical steel housing, allowing the diamond culets to be aligned parallel to each other.

The diamonds themselves, which are hot-pressed into the Be plates to give additional support, do not have matched culet sizes or thicknesses, the authors stating that this facilitates the centering of the sample on the diffractometer. The reasons why this should be so, however, are not clear, as the authors themselves state that the different diamond thicknesses, and therefore different optical

pathlengths, must be accounted for when aligning the sample optically.

To maintain perfect alignment of the diamonds while pressure is being applied, the cell uses a piston-cylinder design – the upper half of the cell being mounted on a piston which fits tightly into the cylindrical chamber of the lower half of the cell. The two halves of the cell are pulled together using a knee arrangement which allows a large force multiplication factor. The two half-angles of the conical apertures in the steel housings are designed such that gasket occlusion is the limiting factor in determining the upper angular limits of the incident and diffracted beams to the cell axis.

The piston-cylinder arrangement is also used in the DAC designed by Kudoh (1984). Combined with the ability to align the diamonds translationally and to ensure their faces are parallel, structural studies to 140kbars have been possible using this cell. The pressure is applied to the cell using a lever-arm loading device originally designed to pressurise DACs for powder-diffraction studies to very high pressures, and is maintained by three bolts positioned symmetrically around the cell edge.

All the DACs described so far have had what is known as the transmission geometry in which the incident and diffracted beams pass through different diamonds (Figure 2.9a). Although this geometry of DAC has been used in the great majority of structural studies using single-crystal techniques, it suffers from the drawback that only 40-50% of all reflections are measurable, this fraction depending on the angular size of the apertures in the steel housings (Merrill and Bassett (1974)). Transmission-geometry cells, though, have the advantage that the absorption correction for the cell is easily made due to the mirror and/or cylindrical symmetry of the cells. To overcome the problem of the limited amount of data measurable, another family of DAC has been developed using a different geometry. In this so-called transverse geometry, the incident and diffracted beams pass through the same anvil (Figure 2.9b). The advantages of this geometry are that a much larger fraction of reflections is measurable out to a considerably higher 2Θ limit. However, the absorption correction for the cell is no longer simple and occlusion by the highly-absorbing gasket is a serious problem especially at low diffraction angles (Figure 2.10). This occlusion, however, may be eliminated by the use of lowly-absorbing gaskets.

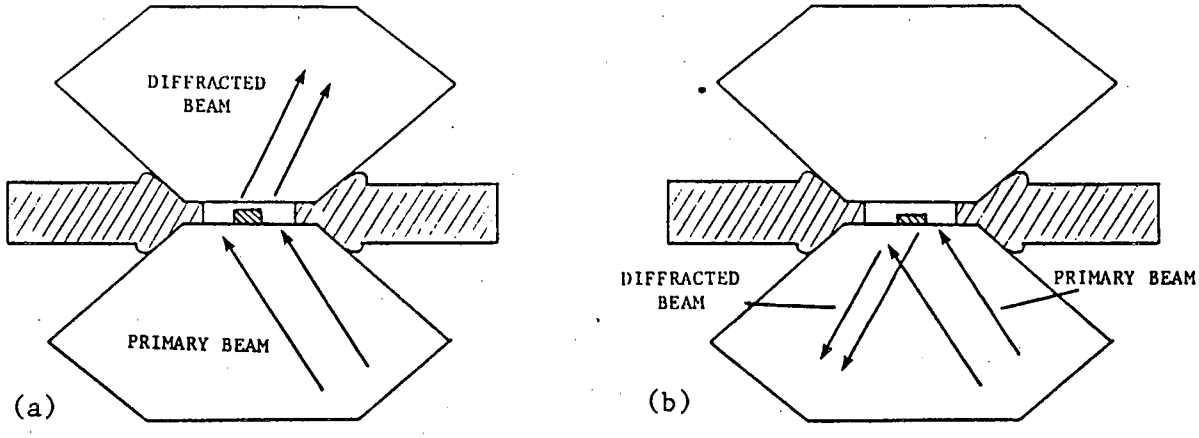

Figure 2.9: The diffraction geometry in the (a) transmission, and (b) transverse geometry design of DAC.

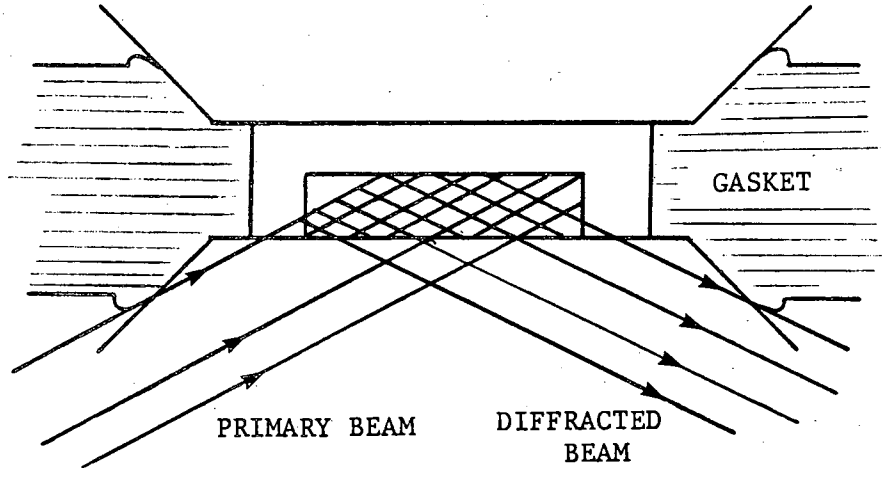

Figure 2.10: A detailed view of the gasket hole in a transverse-geometry DAC. Only the cross-hatched volume of the crystal scatters into the detector without occlusion of either the primary or diffracted beam.

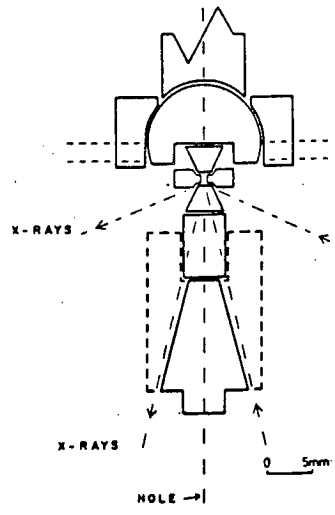

Figure 2.11: The transverse-geometry DAC of Schiferl (1977a) showing the wide angular access available for the incident and diffracted beams. (From Ahsbahs (1987).)

The transverse geometry was first used in a cell designed by Schiferl (1977a) which exhibits a very different design to the M-B type cells. The cell is shown in Figure 2.11. The diamond for which the maximum angular access is required is mounted on a Be cylinder which, in turn, is mounted on a stainless-steel pillar. The steel is cut away as much as possible to maximise access to the sample. The second diamond, which requires no angular access, is mounted so as to be adjustable to align the culet faces. However, no translational alignment of the diamonds is possible. The original cell was subsequently redesigned (Schiferl *et al.* (1978)) to allow a higher pressure limit. Prestressed Be was used as the backing cylinder for the diamond, being stronger than the normally processed Be. (It was from this prestressed Be that Schiferl also made the modified backing plates for the M-B cell). A redesigned upper-diamond mount allowed translational alignment of the diamonds.

The same basic design as Schiferl was adopted by various workers at the MPI in Stuttgart who designed a cell that was both smaller and lighter than Schiferl's original (Koepke *et al.* (1985)). The cell (Figure 2.12) uses the knee arrangement of Keller and Holzapfel to apply the pressure, and was again designed to provide as wide an angular access to the sample as possible. Apart from shadowing from two support pillars, all reflections in a conical belt of 45° half angle are

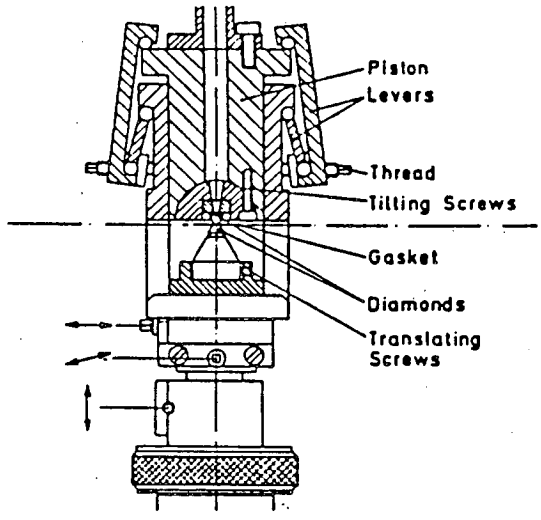

Figure 2.12: The MPI transverse-geometry DAC. (From Koepke *et al.* (1985).)

measurable. For reflections with $2\Theta<45°$, only 5-10% of reflections are affected by shadowing. The diamonds of this cell are not matched and have culets of 0.7mm and 1.3mm. The smaller culet is used on the diamond that the diffracted beam does not pass through as it was found that the gasket bends up around this diamond at high pressure, producing less occlusion of the incident and diffracted beams. Using metal gaskets, pressures of up to 500kbars are possible with this cell as there are no Be supports used – the diamonds being mounted directly onto steel plates. However, the highest pressure at which a structural study has been to date using this cell is 102kbars (Glinneman (1990)). Using Be gaskets, which eliminates the problems of gasket occlusion and allows a simple graphical method for correcting for the resulting absorption, reduces the pressure limit to 40kbars.

A combination of x-ray permeable gaskets and the transmission geometry has also been used in a cell designed by Ahsbahs (1984a,b). The cell was specifically designed for the study of complicated structures up to 30kbars which requires the largest possible data sets. The cell (Figure 2.13) was designed to be small enough to fit onto a Philips PW1100 diffractometer and allows a conical belt of reflections centred on the plane of the gasket to be measured. The limiting criteria for reflections to be measurable is:-

$$\sin^{-1}[\sin\theta \sin\chi] < \beta \qquad (2.2)$$

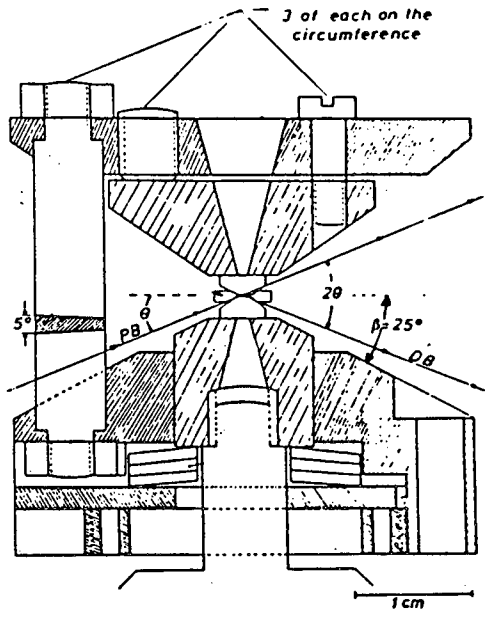

Figure 2.13: The Ahsbahs transverse-geometry DAC showing the primary beam (PB), diffracted beam (DB) and the definition of the angle β. (From Ahsbahs (1984a).)

where β is 25°. The upper pressure limit using Be gaskets was originally 35kbars although better gasket design has increased this to 70kbars.

Finally, a DAC by Malinowski (1987) combines the best features of both the transverse and transmission geometries. As shown in Figure 2.14a, the cell is very similar to an M-B DAC and uses a knee arrangement to apply the pressure and a piston and cylinder arrangement to maintain good diamond alignment. Alignment of the diamonds is permitted by one of the diamondsbeing mounted on a hemispherical steel backing plate. The diamonds have unmatched culets to allow the preferential distortion of the gasket discussed for the MPI Stuttgart cell.

By rotating the cell by 90° (Figure 2.14b), the design modifications allowing the use of the transverse geometry are visible. The lower diamond is mounted on a beam of Be, rather than a plate, removing almost all the absorbing steel from this side of the cell and allowing improved angular access for both transmission and transverse geometries. In the transmission geometry, the absence of any angular restriction on the incident or diffracted beam, except due to the steel fingers holding the Be beam or due to gasket occlusion, allows a larger percentage

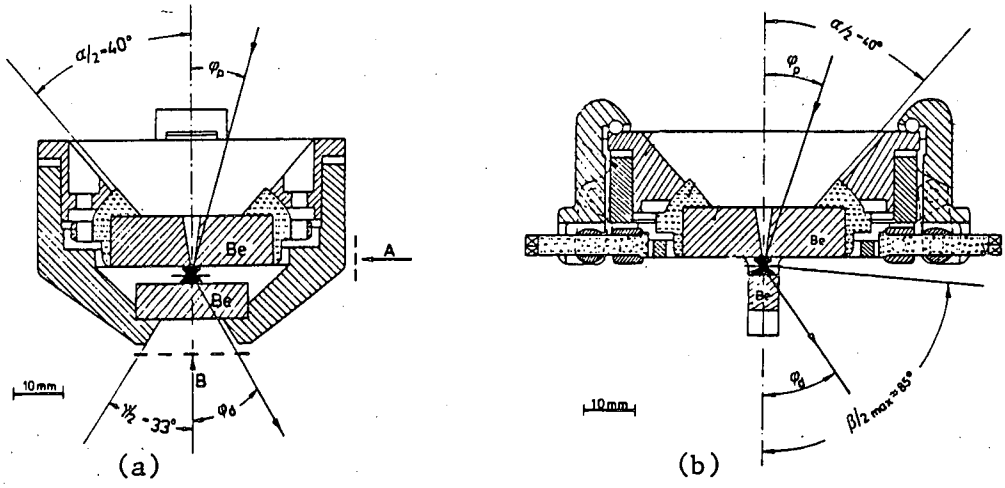

Figure 2.14: Two perpendicular cross-sections through the Malinowski DAC. Showing the (a) transmission and (b) transverse geometry of the cell. (From Malinowski (1987).)

of the Ewald sphere to be measured compared to a more standard DAC design. This cell, however, has yet to be used for a full structural study.

High Pressure–High Temperature Cells

To enable the study of samples at both high temperatures and high pressures (HT-HP) simultaneously, several DACs have been designed with integral heating elements.

The first DAC to allow the structural study of materials at HT-HP was designed by Fourme (1968) for use on precession cameras and was equipped with a resistance heater capable of sustaining 250°C. This cell was employed by Andre *et al.* (1971) in the first combined HT-HP experiment on monochlorobenzene in which the crystal structure was determined at 120°C and 14kbars, a considerable achievement.

Hazen and Finger (1979,1981a) have added a heater to their version of the Merrill-Bassett DAC to enable a pressure-temperature maximum of 400°C at 25kbars. Although similar in design to the DAC designed for ambient-temperature studies, certain features of the HT-HP cell had to be changed. The beryllium used in the backing plates of the ambient-temperature cell became too soft at

temperatures above 200°C to support the diamonds and were therefore replaced by plates made from hot-pressed boron-carbide (B-C). However, despite being a strong material, the B-C weakened with machining, necessitating the removal of the hole in the plates for optical access to the sample to provide additional strength. The B-C plates were also found to have a higher absorption than the beryllium plates, resulting in poorer counting statistics for weak reflections. The cell has only been used for two structural studies of CaF_2 (Hazen and Finger (1981b)), and $CaMgSiO_4$ (Hazen and Finger (1981c)).

Finally, Kudoh has designed a version of his DAC to allow HT-HP studies, and has been used in a HT-HP structural study of quartz (Ogata *et al.* (1987)).

X-ray Powder-Diffraction Pressure Cells

Although very little structural work has been done using x-ray powder-diffraction methods, the cells that have been used will be discussed briefly.

The first high-pressure structural study using this technique was made in 1969 using a powdered sample held in a tetrahedral ram (Barnett *et al.* (1969)). The massive ram held sufficient material to eliminate the problems of obtaining a good powder average and allowed accurate relative intensities to be measured. The tetrahedral ram, however, was soon superceded by the DAC.

As described earlier, the use of Be as a backing plate material for the diamonds produces parasitic scatter in the form of Be powder lines in the collected data, degrading its quality. For this reason Be plates are not generally used in cells designed for powder studies but rather the diamonds are mounted directly onto hardened steel plates. This allows very high pressures to be reached at the cost of reduced angular access to the cell, perhaps to just a narrow slit, in order to provide sufficient support to the backs of the diamonds. Although powder lines can still be produced by the gasket, suitable collimation of the incident x-ray beam, especially of an already highly-collimated synchrotron beam, allows illumination of the sample without simultaneous illumination of the gasket.

Neutron-Diffraction Cells

Comparatively little structural work has been done at high pressures using

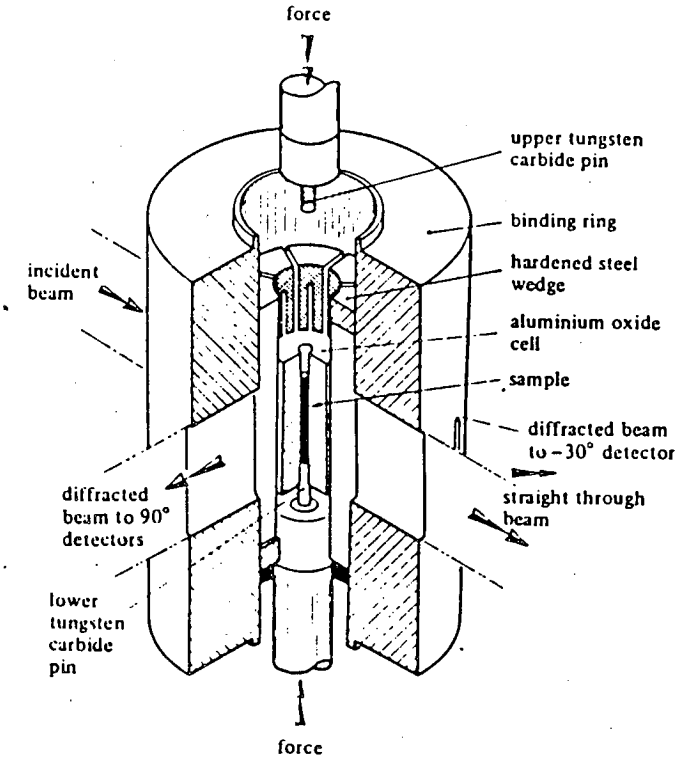

Figure 2.15: The supported piston-and-cylinder pressure cell used in the TOF neutron-diffraction studies of Brugger *et al.* (1966). (From Carlile and Salter (1978).)

neutron-diffraction techniques despite the very detailed structural studies made at atmospheric pressure using these techniques. However, several different pressure cell designs have been used in the collection of the diffraction data.

The earliest pressure cells designed for neutron-diffraction structural studies were used at the Idaho Falls reactor by Brugger and his co-workers (Brugger *et al.* (1966)). Despite being a reactor source rather than a spallation source, TOF techniques were used by employing a mechanical chopper to cut the neutron flux into short bursts. Developing the techniques used earlier by Litvin and Ponyatovskii (1966), the pressure cell used a supported piston-and-cylinder design with fixed windows for entrance and exit of the neutron beams,as shown in Figure 2.15. The pressure vessel is made of sintered alumina (Al_2O_3) because of its very high compressive strength, although it has very low tensile strength. The use of alumina replaces the null-matrix alloys used in earlier cell designs which, although eliminating parasitic coherent scatter in the form of powder

lines, creates a high isotropic background and highly attenuates the incident and diffracted beams through absorption. (A null-matrix material is a mix of elements or isotopes with positive and negative neutron scattering lengths which produces a material with no coherent scattering length. The material thus gives no Bragg reflections or powder lines, but produces an intense, isotropic incoherent scatter. The most frequently used material is an alloy of Ti and Zr). The use of alumina is preferred due to its low incoherent scatter and its low absorption for neutrons. The coherent scatter from the alumina cylinder is eliminated from the diffraction pattern by the fixed scattering geometry of the pressure cell, combined with careful collimation of the incident and diffracted beams.

The alumina is supported by 30° steel wedges contained inside a steel binding ring. Access to the sample is provided by entrance and exit windows which are cut through the binding ring coincident with the gaps between the steel wedges. The cell has been used in structural studies to 27kbars and has prompted similar cells to be built in other laboratories.

The use of sintered alumina for the pressure vessel was also employed by McWhan *et al.* (1974). However, in this cell, the 'cylinder' has a double truncated conical outer surface, as shown in Figure 2.16, and the pressure is applied to the sample while at the same time the alumina is compressed radially inwards. Application of these forces simultaneously eliminates internal compression in the alumina as the internal and external forces are balanced. This design allows pressures up to 50kbars to be reached and allows both the option of a fixed scattering geometry for TOF methods, or full angular access to the sample for monochromatic powder or single-crystal techniques. For single-crystal studies, however, the cell geometry allows only reflections lying in the plane perpendicular to the cell axis to be measured, severly limiting the size of the data set obtainable from one crystal mounting although several mounting may be used.

The same cell geometry was employed by Bloch *et al.* (1976) who designed a cell for structural studies at pressures to 30kbars and temperatures down to 4.2K. The cell (Figure 2.17) uses the idea of compressing the alumina barrel to reduce the internal forces on it, although this is done before applying the sample pressure rather than applying the two forces simultaneously. As with the McWhan design, this cell can be used for either single crystals or

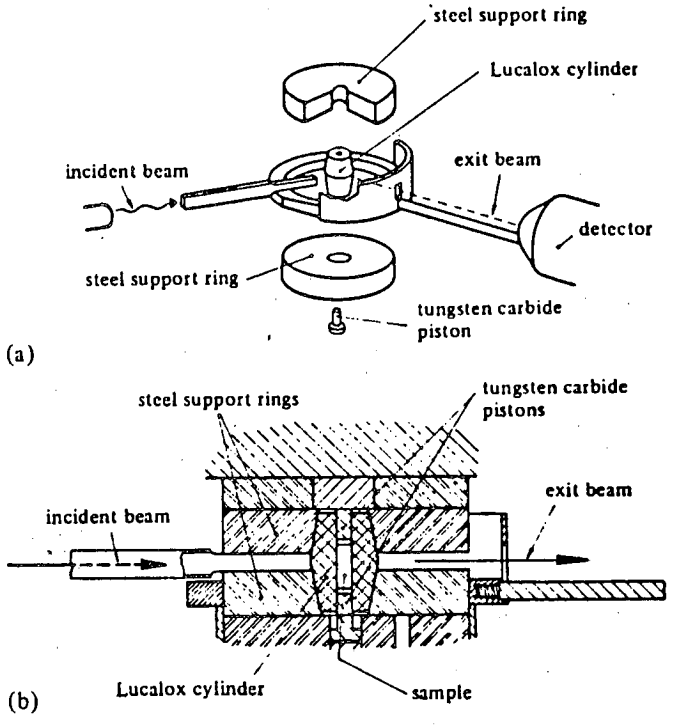

Figure 2.16: (a) Exploded, and (b) cross-sectional view of the directly pressurised supported cylinder cell of McWhan *et al.* (1974). (From Carlile and Salter (1978).)

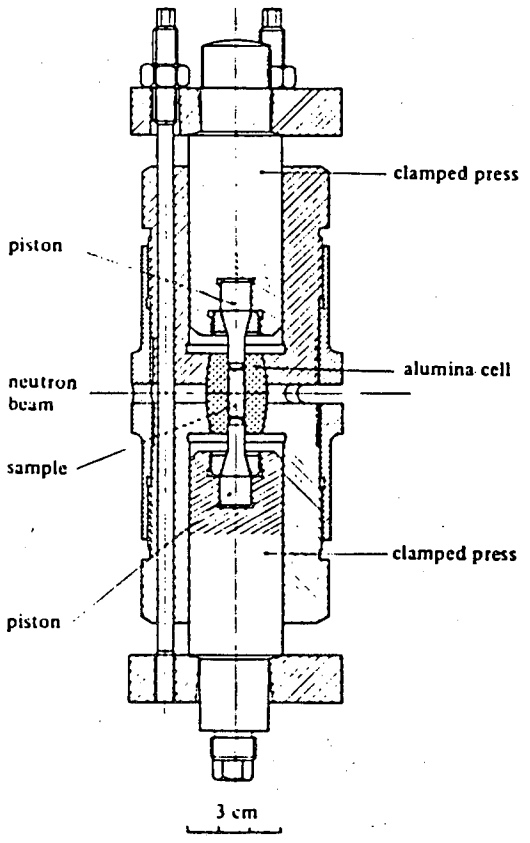

Figure 2.17: A cross-section of the Bloch *et al.* (1976) pressure cell. (From Carlile and Salter (1978).)

powders although the three supporting pillars leads to occlusion of the incident or diffracted beam in single-crystal studies.

Although the cells described above have been able to reach pressures of over 70kbars, this upper pressure limit is accompanied by a greatly reduced sample volume with a corresponding increase in the time necessary to collect quality data (48 hours in the case of the Brugger cell). A number of pressure cells have been designed in which a large sample volume was the main design criterion with the lower pressure limit seen as an acceptable compromise. High-pressure He gas is often used as the pressure medium in these cells, allowing perfectly hydrostatic conditions.

The cell designed by Paureau and Vettier (1975), shown in Figure 2.18, has an upper pressure limit of 6kbars, using He gas, and is capable of working at temperatures as low as 4.2K (the actual pressure-temperature combination used is limited by the freezing temperature of the He at high pressures). The sample volume of the cell is $5cm^3$, or $5000mm^3$, compared to $200mm^3$ for the Brugger and McWhan cells. It is also possible to use large single-crystal samples. The cell body is made of aluminium, which has a very low absorption for neutrons, with the outer shield made of a high-tensile alloy while the main body is made of an alloy chosen for its superior toughness rather than for its tensile strength. The pressure of the helium is adjustable to 5bars (!) allowing great control over the experimental conditions.

The Paureau-Vettier cell is designed for angle-dispersive powder and single-crystal studies and the diffraction data suffer from the strong parasitic powder lines from the aluminium cell body; however, the peaks are few in number and the loss of diffraction data is small. Another He gas cell, designed for the fixed scattering geometry of TOF methods at the IPNS neutron source at Argonne, has been used for structural studies up to 7kbars and at low temperatures, the pressure-temperature range again being determined by the freezing point of helium. The full details of this cell design have yet to be published, but a schematic drawing of a cross-section through the cell is shown in Figure 2.19 and illustrates the most important design innovation of this cell. Surrounding the sample chamber are concentric shields of highly absorbing material which have windows cut in them for entrance and exit of the neutron beams. Combined

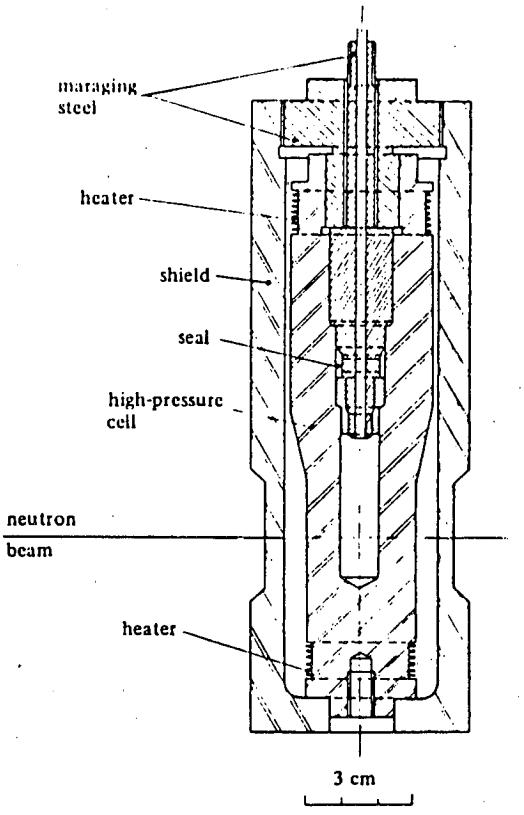

Figure 2.18: The helium-gas pressure cell of Paureau and Vettier (1975). (From Carlile and Salter (1978).)

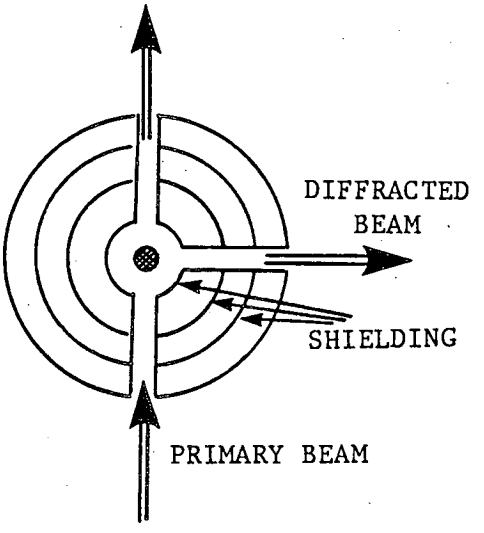

Figure 2.19: A schematic cross-section through the helium-gas cell used at the IPNS, Argonne in a 90° scattering geometry. Concentric layers of heavy shielding prevent multiple scatter from reaching the detector.

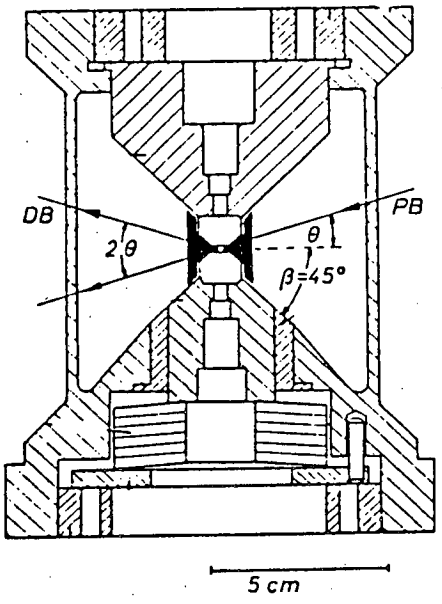

Figure 2.20: The Ahsbahs pressure cell for neutron-diffraction studies. Note the increase in the angle β over the cell for x-ray diffraction (Figure 2.13). (From Ahsbahs (1984a).)

with the heavy shielding on the outside of the cell, these shields prevent any neutrons that are multiply scattered from the cell reaching the detector. The result is a powder pattern with an extremely low, flat background and combined with a large sample volume, allows accurate structural studies to be made in a relatively short time.

Finally, with the great success of the DAC in x-ray structural work, there has been a wish to use a similar design of cell in the study of single-crystals using neutron-diffraction techniques. A neutron-diffraction version of the Ahsbahs transverse-geometry DAC (Ahsbahs (1984a,b)) is shown in Figure 2.20. This cell is basically that of the x-ray design but the low absorption of neutrons by aluminium allows the three pillars of the original x-ray cell to be replaced by a cylindrical aluminium shell. The generally low absorption of neutrons by materials also allows permeable gaskets of Ti-Zr alloy to be used. This alloy, as stated above, has no coherent scatter and so produces no powder lines which would contaminate the ω-2Θ scans needed for measuring Bragg peaks when using neutrons (see Chapter 2.6.2).

The β angle of 25° in the original x-ray cell is increased to 37° or 45° in the

neutron cell, allowing many more reflections to be measured. Optical access to the sample is still available along the cell axis. The anvils of the cell can either be sintered tungsten-carbide (W-C), or single-crystal sapphires, allowing pressures of up to 20kbars or 15kbars respectively. However, absorption of the neutrons by the W-C is considerable and the uncertainty in the absorption correction leads to increased errors on the refined thermal parameters. The most accurate work using this cell is therefore obtained with sapphire anvils.

2.5.2 Gaskets

Although the simplest component in a DAC, the gasket is, in many ways, one of the most critical. Due to the extreme deformation of the gasket at high pressures, selection of the appropriate gasket material and dimensions is an important step in the assembly of a DAC if occlusion of the incident or diffracted beam is to be avoided.

In general, the gasket is made of a hard metal foil approximately 250μm thick. Commonly used materials are Inconel 750X, a moderately hard nickel alloy (Ni:Cr:Fe=72:16:8), and hardened T301 stainless-steel.

The size of the gasket hole used depends both on the size of the sample, and the upper pressure required. For a single crystal of diameter 100μm, the optimum gasket hole diameter is 300-350μm, this diameter preventing, or at least greatly reducing, gasket occlusion. Another method of reducing gasket occlusion has been proposed by Katrusiak and Nelmes (1986b) in which the gasket edge closest to the diamond which the sample is not mounted on (Figure 2.21) is removed, thus allowing a greater diffraction angle before the gasket begins to occlude the diffracted beam. For higher pressures, a smaller gasket hole is used at the expense of a lower sample volume if occlusion is to be reduced. To obtain higher pressures many workers have also used preindented gaskets, that is, the gasket is prepressed between the diamonds before the gasket hole is drilled. Care must be taken, however, to ensure that the gasket is replaced on the diamonds in the same orientation as it was preindented.

The use of a large (1×1cm^2) gasket greatly reduces the background scatter as it

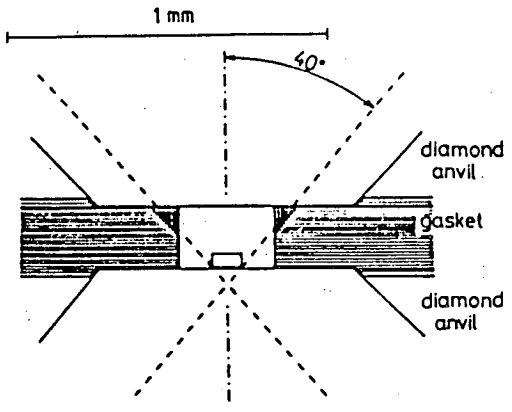

Figure 2.21: The high-pressure chamber of a Merrill-Bassett DAC. The dashed lines represent the limit of accessible angles and the edge of the gasket which is removed is indicated by the cross-hatch shading. (From Katrusiak and Nelmes (1986b).)

absorbs almost all of the parasitic scatter from the Be plate and diamond nearest the x-ray source. The powder lines and diamond reflections are then generated only from the diffracted beam and from that part of the incident beam that passes through the gasket hole. The latter will be only 300-350μm across if the gasket is highly absorbing, greatly reducing the illuminated volume of beryllium compared to that illuminated by the full incident beam.

2.5.3 Pressure Fluids

Although it was stated previously that liquids are used as the pressure transmitting medium in a pressure cell, both solids and crystalline gases have also been used.

Early high-pressure studies, including diffraction studies, used NaCl as a pressure transmitting medium (Jeffrey *et al.* (1966)) allowing the pressure calibrant and pressure transmitting medium to be combined into one. However, the use of solids as pressure media does not allow truly hydrostatic conditions to be achieved, conditions essential for accurate structural work. This prompted the search for liquids that would remain liquids, and thus hydrostatic, to the very high pressures suddenly obtainable using a DAC.

The observation that the R-lines used in the ruby fluorescence method of pressure calibration broadened in the presence of nonhydrostatic conditions, allowed Piermarini *et al.* (1973) to determine the hydrostatic limits of some commonly used liquids. They found that the highest hydrostatic pressure limit was for a 4:1 methanol:ethanol mixture which remained hydrostatic to a glass transition at 104kbars. Addition of a small amount of water to give a 16:3:1 methanol:ethanol:water mixture was later found to raise this limit to 145kbars (Fujishiro *et al.* (1982)), the highest limit known for a fluid. The hydrostatic limit of pure methanol is 70kbars (Piermarini *et al.* (1973)), allowing its deuterated form (to eliminate incoherent scatter of neutrons from the H-atoms) to be used in neutron-diffraction studies. Other pressure fluids that have been used are 1:1 pentane:isopentane, silicon oil, fluorinated hydrocarbons, glycerine and index of refraction oil.

A more recent, and very important, advance in pressure transmitting media, has been the use of crystalline gases such as H_2, N_2, He, Ar, Ne, Xe and CH_4 (LeSar *et al.* (1979), Bell and Mao (1981)). Although these gases crystallise at relatively low pressures (He has the highest freezing pressure at 120kbars), the resulting solids remain soft and ductile to very high pressures providing either hydrostatic, or quasi-hydrostatic, conditions – H_2 and He remain almost hydrostatic to pressures in excess of 600kbars while quasi-hydrostatic Ar has been observed to support a pressure gradient of only 17kbars at a total pressure of 800kbars (Mao *et al.* (1986)). Ar has the additional advantage of also being a pressure calibrant (Chapter 2.6.7).

2.6 High-Pressure Diffraction Techniques

To cope with the many problems that the use of pressure cells introduce into the collection of diffraction data, many techniques have been developed to maximise the quality and quantity of the data measurable, and to reduce the corrections that need to be applied. These methods are discussed under the following headings.

(1) Maximising the data set

(2) Scan type
(3) Crystal centering
(4) Reflection overlap
(5) Absorption
(6) Choice of radiation
(7) Pressure calibration

2.6.1 Maximising the Data Set

The limited amount of data measurable when using a pressure cell reduces the accuracy and precision with which structural changes can be followed as a function of pressure. This reduction in the available data is even more acute if higher pressures are required as this usually entails a further reduction in angular access to the cell. However, the wide use of the DAC for single-crystal studies has prompted much effort into the study of how to maximise the number of individual Bragg reflections measurable. This effort has lead to the development of the transverse-geometry DACs and to optimised methods for using transmission-geometry DACs.

Analysis by Merrill and Bassett (Merrill and Bassett (1974)) showed that at a 2Θ limit of 60°, only 55% of reciprocal space was accessible using their DAC which had a half-angle opening of 50°. However, this calculated volume was for the ideal case in which the cylindrical axis of the cell remained in the diffraction plane for each reflection measured, and was considerably larger than the volume actually accessible using their three-circle diffractometer which forced them to measure all reflections in the bisecting position (ω=Θ). For a four-circle diffractometer, however, measurement in the bisecting position is no longer obligatory and two methods have been developed to increase the percentage of reciprocal space accessible.

The first was developed by Denner *et al.* (1978) who showed that the intensity of a reflection changed as it was rotated around its scattering vector (a ψ-scan) due to cell absorption and gasket occlusion. Following the method of Flack (1974), they made a series of ψ-scans around different reflections and constructed a model for the absorption and occlusion of the pressure cell as a function of

the diffractometer angles. When a sample reflection is then measured using this method, the model is first used to calculate the correction that should be applied to the intensity if the reflection was measured at the bisecting position, and a simulated ψ-scan is then made by the control computer to calculate at what ψ angle this correction is a minimum. The reflection is then measured at this normally non-bisecting position and the correction for absorption and occlusion applied automatically.

This method, however, would seem to have faults. It is not certain to what extent one can 'correct' for occlusion by the gasket, this depending critically on the gasket deformation, thickness (which reduces at higher pressures) and crystal centering in the gasket hole. It is probably safer to try to minimise the gasket occlusion and then delete those reflections which are still suspected to be affected rather than trying to correct for it.

Another, better, method was developed simultaneously by Finger and King (1978) and is called the fixed-ϕ geometry. In this technique, the ideal measurement position originally realised by Merrill and Bassett is obtained by constraining the cylindrical axis of the DAC to lie in the diffraction plane for each reflection measured. This has two very important advantages.

(1) The pathlengths of the incident and diffracted beams through the diamonds and beryllium backing plates are at a minimum for each reflection in this geometry. This reduces the background, through reducing the illuminated volume of beryllium, and maximises the sample intensity through reduced absorption.

(2) The maximum possible number of reflection can be observed in this geometry. For an initial test experiment on a single crystal of NaCl at 32kbars (Finger and King (1978)), it was found that three times as many non-equivalent reflections could be measured using the fixed-ϕ geometry as opposed to the bisecting geometry.

This method allows the optimum angles for individual reflections to be calculated analytically before the reflections are measured, and, although the absorption correction must still be applied, it is dependent only on α_i and α_d, both of which are easily calculable (Chapter 2:6.5). For these reasons the method of Finger and King is widely used.

2.6.2 Scan Type

The intense structured background present in single-crystal studies using a pressure cell has prompted the use of several techniques in order to maximise the quality of the diffraction data. Although x-ray diffraction studies of single crystals at atmospheric pressure are normally made using a coupled ω-2Θ scan, this scan-type scans the detector *across* the beryllium and gasket powder lines in the background, producing extra peaks in the reflection profiles. Although these extra peaks may be separate from the sample Bragg peak, and possibly excluded from the calculation of the integrated intensity of the sample reflection, the powder lines may also lie directly underneath the sample peak, making the accurate measurement of that reflection impossible. This problem, though, may be eliminated by using an ω-scan in which only the sample is rotated while the detector remains stationary (King (1981)). This scan-type scans *along* the powder lines rather than across them and although the background will, in general, be higher, as a powder line will scatter into the detector over the full range of the scan, the background will be flat, allowing the true background level to be accurately determined. The ω-scan method, however, does require that a larger aperture be used compared with an ω-2Θ scan in order to intercept all of the sample intensity over the full width of the scan. This larger aperture will lead to a further increase in the background level. Despite this, however, the ω-scan method is widely used and highly recommended, the lower signal-to-noise ratio, which can be increased by simply counting for longer, being an acceptable compromise in order to correctly determine the true background level and thus make accurate measurements of the integrated intensities.

For single-crystal neutron-diffraction studies using a standard detector, an ω-2Θ scan is essential because the wavelength spread of even a monochromated beam of neutrons requires that the detector be scanned in order to intercept the full intensity of the sample peak over the full scan range. The Ahsbahs cell uses a null-matrix gasket in order to eliminate gasket powder lines but some reflection profiles will still be affected by the powder lines produced by the aluminium body of the cell. For the more usual type of neutron pressure cell, however, the use of Al_2O_3 as a pressure-vessel material produces a large number of powder lines. The correct background level in this case can be estimated by offsetting the sample from the diffracting position after a sample reflection has been measured,

and then making an identical scan through the background, allowing it to be subtracted from the scan containing the sample reflection.

2.6.3 Crystal Centering

Centering a single crystal on a diffractometer at atmospheric pressure is usually achieved using optical means by observing the position of the crystal as the various circles of the diffractometer are rotated. The presence of a pressure cell makes centering somewhat harder as the sample may not be visible from certain angles (parallel to the plane of the gasket in a DAC for example). In order to overcome this problem, a diffraction method has been developed to centre the crystal (King and Finger (1979)). Based on Hamilton's eight-position method (Hamilton (1974)), the procedure is generalised to work in the non-bisecting geometry. Measurement of a reflection in eight different angular settings allows a determination of the crystal centering errors, as well as misalignments of the diffractometer, and allows diffraction angles to be determined that are independent of these errors, allowing very precise unit-cell dimensions to be measured. These are essential if structural changes as a function of pressure are to be followed accurately. However, this technique relies on the initial centering errors being small and the sample must therefore be aligned initially by optical means. This is greatly facilitated in a DAC by the use of matched diamonds, and thus equal optical pathlengths, which allows easier centering perpendicular to the plane of the gasket. For neutron single-crystal studies even initial centering may not be possible by optical means due to the general lack of optical access to the pressure cells. In this case, all centering must be done using diffraction methods although the design of many neutron diffractometers does not allow the detector to be driven to negative-2Θ angles, preventing the use of the eight-position method.

For angle-dispersive neutron-diffraction studies of powders, alignment of the sample at the centre of the diffractometer is essential as even a small misalignment will mean that the sample views the monochromator at a slightly different angle to a well centred sample, thereby selecting a different wavelength to that seen at the centre of the diffractometer. This will mean that unit-cell dimensions will be wrongly determined on an absolute scale although changes on a

relative scale can be determined if the pressure is varied *in situ* (Hewat (1989)). For powder studies on a spallation neutron source, the centering errors in the sample will appear as errors in the time-of-flight of the diffracted neutrons, but as the centering errors will be much smaller than the total flightpath of the neutrons, these errors will be very small, allowing changes on an absolute scale to be accurately determined.

2.6.4 Reflection Overlap

Although little can be done in many cases to completely avoid contamination of the diffraction data by powder lines from the pressure cell or gasket, simultaneous measurement of sample reflections and Bragg reflections from either the diamond or sapphire anvils, or from a pressure calibrant crystal, can be avoided by the use of techniques developed by Denner *et al.* (1977). In this method, the orientation matrices of both the anvils and the calibrant crystal are determined, and a check is then made before each sample reflection is measured to see if reflections from any of these crystals will scatter into the detector simultaneously with the sample reflection. If this is the case, then the sample reflection is omitted, although it may be measured later at a slightly different ψ-angle at which no overlap with the anvil or calibrant crystal occurs.

The number of reflections that will actually be affected by overlapping reflections using a DAC is very limited due to (i) the high symmetry and small lattice parameter of diamond, and (ii) the absence of $\lambda/2$ or $\lambda/3$ reflections if a pulse-height analyser is used in the detector. The identification of diamond reflections is also very easy due to their very high intensity. However, for neutron-diffraction studies using a sapphire-anvil pressure cell, the problem is much more serious due to sapphire's low symmetry, large c-axis lattice parameter, and to the $\lambda/2$ and $\lambda/3$ contamination of the incident beam. This results in an greatly increased number of (weak) sapphire reflections which may be indistinguishable from sample peaks due to the lack of energy discrimination in standard neutron detectors.

2.6.5 Absorption

The correction of the incident and diffracted beams for pressure cell absorption is essential if accurate relative intensities are to be measured. For neutron-diffraction pressure cells, this absorption will be small due to the low absorption coefficients of the materials used in the cell construction. The absorption correction for the Ahsbahs cell is made using the measured pathlengths of the incident and diffracted beams through the cell obtained from a large-scale drawing of the anvils and gasket, along with their measured absorption coefficients. In other pressure cells for neutron diffraction, the absorption correction may be zero as the incident and diffracted beam have the same pathlength through the cell, independent of diffraction angle. This is the case for the Bloch cell as well as those designed for powder-diffraction studies. For pressure cells using TOF techniques, the absorption correction is more complicated as the correction for an individual reflection depends on the wavelength at which it was measured – the absorption of the cell being wavelength dependent. The correction in this case is usually determined experimentally by monitoring the λ-spectrum of the direct beam after it has passed through the cell and comparing it to the λ-spectrum of the incident beam before reaching the cell. The difference in the spectra is due to the cell absorption.

For x-ray diffraction techniques, the absorption of the pressure cell is considerably higher than in the neutron case and an accurate determination of the absorption correction for each reflection is essential. (An exception is the Keller-Holzapfel DAC where the shape of the beryllium backing plates is designed to make the absorption the same for all reflections). The necessity of an absorption correction was realised from the earliest days of the DAC when, in a study of Br_2 at 10kbars, it was shown to greatly improve the internal consistency of the diffraction data (Santoro *et al.* (1968)). However, the analytic technique used in this case required considerable computation and simpler experimental techniques of determining the absorption have been developed. For the transmission-geometry cells, the absorption correction is greatly simplified if the DAC has both cylindrical and mirror symmetry. In this case, the absorption for each half of the cell is assumed to be the same and the absorption is then determined simply by the angle α between the incident or diffracted beam and the cylindrical axis of the cell (Figure 2.22). Two problems, however, remain.

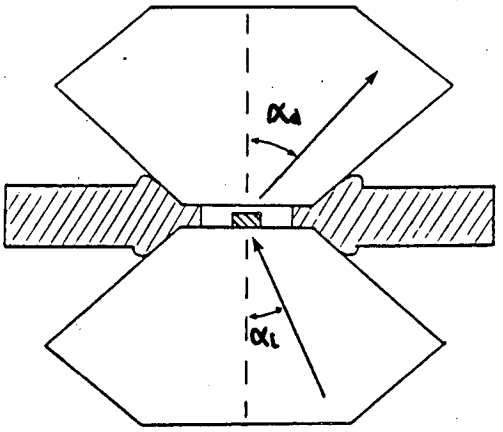

Figure 2.22: The definition of the angles α_i and α_d, the angles between the cell axis and the incident and diffracted beams respectively.

(1) How to determine the absorption as a function of α.
(2) How to calculate the angle between the cell axis and the incident or diffracted beam for each measured reflection.

Early attempts (Hazen (1976)) to determine the absorption correction as a function of α were based on measuring the pathlengths of the x-rays through the beryllium and diamonds and then using the known absorption coefficients to determine the correction. This technique was impractical, however, due to uncertainties in the measured pathlengths and in the accuracy of the published absorption coefficients. The more usual method for determining the α-dependence of the absorption is to monitor the suitably attenuated direct beam after it has passed through the cell as the cell is rotated to vary α from $+40°$ to $-40°$ (Finger and King (1978)). This measurement is usually repeated as the cell is rotated around its cylindrical axis, the results then being averaged. A polynomial fit to the data allows the absorption to be calculated for any value of α.

A second method that has been developed is to measure the intensity of Bragg reflections for a sample crystal both inside the cell at atmospheric pressure and outside, the changes in the integrated intensity of each reflection being due to cell absorption (Hazen (1976)). A comparison of the results obtained with this method and with those obtained by monitoring the direct beam, shows the resulting correction as a function of α to be very similar.

In order to determine the absorption correction for an individual reflection it is necessary to know the values of α_i and α_d, the angles between the the incident and diffracted beams and the cell axis (Figure 2.22). Although these can be calculated from the diffraction angles of each reflection, the answer is especially simple if the fixed-ϕ geometry is used, in which case α_i and α_d are given simply by ω and $2\Theta-\omega$ respectively. The fixed-ϕ geometry also ensures that α_i and α_d are minimised for each reflection, so reducing the absorption correction that must be applied, and is another significant advantage of using the fixed-ϕ geometry.

2.6.6 Choice of Radiation

X-rays

The relatively long pathlengths of the incident and diffracted beams through a pressure cell requires that either MoK_α (λ=0.71Å) or AgK_α (λ=0.56Å) x-rays be used to collect data, the other commonly used type of x-rays, CuK_α (λ=1.54Å), being too highly absorbed. Of these two, AgK_α offers significant advantages over MoK_α.

(1) The shorter wavelength is absorbed less by the pressure cell and sample and thus a smaller absorption correction is needed.

(2) The fixed angular apertures of DACs means that the maximum 2Θ angle is usually limited to 80°. Using MoK_α, this equates to a maximum $\sin\Theta/\lambda$ of $0.9Å^{-1}$ while using AgK_α, a maximum $\sin\Theta/\lambda$ of $1.15Å^{-1}$ is possible, allowing a more detailed study of structural details such as thermal motion and disorder.

Despite these advantages, very few structural studies have been made using AgK_α x-rays, with those that have been made giving considerably poorer results than equivalent studies made using MoK_α. Two possible reasons have been given for this (Levien *et al.* (1980)).

(1) The intensity from a Ag-target x-ray tube is less than that from a Mo-target tube, requiring longer counting times to give the same counting statistics.

(2) The counting efficiency of the detectors used to measure the sample reflections is less for AgK_α than for MoK_α.

The combination of these two effects is to reduce the signal-to-noise ratio for reflections measured using AgK_α radiation, making the accurate determination of the integrated intensity for the sample more difficult. This will reduce the quality of the final refined structure.

Neutrons

Compared to x-rays, the absorption of neutrons in materials is very low, thus although shorter wavelength neutrons are absorbed less than those with longer wavelengths, wavelengths as long as 3Å can be used. The choice of a specific wavelength for single-crystal studies is usually a compromise between the desired real-space resolution ($\sin\Theta/\lambda$ limit) and the neutron flux at a given wavelength, the reduction in flux at the shorter wavelengths being considerable. For monochromatic powder studies, the usual choice of wavelength is 1-2Å to allow a good angular separation of closely spaced peaks. This separation can be further increased using wavelengths as long as 3Å although the real-space resolution of such data will be severly limited. No data exists to compare the quality of structure refinement obtainable using different wavelengths of neutrons.

2.6.7 Pressure Calibration and Measurement

Although not directly affecting the quality of the structure refineable from the collected diffraction data, it is obviously important to accurately determine the pressure at which the data were collected. This is especially important if structural changes as a function of pressure are to be related to changes in physical property determined by a non-diffraction method in which a different pressure calibration technique may have been used.

Two commonly used methods are to determine the pressure in a diffraction experiment; the equation of state (hereafter EOS) of a calibration material (the pressure dependence of its volume) or the ruby fluorescence technique. By far the most important EOS is that of NaCl, almost all other forms of pressure

calibration, including the ruby fluorescence method, being related directly, or indirectly, to it.

The NaCl Equation of State

The original papers on the EOS of NaCl were published by Decker (1965, 1966, 1971). The resulting EOS is not a first principles calculation, but involves simplifications and requires empirical values of the zero pressure bulk modulus and thermal expansion. Decker originally chose NaCl for his calculation as the lattice energy of ionic crystals was well known and sufficient experimental data was available to allow calculation of the required input parameters and to check the results of the calculations. Recalculating his EOS as new, and more accurate, values were determined for these input parameters, the final EOS of NaCl using Decker's technique was published in 1972 (Decker *et al.* (1972)).

In his 1971 paper, Decker stated that the uncertainty in his EOS due to uncertainties in the input parameters, but not including any approximations inherent in the theory, was 1.1% below 50kbars, 1.7% below 100kbars, and 2.4% below 200kbars.

In 1978, Birch (1978) reviewed all the available data on NaCl with the aim of incorporating it all into a consistent framework, and could reconcile all the available data with a second-order Birch EOS given by

$$P(\text{kbar}) = 3K_o f(1+2f)^{5/2}(1+af+bf^2) \qquad (2.3)$$

where $V/V_o=(1+2f)^{-\frac{3}{2}}$, V_o and K_o are the volume and bulk modulus respectively at 1bar, and a and b are variables determined by least squares.

Using the accurately determined values of the bulk modulus and its pressure derivatives (Chabildas and Ruoff (1976), Spetzler *et al.* (1972)), Birch gave the NaCl EOS as

$$P(\text{kbar}) = 714f(1+2f)^{5/2}(1+2.6f-9.5f^2) \qquad (2.4)$$

More recently, Birch (1986) again collected the latest experimental data on NaCl, including the direct measurement of the EOS of NaCl to 32kbars by Boehler and Kennedy (1980), to obtain a new EOS given by

$$P(\text{kbar}) = 716.4 f (1+2f)^{5/2} (1+1.796f - 5.00f^2) \qquad (2.5)$$

This equation fits the Boehler and Kennedy data with a standard deviation of 0.054kbars while, for comparison, the 1972 Decker EOS fits the same data with a standard deviation of 0.34kbars. With the more extensive and accurate input data, it is felt that the 1986 Birch EOS is the most accurate available for NaCl. Despite this, however, the original Decker 1971 EOS is still widely used.

Although both Decker and Birch calculated the EOS of NaCl for temperatures above ambient, no calculations were made for the EOS at temperatures lower than ambient. This problem, however, was tackled simultaneously by Skelton *et al.* (1984) and Menoni and Spain (1984), both of whom calculated the EOS of NaCl to 0K. The results in each case were almost identical.

The disadvantage of the EOS method of determining the pressure is that the lattice parameters must be measured using either x-rays or neutrons. Although this may be of little or no disadvantage in diffraction work, it is a serious drawback in spectroscopic work. Possible disadvantages that may occur in the case of diffraction are the loss of sample volume due to the inclusion of the pressure calibrant in the pressure vessel, or the overlap of Bragg reflection or powder rings of the calibrant and the sample. The development of the DAC in the late 1960's and early 1970's, and the very much higher pressures available for both diffraction and spectroscopy, led to the search for a more convenient method of determining the pressure.

The Ruby Fluorescence Method

In the early 1970's, workers at the NBS developed the ruby fluorescence pressure gauge for all high-pressure apparatus with optical access (Forman *et al.* (1972), Barnett *et al.* (1973)). By including a chip of ruby (Cr^+ doped Al_2O_3) in the pressure chamber of a DAC and illuminating it with a laser, the two fluorescent R-lines at 6927Å and 6942Å could be seen to shift as a function of applied

pressure. However, no theoretical calculation of the pressure dependence of the wavelength shift could be calculated and so the wavelength shift versus pressure could only be calibrated against known fixed points. In the 1972 paper, the shift was calibrated to 22kbars using the known freezing points of CCl_4, H_2O, n-C_7H_{16} and C_2H_5Br, as well as the solid-state transitions in CCl_4 and H_2O. Up to this pressure, the shift was found to be linear with pressure with shifts of –0.77(3) $cm^{-1}kilobar^{-1}$ and –0.84(3) $cm^{-1}kilobar^{-1}$ for the R1 and R2 lines respectively. Preliminary checks to calibrate the wavelength shift against the NaCl EOS suggested that the shift remained linear to 70kbars. It was also observed that significant broadening of the two R-lines occurred when non-hydrostatic conditions were present. This feature has since been exploited to determine the range over which pressure transmitting media remain hydrostatic (Piermarini *et al.* (1973)). Finally, it was noted that the shift of the lines with temperature was $-0.14cm^{-1}kilobar^{-1}$ at room temperature which corresponds to $0.17kbarK^{-1}$. This thus makes a knowledge of the temperature at which the experiment and pressure calibration were made, very important.

The ruby scale was extended in 1975 (Piermarini *et al.* (1975)) to allow calibration to 195kbars at 298K. The line shift was calibrated directly against the Decker (1971) EOS for NaCl and it cannot be stressed too strongly that this established that the ruby scale and the 1971 EOS for NaCl were the same pressure scale to 195kbars. The linear relationship between pressure and wavelength shift, at the 95% confidence level is

$$P(\text{kbar}) = 2.746(14)\,\Delta\lambda \qquad (2.6)$$

where $\Delta\lambda$ in the wavelength shift in Å and the error takes into account both the uncertainties in the x-ray measurements used in the determination of the NaCl lattice parameter, and the uncertainties in the Decker EOS, as mentioned above.

In the same year, Piermarini and Block (1975) calibrated the wavelength shift to 291kbars, the pressure at which NaCl undergoes a first-order phase transition to the CsCl structure. Assuming that the ruby shift was still linear to this pressure gave a transition pressure of 292(5)kbars, indicating that the shift was indeed

still linear to this pressure.

In 1976 and 1978, the ruby shift was calibrated to 1Mbar (Mao and Bell (1976a,b), Mao *et al.* (1978b) against the isothermal EOS obtained from shockwave data for Cu, Mo, Pd and Ag (Carter *et al.* (1971)). Above 100kbars all measurements were made in non-hydrostatic conditions. The wavelength shift to 1Mbar was found to be slightly non-linear and given by

$$P(\text{Mbar}) = A/B\left[\left(\frac{\lambda_o+\Delta\lambda}{\lambda_o}\right)^B - 1\right] \tag{2.7}$$

where λ_o is the wavelength at 1bar and A=19.04 and B=5.

Taking great attention of the possible sources of error in the measurements resulted in the total random error in the pressure calibration between 60kbars and 1Mbar being ±6%. However, a systematic error was also present in the calibration due to the different strengths of the metals and the way they acted differently to the non-hydrostatic stress distribution and the direction of uniaxial stress. This error led to the pressures being slightly underestimated for a given wavelength shift. The problem of this slight underestimation in the pressure was addressed by Zou *et al.* (1982b) who calibrated the R-line shift against the EOS of Ag in a quasi-hydrostatic pressure medium of argon to 600kbars. Although no numbers were quoted for the shift, the results did indeed show the previous non-hydrostatic work to contain a systematic underestimate of the pressure. This analysis was later extended to Cu (Mao *et al.* (1986)) and this data, and the previous data on Ag, were used to calculate a new equation relating the wavelength shift and the pressure. Again using an argon pressure medium the maximum pressure gradient was 17kbars at 700-800kbars. A plot of the R-line shapes at 745kbars showed very little broadening of the peaks thus confirming the quasi-hydrostatic nature of argon at these high pressures. Using the initial slope of Piermarini *et al.* (1975) and the combined Cu and Ag data, gave a shift represented by

$$P(\text{Mbar}) = \frac{19.04}{7.665}\left[\left(\frac{\lambda_o+\Delta\lambda}{\lambda_o}\right)^{7.665} - 1\right] \tag{2.8}$$

which falls within the ±6% error quoted by Mao *et al.* (1978b).

Other Pressure Calibration Methods

Although the NaCl EOS and the ruby fluorescence methods are the most important techniques for measuring the pressure in diffraction experiments, other methods have also been used and these are discussed briefly.

CsCl EOS

In his 1971 paper, Decker used the same method as he used for NaCl to determine the EOS of CsCl to over 400kbars. The uncertainty in the calculated pressures was larger than that for NaCl. To determine the consistency of the two calculated equations of state, a mixture of NaCl and CsCl was compressed to 32kbars and the pressures determined from the two equations of state compared (Decker and Worlton (1972)). The results suggested that the EOS determined for CsCl yielded pressures that were about 2% lower than those obtained from the NaCl EOS. However, up to the highest pressure measured, this discrepancy was within the uncertainties of the EOS itself and similar measurements to higher pressures are required to make any real differences more pronounced.

Gold EOS

Gold is an almost ideal pressure calibrant due to its simple cubic structure, its stability at both extreme pressures and temperatures, and its high atomic number making it a strong scatterer of x-rays. The EOS of gold has been determined by many authors (Ming *et al.* (1983), Heinz and Jeanloz (1984), Yagi *et al.* (1985)) to both very high pressures and temperatures, and calibrated against both the NaCl EOS and the ruby fluorescence scale. In each case the results were in excellent agreement with shockwave data.

Argon EOS

Argon, because of its use as a pressure fluid to enable quasi-hydrostatic conditions to 800kbars, is a good choice of pressure calibrant as it allows calibrant and fluid to be combined into one, thus eliminating loss of precious sample volume. The EOS of single-crystal argon has been calibrated against the ruby fluores-

cence scale to 82kbars (Finger *et al.* (1981)), and separately to 769kbars (Xu *et al.* (1984)), to 600kbars (Zou *et al.* (1982a)) and to 800kbars (Mao *et al.* (1986)) using polycrystalline samples.

CaF_2 EOS

The use of CaF_2 as a pressure calibrant was developed to allow pressure calibration in a high temperature-high pressure DAC which had no optical access to the sample (Hazen and Finger (1981b)). By combining the known values for the compression at room temperature with the thermal expansion at atmospheric pressure, a polynomial function for the unit-cell volume as a function of pressure and temperature was derived. It should be noted, however, that no cross calibration to the NaCl EOS has been made for CaF_2 and so the accuracy of the calculated EOS is uncertain.

2.7 A Comparison of High-Pressure Structural Results

Although it is not possible to review in detail here the results of all the high-pressure structural studies made to date, a comparison of the different structural results for two materials, α-Quartz (SiO_2) and KDP (KH_2PO_4), allows the quality of the results obtainable using different diffraction techniques to be compared. These two materials were chosen for the following reasons.

(1) α-Quartz has been the subject of many high-pressure studies of which three structural studies are compared here. Two use single-crystal x-ray techniques using a Keller-Holzapfel and Merrill-Bassett DAC, while the third uses TOF neutron-diffraction techniques on a powdered sample.

(2) KDP has been the subject of many studies of which two single-crystal x-ray diffraction studies made nineteen years apart can be compared with a monochromatic neutron-diffraction study made using single-crystal techniques.

In the following discussion emphasis is given to the experimental details and the

quality of the results rather than the science involved. For this reason no more than a brief description of the structure of the materials will be given.

SiO_2: trigonal $P3_121$, a=4.85Å, c=5.35Å, Si at $(x,0,\frac{1}{3})$, O at (x,y,z)

The first structural study of α-Quartz at high pressure was made by Jorgenson (1978). Using TOF neutron diffraction and a Brugger-type cell, he followed the structural changes up to 25kbars. The studies were made under hydrostatic conditions using d-methanol as the pressure fluid and the CsCl EOS to measure the pressure. Using a 90° scattering geometry, a pattern free from parasitic scatter from the pressure cell was collected to a minimum d-spacing of 1Å ($\sin\Theta/\lambda$=0.5Å^{-1}). In this region, Rietveld profile refinement was made on 38 independent reflections and the refined parameters were the positional parameters for both the Si and O atoms and an isotropic thermal parameter for each atom. The latter were not quoted and there was no mention of a cell absorption correction having been made. At a pressure of 21kbars, the lattice parameters were determined to be a=4.8262(5)Å and c=5.3358(9)Å while the atomic coordinates were refined with estimated standard deviations (hereafter esd's) of 0.001 to 0.002. This resulted in bondlengths being determined to 0.005Å and bondangles to 0.2-0.6°. Comparison of the results obtained from atmospheric pressure to 25kbars showed no change in the quality of refined structure as a function of pressure.

d'Amour *et al.* (1979) determined the structure of α-Quartz to 68kbars in 1979 using single-crystal x-ray diffraction techniques. Data were collected using a Keller-Holzapfel design of DAC and an Inconel gasket with a 180μm diameter hole. The crystal size was 60×60×80μm^3 and the pressure fluid was a 4:1 mixture of methanol:ethanol. The pressure was calibrated using the CsCl EOS. Using graphite-monochromated MoK$_\alpha$ radiation, 150 reflections (60 independents) were measured to a $\sin\Theta/\lambda$ of 0.53Å^{-1} using ω-scans and the diffraction geometry developed by Denner *et al.* (1978). R-factors after refinement were in the range 5.6–9.9% and the refined parameters at 19kbars are given in column 2 of Table 2.1, with the results of Jorgenson at 21.1kbars included in column 1 for comparison. For the x-ray data, the lattice parameters were not measured using the eight-position method and were determined to be a=4.832(2)Å and c=5.347(4)Å at 19kbars. The esd's on the refined positional parameters were

SiO_2	Jorgenson	d'Amour *et al.*	Levien *et al.*
Pressure(kbars)	21.1	19	20.7
$(\sin\Theta/\lambda)_{max}(\text{Å}^{-1})$	0.5	0.53	0.99
a(Å)	4.8262(5)	4.832(2)	4.8362(5)
c(Å)	5.3358(9)	5.347(4)	5.3439(4)
x(Si)	0.456(2)	0.463(2)	0.4630(2)
x(O)	0.410(1)	0.409(3)	0.4111(6)
y(O)	0.281(1)	0.279(3)	0.2795(4)
z(O)	0.224(1)	0.107(2)	0.1095(2)
av. Si-O(Å)	1.607(5)	1.61(2)	1.607(1)
Si-O-Si(°)	139.5(5)	138.9(11)	139.9(2)
O-Si-O (°)	110.7(2)	111.2(4)	110.7(1)
O-Si-O (°)	108.3(6)	108.3(5)	108.15(4)
O-Si-O (°)	108.8(3)	109.8(9)	109.4(2)
O-Si-O (°)	109.4(6)	110.7(7)	109.7(1)

Table 2.1: The unit-cell dimensions, refined atomic coordinates, average Si–O bondlength, and selected interatomic angles from the structural studies of SiO_2 by Jorgenson (1978), d'Amour *et al.* (1979) and Levien *et al.* (1980). Esd's are given (in parentheses) on the last quoted place. The Si atom in each case was fixed by symmetry at $(x, 0, \frac{1}{3})$.

0.002 to 0.003 giving esd's on the bondlengths of 0.02Å and esd's on the bondangles of 0.4° to 1.1°, both of which are considerably larger than those obtained by Jorgenson. Isotropic thermal parameters were refined for both the Si and O atoms at all pressures but showed no uniform tendency as a function of pressure.

The third refinement of the structure of α-Quartz was made by Levien *et al.* (1980), again using single-crystal x-ray techniques. In this study, however, a Merrill-Bassett DAC was used with an Inconel gasket with a hole 300μm in diameter. The crystal had dimensions $70\times70\times30\mu m^3$ and the pressure fluid was again a 4:1 methanol:ethanol mixture. The pressure was measured using the

ruby-fluorescence method. Attempts were made to collect high-pressure data using AgK_α radiation, but the refined data gave R-factors three times those obtained using MoK_α radiation and the AgK_α results were not reported. All data were subsequently collected using MoK_α. Reflections were measured at pressures up to 61kbars with the lattice parameters being measured at each pressure using the eight-position method. The values of a=4.8362(5)Å and c=5.3439(4)Å at 20.7kbars show the high precision obtainable using this technique compared to the results of d'Amour *et al.*. Data were measured to $2\Theta=90°$ ($\sin\Theta/\lambda = 0.99Å^{-1}$) with those reflections lying on, or near, the powder lines from the beryllium being omitted. No details were given about the scan type used to measure the data, or if the data were collected away from the bisecting position. At 20.7kbars, 390 measured reflections were averaged to 198, of which 170 had intensities of twice their standard deviation. Intensities were corrected for cell and sample absorption and refined to give, at 20.7kbars, esd's of 0.0002-0.0006 on the atomic coordinates and esd's of 0.001Å and 0.1°-0.4° in the bondlengths and bondangles respectively. An isotropic extinction correction and full anisotropic thermal parameters were refined at all pressures, both showing little change with increasing pressure. The refined values at high pressure also agree well with those obtained at atmospheric pressure and show this to be one of the most accurate high-pressure structure determinations using x-ray diffraction techniques to have been made, with the esd's on parameters only a factor of 2-3 times those obtained at atmospheric pressure. The results obtained at 20.7 kbars are listed in column 3 of Table 2.1 for comparison with the other two studies.

Several points thus emerge from comparing these three studies of α-Quartz.

(1) The precision of the lattice parameters obtained from the Rietveld refinement and from the eight-position method are far superior to those obtained when not using the eight-position method. As the estimated errors in the lattice parameters should be incorporated into the calculation of the esd's of the bondlengths and bondangles, a precise determination of the lattice parameters is very desirable.

(2) The most precise results were obtained by single-crystal techniques, as were the least precise. Levien *et al.* state that the low precision of the study by

d'Amour *et al.* was due to the need of a cell absorption correction, even for the Keller-Holzapfel cell, and to the low real-space resolution of their data. They also felt that the crystal-size to gasket hole ratio used by d'Amour *et al.* was too small, and that their data may have therefore been affected by gasket occlusion.

(3) State-of-the-art high-pressure diffraction using single-crystal x-ray techniques would seem to be able to refine crystal structures with esd's on refined parameters being only twice those obtainable at atmospheric pressure. It is also possible to refine physically-sensible anisotropic thermal motion.

(4) Single-crystal techniques, as expected, can give superior results to powder-based techniques. However, great care and effort is needed for this to be so and may not be the case in general, as illustrated by the results of d'Amour *et al.*.

(5) Problems remain over the accuracy of the results obtainable using the Keller-Holzapfel DAC compared to those obtainable using the Merrill-Bassett DAC. A comparison of the refinements of the structure of ruby at high pressure (Finger and Hazen (1978), d'Amour *et al.* (1978)) again shows the esd's in the case of the data collected using a Keller-Holzapfel cell (d'Amour *et al.*) to be 3-4 times larger than those obtained in equivalent studies made with a Merrill-Bassett DAC. The author feels that the increased volume of illuminated beryllium which the hemispherical backing plates introduce, and the resulting rise in the background and cell absorption, far outweigh the advantages of having no absorption correction to make. It is then felt that the most accurate structural studies using x-ray single-crystal techniques can be made in a Merrill-Bassett cell rather than in a Keller-Holzapfel DAC.

KH_2PO_4: tetragonal $I\bar{4}2d$, a=7.5Å, c=6.9Å, K at (0,0,$\frac{1}{2}$), P at (0,0,0), O at (x,y,z), H at (x,y,z)

The first structural of study of KDP at high pressure was made as early as 1971 (Morosin and Samara (1971)) with a single-crystal x-ray study at 3kbars. The pressure cell was a beryllium cylinder with a hemispherical top and kerosene was used as the pressure fluid. Using MoK_α radiation, 26 reflections which calculation showed to be the most sensitive to the O-atom atomic coordinates, were measured using ω-2Θ scans at 1bar and 3kbars, all measurements being made with the sample inside the cell. The structure factors of the high-pressure reflec-

tions were then determined by scaling the intensities obtained from the sample inside the cell at atmospheric pressure to those previously obtained with the sample outside the cell at atmospheric pressure. The refined positional parameters for the O atom (no information was obtainable for the H atom) are given in column 1 of Table 2.2. An isotropic thermal parameters was refined for the O atom while those for the K and P atoms were fixed at their atmospheric pressure values. No detailed results were given for the cell parameters or bondlengths, but the large esd's of 0.005 and 0.007 on the O atomic coordinates suggests that the latter will be poorly determined.

As part of a series of structural work on KDP, the structure was determined at 16.5kbars using single-crystal neutron-diffraction techniques by Tibballs *et al.* (1982a). The data were collected on the D15 normal-beam diffractometer at the Institut Laue-Langevin, Grenoble using a calibrated wavelength of 0.8357(2)Å. The sample was cylindrical in shape with diameter of 3mm and height 3mm and was mounted in a Bloch cell such that the $(h0l)$ plane of reflections was measurable. The hydrostatic fluid was Fluorinert, a mixture of fluorinated hydrocarbons, and the pressure was determined from the previously determined compression of KDP. The cell parameters were determined to be a=7.329(3)Å and c=6.856(3)Å. Using ω-2Θ scans, approximately 200 reflections were collected in the $(h0l)$ layer to a $\sin\Theta/\lambda$ of 1.1Å^{-1}. Averaging gave 73 independent reflections. Scans of reflections affected by powder lines from the Al_2O_3 pressure vessel in the cell had their true background estimated from scans made through adjacent volumes of reciprocal space. No absorption correction was necessary for the pressure cell. Anisotropic thermal parameters were refined for all atoms although the limited data set required some constraints to be made. The final R-factor was 4.9%. The refined atomic coordinates for the O and H atom are given in column 2 of Table 2.2 and show esd's of 0.0001 to 0.0002 on the O atom, and 0.0007 to 0.0012 for the H atom. The increased precision over the 1971 data is immediately obvious and the distance between the H atoms (δ), although only 0.315Å, is determined to 0.011Å while the length of the hydrogen-bond (2R) is determined to 0.003Å.

The most recent structural study of KDP was made using single-crystal x-ray techniques to a pressure of 54kbars using a Merrill-Bassett DAC (Endo *et al.* (1989)). The crystal had dimensions 150×150×70μm^3 and was mounted in the

KH_2PO_4	Morosin and Samara	Tibballs *et al.*	Endo *et al.*
Pressure(kbars)	3	16.5	20
$(\sin\Theta/\lambda)_{max}(\text{Å}^{-1})$	–	1.1	0.7
a(Å)	–	7.329(3)	7.319(2)
c(Å)	–	6.856(3)	6.849(2)
x(O)	0.167(7)	0.1526(1)	0.1531(13)
y(O)	0.077(5)	0.0816(1)	0.0815(15)
z(O)	0.125	0.1267(2)	0.1287(14)
x(H)	–	=x(O)	–
y(H)	–	0.2286(7)	–
z(H)	–	0.1224(12)	–
δ(H-H)(Å)	–	0.315(11)	–
2R(O-O)(Å)	–	2.469(3)	2.467(22)
P–O(Å)	–	1.537(2)	1.545(99)
O-P-O(°)	–	111.2(1)	110.4(7)

Table 2.2: The unit-cell dimensions, refined atomic coordinates and selected interatomic bondlengths and angles from the structural studies of KH_2PO_4 by Morosin and Samara (1971), Tibballs *et al.* (1982a) and Endo *et al.* (1989). Esd's are given (in parentheses) on the last quoted place. Parameters given without esd's were not refined while parameters indicated by '–' were either not determined or their values were not given explicitly by the authors. In all cases the P atom was fixed at (0,0,0) while the K atom was fixed at $(0, 0, \frac{1}{2})$.

DAC such that the b-axis of the crystal was perpendicular to the culet face, allowing maximum access to the ($h0l$) reciprocal plane. The gasket hole was 300μm in diameter and the pressure was measured using the ruby technique. Pressure cell absorption was corrected for by measuring a data set both inside and outside of the cell at atmospheric pressure. The lattice parameters were not determined using the eight-position method and at 20kbars were a=7.319(2)Å and c=6.849(2)Å. Using MoK_α radiation, a quarter sphere of reciprocal space was measured to a $\sin\Theta/\lambda$ of 0.7Å^{-1} using ω-2Θ scans. Refinement on the resulting 26-34 independent reflections gave R-factors of 4-8%. Refinement of the data at 20kbars gave esd's on the O-atom atomic coordinates (again there was no information obtainable on the H atoms) of 0.0013-0.0015, however, at 14kbars this increased to 0.0029. The esd's also increased at higher pressures, a commonly occurring problem. Isotropic thermal parameters were refined for all three heavy (P, K and O) atoms and showed little change to the highest pressures. The accuracy of this study, although significantly better than the earlier 1971 study, is considerably worse than that using neutrons with the hydrogen-bond length being determined to only 0.02 to 0.04Å, some ten times worse than that using neutrons. The refined atomic coordinates for the data set collected at 20kbars are given in column 3 of Table 2.2.

Again several points emerge from comparing these three structural studies.

(1) The lattice parameters of the 1989 x-ray study were not measured using the eight-position method and subsequently have esd's that are again three to four times larger than those in the study of Quartz by Levien *et al.*

(2) The accuracy and precision of the neutron-diffraction study are considerably higher than those of the most recent x-ray study. It is likely that the x-ray study suffers from having been made using ω-2Θ scans rather than ω scans to collect the data, and also from the fact that all possible reflections were not measured in the x-ray case but rather only a quarter of them. It is also uncertain as to how the weaker reflections were measured in the x-ray case, the experimental details suggesting that *all* reflections were measured at a constant scan speed. It is better, especially in the case of high-pressure diffraction, to collect the data to a constant σ(I)/I (Finger *et al.* (1973)), that is, counting the weaker peaks for longer to improve their statistics. It is therefore uncertain as to what extent

the neutron and x-ray results would compare if state-of-the-art techniques had been used in each case.

(3) No mention is made of refining anisotropic thermal parameters in the 1989 x-ray study – not even for the K and P atoms which lie on high symmetry positions. This emphasises the point that the physically-sensible anisotropic thermal parameters obtained by Levien *et al.* are the exception rather than the rule in high-pressure structural studies.

(4) The real-space resolution of the single-crystal neutron-diffraction study is considerably higher than that of any of the x-ray studies described here. This is generally the case, as high-resolution x-ray studies would require the use of AgK_α x-rays rather than MoK_α. This higher resolution allows neutron-diffraction studies to resolve finer structural details, such as disorder, which may only be evident as thermal anisotropy in x-ray studies.

2.8 Conclusions

This chapter has attempted to describe the different methods and techniques used in the determination of crystal structures at high pressure; how the problems associated with high-pressure crystallography come about; and to what extent these problems can be reduced or eliminated. Several conclusions can be reached as to the state-of-the-art of structural studies at high pressure prior to the work described in this thesis.

The wide availability and ease of use of the DAC has allowed great improvements to be made in the quality of refined structures at high pressure using single-crystal x-ray diffraction techniques. The lack of strict time constraints when using laboratory sources of radiation, as opposed to the use of central facility sources, has allowed a large number of diffraction techniques to be developed to maximise the quality and quantity of data collectable using a DAC. Use of these techniques has led to refined structures in which the esd's on the parameters are only a factor of two or three larger than those obtained at atmospheric pressure. However, as shown in the previous section, this quality of refinement can only come about if all the diffraction techniques available – the eight-position method,

fixed-ϕ geometry, counting to constant σ(I)/I, using ω scans, large gasket hole to crystal size ratio, avoiding diamond or pressure calibrant reflections – are utilised, and this factor of two to three in the esd's probably represents the best current accuracy and precision possible. It is also apparent that, to date, very little structural work has been done using the transverse-geometry DACs despite the advantage they offer of very large data sets. It would then seem that the most accurate structural work using a DAC can be done with those having the transmission geometry, with the Merrill-Bassett design of cell allowing higher quality data than the design of Keller and Holzapfel, although very recent results using the MPI design of transverse-geometry DAC illustrate the high quality of results that may now be available using this cell (Glinneman (1990)).

However, despite the large amount of work that has been done to improve the quality of high-pressure structural studies using this technique, very few improvements or developments have been made in recent years, the majority of techniques and equipment having been developed in the 1970's and early 1980's. No solution, therefore, has been found to the problems of using AgK_α radiation, or the problem of the declining quality of refinements as the pressure is increased, problems that will become evermore important with the use of short wavelength radiation from synchrotrons, and the use of smaller crystals enabling considerably higher pressures to be achieved.

Although single-crystal x-ray diffraction accounts for a large percentage of the high-pressure structural studies made, single-crystal neutron-diffraction may, as it does at atmospheric pressure, allow significant improvements to be made in both the quality and detail of diffraction study possible. The previous section illustrated the possibilities offered by this technique even though only a single layer of reflections was measurable. However, in order that single-crystal neutron-diffraction be able to realise its full potential, a more three-dimensional data set needs to be measurable, offering the possibility of studying low-symmetry structures. The neutron-diffraction version of the Ahsbahs cell, with its transverse geometry allowing wide access to reflections, would seem to offer great possibilities in this field.

Of the two neutron powder-diffraction techniques, the wavelength-dispersive TOF techniques offer significant advantages over the angle-dispersive techniques.

The latter suffer from severe problems with parasitic scatter from the Al_2O_3 used as a pressure- vessel material also from problems with centering errors which make the determination of absolute structural changes as a function of pressure very difficult. Both these problems, however, are eliminated with the use of TOF techniques which therefore allow high-quality data to be relatively straight-forwardly measured. The absence of any degradation in the quality of the data as a function of pressure, and the use of the 90° scattering geometry to enable pressure cell to be designed with only small entrance and exit slits to weaken them, allows the prospect of extending the use of wavelength-dispersive techniques to considerably higher pressures. This potential, however, has remained sadly untapped, with very little development in this field during the 1980's and certainly no advancement on the pressure of 73kbars reached by Brugger *et al.* (1969). Indeed with the demise of the 25kbar cell at Argonne (Jorgenson (1988)), almost no work has been done at pressures in excess of 7kbars using TOF techniques in recent years, and little work has been done using angle-dispersive techniques above 10kbars. This would then seem a field with considerable opportunity for development.

The combination of high pressure and non-ambient temperatures has been very infrequently used in structural studies. Although all neutron-diffraction techniques lend themselves to the use of non-ambient temperatures, especially low temperatures, either through the large size of neutron diffractometers having the robustness to accommodate the necessary cryostats and furnaces, or through the absence of pressure cell movement (TOF techniques), the small size of many four-circle x-ray diffractometers prevents the use of standard cryostats of furnaces in experiments using a DAC. Although this problem has been partially solved with the use of resistively heated DACs or, more recently, by DACs heated externally by a furnace (Schiferl *et al.* 1990), the quality of the data has generally been poor due to the high absorption of the materials used to withstand the high temperatures. This general lack of temperature variation thus makes experimental access to the large number of different phases and phenomena discovered at non-ambient pressures and temperatures very limited. The use of a DAC mounted on a closed-cycle helium cryostat would allow considerable advances to be made in this area.

Therefore, although many problems associated with high-pressure diffraction

have been solved, many problems still exist on which much work is still required.

(1) The ability to achieve accurate results in x-ray diffraction studies using AgK_α radiation would significantly increase the resolution of the x-ray data available and allow a greater distinction to be made between, for example, structural disorder and thermal anisotropy.

(2) The reasons for the general decrease in the data quality as pressure is increased in single-crystal studies using a DAC are not yet fully understood. Understanding the reasons for this will be essential if accurate structural studies are to be extended to increasingly higher pressures.

(3) Improvements are needed in the quality of data obtainable using the transverse-geometry DACs.

(4) Development of techniques are needed to allow the refinement of structures from monochromatic x-ray powder data using a DAC. This will allow the possibility of structures being refined at very high pressures.

(5) Development of techniques to allow single-crystal studies using synchrotron radiation are also needed, especially techniques to allow the use of the Laue method. The very high flux from synchrotrons will enable the use of smaller sample crystals, and thus higher pressures, and will also significantly increase the signal-to-noise ratio of sample reflections. The use of the high flux at short wavelengths, however, makes the solution to the AgK_α problem even more urgent.

(6) The use of the Laue technique on spallation neutron sources should be developed.

(7) Higher pressures are needed using TOF powder-diffraction techniques.

(8) Temperature variation is needed in all high-pressure diffraction techniques.

The solutions to some of these problems form the bulk of the present work and are considered in the next chapter.

Chapter 3

Technique Development

3.1 Introduction

The work described in this chapter addresses some of the problems and comments discussed at the end of the Chapter 2 and is divided into four sections, one for each of the four general diffraction methods of x-ray single-crystal and powder diffraction, and neutron single-crystal and powder diffraction. The majority of the work undertaken was concerned with the development of single-crystal techniques, using both x-rays and neutrons, and the work in these areas is therefore described in some detail. However, the author has also been closely associated with two new projects to develop x-ray and neutron powder-diffraction methods with the aim of being able to determine crystal structures using these techniques to significantly higher pressures, and with higher accuracies, than have been possible hitherto. Although both these projects have only recently been started and little, if any, high-pressure diffraction work has been done, they are described in this chapter both for completeness, in light of the aim of this thesis of covering *all* aspects of structure determination at high pressure, and to illustrate the current state-of-the-art techniques now available in these fields as opposed to those available prior to the present work.

3.2 Single-Crystal X-Ray Diffraction

3.2.1 Introduction

Although the techniques associated with high-pressure single-crystal x-ray diffraction are the most highly developed of all high-pressure data collection methods, two new techniques are described in this section that allow diffraction data to be collected with greater accuracy than has been possible hitherto. The first section describes a detailed study of how simultaneous diffraction from the diamond anvils of a DAC affects the intensity of sample reflections and describes a data collection method to allow affected reflections to be identified. The second section describes a study on the use of tungsten gaskets to allow high-quality data to be collected using AgK_α radiation.

3.2.2 The Effects of Simultaneous Diffraction

Although, as described in the previous chapter, techniques have been developed to predict and avoid the situation in which simultaneous diffraction of one or more of the diamond-anvils in a DAC and the sample occurs such that both scatter into the detector, a problem which appears not to have been considered is the possible removal of intensity from either the incident or diffracted beams by this simultaneous diffraction process. The equivalent effect has been observed in energy-dispersive powder-diffraction studies and also in studies of the pseudo-Kossel pattern produced when fluorescence from a powder sample inside a DAC passes through one of the diamonds (Okada and Iwasaki (1980)).

There are two possible forms of simultaneous diffraction process that can reduce the intensity of the measured sample intensity and these are illustrated in Figure 3.1. In the first of these processes, part of the incident beam is diffracted by the diamond between the sample and the x-ray source (the 'incident-beam event' shown in Figure 3.1) and the intensity of the incident beam reaching the sample is therefore reduced. In the second case, the diffracted beam from the sample crystal is further diffracted by the diamond closest to the detector (the 'diffracted-beam event') and is thus reduced in intensity.

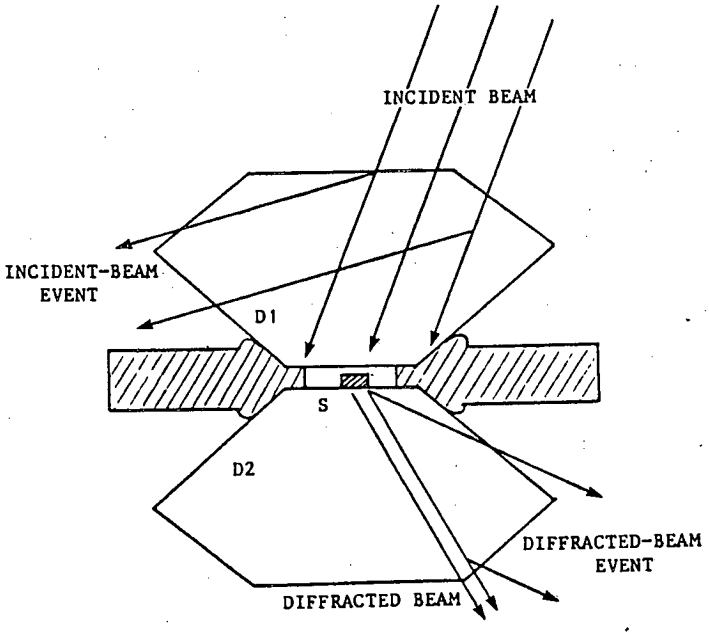

Figure 3.1: A cross-section of the Merrill-Bassett cell showing the x-ray paths for simultaneous diffraction (i) by the diamond (D1) in the beam incident on the sample, and (ii) by the diamond (D2) in the beam diffracted by the sample.

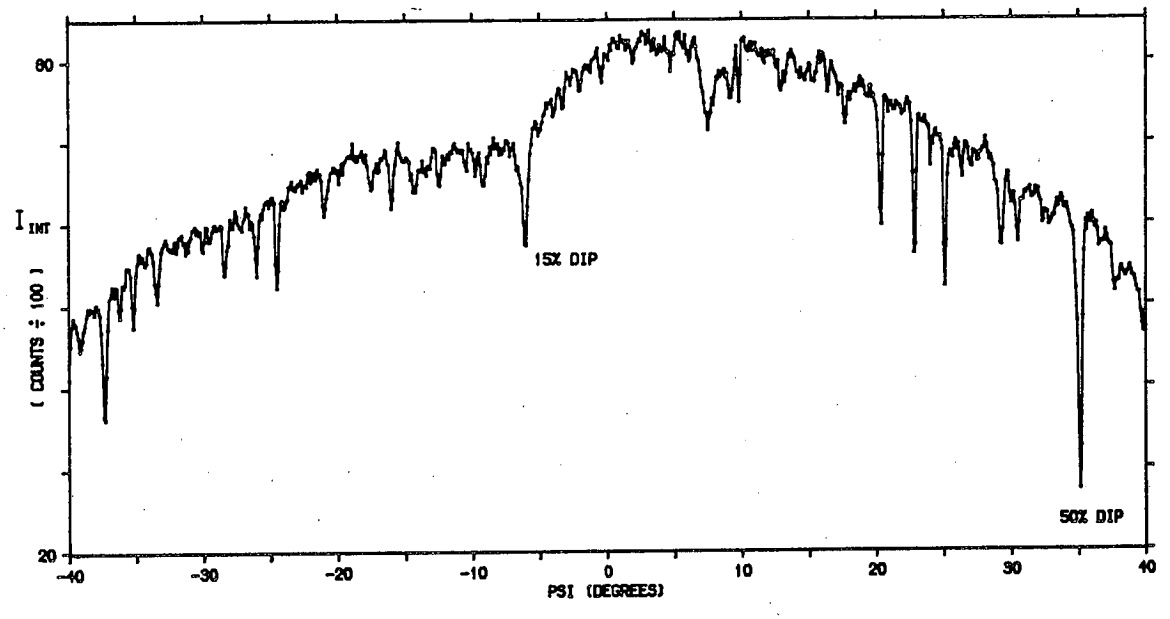

Figure 3.2: Integrated intensity (I_{INT}) versus ψ for the 200 reflection of a $KMnF_3$ sample under pressure in a Merrill-Bassett DAC. I_{INT} is the total integrated intensity at each point, divided by 100.

Initial evidence for these simultaneous diffraction events was encountered during measurements of the variation of the integrated intensity with rotation about the scattering vector of a sample in a DAC (ψ-scans). Figure 3.2 illustrates the integrated intensity as a function of ψ for a sample of the cubic perovskite $KMnF_3$ mounted in a Merrill-Bassett DAC, using a CAD-4 four-circle diffractometer and MoK_α radiation (graphite monochromator). The integrated intensity of the (200) reflection was measured using an ω-2Θ scan performed at successive steps of 0.1° in ψ. It can be seen that in addition to a slow variation in the integrated intensity due to the variation of the DAC and sample absorption as a function of ψ, there are sharp dips of up to 50% which were tentatively attributed to the effects of simultaneous diffraction processes.

In order to prove, however, that these events were in fact due to simultaneous diffraction processes, it was necessary to calculate the conditions under which such processes occurred and to show that the intensity diffracted by the diamonds was the same as that 'missing' from the integrated intensity of the sample reflection.

The angular conditions under which either incident- or diffracted-beam events occurred, and the direction of the resulting diffracted beam, can, in principle, be calculated if the orientation matrices of both the diamond anvils and the sample crystal are known. However, these calculations are hampered by two difficulties. The first is that an orientation matrix for a crystal can only calculate the diffraction angles for a given reflection accurately if that crystal is well centred on the diffractometer – a condition not met by either of the diamond-anvils. The second difficulty is that the simultaneous reflections from the diamonds are not confined to lie on the equatorial plane of the diffractometer but may diffract well away from the plane, making the detection of such reflections using the diffractometer detector, impossible.

Using a computer program written by Dr. J.S. Loveday of this department, it was possible to both predict the occurrence of simultaneous diffraction events and to predict the direction of the diffracted beams. Location of the latter, using Polaroid film as the reflections were inclined at angles of up to 90° to the equatorial plane, showed the program to be working correctly. However, the direction of the diffracted beams from both incident- and diffracted-beam events made the location and measurement of their intensity, even using a second detector, very difficult as many of the reflections were either partially or totally absorbed by the steel components of the pressure cell or the Inconel gasket. In order to remove these restrictions, the sample was removed from the DAC and fixed to the culet of a bare diamond which was then mounted on a steel pin. However, when ψ-scans were made around a number of sample reflections in this case, no dips were observed in the integrated intensity, casting doubt on the earlier assumption that the dips in the previous ψ-scans were due to simultaneous diffraction. In order to examine the initial assumption that the dips were due to simultaneous diffraction, a number of tests were made.

First, it was necessary to investigate whether diamonds in the loaded pressure cell (as used to obtain the results in Figure 3.2) reflected a larger percentage of the incident or diffracted beam than an isolated diamond. A $KMnF_3$ sample was mounted in a Merrill-Bassett DAC which was loaded to give a pressure of 2.5kbars on the sample. The DAC was then mounted on the diffractometer and the CAD-4 detector, with suitable attenuation, was set to monitor the direct beam. Measurements were made as the diamond on the detector side

of the DAC was stepped (in ω) through its (220) reflection. The resulting dip in the intensity of the direct beam is shown in Figure 3.3 and it can be seen that the modest applied pressure of 2.5kbars has dramatically increased the scattering power of the diamond, causing a 10% reduction in the intensity of the direct beam. This was confirmed by using the CAD-4 detector to measure the intensity of the diamond reflection as shown by the dashed line and circular symbols in Figure 3.3: clearly there is a close correspondence in both position (in ω) and intensity between the diamond reflection and the dip in the primary beam. This same technique was then used to monitor the scattering power (the percentage of the primary beam scattered) of various classes of reflection under the same conditions, and it was found that only the five strongest classes of reflection affected the beam significantly – the (111) class by 20-30%, the (220) class by 10-15%, the (311) class by approximately 7% and the (400) and (440) classes by approximately 4%. These effects are some 30 times larger than those obtained for an isolated diamond and the exact explanation for this is uncertain at present. It may be possible to explain the increase in scattering power by the way in which the stress is applied to the diamonds, increasing their mosaic width (the angle over which they satisfy Bragg's law), and a study of how the mosaic width of the diamonds changes with pressure is planned for the future.

Having shown that diffraction by the diamonds can scatter a significant fraction of the incident beam, it was then necessary to show that all the dips in a ψ-scan of a sample reflection could be accounted for by simultaneous diffraction. Figure 3.4 shows a section of a ψ-scan for a sample of $KMnF_3$ and below the scan are marked the predicted values of ψ for incident- and diffracted-beam events involving the five strongest classes of reflection listed above, the relative strengths of which are indicated by the lengths of the marks. There can be seen to be a generally good agreement between the predicted events and the observed dips, in terms of both position and relative magnitude. All the obvious dips correspond to predicted events, and often to a near coincidence of two or more of them: for example, the dip labelled 1 in Figure 3.4 can be seen to arise from the superposition of a (220) incident-beam event and a (220) diffracted-beam event; dip 4 is from two (311) incident-beam events, separated just enough to show up as a broadening of the dip; and the large (50%) dip in Figure 3.2 can be attributed to (111) incident- and diffracted-beam events coinciding. Discrepancies of up to 2-3° (in ψ) between calculated and observed positions are often found, as for dip

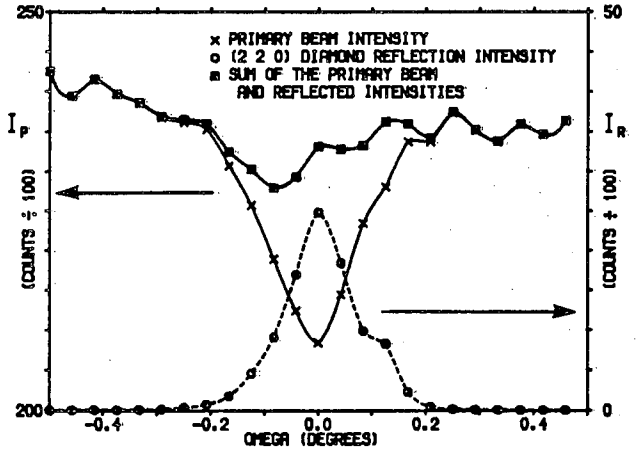

Figure 3.3: An ω scan through a 220 diamond reflection from a DAC under pressure (o), setting ω =0 at the peak, and the intensity of the primary beam (×) measured for each step through the reflection. The sum of the primary-beam intensity (I_P) and the intensity in the reflection (I_R) is also shown (■). I_P and I_R are the recorded counts at each point, divided by 100.

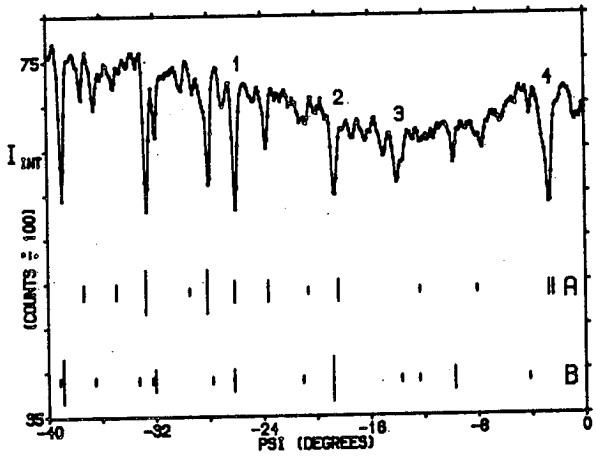

Figure 3.4: Integrated intensity, I_{INT}, versus ψ for the 110 $KMnF_3$ reflection, at a pressure of 2.5kbars. The vertical marks below show the predicted positions of incident-beam events (labelled A) and diffracted-beam events (labelled B). The lengths of the marks represent the relative scattering powers of the diamond reflections involved, as given in the text – the longest is for 111-type reflections, the next for 220, the next for 311 and the shortest for both 400 and 440. I_{INT} is the total integrated counts at each point, divided by 100. The dips labelled 1, 2, 3, and 4 are discussed in the text.

3 in Figure 3.4, and are due to the small errors in the orientation matrices of the diamonds, as discussed earlier, to which the calculations are quite sensitive. Variations in the relative magnitudes of the dips away from the predictions – as for dip 2 in Figure 3.4, which is predicted to be stronger than dip 1 – are believed to arise from the anisotropic stresses on the diamonds. More detailed checks, on this and other ψ-scans, confirmed (i) that there were no dips that could not be accounted for, and (ii) that all predicted events gave rise to dips.

As a final confirmation, a search was made for direct evidence to relate simultaneous diffraction and the ψ-scan dips. For incident-beam events the best method was to monitor the intensity of the primary beam as the ψ-scan of the sample passed through a dip. In all cases studied, the primary beam intensity showed a reduction whose magnitude was consistent with the measured scattering power of the class of diamond reflection predicted to be involved. Furthermore, the magnitude of the dip in the measured sample reflection intensity was simply the percentage reduction of the primary beam intensity.

The technique used to seek direct evidence of diffracted-beam events was more complicated as these events do not affect the intensity of the direct beam (see Figure 3.1) and it is not possible, in general, to measure the reflected beam intensity using the CAD-4 detector, as discussed previously. A second detector, which could be positioned manually, was therefore used to detect and measure these diffracted-beam events, and, in order to put the intensities of the diamond and sample reflections on the same scale, the second detector was also used to measure the sample intensity. Figure 3.5 shows a diffracted-beam event due to a diamond (220) reflection, successfully recorded at the predicted position of the detector. Furthermore, taking into account the uncertainty in the diffractometer setting (0.1° in ψ) and the differences in absorption for the diamond and sample reflections, there is close agreement between the diamond reflection and the dip in the sample intensity in terms of both size and ψ setting.

In view of the large difference in the scattering power of an unstressed diamond and of the diamonds in a DAC at the low pressure used in the studies described above, it is important to know to what extent the scattering power changes at higher pressures and how this alters the affect of simultaneous diffraction. To study this, measurements were made of the scattering power of the diamond-

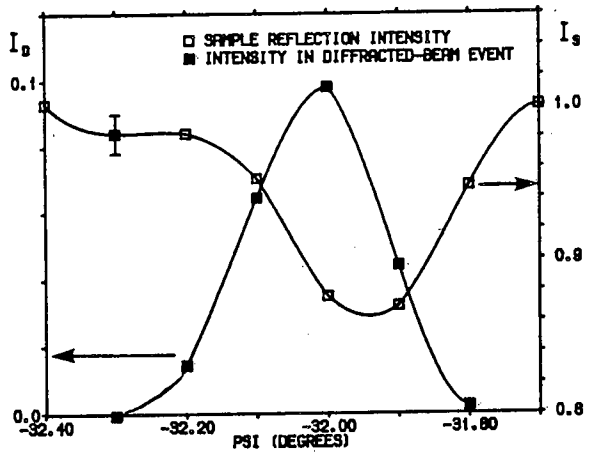

Figure 3.5: The peak intensity of a 220 $KMnF_3$ sample reflection, I_S (□), and the peak intensity of a diffracted-beam event involving a 220 diamond reflection, I_D (■), as a function of ψ at a pressure of 2.5kbars. I_S and I_D were measured with the same detector and have been put onto a common scale normalized to 1.00 at the maximum sample intensity. A typical error bar is shown for one of the points.

anvils in a DAC at pressures of 30kbars and atmospheric pressure, in addition to the 2.5kbars of the studies described above. Measurements were also made with the cell at 30kbars using AgK_α radiation (instead of MoK_α) in order to study any wavelength dependence. The results confirmed the very small scattering power of the diamonds at atmospheric pressure and showed that the (greater) scattering power of the diamonds at 30kbars is the same as that at 2.5kbars. Hence, the dramatic effect of pressure on the scattering power is brought about within the first one or two kilobars of applied load and is not visibly increased at higher pressures. The scattering power was also found to be unaffected by the use of AgK_α (0.56Å) radiation as opposed to MoK_α (0.71Å), and since only the same five classes of reflection give rise to significant events, the typical density of dips is not affected either. It would then seem that neither the poor quality of high-pressure data collected with AgK_α radiation or the decrease in refinement quality as the pressure increases is due to this simultaneous diffraction process.

With the increased use of synchrotron radiation in crystallographic studies at high pressures (see Chapter 6), it was felt important to study the effects of

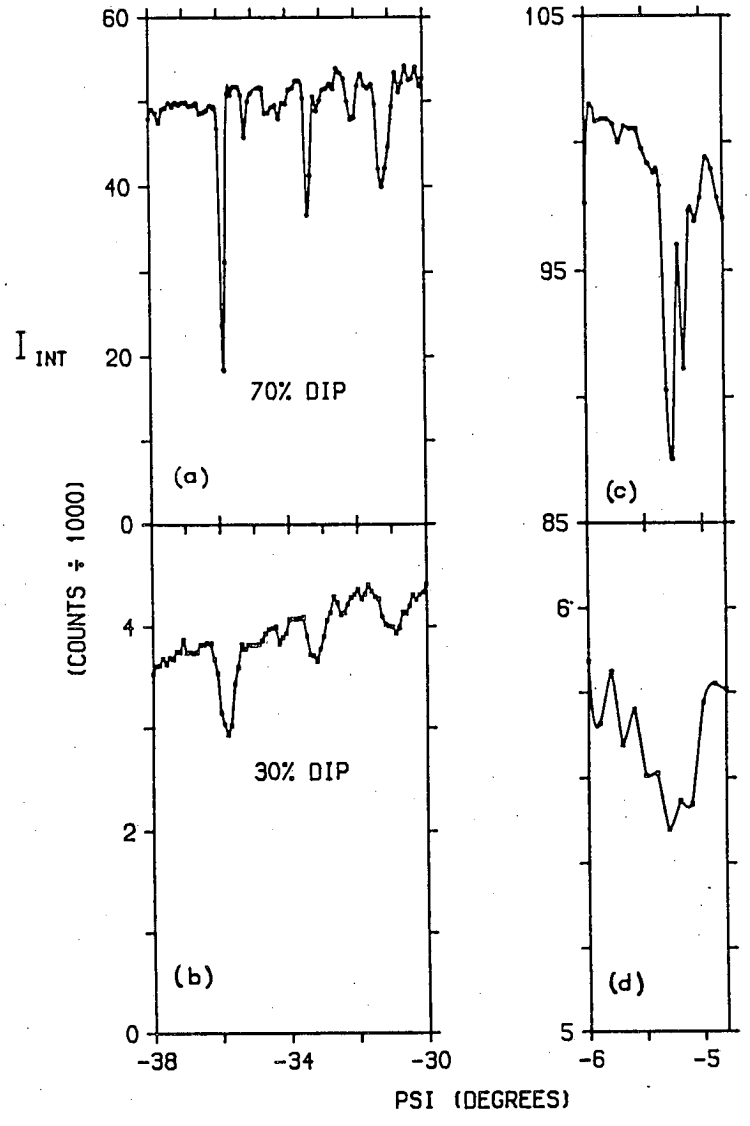

Figure 3.6: Integrated intensity, I_{INT}, versus ψ for the 110 $KMnF_3$ reflection in a DAC at a pressure of 13kbars (a) measured on a synchrotron beam at the Photon Factory, and (b) measured on a laboratory source, with (c) the detail of two resolved dips in the synchrotron measurements and (d) the corresponding unresolved dip in the laboratory-source measurements. I_{INT} is the total integrated counts at each point, divided by 100. Note the difference in ψ scale between the two parts of the figure.

the special characteristics of synchrotron radiation, most specifically the low divergence of the incident beam, on the simultaneous-diffraction events. Integrated intensity ψ-scans were collected on beamline 10A at the Photon Factory, Tsukuba, using the same $KMnF_3$ sample and DAC as for the laboratory-source measurements. Figure 3.6(a) shows one such scan and Figure 3.6(b) shows the same scan collected using the CAD-4 diffractometer, as already described. The dips in the scan obtained with the synchrotron beam are much deeper, and they are also narrower in ψ. The narrowness is further illustrated by the synchrotron measurements in Figure 3.6(c) which resolve the laboratory-source dip in Figure 3.6(d) into two dips only 0.1° apart. These differences in depth and width may be attributable to the absence of the K_α doublet in the synchrotron beam as well as the reduced beam divergence. Further work is required to check this using a laboratory source and a silicon monochromator.

Although it has been shown that simultaneous diffraction can have a dramatic effect on the intensity of a measured sample reflection, it has yet to be shown how many reflections in a measured data set are affected at the value of ψ , ψ_m, at which they are measured (usually that which minimises the cell absorption, see Chapter 2.6.1), and what effect these events will have on the final refined data. To investigate this, and to develop a data collection strategy to avoid simultaneous diffraction, a full data set was collected on the CAD-4 with each reflection being measured at three values of ψ at 0.5° intervals about ψ_m. In order to keep the length of the data collection the same, each of these reflections was collected for only one third of the time that a single reflection would be measured for in a normal data collection. This three-point scan allowed those reflections affected by simultaneous diffraction to be detected, and showed that the integrated intensity of about 20% of all reflections is reduced by more than two standard deviations at the measuring position in a data set collected to a $\sigma(I)/I$ of 3%. Since the average separation of the dips as a function of ψ is determined by the unit-cell dimensions of diamond, a similar result may be expected for any sample, irrespective of unit-cell dimensions.

The points at which the dips occur in a ψ scan appear to be pseudo-randomly distributed and so the main consequence of ignoring the effect maybe simply to reduce the precision of the derived information. However, there is evidence that higher-angle sample reflections are less affected. This is attributable to the

larger angular separation of the K_{α_1} and K_{α_2} reflections at high 2Θ (sample), which prevents them both being affected by the same strong (and, thus, low-2Θ) diamond reflection. To the extent that the average magnitude of dips decreases with increasing 2Θ, the thermal parameters of the sample will be underestimated. (A full account of the 2Θ-dependence also involves consideration of the way the diamond reflections pass through the reflection condition.)

In conclusion, it has been found that a previously unsuspected source of error, the reduction in the sample intensity due to simultaneous diffraction, can reduce the intensity of sample reflections by up to 50%, although a simple three-point measurement procedure allows affected reflections to be identified. However, this simultaneous diffraction process does not seem to be the cause for the reduction in data quality when using AgK_α radiation, a possible solution to which is considered in the next section.

3.2.3 The Use of Tungsten Gaskets

As discussed in the previous chapter, two of the major unsolved problems in collecting diffraction data from single-crystal samples in a DAC are (i) that in many cases the results obtained from refinement of the diffraction data get worse as the pressure is increased, and (ii) that the results are generally worse when using AgK_α radiation rather than MoK_α radiation. It is surprising that despite the large volume of work that has been put into single-crystal x-ray diffraction techniques, that no successful solution has been found to these problems to date. However, with the advantages that shorter wavelength radiation has (less absorption and higher real-space resolution), and the development of techniques for single-crystal diffraction on synchrotron sources which offer both high flux at short wavelengths and the possibility of obtaining higher pressures through the use of smaller crystals, a solution to these two problems has become ever more urgent. A possible solution to these problems is described in this section.

In order to determine what factors may lead to the reduction in data quality when using AgK_α radiation or when going to higher pressures, a list was made of those factors that vary on (a) changing from MoK_α radiation to AgK_α, and on (b) increasing the pressure in a DAC from atmospheric pressure to (say)

50kbars. The differences, as well as some factors which remained constant, are listed below.

(a) Changing from MoK_α to AgK_α

(1) The number of measurable reflections increases.
(2) The cell absorption decreases but is determined in the same way for both MoK_α and AgK_α radiation.
(3) The sample absorption decreases but is determined in the same way for both MoK_α and AgK_α radiation.
(4) The flux from a Ag-target x-ray tube is less than that from a Mo-target tube.
(5) The detector efficiency is less for AgK_α radiation than for MoK_α.
(6) There is a λ^3 dependence of the intensity diffracted from the sample. This term is smaller for AgK_α.
(7) The AgK_α characteristic lines lie on a higher white background than do the MoK_α lines, leading to a higher background.
(8) Penetration of the gasket by the AgK_α radiation is greater than for MoK_α due to the lower absorption of the gasket material. This will result is a higher background from the increased volume of beryllium illuminated on the detector side of the DAC.

(b) Increasing the Pressure

(1) The number of measurable reflections will decrease slightly as the reciprocal lattice expands.
(2) The cell absorption will remain constant.
(3) The gasket will occlude the sample more as the gasket hole shrinks as pressure is initially applied. However, the gasket hole will expand at still higher pressures when the gasket is unable to support the internal pressure. This will again lead to an increase in the illuminated volume of beryllium.
(4) The gasket between the diamonds will thin, leading to greater penetration of the gasket by the primary beam and an increase in the illuminated volume of beryllium, creating a higher background.

Analysing these two lists, it would seem that the cause of the decrease in data quality in both cases may be the same as that which causes diffraction data collected at high pressure to be poorer than that collected at atmospheric pres-

sure, that is, a decrease in the signal-to-noise ratio. In the case of using AgK_α radiation, this decrease is due both to a decrease in the signal ((a) 4, 5 and 6 above), despite a reduction in the DAC and sample absorption, and an increase in the noise ((a) 7 and 8), while on going to higher pressures, the reduction in the signal-to-noise ratio is due principally to an increase in the noise ((b) 3 and 4), the signal strength remaining essentially constant.

Although little can be done to increase the signal using a laboratory-based x-ray source (Ag-target tubes being required to run at a lower current than tubes with a Mo target), it was felt that gains could be made in reducing the noise, specifically the increase in the background that results from the increased penetration of the gasket material surrounding the pressure chamber, a problem present both when using AgK_α radiation ((a) 8) and when the gasket thins at high pressure ((b) 4).

As described earlier, the usual materials used for gaskets for structural studies are Inconel, a nickel alloy, and hardened stainless steel. These gaskets are then primarily composed of nickel, chromium and iron which have linear absorption coefficients of $415cm^{-1}$, $224cm^{-1}$ and $303cm^{-1}$ respectively for MoK_α radiation, and $215cm^{-1}$, $114cm^{-1}$ and $155cm^{-1}$ respectively for AgK_α. The reduction in absorption on moving from MoK_α to AgK_α is very obvious.

The use of tungsten as a gasket material would seem to offer several considerable advantages over those materials used at present.

(1) The absorption coefficient of tungsten for MoK_α is $1913cm^{-1}$, 6 times that of iron and more than 4 times that of nickel. Since the absorption of a material is determined by $\exp(-x\mu)$ where μ is the absorption coefficient and x is the pathlength in the material, the absorption of a tungsten gasket $100\mu m$ thick is more than 3,000,000 times that of nickel.

(2) The absorption coefficient of tungsten is still $1023cm^{-1}$ for AgK_α radiation, 5 times that of nickel at the same wavelength and 6 times that of iron. For a $100\mu m$ thick gasket, the absorption of tungsten is more than 3000 times that of nickel.

(3) Recent work by Katrusiak (1990) has shown that gaskets made from tungsten

deform less than those made from Inconel or stainless steel, leading to less occlusion at lower pressures and a smaller gasket hole at higher pressures, reducing the illuminated volume of beryllium.

In order to test the effect of the very much higher absorption of tungsten on the background from a Merrill-Bassett DAC, a series of 2Θ scans were made of the background using two different gaskets, Inconel and tungsten, and using MoK_α and AgK_α radiation.

The Inconel gasket, 250μm thick and with a gasket hole 250μm in diameter, was centred on the diamond of half a Merrill-Bassett DAC which was then mounted on a CAD-4 diffractometer employing MoK_α radiation (graphite monochromator). The half cell was mounted such that the Be plate and diamond anvil were on the detector side of the gasket. A series of 2Θ scans were made through the powder pattern resulting from the primary beam passing through the beryllium backing plate and the cell was then removed from the diffractometer and replaced by half of another Merrill-Bassett DAC containing a similar, although not identical, gasket made of tungsten. A series of 2Θ scans were then made through the powder pattern obtained when using this gasket. The x-ray tube was then replaced by a tube with a Ag target and the measurements for both gaskets were repeated for the shorter wavelength radiation.

Although it was attempted to keep the gasket dimensions the same for each different material used, this could not be ensured. Combined with the use of two different half-cells (due to diamond failure), and slightly different detector apertures for the MoK_α and AgK_α scans, no direct comparison is possible for the results obtained from the two different gaskets at the same wavelength. However, identical conditions were employed for the study of the same gasket using different wavelengths and a direct comparison of the effect of the change in wavelength for each gasket is possible.

Figure 3.7a shows the powder patterns obtained using MoK_α and AgK_α radiation with an Inconel gasket. Despite the lower flux from the Ag-target tube and the lower detector efficiency, it can be seen that the intensity of the beryllium powder lines is some 3 times higher in the case of the AgK_α radiation with a general increase in the background level of a similar magnitude. This sizable increase in the background level when using AgK_α radiation, coupled with the

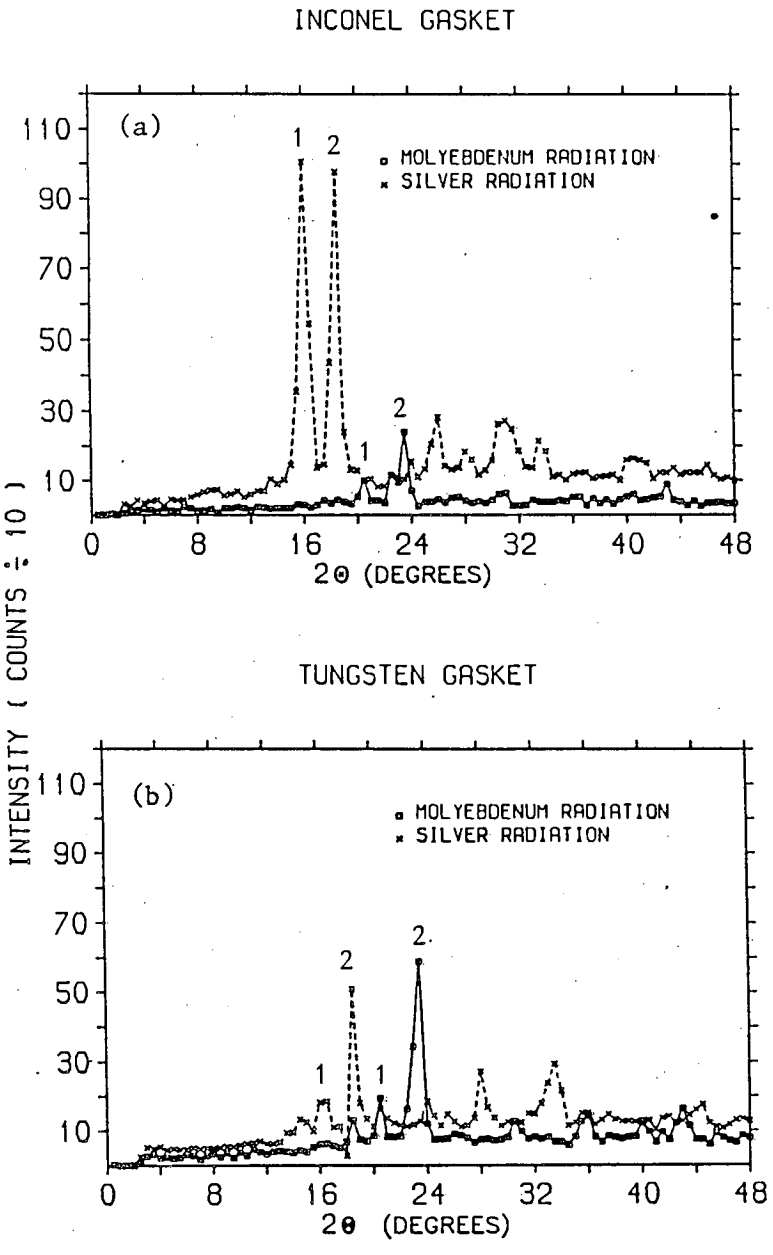

Figure 3.7: A 2Θ-scan through the powder pattern produced by the primary beam passing through the beryllium components of half a Merrill-Bassett DAC for (a) an Inconel gasket using MoK_α (□) and AgK_α (×) radiation, and (b) for a tungsten gasket using MoK_α (□) and AgK_α (×) radiation. The peaks labelled 1 and 2 in (a) and (b) are from the same group of reflections but are shifted in 2Θ by the use of different wavelengths. The differences in relative intensities of the peaks labelled 1 and 2 are not understood at present.

simultaneous decrease in the intensity of sample peaks, would seem a likely cause for the decrease in data quality generally observed on using wavelengths shorter than MoK_α.

Figure 3.7b shows the results of the 2Θ scans made of the cell using the tungsten gasket. In comparison to Figure 3.7a, the difference in the intensity of the powder peaks using the different wavelengths is reduced markedly, with their intensities being comparable. However, the background is still slightly higher in the case of the scan made using AgK_α, indicating that the use of a tungsten gasket may not completely solve the problems of using shorter wavelength radiation.

Although Figures 3.7a and 3.7b demonstrate the effectiveness of tungsten gaskets in reducing the background when using AgK_α radiation close to that when using MoK_α radiation, a considerable amount of work is still required to fully develop the use of tungsten gaskets. Tests, for example, are required to compare the background intensities obtained from identically prepared gaskets of Inconel and tungsten using identical scans, and to determine the dependence of the intensity of the background on the thickness of the gasket and the diameter of the gasket hole. Similarly, further work is required to understand the reasons for the different relative intensities of the powder lines (compare peaks 1 and 2 in Figure 3.7a for MoK_α and AgK_α). Although such a program of measurements is planned for the future, no such measurements have yet been made, the preference being to test the use of tungsten gaskets combined with AgK_α radiation in an actual structural study of a material of interest at pressures above 40kbars. Such a study, of $YBa_2Cu_4O_8$, is described in Chapter 5.

3.3 Single-Crystal Neutron-Diffraction

3.3.1 Introduction

Although, as discussed in Chapter 2.7, single-crystal neutron-diffraction at high pressures has already produced high-quality data with high real-space resolution, the results so far have mainly been derived from single layers of data or from two orthogonal layers of data collected from two different crystal mountings.

However, the recent development of the Ahsbahs cell with its transverse geometry heralds a major breakthrough in single-crystal neutron-diffraction techniques, a breakthrough almost comparable to that made by the introduction of the DAC in single-crystal x-ray studies, with the initial results from the cell (Kuhs *et al.* (1986)) indicating the very high quality of data, and subsequent refined structure, available using this cell. This section describes the cell and the new techniques that have been developed in order to use it for high-resolution ($\sin\Theta/\lambda > 1.0 \text{Å}^{-1}$) structural studies of H-bonded materials – the experimental results of which are presented in Chapter 4. As well as the development of the Ahsbahs cell and associated data collection techniques, development work has also been made on a clamp-type cell similar to that designed by Bloch *et al.* (1976) but which is designed for higher pressures and to present less restrictions on the number of measurable reflections. The application of a newly developed position-sensitive detector for single-crystal studies at high pressure is also described and the advantages and disadvantages for high-pressure structural work are discussed. All the work described was made using the D9 four-circle diffractometer and the D15 equi-inclinational diffractometer at the Institut Laue-Langevin (ILL), Grenoble.

3.3.2 Pressure Cell Development

Clamp Cell

Although the pressure cell designed by Bloch *et al.* (1976) has been used for several successful structural studies at the ILL at pressures up to 20kbars and temperatures down to 4K, this cell has several disadvantages.

(1) The geometry of the cell allows only one layer of reflections to be measured for any one crystal mounting.

(2) The three steel pillars around the outside of the cell obscure a considerable number of reflections in the single layer accessible. This is illustrated in Figure 3.8 which shows the *hk*0 reciprocal layer of reflections for KH_2PO_4. All those reflections lying in the shaded areas have either the incident or diffracted beam obscured by one of the three pillars and are thus not measurable.

(3) The Bloch cell used at the ILL is no longer able to reach pressures above 20kbars.

A new pressure cell has therefore been designed at the ILL in order to obtain pressures of up to 30kbars while doing away with the three steel pillars, so increasing the available data set. No attempt was made, however, to increase the aperture of the cell in order to allow further layers of data to be measured, indeed the aperture was initially decreased in order to provide additional support at the highest pressures. The cell is shown in Figure 3.9a and an enlarged cross-section is shown in Figure 3.9b. The pressure is produced by using the tungsten-carbide pistons to apply a force on the aluminium sample-can which contains a sample glued to an aluminium support pin surrounded by hydrostatic fluid. An alumina barrel surrounds the sample-can to support it while under pressure; the barrel is in turn supported by two thick steel bands. In each loading of the pressure cell, an NaCl crystal is glued to the sample crystal to act as a pressure calibrant, using the NaCl equation of state.

Initially, the cell was designed to work in two different configurations. For the first, the height of the window between the steel bands was 9mm and thus for a sample 3mm high, allowed a gap of 3mm at both the top and the bottom. This configuration was designed for studies up to 23kbars. For pressures up to 30kbars, the height of the window was reduced to only 5mm, placing great emphasis on the alignment of the sample in the window if the sample reflections were not to be occluded by the steel bands. For a perfectly-centred sample 2mm high and 2mm in diameter, this means only a 1.5mm clearance from the steel rings. As these rings have an outer diameter of 58mm, the reciprocal lattice plane to be measured has to be horizontal to within 2.8° to ensure that the high-angled reflections are not occluded. This compares to an alignment of 5.6° which would be required for a 3mm high sample in the 9mm high window. It should be noted, however, that these required alignment angles represent the ideal case of a perfectly-centred sample. In practice, both the height of the sample, and its alignment, change as pressure is applied, and a sample that is therefore well centred in the window at atmospheric pressure may become tipped and occluded at high pressure. For this reason, initial development work was done using the 23kbar arrangement as the alignment criterion was less severe, and the larger sample volume allowed the easier observation and measurement

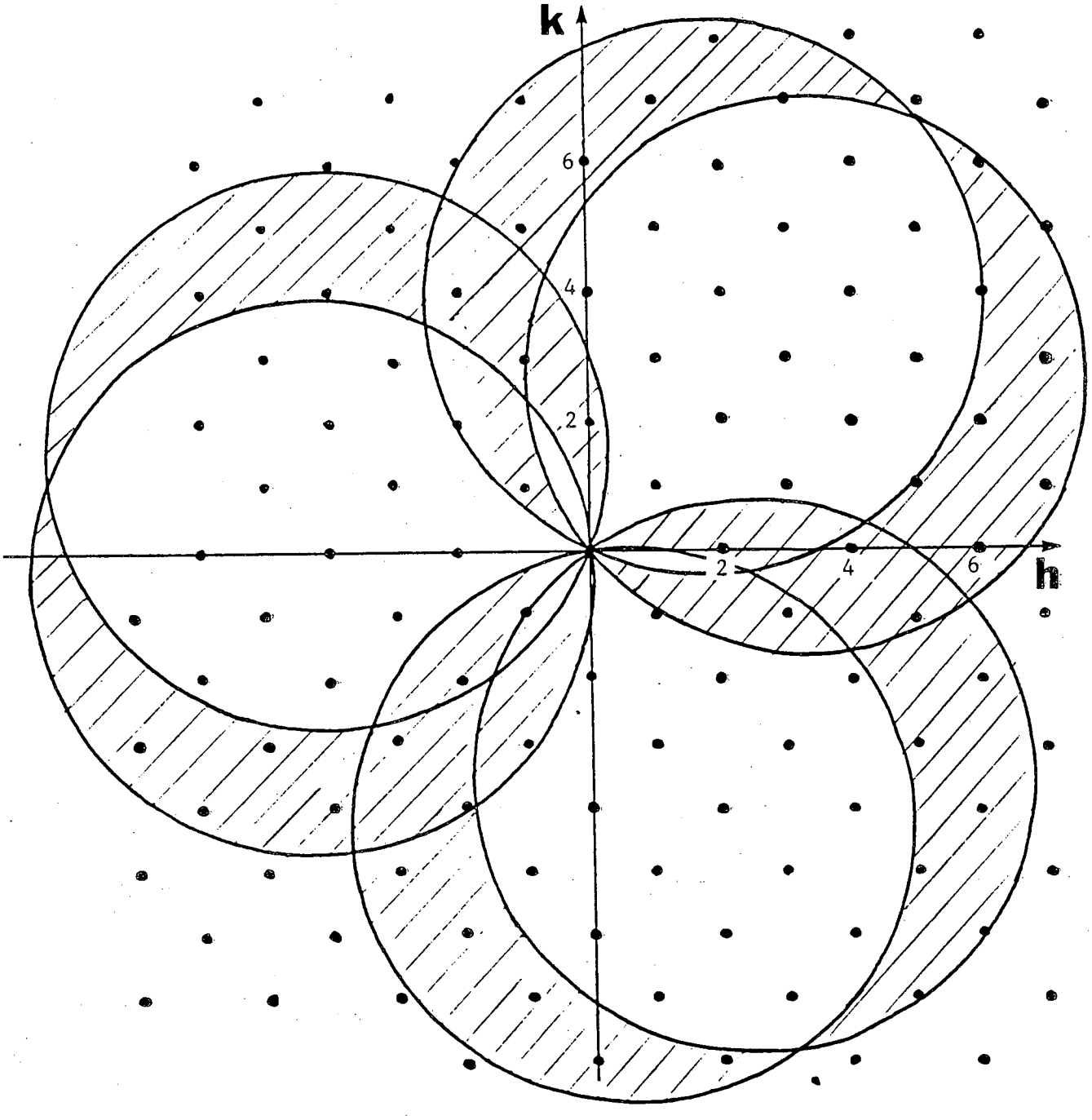

Figure 3.8: The $hk0$ reciprocal layer in KH_2PO_4. Those reflections in the shaded areas are occluded by the three supporting bolts of the Bloch *et al.* pressure cell.

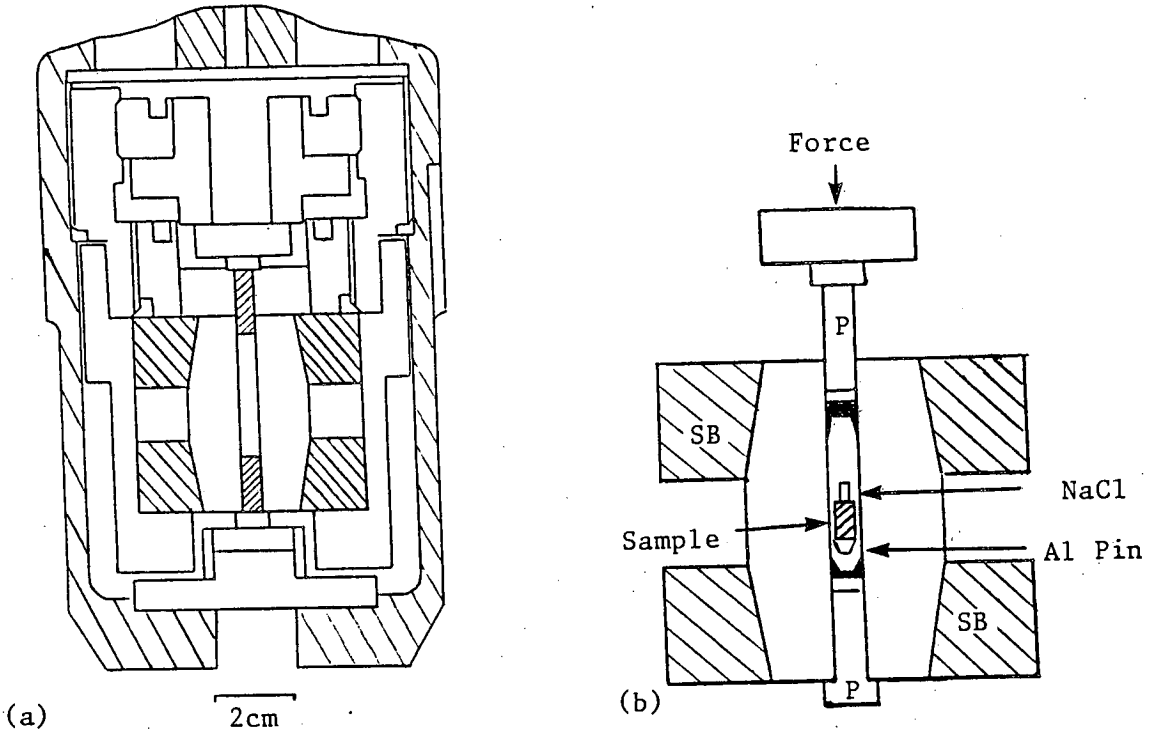

Figure 3.9: (a) A cross-section through the new ILL clamp-type pressure cell, and (b) a close up of the pressure chamber of alumina supported by two steel bands (SB). The sample is glued to an aluminium pin and a NaCl crystal is glued to the top of the sample crystal. The sample is placed in an aluminium sample can and surrounded by hydrostatic fluid. Pressure is applied by pressing down on the top piston (P).

of sample reflections.

In order to collect data with the new cell it was first necessary to determine the configuration of the lower piston with respect to the alumina barrel in order to place the sample accurately in the centre of the window between the steel bands. This was done at atmospheric pressure using a test crystal of NaCl for alignment purposes. The first sample crystals used in the new cell were KD_2PO_4 and $ND_4D_2PO_4$ and unfortunately all the crystals were crushed due to failure either of the pistons or of the sample cans. These results, however, identified several operational problems:

(1) The sample-can height was too great compared to the height of the alumina barrel and stood proud of the top of the alumina.

(2) The upper piston was not sufficiently well guided into the alumina barrel. This had two causes: the height of the sample can prevented the piston from being located inside the alumina barrel before pressure was applied to the cell and had therefore to be balanced on top of the sample can; no support was provided for the piston or for the upper plate which pushes down onto the piston. This meant that their alignment with respect to each other was poor and allowed a sideways load to be applied to the piston, causing it to shatter or to deform the sample can preferentially on one side.

(3) The pressure transmitting fluid was found to be an important factor in the successful loading of the cell. For studies below 20kbars, the preferred fluid was Fluorinert, a mixture of fluorinated hydrocarbons, due to its low compressibility compared to d-methanol, the other fluid normally used. However, Fluorinert becomes very viscous and non-hydrostatic above 18kbars. Another fluid tested was a 1:1 mixture of d-pentane:d-isopentane, but this was found to have too high a compressibility, resulting in the crushing of the sample-can before a pressure of 20kbars was reached. This problem of the most suitable pressure fluid has still to be solved. The necessary criteria for a good fluid are that it must be free of hydrogen (to eliminate incoherent scatter) and must be hydrostatic to 30kbars while at the same time being relatively incompressible.

(4) The frictional losses in the new cell were usually severe, although not as severe as in the old Bloch cell, resulting in a non-linear relationship between the

applied load to the cell and the resulting pressure. Attempts to overcome this problem were made by using sample cans made from Teflon; however, it was found that while applying pressure to the cell, the small aluminium support pin for the sample cut through the Teflon causing the sample can to rupture.

Subsequent redesigns of the pistons, alumina barrel and sample-can parts removed the problems with the sample-can height and upper piston alignment and have reduced the frictional losses. However, it has not been possible to reach pressures of 30kbars and the cell is now only used in the 23kbar configuration which allows pressures of 20kbars to be reached quite reliably. Further design modifications are in progress to allow pressures of 30kbars to be reached.

A final advantage of this new cell over the old Bloch cell was discovered during the first high-pressure low-temperature experiment using this cell. In a study of $NH_4H_2PO_4$, the pressure in the new cell was found to fall from 12kbars at room temperature to 8.5kbars on cooling to 130K. Although this requires that the pressure in the cell at room temperature be considerably higher than that required at low temperature in order to allow for the pressure loss on cooling, the pressure loss is considerably smaller than that found when using the Bloch cell. In an early attempt to study the quantum paraelectric state of KH_2PO_4 (Chapter 4.5) using the Bloch cell, the pressure was found to fall 9kbars on cooling from room temperature to 40K, most of the drop in pressure occurring in the first 150K. This very large loss of pressure on cooling, and the inability of the Bloch cell to reach pressures of 20kbars, severely limit the pressure-temperature field in which the old cell can operate. Although the new pressure cell also loses pressure on cooling, the pressure-temperature range available for structural studies is increased considerably. The study of the quantum-paraelectric state of KH_2PO_4 described in Chapter 4.5 was therefore only possible with the development of this new cell.

Ahsbahs Cell

Although the author was not personally involved in the design modifications made to the Ahsbahs cell during the current work, these modifications, which allowed the cell to be both heated and cooled, offering a temperature range of

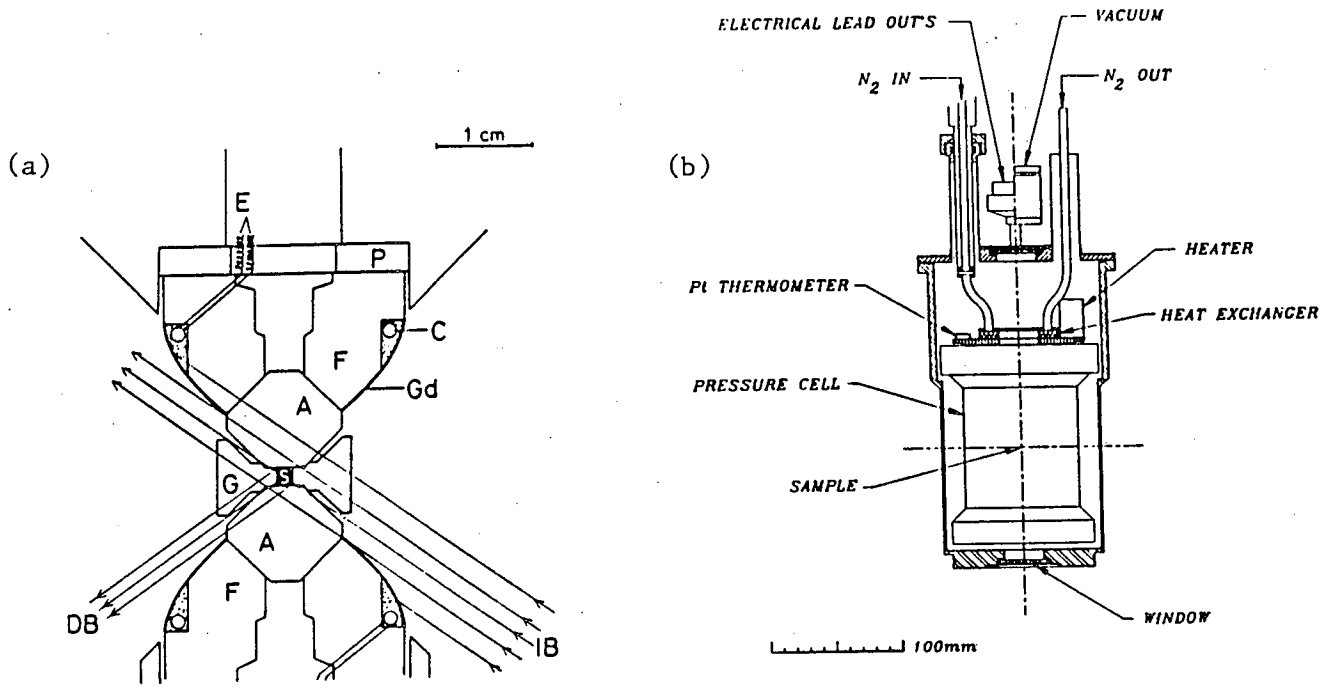

Figure 3.10: (a) Schematic drawing of the inner part of the high-temperature Ahsbahs cell. A –sapphire anvils, G –Ti-Zr gasket, S –sample, F –anvil seat, P –pyrophyllite disk, C –heating coil, E –electrical connections, Gd –gadolinium paint, IB –incident beam, DB –diffracted beam. (From Kuhs *et al.* (1989).) (b) A cross section through the cryostat used with the Ahsbahs cell.

350K to 150K, are described below.

High-Temperature Cell

Although the basic design features of this cell are the same as those for the original design as discussed by Ahsbahs (1984a,b), several improvements to the initial design now allow higher pressures to be reached and the ability to heat the sample (Kuhs *et al.* (1989)). The cell is shown in Figure 3.10a. The main alteration is in the design of the sapphire anvils with the use a double-conical shape which allows a smoother stress distribution within the anvil. The

sapphires are aligned such that their (001) axis is along the cylindrical axis of the cell within a few degrees. The gaskets, as described earlier, are made of a null-scattering Ti-Zr alloy and are machined such that the first contact with the sapphires on pressurising is with the conical region of the anvil which prevents cracking of the sapphires. The steel anvil seats are coated with highly absorbing gadolinium paint to avoid any parasitic scatter, and are thermally insulated from the rest of the cell by two pyrophyllite disks. Heat is applied to the sample by heating the steel anvil seats, and the temperature is measured by a thermocouple and controlled by a standard ILL temperature controller.

Low-Temperature Cell

The cryostat used to cool the pressure cell down to temperatures of 150K is shown in Figure 3.10b. The cell is cooled by N_2 gas which is cooled in liquid nitrogen before passing through the heat exchanger attached to the top of the pressure cell. The temperature is regulated by a heater attached near the heat exchanger and is again controlled by an ILL temperature controller. The temperature is measured with a Pt thermocouple. The outer shell of the cryostat has plexiglass windows to allow optical access to the sample for growing single crystals from the melt, or for pressure calibration using the ruby method.

3.3.3 The Use of a Small Position-Sensitive Detector for High-Pressure Structural Studies

Introduction

Although position-sensitive detectors (PSDs) have been used extensively for many years in powder-diffraction studies (Convert and Forsyth (1983)) or in the study of proteins where the large number of Bragg reflections requires the ability to measure many different reflections simultaneously (Convert and Forsyth (1983), Arndt (1985)), it is only very recently that such detectors have been used for single-crystal neutron-diffraction studies of samples with small unit cells (Lehmann *et al.* (1989)). These detectors have advantages in the study of twinned crystals or of samples that are poorly crystallised and in this section

the advantages that such detectors offer the study of single crystals under pressure are discussed. After first briefly introducing the basic design features of the detector, the following topics are discussed:

(1) Initial sample alignment.
(2) Reflection centering.
(3) Data collection and scan type.
(4) The separation of sample peaks and sapphire reflections.
(5) Calculation of the integrated intensity.

It should be emphasised at this point that the work described in this section has been developed to allow accurate high-resolution structural studies of complicated crystal structures at high pressure. The majority of the techniques have thus been developed to solve problems specifically associated with the collection of high-quality diffraction data from small sample crystals inside pressure cells and are therefore not in general use.

The Detector

The small two-dimensional PSD described in this section is now the standard detector on the D9 and D15 diffractometers at the ILL and have been described in detail elsewhere (Lehmann *et al.* (1989)). Therefore only a brief description will be given here.

The detector has a 32×32 pixel layout, which, with a typical sample to detector distance of 45cm and a 2×2mm^2 pixel size, results in an angular pixel size of 0.25°×0.25°. Since a typical Bragg reflection dimension at the detector is ~8mm this means that the reflection will cover several pixels in either direction. The detector gas is ^{3}He mixed with C_3H_8 and is enclosed in a heavily shielded cylinder of stainless steel. The detector efficiency at a wavelength of 0.8Å is 75%. In order that accurate integrated intensities should be measurable, the detector must be homogeneous in response. Tests have shown this to be the case with any deviations from homogeneity being within the statistical error.

Initial Sample Alignment

When a single-crystal sample is placed on a diffractometer the first step is to find sample reflections and correctly index them in order to determine the crystal orientation. This is straight-forward at atmospheric pressure where a large sample of probably known alignment is used, and so the sample peaks are easy to find. However, the initial alignment of the sample in a high-pressure experiment is somewhat more difficult. For the present work done on D15 using the new clamp cell described in Chapter 3.3.2, the samples were large, $3\times3\times3mm^3$, and their orientation was necessarily well known and finding the sample reflections was therefore relatively simple. This was not the case, however, for the work done using the Ahsbahs cell on D9. The samples in this case were much smaller, on the order of 0.5mm high and 1mm in diameter, and due to their cylindrical shape to maximise the sample volume in the gasket hole, only the crystal axis along the cylindrical axis of the cell was generally known. This, combined with the fact that the crystal structures studied on D9 were more complicated (monoclinic) than those studied on D15 (tetragonal), meant that their orientation was not generally known inside the pressure cell.

The determination of the crystal alignment was also made more difficult on D9 by the large number of reflections from the sapphire anvils of the pressure cell. Although these could usually be identified as sapphire reflections by their high intensity, this was not the case for those reflections arising from $\lambda/2$ and $\lambda/3$ components in the incident beam, these reflections being similar in intensity to those from the sample.

A final, and serious problem arose from the use of the PSD itself. The background count using the multidetector may be of the order of 500 counts/second because of the parasitic scatter from the pressure cell. Although this may seem very high, the total count is spread over the 1024 pixels of the detector and therefore amounts to an average countrate of only 0.5 counts/second in each pixel. Due to the small volume of the sample crystal, the sample peaks will be both small in size and low in intensity and may only have a maximum countrate of 50-100 counts/second. Although a countrate of this size would be very obvious on a single-detector, the 50-100 counts/second do not give a significant increase in the total countrate of the 1024 detector pixels, increasing it by only

10-20% in this case. It is thus very hard to see the effect of the sample reflection on the *total* countrate of the detector although examination of the countrate of the individual pixels makes the presence of the reflection obvious. This means that the standard peak-finding method of manually scanning the diffractometer angles while monitoring the countrate from the detector using a ratemeter, will, in general, be unable to distinguish sample reflections from fluctuations in the general high background of the detector. Although it is hoped in the future to be able to turn the PSD into a single-detector for finding reflections by 'switching off' those pixels outside the central region of the PSD, and thus make the finding of reflections from the sample in a pressure cell much easier, the software needed for this is still under development and the following technique has therefore been developed in order to determine the alignment of the sample.

(1) A list of reflection intensities for both the sample and the sapphires is produced and the strongest sample reflections with 2Θ angles less than the lowest-angle sapphire reflections are determined. Sample reflections lying along the cylindrical axis of the cell are omitted from this list as the $(00l)$ reflections from the sapphires lie along this direction and are very numerous due to the large c-axis lattice parameter of sapphire.

(2) A search is made for these strong sample reflections in the standard manner by slowly scanning the diffractometer angles while monitoring the total countrate from the PSD. If the alignment of the sample crystal is partially known then it may be possible to find sample reflections quite quickly using this method. Although there should be no sapphire reflections at these low 2θ angles, reflections from the $\lambda/2$ and $\lambda/3$ components of the neutron beam will be present. These are distinguished from sample reflections by slowly shielding first one sapphire and then the other from the incident beam with a piece of highly-absorbing cadmium and determining where the intensity of the found reflection begins to fall. If the intensity falls before the cadmium fully shields one of the sapphires then the reflection comes from that anvil and can be rejected as a sample reflection. Filters to reduce the $\lambda/2$ component in the incident beam are used during this process and are highly recommended.

(3) If sample reflections cannot be found by hand, then the searching process is put under computer control. A series of stepped scans through reciprocal space

are made with a stationary count for 60 seconds at each step. The step size of the scans is chosen to be small enough such that any reflection will show up on two or three successive steps and therefore allows reflections to be distinguished from merely statistical fluctuations. Once a reflection is found, then sample and sapphire reflections are distinguished as in (2) above. This method, although eventually finding sample reflections, is very slow and may take 12 hours to find enough sample reflections to refine an orientation matrix.

Reflection Centering

In order to determine if the sample is well centred on the diffractometer, and to measure the lattice parameters of the sample once it is well centred, it is necessary to determine accurately the centre of a number of sample reflections. Although the centering of sample reflections may be done using a standard single-detector, the process is very slow in high-pressure studies as the low intensity of the sample reflections requires long counting times in order to accurately determine the position of the peak maximum. The speed of this centering process, however, is greatly increased by the use of the PSD because whereas the single-detector must make an iterative series of scans through the ω, χ and 2Θ diffraction angles in order to determine the position at which the maximum of intensity goes through the detector aperture, in the case of the PSD only the ω angle with the maximum intensity need be determined, with the other angles being determined by the location of the detector pixel with the maximum intensity at that ω. Thus only two scans, a course ω scan and a fine ω scan, are required for the PSD, resulting in a much faster determination of the peak centres. The saving in time using the PSD may be crucial if many orientation matrices or cell parameters need to be determined during the course of an experiment – monitoring the pressure by using the NaCl equation of state while cooling the pressure cell for example.

Data Collection and Scan Type

The use of a PSD rather than a single-detector offers considerable advantages to the collection of diffraction data and these advantages are very pronounced in the

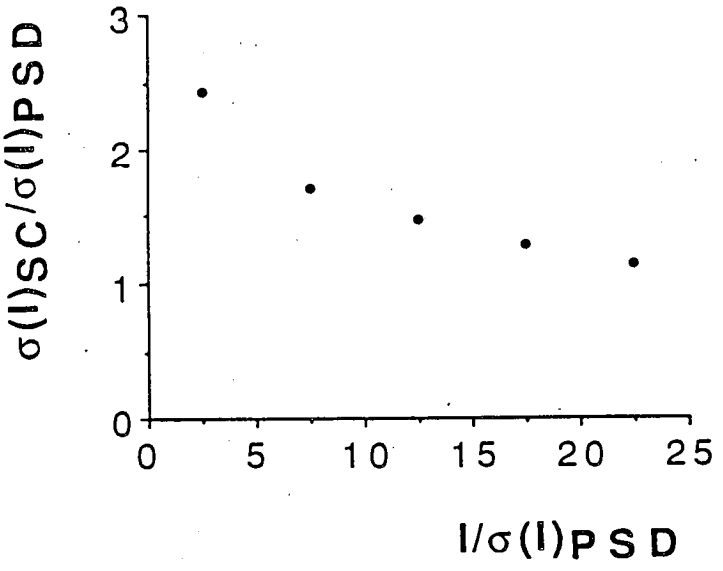

Figure 3.11: The ratio of the estimated standard deviation, σ(I), for two sets of data recorded on ice VI at high pressure, versus the strength of the reflection, expressed as I/σ(I). SC stands for single detector, while PSD stands for the two-dimensional detector. (From Lehmann *et al.* (1989).)

study of samples at high pressure. This is best illustrated by a study of an H_2O ice VI single crystal at 8.5kbars and 281K where identical data sets were collected with a PSD and with a single-detector and the results compared (Lehmann *et al.* (1989)). It was found that the PSD gave a considerable improvement in the precision with which data could be collected. This is shown in Figure 3.11, where the ratio of the errors from the two detectors is plotted against the I/σ(I) ratio for the PSD. It can be seen that for the weaker sample reflections the use of the PSD resulted in an improvement by a factor of 2.5 in the precision with which they could be measured. This improved determination of weak peaks is essential for high-pressure studies using small samples, especially if data is to be collected to high angles, and it is certain that the high-pressure structural study of $PbDPO_4$ described in Chapter 4.3 would not have been possible without the use of the PSD.

The PSD also allows the use of ω scans to collect the diffraction data rather than the more usual ω-2Θ scans. This is because the detector area is large enough to accept the full Bragg peak as it moves across the detector during a scan. As discussed in Chapter 2.6.2, the use of ω scans has considerable advantages

for high-pressure studies as it allows scans to be made along parasitic powder lines rather than across them. Although the background on the two-dimensional detector surface is no longer flat for an ω scan, but rather the powder line can be observed as a ridge of intensity, a background correction can be made to the sample reflection based on the background outside of the peak. However, although all data collected with the PSD in the present work was collected with ω scans, the necessary software for correcting for powder lines has not yet been fully developed although some preliminary work has been done on the problem. Some of the collected diffraction data had therefore to be rejected due to severe contamination.

The Separation of Sample and Sapphire Reflections

Although techniques have been developed to avoid measuring those sample reflections which are affected by diamond-anvil reflections when using x-ray diffraction techniques and a DAC (Denner *et al.* (1977)), the techniques have yet to be employed for studies using the Ahsbahs cell. There are two reasons for this.

(1) The large amount of data available means that, in general, symmetry equivalent reflections are measured for each reflection. If one of these these reflections is affected by sapphire reflection and rejected, the other equivalents allow that reflection still to be used for subsequent analysis.

(2) The determination of the orientation matrices for both sapphires requires the use of valuable experimental time.

It is, however, obviously better to measure as few reflections as possible which must later be rejected, and to spend the time more profitably on unaffected reflections. The number of reflections that *are* badly affected by sapphire reflections is considerably less when using the PSD than when using a single-detector, due to the unambiguous spatial separation of the sample and sapphire reflections. Figure 3.12 shows the $(1\bar{2}\bar{3})$ reflection from the study of $PbDPO_4$ described in Chapter 4.3 and illustrates the three-dimensional (3-D) separation of the sample reflection in the centre of the scan and the sapphire reflection at the edge of the scan. This 3-D separation allows the intensity of the sample reflections to be

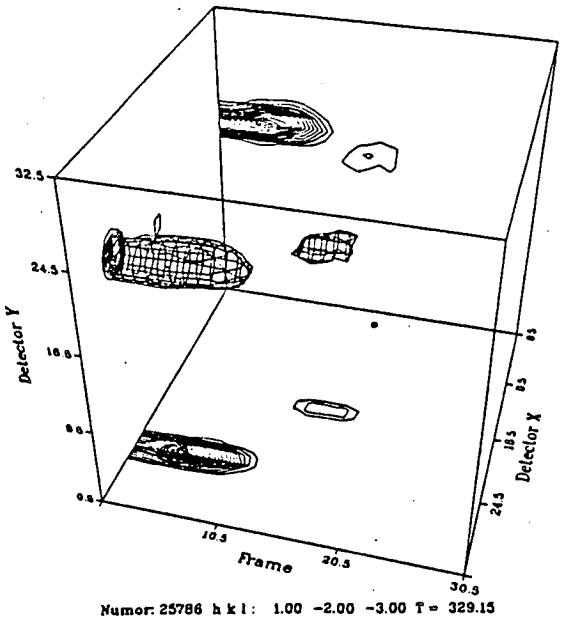

Figure 3.12: A 3-D representation of the scan through the $1\bar{2}\bar{3}$ reflection from $PbDPO_4$ at 13.8kbars and 330K. The axes are the scan-step in ω (frame), and the horizontal (X) and vertical (Y) detector axes. The reflection at the centre of the scan (in X, Y and ω) is from the sample, while the off-set reflection is from one of the sapphire anvils.

determined even though there is a sapphire refection in the same scan, resulting in far fewer rejected reflections. More than 30% of reflections that would be rejected when using a single-detector can be recovered in this way (Lehmann *et al.* (1989)).

Calculation of the Integrated Intensity

Although the determination of the integrated intensity from a one-dimensional profile of scan-angle versus intensity is simple and well understood, the determination of the intensity from a 3-D array of counts as a function of angle and the position (X,Y) on the PSD is more difficult and complex. The method used for the PSD (Wilkinson *et al.* (1988)) is based on the minimum $\sigma(I)/I$ method of Lehmann and Larson (1974) and describes the reflection boundary by an ellipsoid. The precision of the weak reflections is optimised by using peak shapes determined from the strong reflections with similar 2Θ angles, increasing

the signal-to-noise ratio for these reflections. However, this technique requires that a 'library' of strong reflection peakshapes exist up to the highest 2Θ angle required. Although this is not a problem for standard crystallographic studies using the PSD, for high-pressure structural studies with small crystals, and indeed for very high resolution studies at atmospheric pressure, a problem arises in that it is not possible to find suitably intense reflections at the highest angles in order to determine the peakshape accurately. It is therefore not possible to accurately determine the integrated intensities of high-angled weak reflections. Three possible solutions to this problem have been developed.

(1) The strongest reflections at high angles are remeasured until the reflection acquires the necessary precision to be defined as 'strong' and to have an accurately determined peakshape.

(2) The peakshape parameters used to describe the defining ellipsoids at low angles are extrapolated to determine peakshapes at higher angles.

(3) *All* measured reflections within, say, a 5° interval in 2Θ are superimposed in order to define a 'strong' reflection for that range of 2Θ angles from which a peakshape can be determined.

Although the first method can be used to moderately high angles, the counting time required at still greater angles becomes prohibitively long and the second technique has therefore been used for the work described in this thesis. Great care, however, had to be taken when using this method as the integrating volume, and therefore the integrated intensity, is very sensitive to the values of the extrapolated peakshape parameters. The third method described above, although tried, still requires additional software developments to be fully implemented but will probably prove to be the best method for determining peakshapes in the future.

The method used to determine the integrated intensity does, however, have an advantage over the single-detector in determining precise lattice constants. When determining the peakshapes for the 'strong' reflections, the position of the centre of each strong peak is written to a file. This file of accurately determined reflection centres, all of which are determined during data collection, can be used to refine the orientation matrix and, more importantly, the lattice parameters.

This has two advantages.

(1) Least-squares refinement of the lattice parameters can be based on the positions of 200 or more reflections, giving very precise values.

(2) Comparison of the *calculated* position of the centre of a strong reflection (using the calculated orientation matrix) and the *measured* position (determined by the integration procedure) allows those off-centre strong reflections, i.e. sapphire reflections, to be determined. This procedure will indicate sapphire reflections that are off-centred in either ω or pixel number (X,Y) which may not have been noticed earlier.

Thus, despite the problems of initially determining the alignment of the sample, in correcting sample reflections for powder lines, and in determining the peakshape parameters for weak reflections at high angles, the use of a PSD for high-pressure single-crystal neutron-diffraction experiments allows considerable improvements to be made in the quality of the data measurable. The improved signal-to-noise ratio for weak reflections and improved sample-sapphire discrimination, fully optimise the limited experimental time available for neutron-diffraction studies and, with the future development of suitable software, the three present problems associated with the use of a PSD for high-pressure studies will soon be removed. It should be reemphasised at this point that none of these problems exist for general structural studies at atmospheric pressure and the software developments presently in progress have come about through the present work. These improvements, however, will have advantages outside of high-pressure studies, with the improved peak-finding methods applicable to the use of any small or weakly scattering sample, and the ability to determine peakshapes at high angles having application to both very high resolution and very high temperature studies, both of which will have weak reflections at high angles.

3.3.4 An Optimised Data Collection Strategy

Introduction

For single-crystal studies using a DAC on a laboratory-based x-ray source, the limited number of reflections measurable, and the lack of time constraints, allows the measurement, and possibly remeasurement, of *all* reflections to high precision. However, when using central x-ray or neutron facilities, the experimental time is severely limited and it is essential to make the maximum use of the time available through optimised data collection strategies. This section describes such a strategy developed by the author and Dr. R.O. Piltz of this department for high-pressure single-crystal neutron-diffraction studies on the D9 and D15 diffractometers, as well as for very high resolution ($\sin\Theta/\lambda > 1.4\text{Å}^{-1}$) neutron-diffraction studies at atmospheric pressure. Although developed for neutron-diffraction studies, the techniques are applicable, for example, to x-ray structural studies on synchrotrons where experimental time can also be expected to be severely limited.

Data Collection Strategy

One of the main experimental problems posed by the use of the Ahsbahs cell for high-resolution studies was that although there were many reflections that could be measured, their low intensity and the limited experimental time prevented measurement of them all. It was therefore necessary to determine a strategy that would allow the required structural information to be measured with sufficient precision in the time available. The following method was developed.

At low 2Θ angles all reflections from the sample are measured. This allows a correct determination of the scale and anisotropic extinction parameters, and the measurement of the maximum number of symmetry equivalent reflections allows a check to be made for effects such as occlusion, absorption, and very anisotropic extinction, all of which should be visible as causing differences in the intensities of equivalent reflections. This phase of the data collection usually takes 2-3 days and the upper 2Θ limit, and the scan speed used to measure the reflections, are balanced against each other in order to allow the data to be collected in this

time. At this stage it is essential that the integrated intensities of reflections are calculated and compared as soon as possible in order to allow any problems to be spotted early and rectified with the minimal loss of experimental time.

Once the full sphere of data has been collected and reduced to integrated intensities, initial refinement of scale, extinction and perhaps atomic coordinates can begin. Other parameters, such as those describing anisotropic thermal motion, are held fixed at their atmospheric pressure values at this point.

In the next stage of the data collection, only a portion of reciprocal space that contains two symmetry equivalents is measured, allowing each reflection to be checked for the effects of contamination by parasitic scatter. The data at this stage are also collected at a slower rate than that used at lower angles as the reflections will, in general, be weaker. The data are reduced to integrated intensities, and the refinements continually upgraded, while reflections are still being measured. Refinements at this stage will include anisotropic thermal parameters although some parameters may still be too highly correlated to be refined freely and must wait for the collection of higher angled data. However, at this stage, the basic structure should have been determined and this is essential for the collection of the highest-angle data.

At high 2Θ angles, the sample reflections are very numerous and, on the whole, weak and it is therefore not possible to collect all reflections with the slow scan speed that each requires. The data collection for these reflections is then based on the fact that all reflections do not contain the same amount of structural information, and that only those reflections that are sensitive to the required structural information, plus a general selection of other reflections to avoid any bias in the final refined structure, need be measured. It is therefore important to determine those details of the structure which are of the most interest – atomic coordinates, bondlengths, structural details that allow a distinction between two different structural models – and then to determine which of the reflections *still to be measured* have intensities that are sensitive to the required structural information. In order to identify these important reflections their intensity must first be determined. This is calculated using the refinement of the data collected to this point as follows.

The reflections still to be measured, hereafter 'non-measured reflections', are all

assigned very low intensities with large esd's and are made into a file identical in format to that used to input measured reflections for refinement. This file is then appended to the file of measured reflections and all the non-measured reflections are flagged as 'weak' while those reflections that *have* been measured are flagged 'strong'. The data are then refined such that 'weak' reflections are not included in the refinement (and therefore the refinement proceeds as if the non-measured reflections were not present), but only have their structure factors calculated once the refinement has fully converged. This process thus calculates the structure factors for the non-measured reflections based on the structure refined from the measured reflections, and the predicted structure factors can simply be upgraded as further data is collected.

At this point, those non-measured reflections with predicted intensities (squared structure factors) which are large enough to allow them to be measured to a precision of $I/\sigma(I)$>3-4 in a reasonable time are sorted to a file to be measured. Although only the intensity, and not the esd, of non-measured reflections is predicted at this point, the latter can be obtained by comparison with measured reflections with the same intensity and by taking into account the relative counting times. The measurement of this group of reflections allows the precision of all structural parameters to be improved through the collection of a general set of high-angled data, and also prevents bias in the final structure which may be brought about by the measurement of only a few highly-selective reflections. In order to determine these sensitive reflections two methods have been used.

(1) The structure factors of the non-measured reflections are predicted from the refined data using the above method. All the structural parameters are then fixed at their final refined values. The structural parameter of interest – atomic coordinate, thermal parameter, occupancy – is then changed by 5 or 10 times its esd, fixed at this value, and a list of structure factors calculated for the non-measured reflections. Comparison of the two lists of structure factors will show those non-measured reflections whose intensity is most sensitive to the change made in the structure. In determining which of the sensitive reflections to measure, the probable precision with which that reflection will be measured must be taken into account. It is the author's experience that it is the weaker reflections which show the largest percentage change in intensity, but that the esd of these reflections will be far larger than the magnitude of the change. Those

reflections that should be measured, therefore, are those in which the change in intensity is comparable with their expected esd.

(2) After the structure factors for the non-measured reflections have been predicted using the refined data, the structural parameter of interest is again changed by 5-10 esd's and then fixed. However, the rest of the parameters are allowed to refine freely and another list of structure factors are thus calculated with the one parameter fixed. Comparison of the two lists of structure factors will show reflections with shifts in calculated intensity that are due to the change in the value of the fixed parameter but which cannot be eliminated by the refinement of all the other parameters. As for the first technique, the reflections to be measured should be chosen for their shift in intensity as a fraction of their esd.

A comparison between the two techniques shows that the sensitive reflections indicated by each are the same although, as might be expected, they differ in the predicted shift in intensity. It is not clear at present which method gives the most accurate predictions and more work is required in this area.

While these sensitive high-angled data are being collected, the refined structure is continually upgraded, allowing a continual monitoring of the most sensitive reflections to the required structural information. The above techniques also allow the determination of which *measured* reflections are most sensitive to specific structural details, and as these reflections already have both measured intensities and esd's, it is simpler to decide which reflections to remeasure, and for how long.

Very recently the determination of which measured reflections are most sensitive to the structural details of interest has been made using a program written by Dr. L.W. Finger (Hazen and Finger (1989)) based on the ideas of 'Leverage' put forward by Prince and Nicholson (1985). This program, now incorporated into the least-squares refinement program of the PROMETHEUS suite of crystallographic programs (Zucker *et al.* 1983)) by Dr. R.O. Piltz, calculates the partial derivative of the calculated intensity of a reflection with respect to each of the refined structural parameters, and then calculates the percentage decrease in the esd of each parameter if that reflection were to be remeasured to the same precision. The program thus offers a very simple method of determining which

reflections should be remeasured, and to what precision, in order to increase the precision of the required structural information. The program, however, has only been used to calculate which *measured* reflections should be remeasured rather than to determine sensitive reflections that have still to be measured. Work is in progress to use the program for prediction purposes and will involve calculation of not only the intensity of high angled reflections but also a sensible esd.

The programs to allow this process of prediction, refinement and comparison have now been fully incorporated into the PROMETHEUS suite of programs used both at the ILL and in this department. All comparisons of intensities are performed by the computer using the binary output files produced by the refinement program and the comparison of the intensities of many hundreds of reflections takes only a few seconds. *All* single-crystal structural studies made by members of this department, both on in-house x-ray equipment and at external neutron sources, now use this system of programs, which allow the maximum use of experimental time in determining the required structural details.

3.4 X-ray Powder-Diffraction

3.4.1 Introduction

As discussed earlier in Chapter 2.4, the use of monochromatic angle-dispersive x-ray powder-diffraction (ADXRD) techniques for solving crystal structures at high pressure was used very rarely prior to 1987 as the sample volume available when using a DAC is too small to enable the necessary degree of orientational averaging needed in the powder sample to allow the determination of accurate relative intensities. However, very recently, structure determination from high-pressure x-ray powder-diffraction data has been successfully pioneered at the Photon Factory (PF) in Japan using a new type of area detector, an imaging plate (IP), which has allowed the determination of the structure of polycrystalline Br_2 to 800kbars (Fujii *et al.* (1989)) with esd's on the refined positional parameters of ± 0.0005. This is a remarkable achievement, and offers a new, and very precise, method of determining crystal structures to very high pressures for

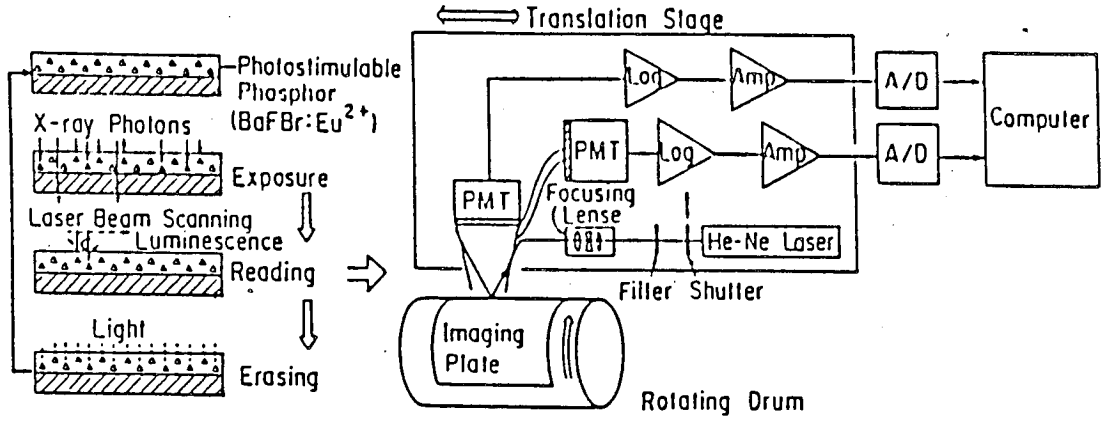

Figure 3.13: Schematic diagram of the Photon Factory imaging plate system.

the first time, finally allowing structural studies in areas that have hitherto only been accessible to spectroscopic or energy-dispersive diffraction techniques. In this section, the IP system developed at the PF is described, and the advantages that such a system offers for precise structural studies to very high pressures will be discussed. Also discussed will be the present project the author is involved in of developing an IP system for use at the Synchrotron Radiation Source at the Daresbury Laboratory. As this work has just started, and no experimental data has yet been collected, the discussion here is limited to the necessary future developments of the system in order to improve upon the Japanese work to date.

3.4.2 The Use of an Imaging Plate in High-Pressure Powder-Diffraction Studies

Figure 3.13 is taken from the 1988 Annual Report of the Photon Factory and shows, schematically, how the Imaging Plate system installed there 'works' and how the plate is read. The plate itself is a flexible plastic sheet $20\times25cm^2$ covered in photostimulable $BaFBr:Eu^{2+}$ phosphor. X-rays incident on the plate create trapped electron states which are stabilised by the Br vacancies. For a phosphor coat $150\mu m$ thick, the x-ray absorption is 100% for wavelengths greater than 1Å and is still 70% for a wavelength of 0.5%. After exposure, the plate is placed in a reader which rasters the plate with a focussed He-Ne laser. This causes the trapped electrons to decay, emitting photons at a wavelength (390nm)

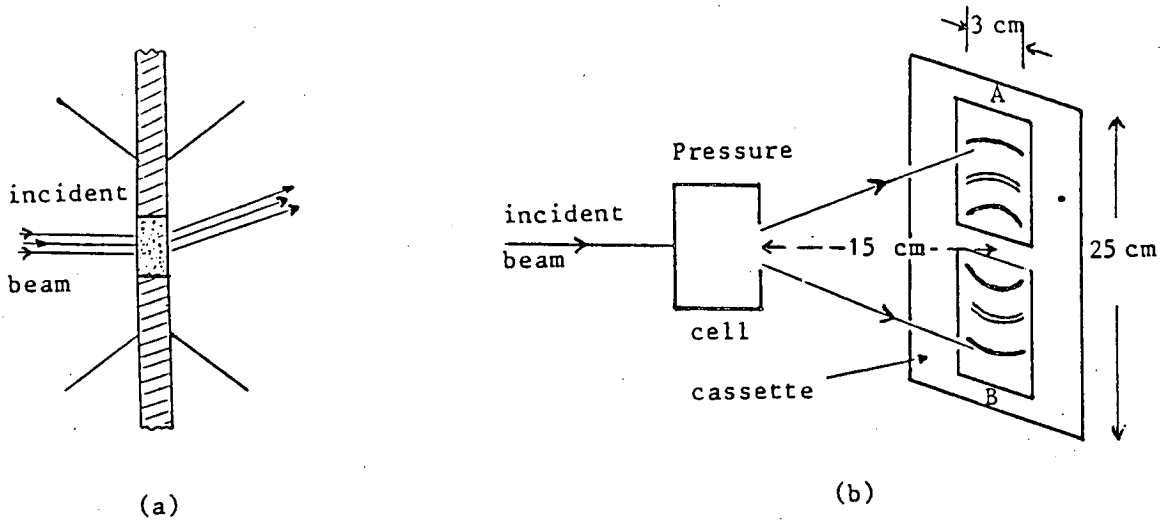

Figure 3.14: (a) The sample chamber of the DAC; (b)the pressure cell and imaging-plate detector set up to record a high-pressure powder pattern.

sufficiently far from that of the laser to be detected with high efficiency by a photomultiplier. The efficiency of this process as an x-ray detector is some 30 times that of standard x-ray film. In the PF system shown, the laser gives a pixel size of $100\times100\mu m^2$ and the imaging plate has a dynamic range of 10^4-10^5 (some 100 times that of film) while the very low intrinsic noise level of the imaging plate is some 300 times smaller than the intrinsic chemical fog of x-ray film.

The plates have an image half-life of approximately 16 days with the main degradation coming from incident cosmic rays which cause saturation within an area smaller than a single pixel and thus appear as spikes in the readout. In the PF system shown, it takes 3 minutes to read the plate and store the digitised image in 2000×2500 pixels. The plates can be used up to 1000 times.

The combination of high efficiency, very large dynamic range and very low intrinsic noise makes the imaging plate an ideal detector for high-pressure powder-diffraction experiments and offers considerable gains to be made when using monochromatic ADXRD techniques, the experimental setup for which is shown in Figure 3.14. The finely-ground sample is enclosed between the diamonds of a DAC and is some $100\mu m$ in diameter and $50\mu m$ thick at high pressure. This

small sample volume emphasises the need for the very intense and collimated radiation available from a synchrotron. The imaging plate, held in a flat cassette, is positioned to collect the diffraction pattern at a distance of ~15cm from the pressure cell. The diffraction pattern itself consists of a strip containing a portion of each Debye-Scherrer ring, the shape of the strip being determined by the shape of the exit window on the pressure cell. By recording a substantial portion of each powder ring, and integrating along it, the signal is greatly enhanced compared to that available using a one-dimensional detector. This integrating procedure also averages out small inhomogeneities in the sample pattern, greatly improving the powder average, while also giving a much better determination of the true background level. To obtain integrated intensities for structure refinement, a gaussian function is fitted to each individual peak by least-squares, thus deriving the peak position and integrated intensity. The peak positions are then converted to d-spacings using the sample-to-plate distance obtained from a calibration run with a standard, such as Si. The use of this integrating procedure, combined with the high efficiency and low background of the system and the use of synchrotron radiation, have made it possible to extend crystal structure determination to high pressures using ADXRD techniques. The availability of this technique offers many advantages for high-pressure structural studies.

(1) The use of powder-based techniques allows samples that cannot be grown as single crystals to be studied. Structural studies of phases which occur after a strongly first-order phase transition that would cause single crystals to shatter can also be studied.

(2) X-ray powder patterns have been collected using energy-dispersive techniques to pressures in excess of 2Mbars. ADXRD techniques may allow full structures to be refined at these extremely high pressures.

(3) The use of high-intensity synchrotrons allows powder patterns to be collected in only a few hours, enabling many diffraction patterns to be collected in a limited amount of experimental time.

The high-pressure powder-diffraction system using the imaging plate at the Photon Factory is the only operating system in the world and the description of the techniques above thus represents the current state-of-the-art in this field. However, the imaging plate, with its ability to measure very high quality data, merits

more sophisticated data analysis techniques than those presently employed at the Photon Factory, and the current project on developing an imaging plate system to allow Rietveld refinement of the diffraction pattern is discussed in the next section.

3.4.3 The Development of the Edinburgh Imaging Plate

As discussed above, this project has only just commenced with the imaging plate system having only been recently purchased. Despite this, and the fact that no high-pressure diffraction data have yet been collected, considerable effort has been devoted to ideas for the future development of the system with the aim of refining full crystal structures to very high pressures at the Daresbury Laboratory. The proposed developments are discussed here.

The main development will be the implementation of full Rietveld techniques to the refinement of the diffraction data. As discussed above, the present practice at the Photon Factory is to fit a gaussian function to each peak in order to extract the integrated intensity; however, this technique makes no attempt to fit overlapping peaks and although sufficient for studies of simple systems such as Br_2, which has few refineable parameters, the method is not generally sufficient for more complex systems. The use of the Rietveld technique will allow an accurate determination of integrated intensities and peak positions, allowing the precise determination of structural details. Development of the Rietveld method, though, will require numerous technique and software developments to overcome the present limitations of the Photon Factory system.

For Rietveld refinement it is essential that the line shape of each peak is constant and that it can be modelled accurately. The use of a flat plate to detect the diffraction pattern will cause the width of the peaks to vary at higher 2Θ angles and although this can be solved by the use of a curved detector plate, it is then essential that the plate remains a constant distance from the sample as a function of 2Θ. The width of the peaks will also be affected by misalignments of a flat detector plate which if not accurately perpendicular to the incident beam, will cause the powder rings to depart from being true circles. Subsequent integration around the rings on the assumption that the rings *are* circular will

result in broadened peaks and an altered line shape.

More work is needed on the integration process itself. Initial tests have shown that it is not easy to determine the true centre of the powder rings (determined at the Photon Factory by allowing the attenuated primary beam to fall onto the plate) and this will affect the integration process. A more general method may therefore be needed. It would also be preferable to have the diffraction pattern intensity determined as a function of 2Θ rather than pixel number and it is hoped to adapt the present integration method to achieve this. The integrating procedure must also be adapted to deal with strong spots arising from diamond-anvil reflections or cosmic rays, omitting them from the integrated profile.

A series of corrections will also have to be applied to the data in order to obtain accurate relative intensities. The polarisation factor varies strongly away from the vertical median line (AB in Figure 3.14b) due to the polarisation of the synchrotron beam, and must be corrected for. Corrections must also be applied for pressure cell and sample absorption, and also for the absorption factor of the imaging plate at higher 2Θ angles (due to the increasing pathlength of the diffracted beam through the phosphor coating).

Although careful sample preparation coupled with integration of the powder lines overcomes preferred orientation of the type that shows up as a variation in intensity around a powder ring, there may still be problems with preferred crystallite orientation with respect to the cell axis, i.e. elongated crystallites tending to align more along the cell axis than perpendicular to it. This will affect the intensity of a whole powder ring rather than vary the intensity around it and is one of the limits on the accuracy of the high-pressure results. It is intended to investigate this problem by recording the same powder rings at different 2Θ angles using different wavelengths, and anticipate that this will yield enough information to characterise any significant axial preferred orientation.

Improvements of these kind will allow an accurate diffraction profile to be obtained containing true relative integrated intensities suitable for Rietveld refinement. Initial tests with the system on the 9.1 powder-diffraction station at the Daresbury Laboratory using a Si sample have also indicated that the line width available is comparable with that obtainable using a standard one-dimensional PSD and thus offers the possibility of *ab initio* unit cell indexing

of unknown structures. Combined with the ability to use direct methods on powder-diffraction data for structure solution, the use of the imaging plate system for high-pressure powder diffraction may allow the accurate determination of the structures of newly discovered phases to pressures of 1-2Mbars, a goal though impossible until a year ago, but which now has to be accepted as challenging, but obtainable.

3.5 Neutron Powder-Diffraction

3.5.1 Introduction

The upper pressure limit for structure determinations using neutron powder-diffraction techniques has been limited to 20-30kbars since the late 1960's because of the large, 10 to 100 mm^3, samples needed. These large samples, and the correspondingly larger forces required in order to apply the pressure, have resulted is massive pressure cell construction with limited angular access for the incident and diffracted beams and high background scatter. The use of a 90° scattering geometry when using a pulsed neutron source has eliminated a lot of the problems associated with high-pressure diffraction, allowing high-quality data to be collected. Such techniques have been developed almost entirely at the IPNS pulsed source, Argonne, where many successful experiments at pressures up to 20kbars have been made (for example Jorgenson (1978)). However, the available neutron fluxes have not been high enough to encourage work at pressures into the 30-40kbar region, or even higher, which would require smaller samples.

A number of recent advances, though, now offer the possibility of extending the pressure range of high-pressure neutron powder-diffraction studies significantly.

(1) The very high flux available from the ISIS pulsed neutron source at the Rutherford Appleton Laboratory would allow sample volumes to be reduced while still enabling a high-quality powder pattern to be collected.

(2) Large sintered-diamond compacts, up to 25mm in diameter, are now available

through developments in the tool industry. Anvils made from this material would be significantly stronger and harder than those made from tungsten-carbide.

(3) The development of the toroidal anvil (Khvostantsev (1984)) allows a significant increase in the sample volume to be made while still permitting the attainment of higher pressures than have been available to date.

Combining these three significant advances, a pressure cell designed specifically for neutron-diffraction with a 90° scattering geometry has been built in collaboration with a group from the Université Marie-Curie, Paris with the aim of collecting high-quality diffraction data to pressures in excess of 100kbars. This will open up a completely new area of science, not possible anywhere else, in the study of light-atom materials, in magnetism, and in the study of thermal motion under pressure. The details of the cell design and work done so far are described in the next section.

3.5.2 The Paris Cell

The 50kbar test version of the cell on which the work so far has been made is shown in Figure 3.15, with an enlarged view of the anvil geometry shown in Figure 3.16a, and a schematic diagram of the toroidal-anvil geometry shown in Figure 3.16b. The design is based on the Bridgman anvil cell of Brugger and coworkers (Brugger *et al.* (1969)) which was capable of reaching pressures of 73kbars although no structures were refined at this pressure.

The incident neutron beam enters the cell along its axis where it is collimated both by the cell housing and by an absorbing boron-carbide disc which prevents the primary beam from hitting the cell and producing a large amount of scatter. To date, most of the testing has been done using tungsten-carbide (WC) anvils and due to the high absorption of this material for neutrons, the back of the anvils is hollowed out to reduce attenuation (shown for the toroidal anvil in Figure 3.16b). The diffracted beam from the sample exits at 90° through the gasket, which is made of concentric rings of pyrophyllite and beryllium-copper, to the detectors. This need for 90° detectors has limited work so far to the Polaris diffractometer at the Rutherford Laboratory but the installation of 90°

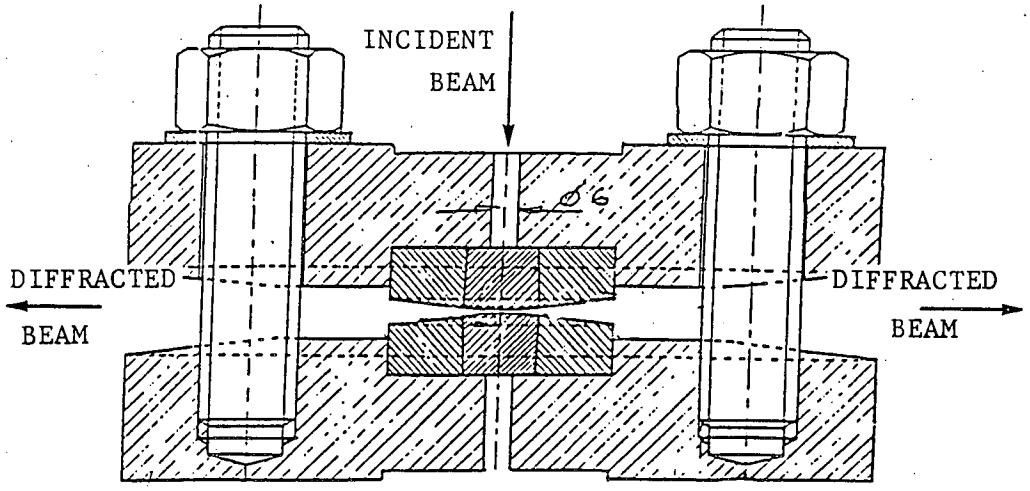

Figure 3.15: A cross-section through the Paris cell.

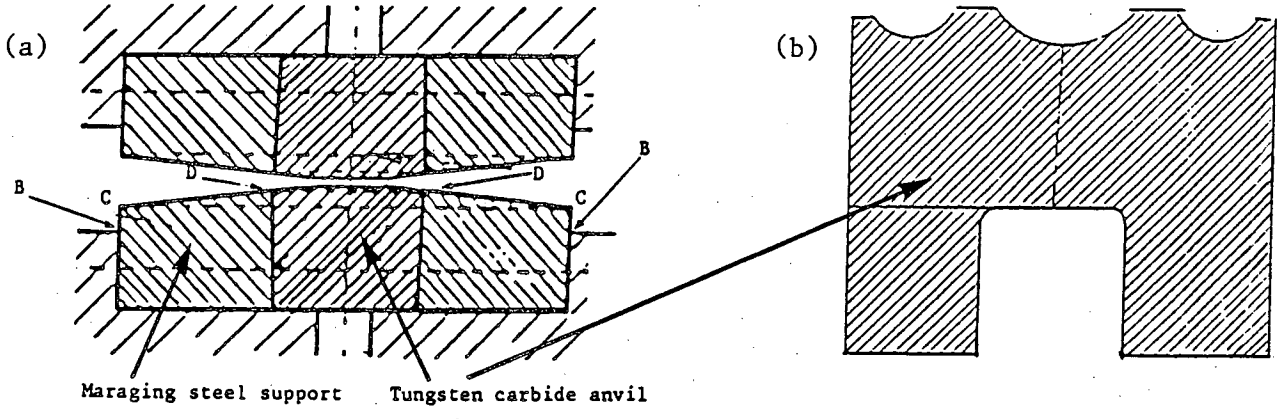

Figure 3.16: (a) An enlarged view of the anvil geometry of the paris cell, and (b) a schematic drawing of the torroidal anvil geometry. The points labelled B to D in (a) are discussed in the text.

detectors on HRPD (the High Resolution Powder Diffractometer) will also allow the use of the cell on this instrument. As discussed in Chapter 2.5, in order to achieve a diffraction pattern free from parasitic scatter, and thus suitable for accurate refinement, the cell must be collimated such that only the sample is both illuminated by the primary beam and viewed by the detectors simultaneously. A series of tests were therefore made to measure the effectiveness of the screening used to reduce the amount of cell scattering entering the detectors.

Using a paint made of highly-absorbing gadolinium oxide and Araldite, various sections of the cell were shielded to see where the scatter from the cell originated and to what extent it could be eliminated. These tests showed:-

(1) A completely unscreened cell (no GdO paint) with flat-tipped anvils gave WC peaks that were as strong as those obtained from a strongly scattering sample such as iron.

(2) Of this scattering, 20% came from the anvil tip (D to D in Figure 3.16a), 60% from the maraging steel face (D to C in Figure 3.16a) and 20% from the maraging steel supports (C to B in Figure 3.16a).

As stated, these results apply to the flat-tipped anvils and similar tests were made with indented anvils. It was found that under identical screening conditions, the intensity of the WC peaks from the indented anvils were a factor of 3 smaller than those from the flat-tipped anvils. The reasons for this are not completely clear at the moment as although the indented anvils reduce the illuminated volume of WC, while at the same time increasing the sample volume, most of the illuminated volume of WC remains and can be viewed by the detectors through the bevel in the maraging steel. A fuller understanding of the relevant scattering processes is still needed.

The results presented so far refer to the use of WC anvils which have been used in the 50kbar test cell. However, the attainment of pressures above 100kbars will require the use of sintered-diamond anvils. Tests on the attenuation coefficients of two types of sintered diamond, one with a heavy (cobalt) binder and one with a light binder, show the latter to be preferable as an anvil material due to its lower attenuation and reduced wavelength-dependent absorption correction. The tests also showed the diamond with the light binder to be less attenuating than the

WC, increasing the signal that will be available from the sample. However, the diamond itself can be expected to scatter more strongly (by a factor of two) than the WC and into a smaller number of reflections and the parasitic scatter from the diamond can therefore be expected to be some four times higher than that from the WC. The greater separation of the diamond peaks, though, may allow them to be simply excluded from the diffraction pattern and tests are still required to determine to what extent these diamond peaks can be screened out with the use of GdO paint.

Although work has been done on the 50kbar test cell to minimise absorption and maximise the signal-to-noise-ratio, and the cell has been used successfully to determine the equation of state of ^{7}LiD to 60kbars (Besson *et al.* (1990)), a pressure only bettered by Brugger *et al.* (1969), much work is still required in order to develop the full potential of the pressure cell.

(1) Both absorption and collimation processes still need to be fully understood, with the aim of improving the signal-to-noise ratio.

(2) Further development of the gasket and anvil designs is needed in order to allow higher pressures to be reached while maintaining $\overset{as}{\Lambda}$ large as possible sample volume.

(3) Development of the Polaris 90° detector banks is needed to reduce the background and to improve collimation. The use of two permanent detector banks at $\pm 90°$ needs to be developed while future cell designs will be able to maximise the signal by nearly encircling the sample – in the plane perpendicular to the incident beam – with a detector.

(4) Reduction in the noise – necessary for the refinement of weakly-scattering samples – will be required through extra collimation of the cell and detectors.

The successful use of this pressure cell in the future to obtain refineable diffraction patterns at pressures up to 100kbars will more than treble the presently available upper pressure limit for neutron powder-diffraction, and when combined with variable temperature, will provide unparalleled opportunities in high-pressure research.

Chapter 4

High-Pressure Structural Studies of H-Ordering Materials

4.1 Introduction

High-pressure studies of this group of materials have been made by members of this department since the late 1970's (for example Nelmes *et al.* (1982), Tibballs *et al.* (1982a,b), Nelmes (1987)) and account for a large percentage of the total number of high-pressure single-crystal neutron-diffraction studies made to date. However, although these studies have contained very detailed investigations of structural disorder and thermal motion, the materials studied have mostly been confined to simple tetragonal structures. The work contained in this chapter extends this series of structural studies to two monoclinic systems – using the Ahsbahs cell – and to a tetragonal system using the new ILL clamp-type cell, and presents results that cannot be explained by the long-accepted model for the hydrogen-ordering phase transition in these materials.

4.2 H-ordering Systems

This group of materials undergo a hydrogen-ordering (H-ordering) structural phase transition from a paraelectric phase to a ferroelectric or antiferroelectric phase on cooling through the phase transition temperature T_c. The details of

the transition will be discussed using the prototype material KH_2PO_4 (KDP) as an example.

The crystal structure of KDP (Nelmes *et al.* (1987)) is shown in Figure 4.1. Above T_c, in the paraelectric phase, the H-atoms are 50:50 disordered over two sites, δ apart, in short O-H-O bonds of length 2R linking the PO_4 groups. Below T_c, in the orthorhombic ferroelectric phase, the H-atoms order fully onto one of the two sites and there is an accompanying displacement of the heavy atoms along the *c*-axis.

T_c is very sensitive to both deuteration and pressure with T_c rising from 122K to 229K on deuterating KDP to KD_2PO_4 (DKDP) and T_c falling by $4.6Kkbar^{-1}$ in KDP (Samara (1987)). These changes in T_c with pressure and deuteration are currently explained using the tunnelling model of the transition (Blinc (1960)) in which the H atoms (or D atoms in DKDP) are treated as being in a double-potential well (Figure 4.2) and the increase in T_c on deuteration is explained by the heavier deuterons having a much lower tunnelling frequency through the potential barrier separating the two minima than the protons. This allows the deuterated material to order at a considerably higher temperature. The decrease in T_c with applied pressure is assumed to be due to a shortening of the H(D)-bonds which leads to a lower potential barrier between the minima and a higher tunnelling frequency. However, accurate high-pressure and atmospheric-pressure structural studies of KDP and DKDP using single-crystal neutron-diffraction (Tun *et al.* (1988), Meyer *et al.* (1980), Tibballs *et al.* (1982a,b)) have cast doubts on this explanation for the deuteration and pressure effects on T_c. More specifically:

(1) The compression of the H(D)-bonds is far less than was expected, throwing uncertainty on the explanation for the pressure dependence of T_c.

(2) The increase in T_c on deuteration is accompanied by significant increases in both δ and 2R, structural changes that are not explicitly taken into account in the tunnelling model.

(3) High-pressure studies show that δ and 2R decrease with applied pressure, as does T_c, indicating, along with (2) above, that there may be some relationship between T_c and the H-bond dimensions.

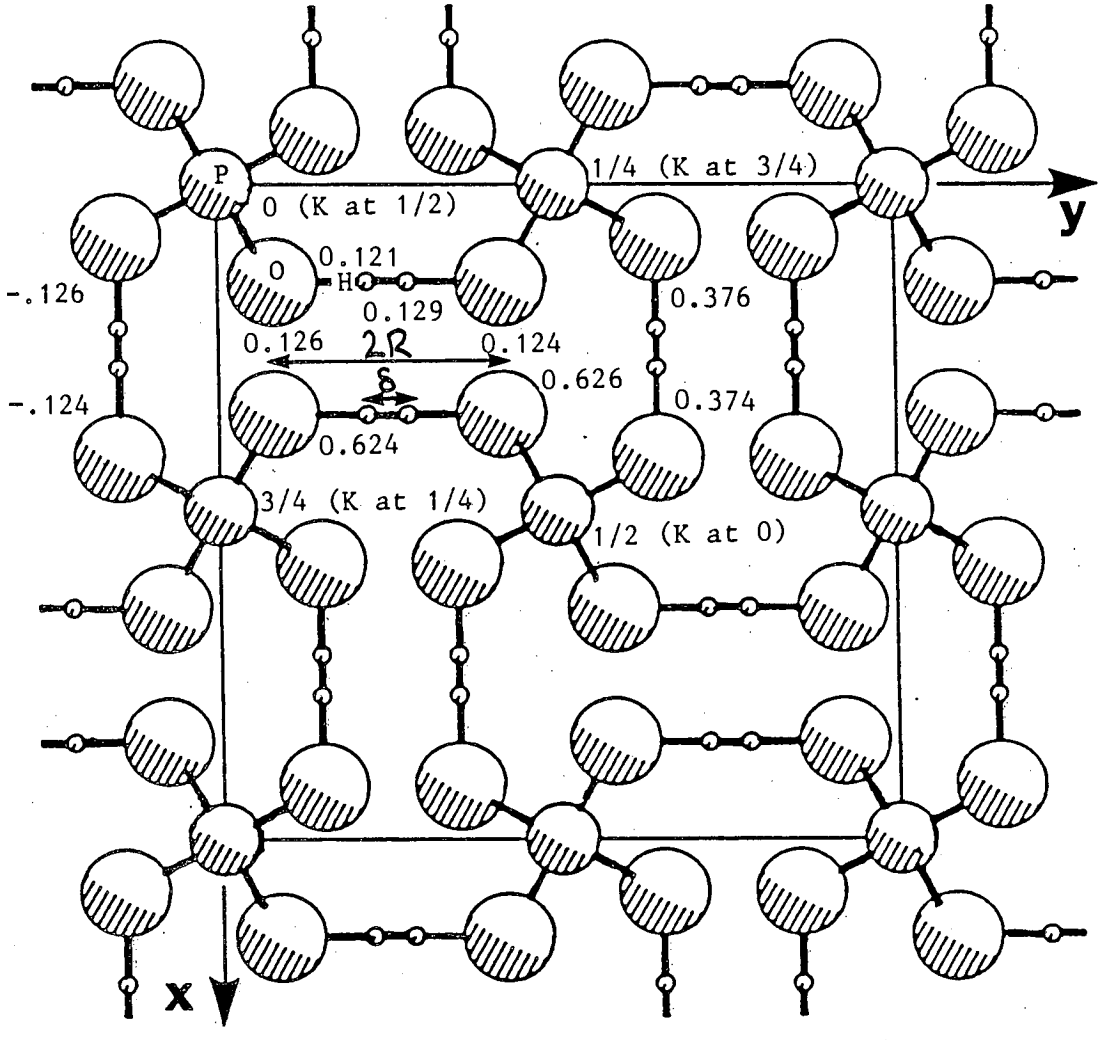

Figure 4.1: The tetragonal structure of KH_2PO_4 (KDP) viewed along the z axis. The K atoms, at positions displaced c/2 from each P atom, are superimposed onto the P atoms in this projection. Fractional coordinates along z (fixed by symmetry for the K and P atoms) are given for some of the atoms. The bondlengths 2R and δ are shown.

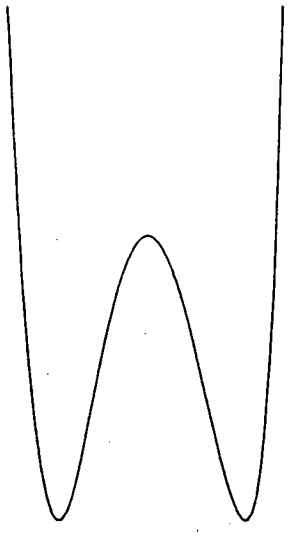

Figure 4.2: A schematic drawing of the double-well potential in which the H atoms sit in the paraelectric phase of KH_2PO_4.

Ichikawa (1981) and Ichikawa *et al.* (1987) have shown that for a number of KDP isomorphs and their deuterated analogues that there is an approximately linear relationship between T_c and 2R. It was concluded that the increase in T_c on deuteration arises from the increase in 2R alone, without needing to invoke tunnelling, and termed this the 'geometrical isotope effect' (Ichikawa (1978)). However, a more precise examination of the variation of T_c with 2R in KDP and DKDP (Nelmes (1988)) has shown that although the difference in T_c is much reduced when KDP and DKDP are compared at the same 2R, it is still 40K (Figure 4.3a). Moreover, it was shown that if the comparison is made instead at the same δ, then the difference in T_c is reduced to only 15K or less (Figure 4.3b), suggesting that δ is the more important geometrical determinant of T_c.

This relationship between T_c, 2R and δ has also been the subject of studies in another H-ordering system $H_2C_4O_4$ (Squaric Acid or H_2SQ.) where Tatsuzaki and Yamamaka (1987) have reached a similar conclusion to Ichikawa *et al* and related T_c to 2R. Accurate structural studies (Tun *et al.* (1987)), however, have suggested that a relationship might exist between T_c, δ and 2R between <u>different</u> systems and that the much larger T_c in H_2SQ. (T_c=374K at atmospheric pressure) is mainly the result of a much larger δ: about 75% of the difference in T_c being removed when H_2SQ. is at the pressure required to make its δ-value equal

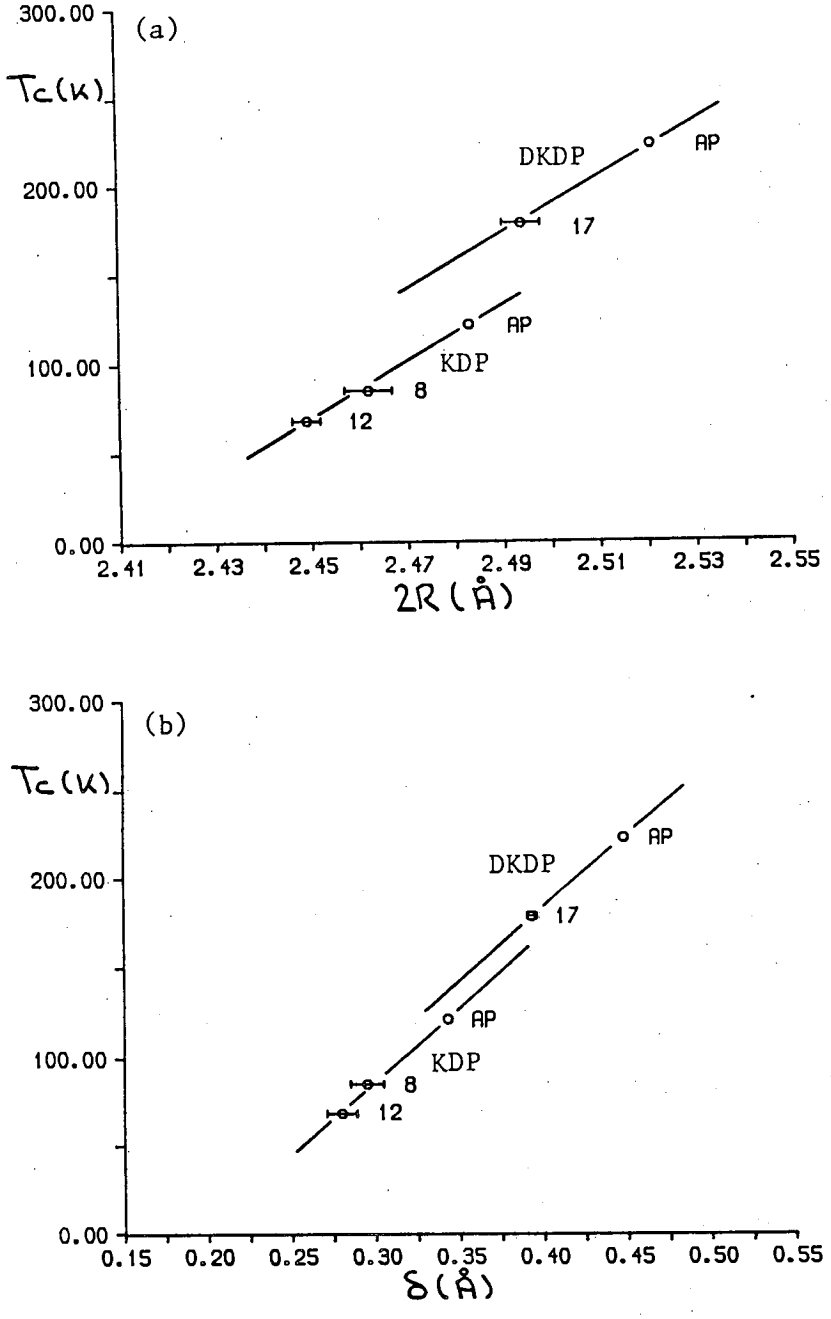

Figure 4.3: (a) The variation of T_c with the O-H-O bondlength, 2R, and (b) the variation of T_c with the H-site separation, δ, in KH_2PO_4 (KDP) and KD_2PO_4 (DKDP). The pressure is given against each point as AP (atmospheric pressure) or the number of kilobars applied. Where error bars are not shown, the errors are less than the size of the symbols used to plot the point. The lines are guides for the eye only.

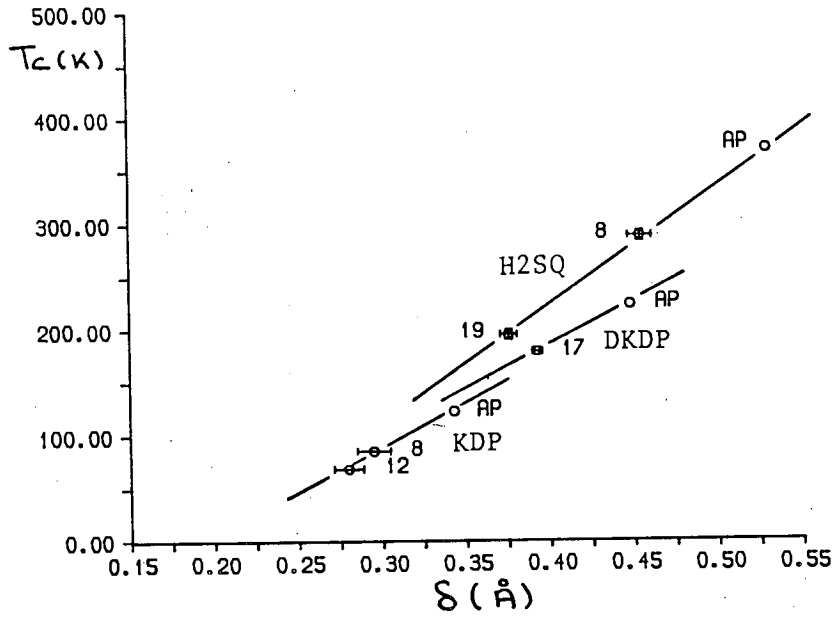

Figure 4.4: The variation of T_c with the H-site separation, δ, in KH_2PO_4 (KDP), KD_2PO_4 (DKDP) and $H_2C_4O_4$ (H_2SQ.). The pressure is given against each point as AP (atmospheric pressure) or the number of kilobars applied. Where error bars are not shown, the errors are less than the size of the symbols used to plot the point. The lines are guides for the eye only.

to the atmospheric-pressure δ-value in KDP (Figure 4.4).

However, a subsequent high-pressure structural study of another H-ordering material $PbHPO_4$ (LHP) (Restori *et al.* (1987)), again using single-crystal neutron-diffraction techniques, suggested that this material's behaviour was very different to that of KDP and H_2SQ. and that the simple relationships detailed above may not be applicable to H-ordering transitions in general. It was found for LHP that the pressure required to reduce δ to the atmospheric-pressure value of KDP would be only 5kbars, a pressure at which the value of T_c would be at least 260K, 138K higher than in KDP. A doubt, however, remained over the accuracy of the structural study of LHP, which has a relatively complicated monoclinic structure, especially over the geometry of the H-bonds which were found to have H-H, the line joining the two H-sites, almost perpendicular to the O-O line, in contrast to a previous study of LHP at atmospheric pressure which showed H-H inclined at only 8.4° to O-O.

Resolving these two apparent anomalies in the LHP system through more accurate structural studies is an ideal problem for the Ahsbahs cell. To determine the accurate dimensions of the H-bond, especially δ which is only 0.3-0.4Å, requires high-resolution single-crystal neutron-diffraction techniques while the complicated structure requires a three-dimensional data set. A more accurate determination of monoclinic structures would also allow high-pressure structural studies of another H-ordering system, CsH_2PO_4-CsD_2PO_4, which is unique amongst H-ordering systems in that both CsH_2PO_4 and CsD_2PO_4 can be cooled to either a ferroelectric phase or an antiferroelectric phase depending on the applied pressure (Samara (1987)).

4.3 A High-Pressure Structural Study of $PbDPO_4$

4.3.1 Introduction

To test the relationship between T_c, 2R and δ decisively in the KDP-DKDP system, it would be necessary to determine the crystal structures of KDP and DKDP under conditions where they had the same value of T_c. However, a pressure of 40kbars would be required to reduce T_c in DKDP to 122K and, as discussed in Chapters 2 and 3, such a pressure is as yet unobtainable using single-crystal neutron-diffraction techniques. Hence the conclusions on the relationship between the isotope effect on T_c and the accompanying structural changes has been based on measurements made up to 17kbars. However, the $PbHPO_4$-$PbDPO_4$ (LHP-LDP) system does allow the comparison of the hydrogenous and deuterated materials at the same T_c.

LHP undergoes an H-ordering transition at 310K, substantially higher than KDP, and possesses a very different crystal structure. The spacegroup of the low-temperature ferroelectric phase is Pc and that of the paraelectric phase has generally been assumed to be P2/c. The crystal structure viewed down the *b* axis is shown in Figure 4.5. The PO_4 groups are linked by H-bonds in only one dimension, as opposed to KDP in which the PO_4 groups are linked into a

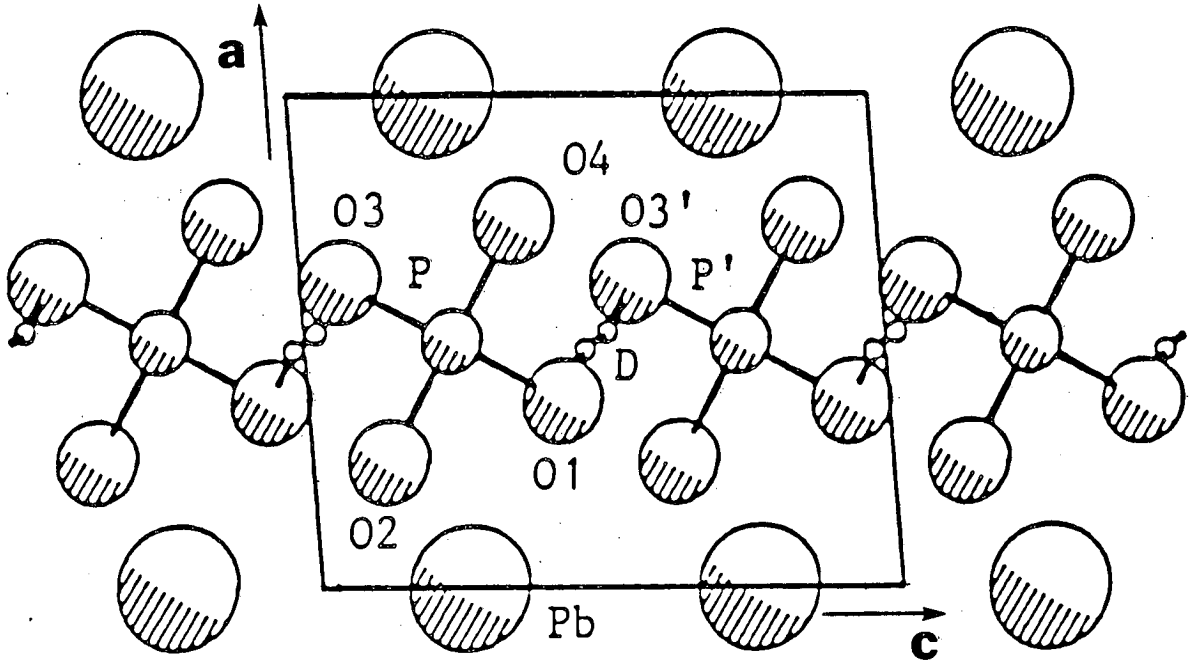

Figure 4.5: The crystal structure of $PbDPO_4$ above T_c viewed along the b axis. The two formula units in the unit cell are related by a c glide plane perpendicular to the b axis. With the origin in the glide plane, the approximate b-axis fractional coordinates of the labelled atoms are 0.21(Pb), 0.79(P), 0.65(O1, O3), 0.92(O2, O4), 0.34(O3') and 0.21(P'). The D atoms are disordered over two sites, as shown, in the O-D-O bonds that link the PO_4 groups along the c axis.

three-dimensional network, and form HPO_4 chains along the *c* axis (Negran *et al.* (1974)). In the high-temperature phase, assuming spacegroup P2/c, the H-atoms are 50:50 disordered over two sites δ apart while the Pb and P atoms lie on twofold axes. The transition is associated with the ordering of the H atoms and displacement of the Pb and P atoms to sites of lower symmetry. However, recent work (Tun *et al.* (1990)) has suggested that the heavy-atom structure retains the lower symmetry Pc spacegroup of the ferroelectric phase above T_c. This has yet to be decisively resolved.

Despite these differences in structure to KDP, the isotope effect on T_c in LHP is similar to that in KDP with T_c rising to 452K in LDP (Negran *et al.* (1974)) – a ΔT_c of 142K. Hydrostatic pressure decreases T_c in LHP and LDP much more strongly than in KDP with a dT_c/dP of about $11 K kbar^{-1}$ in both cases (Mylov *et al.* (1979), Piltz *et al.* (1988)). This means that only a relatively modest pressure of ~14kbars is required to reduce T_c in LDP to 310K, a pressure within the range of the Ahsbahs cell.

4.3.2 Experiment and Data Analysis

The sample crystal of LDP was a cylinder of diameter 1.2mm and height 0.4mm and was obtained from a larger crystal provided by Dr D.J. Lockwood, NRC Canada. The sample was loaded into the resistively-heated pressure cell described in Chapter 3.3.2 in Marburg by Drs. W.F. Kuhs and H. Ahsbahs and was pressurised to 12.0(5)kbars at 298K. The pressure was measured using the ruby method and the pressure fluid was d-methanol.

The diffraction data were collected on the D9 diffractometer at the ILL using a calibrated wavelength of 0.7071(1)Å and a PSD. Initial alignment of the pressure cell and sample was very difficult due to the use of such a small sample crystal and the high background count on the PSD.

In order to collect the diffraction data just above T_c in the paraelectric phase, the sample was warmed by heating the anvil seats of the cell as described in Chapter 3.3.2. The determination of T_c in LHP and LDP is very difficult using diffraction methods as the systematic absences and lattice-type of spacegroups

Pc and P2/c are the same. A previous atmospheric-pressure (AP) study of LDP (Piltz and Nelmes (1990)), however, had shown that the intensity of the (−508) reflection could be used to determine T_c as shown in Figure 4.6a. This reflection was therefore monitored as the cell was warmed and the resulting intensity as a function of temperature is shown in Figure 4.6b which allowed T_c to be determined as 313(2)K. From a later determination of how the pressure in the cell changed as a function of temperature (Kuhs (1989)), the pressure at this temperature was 12.9(5)kbars. This pressure-temperature point, and the value of T_c at atmospheric pressure (452(1)K) allow a value of $-10.7(6)\text{Kkbar}^{-1}$ to be calculated for dT_c/dP. To collect data in the paraelectric phase, the temperature was raised to 330(2)K, resulting in a pressure of 13.8(5)kbars and thus, using the value of dT_c/dP above, a T_c of 308(10)K, the same, within error, as that for LHP at AP (310(1)K). (The error of 10K on T_c reflects the relative error in the determination of the sample pressure, affecting the T_c via dT_c/dP).

The unit cell parameters at 330K and 13.8kbars were determined only roughly at first but were later refined from the positions of 329 'strong' reflections as a=4.6430(4)Å, b=6.5669(7)Å, c=5.7434(5)Å and β=96.748(3)°. The high precision possible in determining lattice parameters when using the PSD is very apparent.

All reflections were collected for $\Theta<25°$, and a quarter $(+h,-k,\pm l)$ of reciprocal space for $25°<\Theta<30°$ and for $30°<\Theta<35°$.

Refinements of the data collected to this point allowed sapphire reflections to be detected and deleted. Trial refinements also allowed those reflections still to be measured that were most sensitive to the dimensions of δ and 2R to be identified. All such reflections were measured carefully. Finally, the strongest reflections were measured in the $35°<\Theta<40°$ and $40°<\Theta<45°$ shells along with those reflections which refinements showed to be sensitive to δ and 2R. A total of 1650 reflections were measured to $\sin\Theta/\lambda=1.1\text{Å}^{-1}$. Only 85 reflections were affected by simultaneous reflections from the sapphires and were deleted from further analysis.

The scan profiles were converted into integrated intensities using the method of Wilkinson *et al.* (1988). Peakshape parameters for $\Theta>35°$ had to be obtained by extrapolation from those values obtained at lower angles. The data were

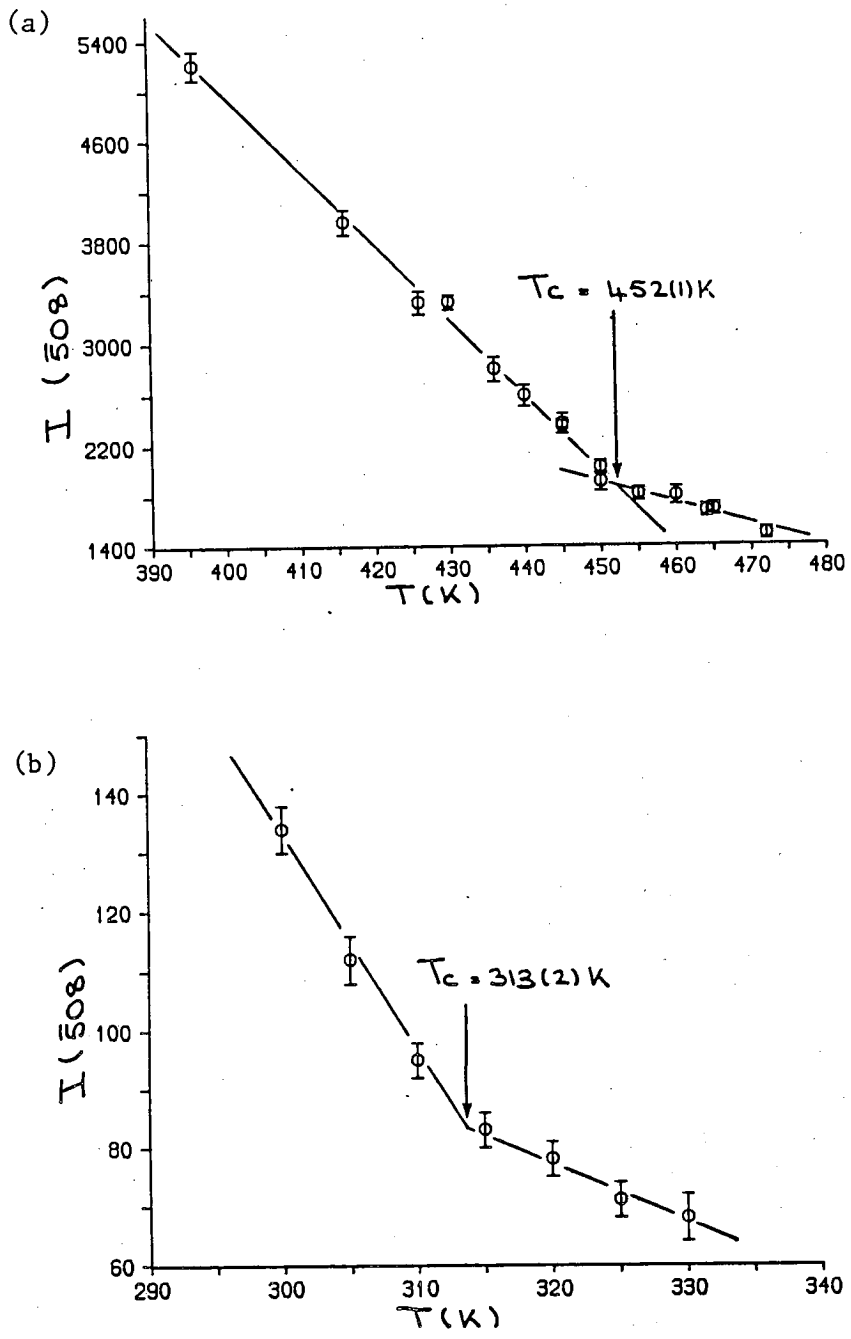

Figure 4.6: The variation of the integrated intensity, I, of the -508 reflection in $PbDPO_4$ at (a) atmospheric pressure, and (b) at high pressure. The determined values of T_c are indicated.

corrected for cell absorption (using measured absorption coefficients of sapphire and Ti-Zr, and the pathlengths obtained from enlarged drawings of the pressure cell) and for sample absorption. No correction for thermal diffuse scattering (TDS) is yet available for data collected using the PSD. After the corrections, reflections with integrated intensities $I_{obs}<10\sigma_c(I_{obs})$ were averaged for 2/m Laue symmetry, where $\sigma_c(I_{obs})$ is the estimated standard deviation (esd) from counting statistics. Stronger reflections were left unaveraged as their intensities may differ significantly due to the effect of anisotropic extinction. After correcting the data for anisotropic extinction all reflections were finally averaged giving internal and statistical R-factors of 2.9% and 3.4% respectively. The number of reflections included in the refinements was 1007.

The data were initially refined (all structure refinements described in this Chapter were made using the PROMETHEUS suite of programs (Zucker *et al.* (1983)) in the spacegroup P2/c and gave an R-factor of 5.10%. The refined atomic coordinates are given in column 1 of Table 4.1 along with the results obtained by Restori *et al.* (1987) for LHP using the Bloch cell. Comparison of the esd's on the heavy atoms (Pb, P, O) in the two studies shows them to be similar, which is surprising considering the higher quality of the present data. However, the esd's on the D-atom atomic coordinates are slightly smaller than those on the H atom and combined with less correlation between parameters, results in a considerably more accurate determination of δ. The most obvious difference in the two results is the y-coordinate of the H and D atoms and the resulting inclination of H-H and D-D, the lines joining the H and D sites, to O-O, the line joining the two O atoms of the H(D)-bond: for LHP, H-H is almost perpendicular to O-O while D-D is inclined at only 7.1°. Considerable emphasis was placed on this difference by Restori *et al.* but it can be understood as arising solely from the limited data collection in that case as follows.

The LHP experiment was performed on D15 using the Bloch cell and was limited to collecting only the $(hk0)$ and $(h0l)$ layers of reflections. All structural information of the y-coordinates therefore came from the $(hk0)$ layer. The equivalent positions in the P2/c spacegroup are (x,y,z), $(x,-y,\frac{1}{2}+z)$, $(-x,-y,-z)$ and $(-x,y,-z+\frac{1}{2})$ and for a projection of the structure onto the ab plane (the 'view' of the structure seen by the $(hk0)$ layer of reflections) this simplifies to $(-x,y,0)$, $(-x,-y,0)$, $(x,y,0)$ and $(x,-y,0)$. If y(D)=0.48 then $-y$(D)=0.52

	$PbDPO_4$ 13.8kbars, 330K	$PbHPO_4$ 15kbars, 298K	$PbHPO_4$ 15kbars, 298K
a(Å)	4.6430(4)	4.637(2)	4.637(2)
b(Å)	6.5669(7)	6.537(2)	6.537(2)
c(Å)	5.7434(5)	5.731(2)	5.731(2)
β(°)	96.748(3)	96.65(3)	96.65(3)
y(Pb)	0.2059(2)	0.2078(2)	0.2077(2)
y(P)	0.7942(3)	0.7934(3)	0.7933(3)
x(O1)	0.3729(2)	0.3714(3)	0.3714(3)
y(O1)	0.6537(2)	0.6558(3)	0.6558(3)
z(O1)	0.4323(2)	0.4326(3)	0.4325(3)
x(O2)	0.2567(2)	0.2565(2)	0.2564(2)
y(O2)	0.9234(2)	0.9242(2)	0.9242(2)
z(O2)	0.1251(2)	0.1245(2)	0.1246(2)
x(D,H)	0.4828(16)	0.4837(16)	0.4862(18)
y(D,H)	0.5236(11)	0.4829(11)	0.5166(12)
z(D,H)	0.4805(12)	0.4852(16)	0.4854(16)
2R(Å)	2.460(2)	2.441(3)	2.440(3)
δ(Å)	0.404(7)	0.310(17)	0.294(20)
P–O1(Å)	1.549(1)	1.551(2)	1.550(2)
P–O2(Å)	1.524(1)	1.528(2)	1.528(2)

Table 4.1: The refined fractional coordinates and selected interatomic distances for $PbDPO_4$ at 13.8kbars and 330K refined in the P2/c spacegroup. Column 2 gives the results of the study of $PbHPO_4$ at 15kbars and 298K, as reported by Restori *et al.* (1987), for comparison, while the third column gives the results from the rerefinement of the data of Restori *et al.* with y(H)$\sim$0.52. Esd's are given (in parentheses) on the last quoted place. The position of the Pb and P atoms are fixed by symmetry in the P2/c spacegroup at $(0,y,\frac{1}{4})$ and $(\frac{1}{2},y,\frac{1}{4})$ respectively.

while if y(D)=0.52 then $-y$(D)=0.48 i.e. there is no way of determining y=0.48 from y=0.52 with only the ($hk0$) layer of data. The data set of Restori *et al.* did, however, contain a few ($h \pm 1l$) reflections which are enough to break this correlation. Rerefinement of the data starting y(D) at 0.52 refines smoothly to give the results given in column three of Table 4.1 along with the recalculated H-bond dimensions. The incorrect results previously published for LHP are thus a direct result of the limited data set collectable in the Bloch pressure cell and illustrate the problems that arise from using this cell for low-symmetry structures. Such a problem did not arise from the use of the Ahsbahs cell and attempts to place y(D) at 0.48 at the start of a refinement always resulted in a refined value close to 0.52.

The sizeable wR-factor for the refinement based on the P2/c spacegroup prompted trial refinements of the data based on models using the Pc spacegroup, previous refinements of LHP and LDP at atmospheric pressure (Tun *et al.* (1990), Piltz and Nelmes (1990)) showing very significant improvements in fit using lower symmetry models. In the simplest model, the P atom was allowed to move away from the $(\frac{1}{2}, y, \frac{1}{4})$ position while the rest of the structure was constrained to be P2/c. This resulted in a final wR-factor of 4.49%, indicating that the original P2/c model could be rejected at the 99.5% confidence level (Hamilton (1965)). However, this model resulted in a highly distorted PO_4 group and was therefore unphysical. Further tests with less restrictive models showed that adding more degrees of freedom reduced this distortion. The final model chosen, and most physically plausible, was the same as that used in the atmospheric-pressure refinements of both LHP and LDP in which the P atom was allowed to move from the $(\frac{1}{2}, y, \frac{1}{4})$ position and the positional parameters of the four non-equivalent O atoms in the Pc spacegroup were allowed to refine freely. The thermal motion of these O atoms, however, was constrained such that the O atoms which would be equivalent in the P2/c spacegroup had the same thermal parameters. Constraints were also applied to the positional and thermal parameters of the D atom such that the occupancy of each site was 50% and one of the sites was related to the other by an inversion through the midpoint of the O..O line.

The final wR-factor for this model was 4.41% (goodness of fit 1.11) for 51 refined parameters. The significantly better fit of the present data to this model based on the Pc spacegroup rather than P2/c suggests that the surprisingly large esd's

	$PbDPO_4$ 13.8kbars 330K	$PbDPO_4$ AP 457K		$PbDPO_4$ 13.8kbars 330K	$PbDPO_4$ AP 457K
a(Å)	4.6430(4)	4.691(1)	x(O3)	0.2629(7)	0.2570(5)
b(Å)	6.5669(7)	6.673(1)	y(O3)	0.9227(7)	0.9226(4)
c(Å)	5.7434(5)	5.800(1)	z(O3)	0.1201(7)	0.1236(3)
β(°)	96.748(3)	97.21(1)	x(O4)	0.7560(7)	0.7439(5)
y(Pb)	0.2059(2)	0.1986(1)	y(O4)	0.0754(7)	0.0784(4)
x(P)	0.5096(11)	0.5016(5)	z(O4)	0.8700(7)	0.8664(3)
y(P)	0.7945(2)	0.7939(1)	x(D1)	0.4928(17)	0.4827(7)
z(P)	0.2451(10)	0.2429(3)	y(D1)	0.5197(11)	0.5227(4)
x(O1)	0.3832(10)	0.3814(4)	z(D1)	0.4732(13)	0.4694(5)
y(O1)	0.6539(5)	0.6562(3)	x(D2)	0.5280	0.5208
z(O1)	0.4258(8)	0.4273(3)	y(D2)	0.4737	0.4687
x(O2)	0.6376(9)	0.6220(4)	z(D2)	0.5138	0.5181
y(O2)	0.3394(5)	0.3354(3)	2R(Å)	2.460(2)	2.496(1)
z(O2)	0.5613(8)	0.5601(3)	δ(Å)	0.402(9)	0.476(5)
			P–O(Å)	1.536(5)	1.538(3)

Table 4.2: The unit cell dimensions, refined fractional coordinates, D-bond dimensions, and the average P–O bondlength for $PbDPO_4$ at 13.8kbars and 330K refined in the Pc spacegroup compared with those obtained from the data at atmospheric pressure (AP) and 457K by Piltz and Nelmes (1990). Esd's are given (in parentheses) on the last quoted place. In both cases the D-atom distribution was constrained to be 50:50 with D2 related to D1 by inversion through the midpoint of the line joining O1 and O2.

commented upon for the P2/c refinement reflect the use of the wrong structural model and a resulting poor fit to the data rather than resulting from poor quality data. The final refined atomic coordinates and anisotropic thermal parameters are given in Tables 4.2 and 4.3 respectively along with those of the atmospheric-pressure study of LDP at 457K (T_c+5K) for comparison.

	$PbDPO_4$ 13.8kbars 330K	$PbDPO_4$ AP 457K		$PbDPO_4$ 13.8kbars 330K	$PbDPO_4$ AP 457K
U^{11}(Pb)	1.21(3)	2.06(1)	U^{12}(O1)	0.41(4)	0.48(3)
U^{22}(Pb)	1.37(4)	1.59(2)	U^{13}(O1)	1.15(4)	1.62(2)
U^{33}(Pb)	1.35(3)	2.21(1)	U^{23}(O1)	0.92(4)	1.26(3)
U^{12}(Pb)	−0.09(9)	0.11(8)	U^{11}(O3)	1.11(3)	1.53(1)
U^{13}(Pb)	0.06(2)	−0.09(1)	U^{22}(O3)	1.78(4)	2.12(2)
U^{23}(Pb)	−0.26(9)	0.14(7)	U^{33}(O3)	1.16(3)	1.50(1)
U^{11}(P)	1.04(5)	1.25(1)	U^{12}(O3)	0.26(3)	0.27(2)
U^{22}(P)	1.06(6)	1.10(3)	U^{13}(O3)	−0.14(2)	−0.19(1)
U^{33}(P)	1.34(5)	1.65(2)	U^{23}(O3)	0.06(3)	0.17(2)
U^{12}(P)	0.15(17)	0.20(13)	U^{11}(D1)	2.47(16)	2.79(7)
U^{13}(P)	−0.14(4)	−0.01(1)	U^{22}(D1)	2.04(3)	1.99(9)
U^{23}(P)	−0.85(15)	−0.40(11)	U^{33}(D1)	2.23(19)	2.94(9)
U^{11}(O1)	2.21(4)	3.06(2)	U^{12}(D1)	−0.21(15)	−0.19(8)
U^{22}(O1)	1.41(5)	1.84(3)	U^{13}(D1)	0.50(12)	0.58(6)
U^{33}(O1)	2.71(5)	3.61(3)	U^{23}(D1)	0.16(12)	0.19(7)

Table 4.3: The refined anisotropic thermal parameters ($\times 10^{-2}$Å^2) for $PbDPO_4$ at 13.8kbars and 330K compared with those obtained from the data at atmospheric pressure (AP) and 457K by Piltz and Nelmes (1990). Esd's are given (in parentheses) on the last quoted place. In both cases the thermal parameters of the O2, O4 and D2 atoms were constrained to be equal to the thermal parameters of the O1, O3 and D1 atoms respectively.

4.3.3 Discussion and Conclusions

Comparison of the positional parameters of the two LDP studies shows that the esd's in the present study to be only a factor of 2-3 times those obtained in the AP study despite the fact that the latter experiment used a sample crystal that had a volume some 15 times that of the high-pressure experiment. Comparison of the results in Table 4.1, however, shows the esd's from the refinement using the Pc model to be 3-5 times those obtained using the P2/c model despite the better fit of the former. This is due to high (90%) correlations present in the Pc model between the positional parameters of the pairs of O atoms which would be symmetry equivalents in the P2/c spacegroup. These correlations, however, do not seriously affect the esd's on the calculated D-bond dimensions.

Comparison of the two sets of thermal parameters again shows the esd's on the high-pressure results to be 2-3 times those of the AP results. Comparison of the absolute values of the parameters is complicated by the fact that the data were collected at very different temperatures and pressures, and that neither data set has been corrected for TDS. Despite these difficulties, the general trend of the thermal parameters is very similar in each case with the values from the atmospheric-pressure study a factor of 1.3 larger, on average, than those of the present study. If the thermal parameters are taken as scaling directly with the temperature, then it would be expected that the AP values would be a factor of 1.37 times larger than the high-pressure values, in good agreement with the results obtained.

Table 4.4 contains the values of δ and 2R derived from the refined coordinates of the present study as well as those from the previous atmospheric-pressure (AP) studies of LHP at 316K (T_c+5K), LDP at 457K (T_c+5K) and a preliminary study of LHP just above T_c at 6.9kbars – all obtained by single-crystal neutron-diffraction techniques. The values of 2R are plotted against T_c in Figure 4.7a and, if LHP and LDP are compared at the same 2R (e.g. 2.470Å), it can be seen that although ΔT_c is greatly reduced from its AP value of 142K, it is still ~40K and it is <u>not</u> reduced to zero. However, if T_c is plotted against δ, as in Figure 4.7b, it emerges that ΔT_c <u>is</u> reduced to zero, within 10K, if the comparison is made at the same δ – i.e. LHP and LDP have the same T_c at the same δ.

Parameter	$PbDPO_4$	$PbHPO_4$	$PbDPO_4$	$PbHPO_4$
T(K)	330(2)	316(1)	457(1)	230(1)
P(kbar)	13.8(5)	AP	AP	6.9(8)
T_c(K)	308(10)	310(10)	452(1)	221(4)
a(Å)	4.6430(4)	4.6829(2)	4.691(1)	4.656(1)
b(Å)	6.5669(7)	6.6447(2)	6.673(2)	6.581(4)
c(Å)	5.7434(5)	5.7798(2)	5.800(1)	5.749(1)
$\beta(°)$	96.748(3)	97.150(3)	97.21(1)	96.85(3)
δ(Å)	0.402(9)	0.391(5)	0.476(5)	0.301(29)
2R(Å)	2.460(2)	2.470(1)	2.496(1)	2.449(2)

Table 4.4: Column 1 gives T_c, the lattice parameters and D-bond dimensions of $PbDPO_4$ at 330K and 13.8kbars. The results obtained from previous atmospheric-pressure (AP) studies of $PbHPO_4$ (Tun *et al.* (1990)) and $PbDPO_4$ (Piltz and Nelmes (1990)), and from a preliminary study of $PbHPO_4$ at 6.9kbars (Piltz *et al.* (1990)) are included for comparison. Esd's are given (in parentheses) on the last quoted place. The data in the study of $PbHPO_4$ at 6.9kbars gave a value of δ that is felt to be unreliable. The relatively large esd's on the cell parameters and δ in the AP study of $PbDPO_4$ are due to uncertainties in the neutron wavelength used.

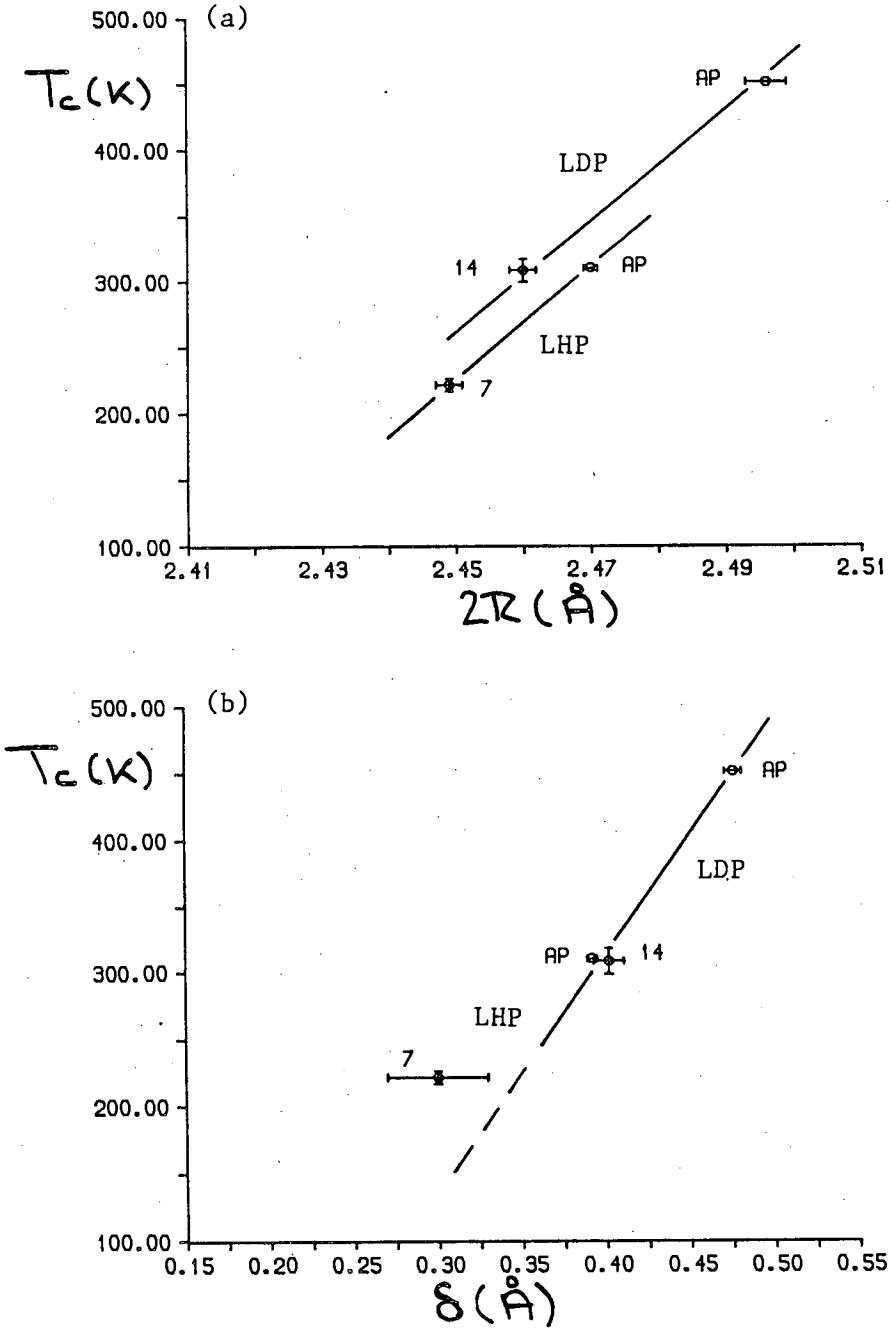

Figure 4.7: (a) The variation of T_c with the O-H-O bondlength, 2R, and (b) the variation of T_c with the H-site separation, δ, in $PbHPO_4$ (LHP) and $PbDPO_4$ (LDP). The pressure is given against each point as AP (atmospheric pressure) or the number of kilobars applied. Where error bars are not shown, the errors are less than the size of the symbols used to plot the point. The lines are guides for the eye only. The value of δ for the study of LHP at 6.9kbars is felt to be unreliable.

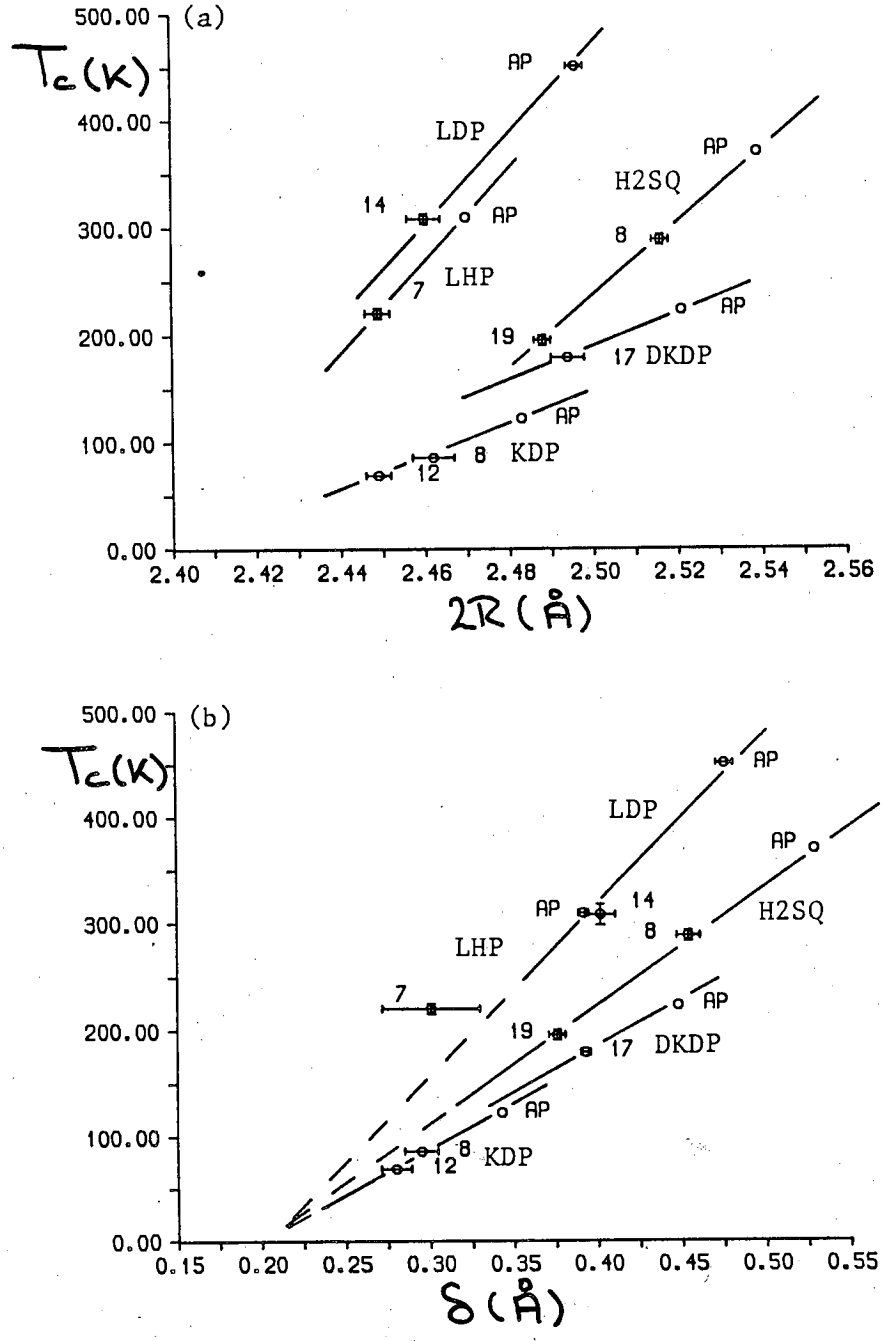

Figure 4.8: (a) The variation of T_c with the O-H-O bondlength, 2R, and (b) the variation of T_c with the H-site separation, δ, in KH_2PO_4 (KDP), KD_2PO_4 (DKDP), $H_2C_4O_4$ (H_2SQ.), $PbHPO_4$ (LHP) and $PbDPO_4$ (LDP). The pressure is given against each point as AP (atmospheric pressure) or the number of kilobars applied. Where error bars are not shown, the errors are less than the size of the symbols used to plot the point. The lines are guides for the eye only.

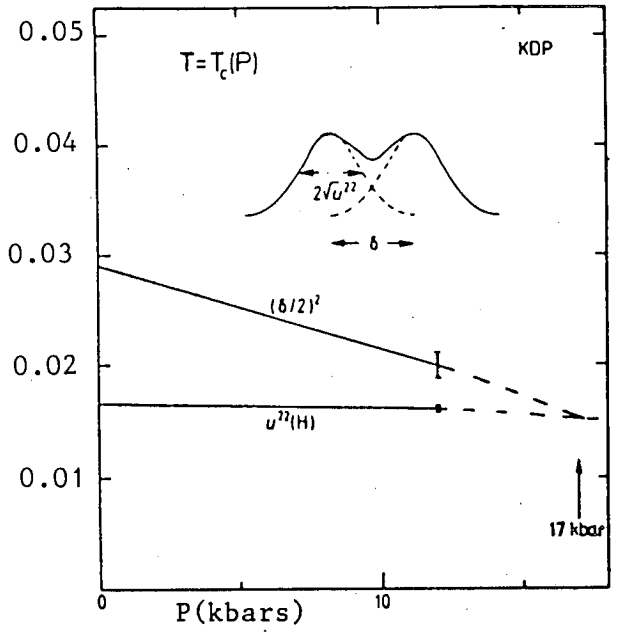

Figure 4.9: The parameters δ – as $(\delta/2)^2$ – and U^{22}, which describe the along-bond H distribution as illustrated, evaluated at the pressure-dependent transition temperature T_c. From Tibballs *et al.* (1982a).

This result clearly and decisively secures the conclusions indicated earlier in the KDP-DKDP system (Nelmes (1988)). Although the results from the KDP-DKDP system are based on extrapolation of low-pressure data and are thus less well determined, it does seem that these two very different H-ordering systems behave in remarkably similar ways in terms of both δ and 2R.

Another striking similarity between different H-bonded systems is evident if the values of T_c, δ and 2R for the LHP-LDP system are plotted with those obtained previously for the KDP-DKDP system and for H_2SQ. Figure 4.8a shows how T_c varies in relation to 2R in each of these systems and although T_c appears to vary linearly with 2R in each case, as shown by the three points for H_2SQ. and KDP, there is no evidence of a simple relationship between them, contrary to the conclusions of Ichikawa (1981) and Ichikawa *et al.* (1987). But when T_c is plotted against δ instead, as in Figure 4.8b, a striking relationship emerges. In all these systems, deuterated and undeuterated, T_c extrapolates to 0K at the same value of δ of ~0.2Å, a remarkable result considering the very different crystal structures and form of H-bonding.

The results of this experiment then give strong evidence that δ – rather than 2R – is the structural parameter most directly associated with T_c and that the isotope effect on T_c may be attributed entirely, or almost entirely, to the accompanying increase in δ and no quantum tunnelling arguments need be used. The critical δ value of 0.2Å as $T_c \rightarrow 0K$ would also seem to have some fundamental significance common to the three systems studied so far. In the case of KDP, it has been shown previously (Tibballs *et al.* (1982a)) that when δ falls to 0.2Å the r.m.s. along-bond zero-point motion of the H atom exceeds the half-distance, $\delta/2$, between the H sites (Figure 4.9). Then the thermal motion is always sufficient to take the H atom from one minimum of the potential well to the other. Such an explanation suggests that the H ordering might be generally understood in terms of thermal excitation over the potential barrier between the sites, rather than tunnelling through it. This explanation might also account for the geometrical isotope effect although T_c is not necessarily expected to be the same at precisely the same δ in that case, because the pressure required to get the same δ will make 2R smaller in the deuterated form (see Figures 4.7a and 4.7b). This difference in 2R, and any other dependence of the thermal motion on the particle mass, mean that the along-bond thermal motion of H and D will generally differ at the same δ and temperature.

4.4 A High-Pressure Structural Study of CsD_2PO_4.

4.4.1 Introduction

The results of the LDP experiment suggest that the three very different H-ordering systems, KDP-DKDP, LHP-LDP and H_2SQ_4, behave very similarly in their dependence of T_c on δ, and that there is a systematic increase in the magnitude of $dT_c/d\delta$ on going from a three-dimensionally H-bonded system, KDP-DKDP, to a one-dimensionally H-bonded system LHP-LDP (Figure 4.8b). These similarities prompted the study of another H-bonded system CsH_2PO_4-CsD_2PO_4 (CsDP-DCsDP) that was very different from those already studied.

The CsDP system is unique amongst H-ordering materials with both a very different crystal structure and phase diagram. CsDP undergoes an H-ordering phase transition on cooling through T_c=159K (Samara (1987)). This transition temperature is again very sensitive to deuteration with T_c rising to ~268K in DCsDP, a ΔT_c of 106K. CsDP is a one-dimensional (1-D) H-ordering material like LHP but the crystal structure is very different (Nelmes and Choudhary (1978)) and is shown in Figure 4.10. Above T_c, in the paraelectric phase, CsDP is monoclinic (and is therefore again well suited to the use of the Ahsbahs cell) with spacegroup $P2_1/m$. In this phase the PO_4 groups are held together by two types of H-bond: ordered asymmetric O–H..O bonds nearly parallel to the *c* axis (O2-H2-O2 in Figure 4.10) and symmetric O–H–O bonds along the *b* axis in which the H atoms are disordered over two sites, δ apart (O3-H1-O3 in Figure 4.10). Thus the structure consists of 1-D chains along the *b* axis which are crosslinked by the ordered H-bonds. Below T_c, in the ferroelectric phase, the spacegroup is $P2_1$ (Iwata *et al.* (1980)) and the transition involves ordering of the H-atoms onto one of their sites with an accompanying displacement of the heavy atoms along the *b* axis.

The pressure dependence of CsDP and DCsDP is unique amongst H-ordering systems with both materials having a paraelectric:ferroelectric:antiferroelectric (PE:FE:AFE) triple-point at low pressures (3.3kbars in CsDP and 6kbars in DCsDP) (Gesi and Ozawa (1978), Yasuda *et al.* (1979)). The phase diagram of the materials is shown in Figure 4.11 which also illustrates the change in the magnitude of dT_c/dP for the PE-FE and PE-AFE phase boundaries. This feature of the CsDP-DCsDP system is particularly interesting in the present context of relating the changes in T_c to the accompanying changes in the H-bond dimensions, and suggests a similar discontinuity in either the relationship between T_c and 2R, between T_c and δ, or a discontinuity in the pressure dependence of the structure.

Before the present study of DCsDP (which is the first high-pressure study of this material) the atmospheric-pressure structure of DCsDP was determined at T_c+5K (273K) (McMahon *et al.* (1990b)) using single-crystal neutron-diffraction techniques. Combined with the atmospheric-pressure structure of CsDP determined by Semmingsen and Thomas (1990) at 200K (T_c+47K), the resulting graphs of T_c plotted against 2R and δ are shown in Figures 4.12a and 4.12b re-

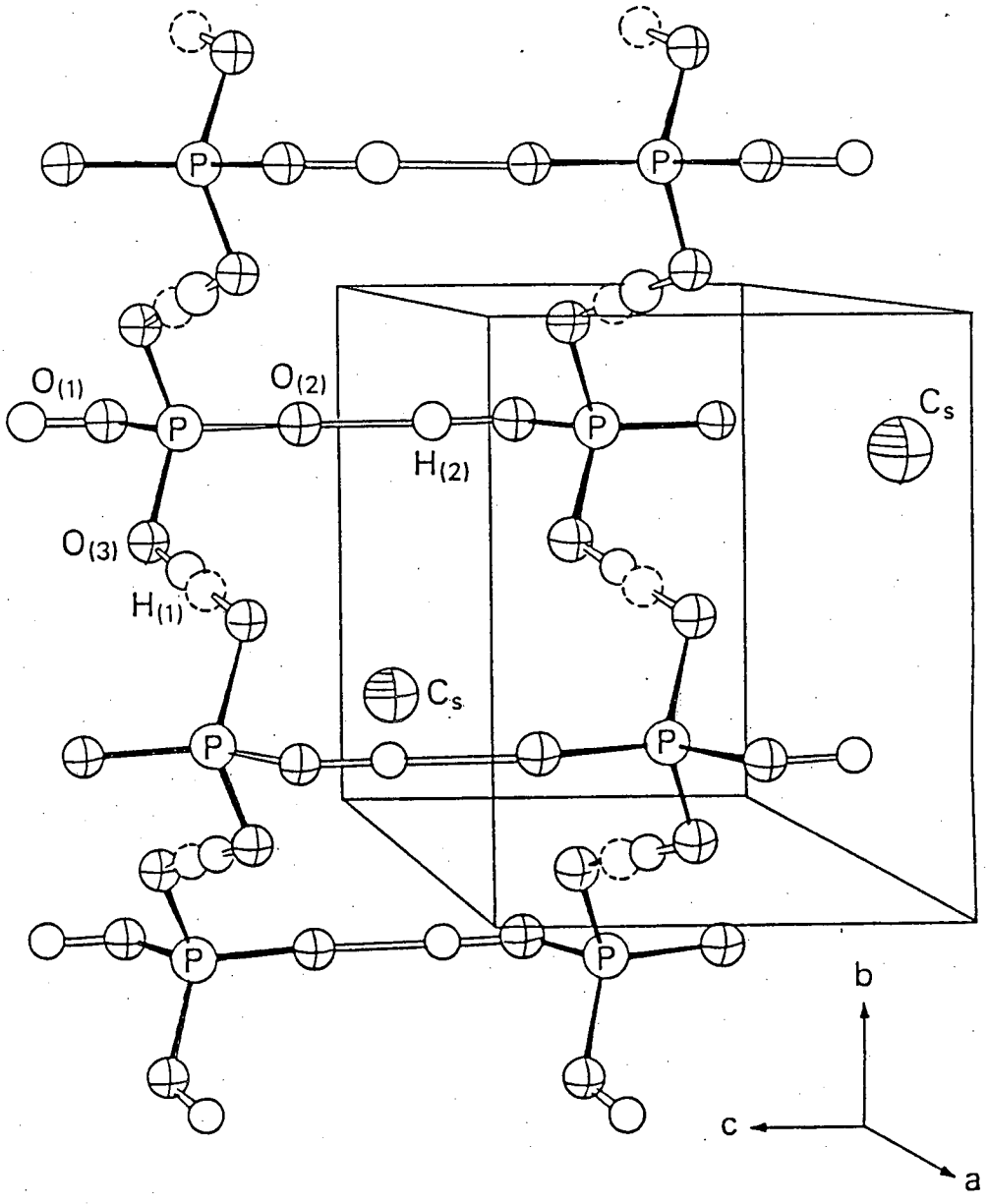

Figure 4.10: The crystal structure of CsH_2PO_4 showing the two types of hydrogen bond – the disordered O3-H1-O3 bond, and the ordered O2-H2-O2 bond. (From Kojyo and Onodera (1988).)

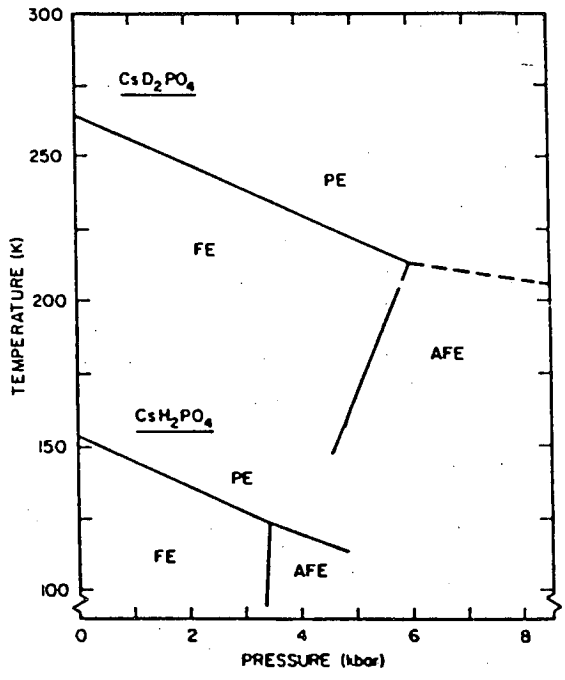

Figure 4.11: The pressure-temperature phase diagram of CsH_2PO_4 and CsD_2PO_4. (From Samara (1987).)

spectively. It can be seen that (i) the variation of T_c with δ does not extrapolate to 0.2Å but to a rather larger value of 0.3Å, and (ii) that the rate of change of T_c with δ is *much* less than that in LHP and LDP, illustrating that the magnitude of $dT_c/d\delta$ is not generally related to the dimensionality of the H-bonding in a system. These two points thus raised several questions that made a knowledge of the pressure dependence of the structure essential, and two high-pressure studies of DCsDP in the paraelectric phase, using the Ahsbahs cell on D9, were planned: one as close as possible to the triple point at 6kbars just above the FE phase, and another at 15kbars just above the AFE phase.

4.4.2 Experiment and Data Analysis

The sample crystals of DCsDP were prepared from a larger crystal provided by Dr. A. Levstik, Ljubljana, and were cylinders of diameter 1.1mm and thickness 0.7mm. Two pressure cells were loaded in Marburg to pressures of 6.3(5)kbars and 12.1(5)kbars. The pressure was measured using the ruby method and the

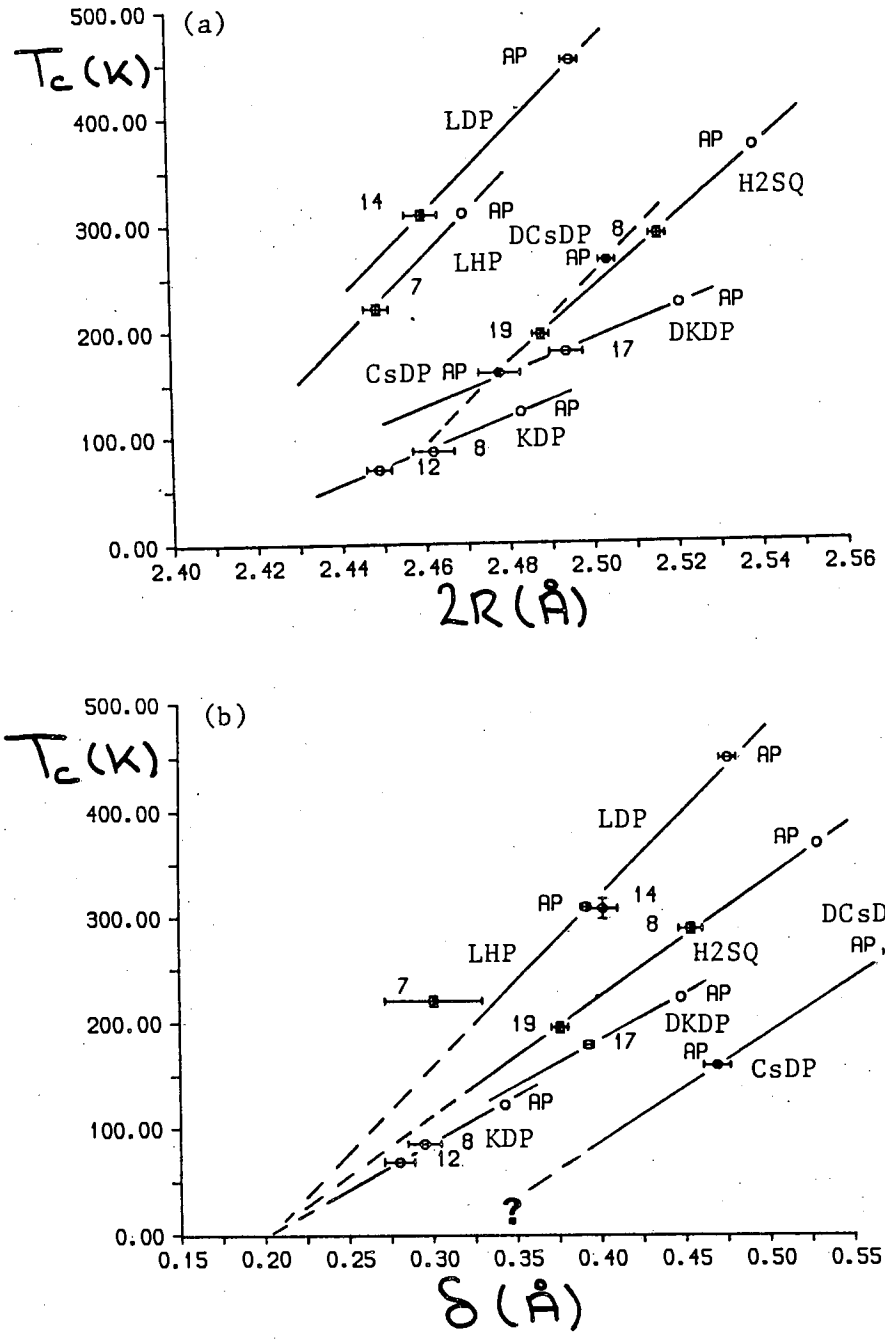

Figure 4.12: (a) The variation of T_c with the O-H-O bondlength, 2R, and (b) the variation of T_c with the H-site separation δ in KH_2PO_4 (KDP), KD_2PO_4 (DKDP), $H_2C_4O_4$ (H_2SQ.), $PbHPO_4$ (LHP), $PbDPO_4$ (LDP), CsH_2PO_4 (CsDP) and CsD_2PO_4 (DCsDP). The CsDP and DCsDP points are represented by filled circles. The pressure is given against each point as AP (atmospheric pressure) or the number of kilobars applied. Where error bars are not shown, the errors are less than the size of the symbols used to plot the point. The lines are guides for the eye only and a dashed line is used for the CsDP-DCsDP points in (a) for clarity.

pressure fluid was d-isopropanol, the crystals dissolving in d-methanol.

As the expected values of δ were in the range 0.5-0.6Å (Figure 4.12b), the resolution of the data required in these experiments was less than that required in the LDP experiment and the data were therefore collected on D9 using a calibrated wavelength of 0.8460(1)Å. This wavelength also resulted in the maximum intensity for measured reflections (taking into account the neutron flux and the efficiency of the detector as a function of wavelength). Although the experiments were to use the cryostat described in Chapter 3 in order to collect data just above the FE or AFE phases, initial alignment of the sample was simplified by mounting the pressure cell outside the cryostat. Initial alignment was also simplified by the use of a larger crystal than in the LDP experiment, although a systematic search for sample reflections under computer control was still required.

After aligning the 6.3kbar sample, and noting its orientation with respect to the pressure cell, the cell was mounted in the cryostat and cooled to 260K. A similar problem to that faced in the LDP experiment then arose in that the transition was hard to find using diffraction techniques. Using the previously refined structure at T_c+5K and the structure in the FE phase determined by Semmingsen and Thomas (1990), the intensities of the (106) and (343) reflections were found to be sensitive to the transition. These reflections were therefore measured as a function of temperature as the cell was cooled, however, the transition was found from a sudden, reversible, change in the crystal orientation at 231(2)K. From the phase diagram of DCsDP (Gesi and Ozawa (1978), Yasuda *et al.* (1979)) this meant that the pressure was 4.0(2)kbars.

The temperature was then increased to 236K and the unit cell parameters determined from 79 strong reflections as a=7.760(3)Å, b=6.265(3)Å, c=4.866(2)Å and β=107.48(2)°. The reason for the relatively poor precision of these parameters is discussed below.

Two attempts were made to collect data using the PSD but both gave very poor results – unphysically high extinction and negative thermal parameters – suggesting that something was wrong with the data. The problem was traced to the detector itself which was determined to have several 'dead' pixels at the centre of the detector surface. The resulting correction for these pixels in order

to normalise their intensities was very large, making the collection of accurate data impossible. The PSD was therefore replaced with a single-detector. The fault with the PSD also resulted in the relatively few 'strong' reflections used to determine the lattice parameters given above and explains their relatively poor precision. No attempt was made to improve upon the precision of the lattice parameters by centering reflections using the single-detector as (i) experimental time was severly restricted, and (ii) previous experience had shown that no significant increase in precision would result from the use of the single-detector.

Although the fault with the PSD had been determined early in the data collection, less than half the experimental time remained once the single-detector was mounted and only the experiment at 236K and 4kbars was attempted. Time was saved, however, as the PSD data sets, although too poor to refine, did allow those reflections that were affected by sapphire reflections to be omitted from the final data collection.

The data collection strategy was very similar to that used in the LDP experiment with data being collected in shells in Θ from 0°-24°, 24°-35°, 35°-41° and 41°-48°. Trial refinements made during the data collection enabled those reflections sensitive to δ and 2R to be measured with increased precision while use of the 'Leverage' program (Hazen and Finger (1989)) allowed the most sensitive measured reflections to be determined and remeasured.

A total of 1026 reflections were measured to $\sin\Theta/\lambda$=0.98Å^{-1} with only 21 reflections having to be rejected due to contamination by sapphires. The scan profiles were converted into integrated intensities using the method of Lehmann and Larson (1974) and the data were corrected for pressure-cell and sample absorption as in the LDP experiment. No correction was made for TDS. After averaging weak reflections and correcting the data for anisotropic extinction, the data were averaged to give 489 independent reflections. The internal and statistical R-factors on final averaging were 4.87% and 7.71% respectively.

The data were refined in spacegroup $P2_1/m$, trial refinements in the $P2_1$ spacegroup having shown the D-site occupancies to be 50(1)%:49(1)% and therefore that the data was collected above T_c. The final wR-factor was 5.61% (goodness of fit 1.30) for 48 refined parameters. The final refined atomic coordinates, the D-bond dimensions, and other bondlengths are given in Table 4.5 along with

	CsD_2PO_4 4kbars 236K	CsD_2PO_4 AP 269K		CsD_2PO_4 4kbars 236K	CsD_2PO_4 AP 269K
a(Å)	7.760(3)	7.9301(13)	x(O3)	0.1307(4)	0.1285(1)
b(Å)	6.265(3)	6.3799(7)	y(O3)	0.5495(3)	0.5534(4)
c(Å)	4.866(3)	4.9008(7)	z(O3)	0.4139(5)	0.4165(2)
$\beta(°)$	107.48(2)	107.799(7)	x(D1)	0.3632(4)	0.3571(1)
x(Cs)	0.2624(4)	0.2649(2)	z(D1)	0.1734(5)	0.1759(2)
z(Cs)	0.0201(6)	0.0313(3)	x(D2)	−0.0311(16)	−0.0293(3)
x(P)	0.2434(4)	0.2396(2)	y(D2)	0.4888(15)	0.4816(8)
z(P)	0.5266(5)	0.5294(2)	z(D2)	0.5112(28)	0.5143(5)
x(O1)	0.4024(4)	0.3931(1)	2R(Å)	2.494(5)	2.503(2)
z(O1)	0.3881(5)	0.3885(2)	δ(Å)	0.543(9)	0.573(5)
x(O2)	0.3241(5)	0.3239(2)	P–O1(Å)	1.573(4)	1.567(1)
z(O2)	0.8440(5)	0.8455(2)	P–O2(Å)	1.482(4)	1.483(2)
			P–O3(Å)	1.535(3)	1.533(2)

Table 4.5: The unit-cell dimensions, refined fractional coordinates, D-bond dimensions and the P–O bondlengths for CsD_2PO_4 at 4kbars and 231K compared with those obtained from the data at atmospheric pressure (AP) and 267K by McMahon *et al.* (1990b). Esd's are given (in parentheses) on the last quoted place. Parameters given without esd's are fixed by symmetry. In each case, the Cs atom was fixed by symmetry at $(x, \frac{1}{4}, z)$ while the P, O1, O2 and D1 atoms were fixed at $(x, \frac{3}{4}, z)$.

the results from the atmospheric-pressure study of DCsDP for comparison. The anisotropic thermal parameters for both studies are given in Table 4.6.

4.4.3 Discussion and Conclusions

Comparison of the precision of the refined atomic coordinates in Table 4.5 shows the esd's in the high-pressure (HP) study to be generally 3-4 times those in the atmospheric-pressure (AP) study and the esd's on the D atoms to be up

	CsD_2PO_4 4kbars 236K	CsD_2PO_4 AP 269K		CsD_2PO_4 4kbars 236K	CsD_2PO_4 AP 269K
U^{11}(Cs)	2.4(2)	2.62(6)	U^{11}(O3)	4.2(2)	3.88(6)
U^{22}(Cs)	1.6(1)	2.74(27)	U^{22}(O3)	1.7(1)	3.34(20)
U^{33}(Cs)	1.6(1)	2.26(5)	U^{33}(O3)	2.9(1)	4.41(5)
U^{13}(Cs)	0.8(1)	0.45(5)	U^{12}(O3)	−0.9(1)	−1.33(7)
U^{11}(P)	2.5(1)	1.85(5)	U^{13}(O3)	2.2(1)	2.32(5)
U^{22}(P)	1.4(1)	2.83(22)	U^{23}(O3)	−0.9(1)	−1.44(7)
U^{33}(P)	0.8(1)	1.26(4)	U^{11}(D1)	3.6(2)	2.94(6)
U^{13}(P)	1.1(1)	0.66(4)	U^{22}(D1)	2.3(1)	3.32(20)
U^{11}(O1)	3.2(2)	1.79(4)	U^{33}(D1)	1.5(1)	2.16(4)
U^{22}(O1)	2.7(1)	3.66(20)	U^{13}(D1)	1.3(1)	1.21(4)
U^{33}(O1)	0.8(1)	1.56(4)	U^{11}(D2)	2.3(2)	3.21(9)
U^{13}(O1)	1.0(1)	0.68(3)	U^{22}(D2)	2.4(2)	2.63(32)
U^{11}(O2)	3.6(2)	3.90(7)	U^{33}(D2)	2.8(2)	3.56(7)
U^{22}(O2)	4.3(2)	5.39(25)	U^{12}(D2)	0.3(3)	−0.52(14)
U^{33}(O2)	0.6(1)	1.38(4)	U^{13}(D2)	0.4(4)	0.96(6)
U^{13}(O2)	1.0(1)	1.02(4)	U^{23}(D2)	−0.5(2)	−0.09(11)

Table 4.6: The refined anisotropic thermal parameters ($\times 10^{-2}$Å^2) for CsD_2PO_4 at 4.0kbars and 236K compared with those obtained from the data at atmospheric pressure (AP) and 267K by McMahon *et al.* (1990b). Esd's are given (in parentheses) on the last quoted place. The relatively large esd's of the U^{22} parameters in the atmospheric-pressure study are due to the relatively low resolution of the data along the b-axis.'

to 5 times those of the AP study, indicating the poorer precision of the HP experiment. Comparison of the thermal parameters in the two studies (Table 4.6) shows the esd's in the HP experiment to be a factor of 2-3 larger than those obtained in the AP study, although the U^{22} parameters are better determined in the present experiment due to the low number of high k-index reflections that were measured at AP.

Comparison of the absolute values of the thermal parameters in the two experiments shows the present HP results to be rather poorly related to those obtained at AP. This, and the fact that the precision of the refined structure in this experiment is a factor of approximately two lower than the LDP experiment described in the previous section, is felt to be due mainly to two differences.

(1) The data in the DCsDP experiment were collected with the single-detector rather than the PSD. The significantly higher precision with which the PSD allows weak peaks to be measured is felt to be essential for the most accurate structural studies.

(2) The experimental time eventually available for the collection of the DCsDP data was approximately half that available for the LDP experiment.

It should be noted, though, that when parameter correlations are taken into account, the effect of the poorer precision of the refined atomic coordinates in the present study on the calculated bondlengths is to increase their esd's by a factor of only two over those obtained at AP. This precision in the calculated bondlengths is therefore higher than that obtained in an early structural study of CsDP at atmospheric pressure (Nelmes and Choudhary (1978)) where 2R was determined to only 0.01Å and δ to 0.04Å.

Figures 4.13a and 4.13b show how T_c in CsDP and DCsDP varies with 2R and δ respectively, using the values from the present study of DCsDP along with those from the AP studies of CsDP (Semmingsen and Thomas (1990)) and DCsDP (McMahon *et al.* (1990b)), and suggests that the CsDP-DCsDP system behaves very differently from the LHP, KDP and H_2SQ. systems. Three interesting points emerge.

(1) The three points on the T_c-2R graph lie on a straight line, in contrast to

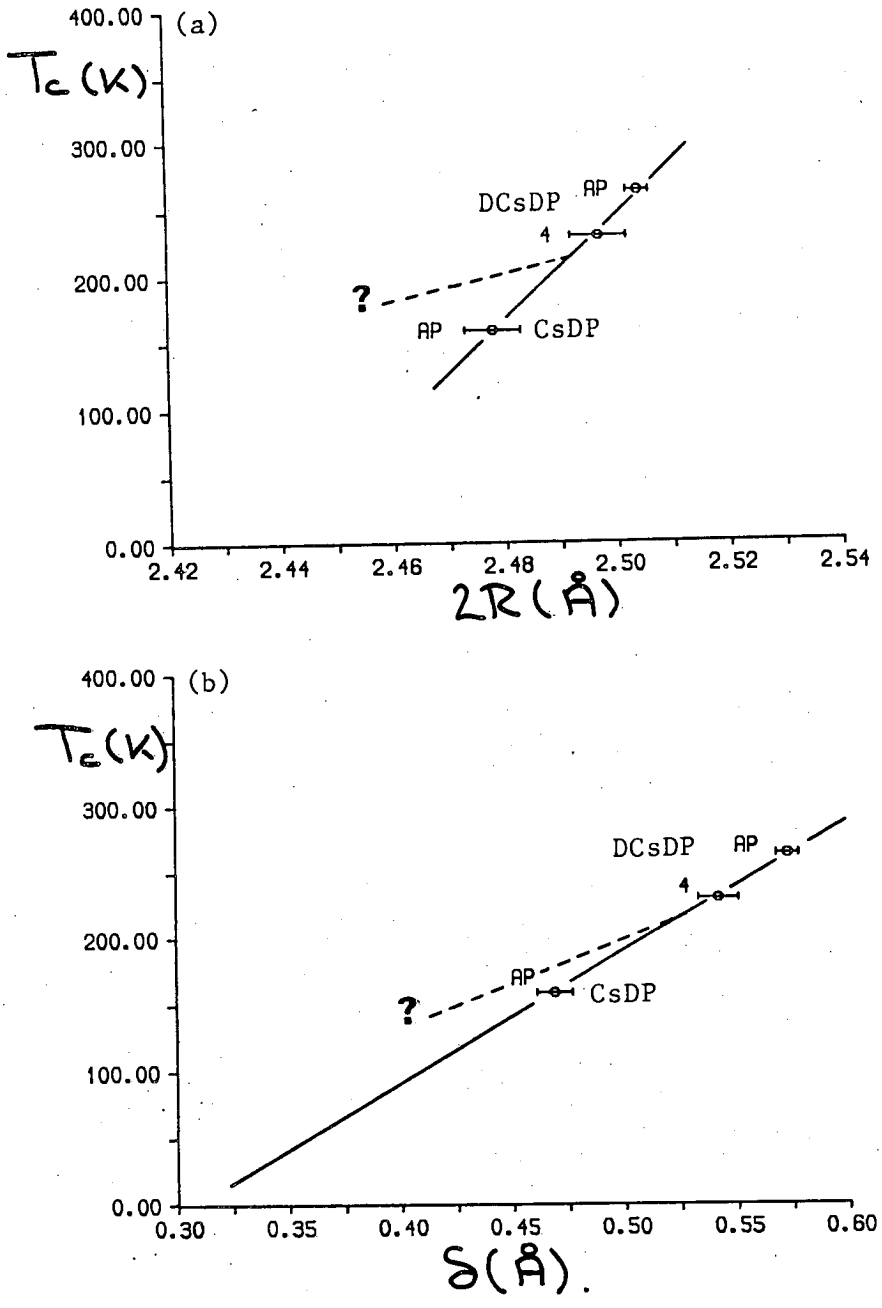

Figure 4.13: (a) The variation of T_c with the O-H-O bondlength, 2R, and (b) the variation of T_c with the H-site separation, δ, in CsH_2PO_4 (CsDP) and CsD_2PO_4 (DCsDP). The pressure is given against each point as AP (atmospheric pressure) or the number of kilobars applied. The dashed lines show the discontinuities in 2R and δ required at the triple point in DCsDP for the CsDP-DCsDP system to behave similarly to the KDP-DKDP and LHP-LDP systems, as discussed in the text.

the other systems studied to date. If T_c *is* related to 2R in the same way as the other systems then one might expect a ΔT_c of ~40K when 2R in the deuterated system was compressed to be the same as 2R in the hydrogenous system. This would require a sudden, and dramatic, discontinuity in the T_c-2R relationship, perhaps at T_c=214K, the triple point temperature. The resulting relationship between T_c and 2R is indicated in Figure 4.13a by the dashed line.

(2) The three points on the T_c-δ graph also lie on a straight line, as is observed for the other systems studied, but this line extrapolates to 0.3Å rather than 0.2Å as $T_c \rightarrow$0K. If, however, there is a discontinuity in the T_c-2R relationship then it would seem likely that this would be accompanied by a discontinuity in the T_c-δ relationship in DCsDP, perhaps at T_c=214K, and also in CsDP at its triple point temperature. These discontinuities might decrease the value of dT_c/dP, resulting in $\delta \rightarrow$0.2Å as $T_c \rightarrow$0K. This possible discontinuity for DCsDP is shown by the dashed line in Figure 4.13b.

(3) If T_c is related to δ and 2R then the dramatic change in dT_c/dP must be accompanied by a dramatic change in the pressure dependence of the PE structure on moving from just above the PE-FE phase boundary to just above the PE-AFE phase boundary. Why this change should occur, however, is uncertain, as no phase transition is involved, the crystal staying in the same PE phase, while high-pressure structural studies of the $NH_4H_2PO_4$-$ND_4D_2PO_4$ system (Piltz *et al.* (1990)), which is isomorphous with KDP above T_c but orders antiferroelectrically below T_c, have shown that the nature of the ordering below T_c has little effect on the relationship between T_c, 2R and δ.

This initial high-pressure study of the CsDP-DCsDP system has thus posed some interesting questions for the model of the transition based on structural arguments to answer and indeed the very different behaviour of the system poses some stringent tests for *any* model of the H-ordering transition. Much structural work is still needed on this system, especially at high pressures, in order to determine the nature of the relationship between T_c and 2R and T_c and δ. Although a high-resolution study of CsDP at AP and T_c+5K is needed to confirm the results of Semmingsen and Thomas (1990), the crucial experimental question is whether the discontinuity in dT_c/dP at the triple points results in a discontinuity in $dT_c/d2R$, $dT_c/d\delta$ or a change in the pressure dependence of the

structure. Experiments are in hand to study the pressure dependence of 2R just above T_c in the region of the triple point using powder-based neutron-diffraction techniques, but a detailed examination of the pressure dependence of δ in the same region poses an exciting, and very exacting, experimental challenge for the future.

4.5 A High-Pressure Structural Study of Quantum-Paraelectric KH_2PO_4.

4.5.1 Introduction

KDP was the first known H-ordering system in which T_c could be reduced to 0K by the application of hydrostatic pressure: T_c initially decreases at -4.6Kkbar^{-1} but at higher pressures the magnitude of dT_c/dP increases until, as shown in Figure 4.14, $T_c \rightarrow$0K at 17.1kbars (Samara (1971)). The term 'quantum-ferroelectric' (QFE) (Hochli (1981)) has been used to describe the low-temperature region (T_c <40K) in which the ordering temperature is determined by the balance between ordering forces and zero-point quantum fluctuations which favour disorder. Although T_c in mixed systems, such as $K_{1-x}Na_xTaO_3$, has been reduced to sufficiently low values by chemical substitution (Hochli and Boatner (1979)), KDP at high pressures (15kbars to 17.1kbars) was the first known case of a QFE state in a pure system.

Previous high-pressure neutron-diffraction studies have enabled the dimensions of 2R and δ at the critical conditions of 17kbars and 0K to have been estimated as 2.428(10)Å and 0.240(14)Å respectively (Tibballs *et al.* (1982a)). It was also possible to estimate the thermal parameters of the H-atom and the results suggested that the along-bond zero-point motion of the protons was sufficient to take them over the potential barrier from one potential minimum to the other, suppressing the ordered phase.

This explanation for the loss of the ordered phase, however, relies on the H atoms still being disordered over two sites at 17kbars and 0K, a situation which

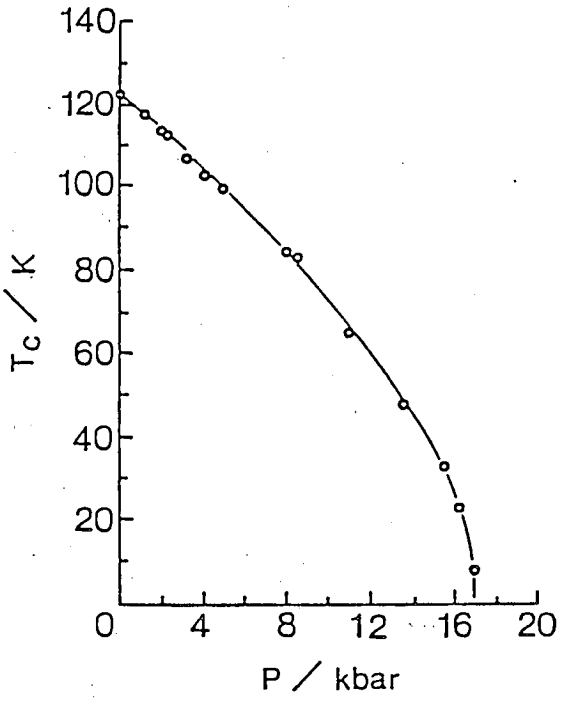

Figure 4.14: The pressure dependence of T_c in KH_2PO_4. (From Motida and Ichikawa (1989).)

is by no means certain. X-ray studies of KDP (Morosin and Samara (1971)) have suggested that $\delta \rightarrow 0$Å as $T_c \rightarrow 0$K, the H atoms becoming centred on a single site in a symmetric O–H–O bond, and this may explain the loss of the ferroelectric phase.

In order to determine whether or not the H atoms do indeed become centred in the O–H–O bonds, and to test the earlier explanation for the loss of the ordered phase, a structural study of KDP as close as possible to the critical conditions of 17kbars and 0K would be required. A determination of H-bond dimensions in KDP as $T_c \rightarrow 0$K would also allow the validity of the proposed extrapolation of δ to 0.2Å in all H-ordering systems described in the two previous experiments, to be tested experimentally for the KDP-DKDP system.

Two early attempts to reach the conditions of 17kbars and 0K using the Bloch cell resulted in failure as the pressure loss on cooling the cell was too great. However, the new pressure cell now available at the ILL lost comparatively little pressure on cooling (as described in Chapter 3.3.2), allowing the critical conditions to be achieved. This section describes the first structural study of an

H-bonded system in its quantum limit.

4.5.2 Experiment and Data Analysis

The experiment was performed on the D15 diffractometer using the new pressure cell described in Chapter 3.3.2 and a PSD. The sample crystal was approximately cylindrical in shape with diameter 3mm and height 3mm and was shaped from a crystal purchased from Lasermetrics Incorporated, New Jersey. A small $2\times2\times2mm^3$ cube of NaCl was mounted on top of the KDP sample for pressure calibration purposes. The sample was mounted in the pressure cell with the *b*-axis aligned along the cell axis allowing only the $(h0l)$ reciprocal layer of reflections to be measured. The pressure transmitting fluid was d-methanol and although this fluid known to dissolve KDP at high pressures, the fluid was frozen before this could occur.

Pressure was applied to the cell at room temperature and, using a calibrated wavelength of 1.1760(2)Å, the lattice parameter of the NaCl was determined to be 5.5176(44)Å corresponding to a pressure of 18.3(7)kbars (Decker (1971)). The pressure cell was then cooled to 10K over 36 hours. While cooling, the (600) and (404) reflections from the KDP were monitored to determine T_c, the (600) reflection splitting in the orthorhombic ferroelectric phase. No evidence of the phase transition was observed.

At 10K, the NaCl lattice parameter was determined to be 5.4960(8)Å, corresponding to a pressure of 16.5(1)kbars (Skelton *et al.* (1984)). The measurements to this point were made using the PSD but the detector developed a serious fault which prevented it from being used for data collection purposes. The loss of the PSD also prevented a very precise determination of the lattice parameters of KDP which had to be determined using the single-detector. The lattice parameters of KDP at 16.5kbars and 10K were determined to be $a=b=7.2767(35)$Å and $c=6.0811(29)$Å.

Using a $\lambda=1.1760(2)$Å, 156 reflections were measured to $\sin\Theta/\lambda=0.75$Å^{-1}. The wavelength was then reduced to 0.8551(2)Å and a further 193 reflections were measured to $\sin\Theta/\lambda=1.05$Å^{-1}. A slight tilt of the sample crystal allowed a

number of reflections in the $(h \pm 1l)$ layer to be measured and a number of identical reflections were included in both data sets to allow the two data sets to be put onto a common scale.

Trial refinements during the data collection enabled the most sensitive reflections to the H-atom distribution to be determined and these reflections were measured with a slow scan speed. Use of the 'Leverage' (Hazen and Finger (1989)) program also allowed sensitive reflections to be determined and remeasured to improve their statistics.

The scan profiles were converted into integrated intensities using the Lehmann-Larson (1974) method and the intensities were then corrected for sample absorption. No absorption correction for the pressure cell was necessary. On averaging those reflections with $I<10\sigma(I)$, several reflections were found to be severly affected by powder lines from the Al_2O_3 in the pressure cell and were deleted. Three reflections were also found to have been occluded by the pressure cell and were also deleted. After correcting for isotropic extinction, final averaging gave internal and statistical R-factors of 6.0% and 6.4% for λ=0.8551Å and 6.6% and 7.2% for λ=1.1760Å. Combining the two data sets gave 149 independent reflections.

Although no evidence of a phase transition to the ferroelectric phase was observed on cooling to 10K, the data were initially refined in the orthorhombic Fdd2 spacegroup. The H-atom distribution was determined to be 49(1)%:51(1)% while the P and K atoms refined to the special positions they occupy in the paraelectric phase. It was therefore concluded that the sample had indeed been in the tetragonal paraelectric phase.

The data were therefore refined in the $I\bar{4}2d$ spacegroup and the tetragonal symmetry allowed all the structural parameters to be refined from the $(h0l)$ data except the U^{12} thermal parameters which were fixed at values used in previous high-pressure low-temperature studies of KDP (Tibballs *et al.* (1982a)). In addition, the x(H) positional parameter was constrained to be equal to x(O) as the near coincidence of the O and H atoms when viewed along the b axis (see Figure 4.1) prevented the independent refinement of the x(H) and U^{11}(O) parameters. Various models were used to model the H-atom distribution.

Model	(1)	(2)	(3)	(4)
R-factor(%)	4.258	4.227	4.180	4.216
N	17	18	18	17
δ(Å)	–	–	0.248(22)	0.217(23)
2R(Å)	2.443(3)	2.442(3)	2.442(3)	2.442(3)

Table 4.7: The weighted R-factor, number of refined parameters (N) and resulting H-bond dimensions δ and 2R for various models of the H-atom distribution in KH_2PO_4 at 16.5kbars and 10K. The various models are discussed in the text. Models (1) and (2) are single-site models for the H atom and therefore do not give a value of δ – the H-atom separation.

(1) A single central site with anisotropic thermal motion.
(2) A single central site with anisotropic thermal motion and an additional along-bond anharmonic term.
(3) Two half-occupied sites each having *anisotropic* thermal motion but with $U^{22}(H)=U^{11}(H)$.
(4) Two half-occupied sites each having *isotropic* thermal motion.

In each model only the diagonal terms in the thermal parameter tensors of the H atoms were allowed to refine.

The final wR-factors for each model are given in Table 4.7 along with the number of parameters refined in each case and the resulting H-bond dimensions. Comparison of the various models using Hamilton's R-factor test (Hamilton 1965) shows that the improvement in fit of model (2) over model (1) is significant at only the 75% confidence level while a comparison of the two two-site models shows the improvement in fit of model (3) over model (4) to be also significant at only the 75% confidence level. However, comparison of models (1) and (4), and (2) and (3) shows the two-site models (models (3) and (4)) to give a better fit to the data than the single-site models using the same number of parameters, indicating that the H-atoms *may* be disordered. The refined positional and thermal parameters for model (4), the simplest two-site model, are given in Table 4.8 along with calculated bondlengths. The results from the high-pressure study

at 16.5kbars and 298K of (Tibballs *et al.* (1982a)) are given for comparison.

4.5.3 Discussion and Conclusions

Comparison of the precision of the results obtained in the present study with those obtained in the room-temperature study shown the esd's to be generally very similar, not surprising considering the similar quality and quantity of the data collected, except for the case of the H atom. This inability of the present study to probe the fine details of the H-atom distribution results from the resolution limit of the data (1.05Å^{-1}), which although much higher than the majority of high-pressure structural studies to date, is not high enough to decouple the H-atom positional and thermal parameters sufficiently to discriminate between a one-site and two-site distribution.

Trial refinements using data from numerous atmospheric-pressure structural studies of H-ordering systems has established an empirical relationship between the maximum resolution of the diffraction data and the magnitude of δ. The results show that in order to determine δ accurately with anisotropic thermal motion refined about each site, the resolution of the data must be high enough such that.

$$\frac{\sin\theta}{\lambda} \cdot \delta > 0.25\text{-}0.30 \qquad (4.9)$$

Failure to collect data to a high enough resolution will result in δ being overestimated. In the case of δ in this experiment, the estimated value of 0.22-0.23Å suggests that data would have to be collected to $\sim$1.3-1.4Å^{-1} in order to determine the form of the H-atom distribution accurately. The value of 0.248(22)Å for δ in the two-site anisotropic model (model (3)) used above is thus probably an overestimate. Collection of data to the required resolution is not possible on D15, where the minimum useful wavelength of 0.855Å allows a $(\sin\Theta/\lambda)_{max}$ of $\sim$1.1Å^{-1}, and would require a wavelength of $\sim$0.5Å which is available, for example, on the D9 or D3 diffractometers at the ILL. However, it is unlikely that the collection of diffraction data, even to a resolution of 1.6Å^{-1}, would show *conclusively* that the H-atom was either ordered or disordered, i.e. that

	KH_2PO_4 16.5kbars 10K	KH_2PO_4 16.5kbars 293K
a(Å)	7.277(4)	7.329(3)
c(Å)	6.801(3)	6.856(3)
U^{11}(P)	0.03(6)	1.06(4)
U^{33}(P)	0.43(8)	1.33(4)
U^{11}(K)	0.46(9)	1.74(7)
U^{33}(K)	0.27(10)	1.23(6)
x(O)	0.1539(3)	0.1536(1)
y(O)	0.0823(2)	0.0816(1)
z(O)	0.1285(3)	0.1267(2)
U^{11}(O)	0.37(5)	1.53(3)
U^{22}(O)	0.33(6)	1.53(3)
U^{33}(O)	0.49(5)	1.79(3)
U^{12}(O)	0	0
U^{13}(O)	−0.05(5)	0.60(9)
U^{23}(O)	−0.02(5)	−0.42(3)
x(H)	=x(O)	=x(O)
y(H)	0.2638(16)	0.2286(7)
z(H)	0.1187(22)	0.1224(12)
B(H)/U^{11}(H)	1.13(12)	2.54(14)
U^{22}(H)		=U^{11}(H)
U^{33}(H)		2.66(10)
2R(Å)	2.442(3)	2.469(3)
δ(Å)	0.217(23)	0.315(11)
P–O(Å)	1.542(2)	1.537(2)

Table 4.8: The unit-cell dimensions, refined fractional coordinates, anisotropic thermal parameters ($\times 10^{-2}$Å^2), the H-bond dimensions and the P–O bondlength for KH_2PO_4 at 16.5kbars and 10K compared with those obtained from the data at 16.5kbars and 293K by Tibballs *et al.* (1982a). Esd's are given (in parentheses) on the last quoted place. Parameters given without esd's were fixed at the values shown. For the study at 10K, the thermal motion of the H atom was constrained to be isotropic and is given in units of Å^2.

the probability density function (PDF) of the H atoms was either single-peaked or double-peaked.

Although the present high-pressure data do not allow a complete description of the H-atom distribution, the accurate determination of 2R *does* allow a model of the H-bond potential to be constructed and, using the method of Lawrence and Robertson (1980a), allows a determination of δ to be made from the calculated energy levels and associated wave functions of the proton in such a potential.

The Lawrence and Robertson calculations, which have shown to give an accurate determination of δ in both KDP and DKDP at atmospheric pressure (Lawrence and Robertson (1980b,1981)), are based on an H-bond potential comprised of two identical Morse potentials placed back to back. The parameters needed to describe the potential for KDP were obtained by fitting the known bands in the infra red spectrum to the diffraction values of 2R and δ. The potential for different temperatures and pressures in then simply obtained by varying the input value of 2R. For KDP at 16.5kbars and 10K, using the calculated 2R of 2.442(3)Å, the potential is shown in Figure 4.15a. It should be noted that the potential has a double-well. Using a computer program written by Mr. N.G. Wright of this department, the energy levels, and corresponding wavefunctions, were calculated for a proton in this potential and the first two energy levels are shown in Figure 4.15a. From these wavefunctions it was possible to calculate the probability density function (PDF) of a proton lying in the lowest energy level of the potential, the only level occupied at a temperature of 10K. This is shown in Figure 4.15b. The important thing to note in this figure is that the calculated PDF is two-peaked and therefore the proton is still disordered over two-sites – according to this model for the potential. That this should be so is illustrated by the location of the lowest energy level in Figure 4.15a which is below the potential barrier separating the two minima. This result is in disagreement with the calculations of Matsushita and Matsubara (1982) which suggested that the proton PDF would be single-peaked for 2R<2.47Å.

In order to calculate δ, the PDF was fitted with a pair of identical gaussian functions by least-squares, thus mimicking the fitting process in the least-squares refinement of the diffraction data which fits the H-atom distribution with two gaussian functions to describe the harmonic thermal motion around each site.

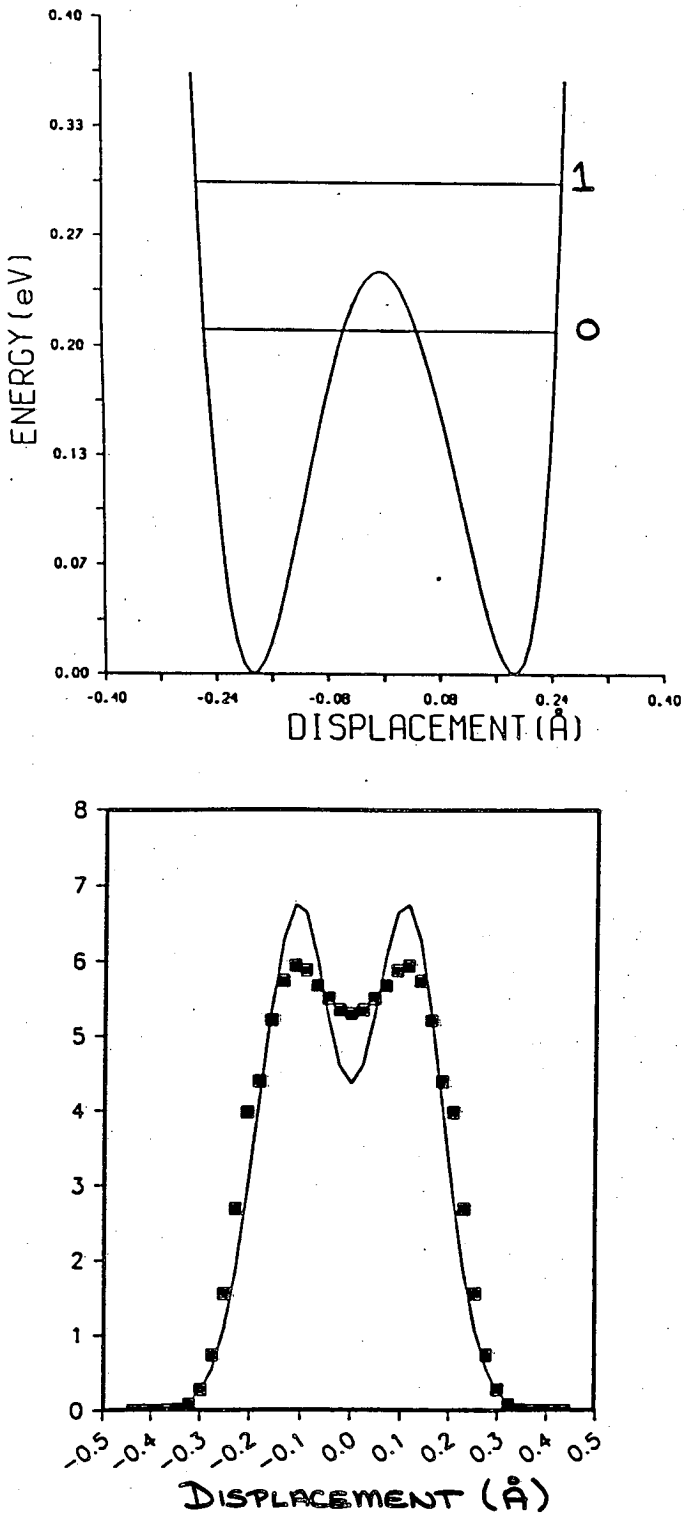

Figure 4.15: (a) The double-well potential for the measured O-H-O bondlength of 2.442Å in KDP at 16.5kbars and 10K. The location of the first two energy levels are marked. (b) The calculated probability density function (PDF) for a proton occupying the lowest energy level in the potential in (a) versus the distance (in Angstroms) from the centre of the bond. The solid line is a least-squares fit of two identical gaussians to the PDF

The value of δ obtained from fitting the PDF in this manner is 0.22Å, in excellent agreement with the two-site isotropic model which gives δ=0.217(23)Å. It should be noted, however, that the PDF of the H atom shown in Figure 4.15b would be better modelled by two anharmonic non-symmetric functions. It is not possible, however, to refine such a model for the H-atom distribution using the present diffraction data.

The two-site isotropic model therefore gives both a good fit to the present diffraction data and a value of δ that is consistent with that calculated using the Lawrence and Robertson model for the potential. Using this description for the H-atom distribution, the along-bond zero-point thermal motion is 0.120(6)Å, slightly larger than the value for $\delta/2$ of 0.109Å, in agreement with the earlier explanation (Tibballs *et al.* (1982a)) for the loss of the ordered phase in terms of the zero-point thermal motion being too large in comparison to δ to allow the system to order.

Three important conclusions thus emerge from this study of KDP.

(1) The protons are very probably disordered over two-sites at the critical conditions of 17kbars and 0K with a separation of H-site separation of ~0.22Å. This is in contrast to predictions that the H-bond would be centred under these conditions.

(2) The along-bond zero-point thermal motion of each proton at 16.5kbars and 10K is sufficient to carry the proton from one potential minimum to the other, preventing the system from ordering.

(3) The extrapolation of the KDP-DKDP system to a δ of ~0.2Å as $T_c \rightarrow$0K is valid and this may be true for the other systems as well.

Although this structural study of KDP has allowed the three points raised in the introduction to be answered, it would desirable to repeat the experiment to higher resolution to enable the true form of the H-atom potential to be determined experimentally, and to allow a comparison of the measured distribution to that calculated using the methods of Lawrence and Robertson. It would also be of great interest to make a structural study of another H-ordering system in the T_c=0K region and both RbH_2PO_4 and $NH_4H_2PO_4$ are possible candi-

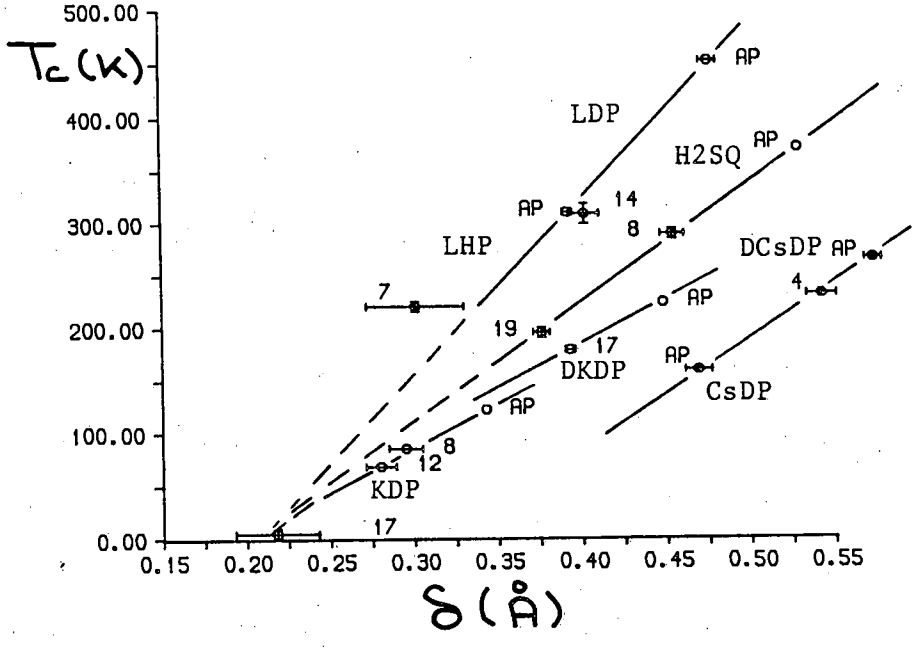

Figure 4.16: The variation of T_c with the H-site separation, δ, in KH_2PO_4 (KDP), KD_2PO_4 (DKDP), $H_2C_4O_4$ ($H_2SQ.$), $PbHPO_4$ (LHP), $PbDPO_4$ (LDP), CsH_2PO_4 (CsDP) and CsD_2PO_4 (DCsDP). The CsDP and DCsDP points are represented by filled circles. The pressure is given against each point as AP (atmospheric pressure) or the number of kilobars applied. Where error bars are not shown, the errors are less than the size of the symbols used to plot the point. The lines are guides for the eye only.

dates, having been observed to lose their ordered phases at pressures greater than 15.2kbars (Peercy and Samara (1973)) and 33kbars (Samara (1971)) respectively. It would also be of great interest to study a deuterated system under the same conditions to see what effect the heavier deuteron has on the value of δ, but this would require a pressure of 70kbars in DKDP (Samara (1979)) and must therefore await improved experimental techniques in the future.

4.6 Conclusions

The use of the Ahsbahs and new ILL clamp cells, and associated data collection techniques, has allowed experiments to be performed with either an unprecedented degree of accuracy, or that were in fact impossible prior to the present work, and have resolved long-standing uncertainties arising from earlier structural work. The results are briefly summarised below.

(1) The study of LHP and LDP under conditions were they have the same T_c has established that they also have the same value of δ, within error, decisively securing a conclusion indicated earlier in the KDP-DKDP system. The results also conclusively show that T_c is not the same if the two materials are compared at the same 2R, again securing a result previously indicated in the KDP-DKDP system and in contradiction to earlier claims. The high-pressure experiment has also allowed the unusual results observed in an earlier high-pressure study of LHP to be explained as arising from the limited data collection in that case, and has shown that the LHP-LDP system does indeed behave similarly to the KDP-DKDP and H_2SQ_4 systems with δ in all three systems extrapolating to δ=$\sim$0.2-0.22Å as $T_c \rightarrow$0K.

(2) The high-pressure study of DCsDP suggests that it is the CsDP-DCsDP system that does now not behave in a similar way to the other systems studied so far. However, the presence of the triple points, and the discontinuities in dT_c/dP, makes the dependence of T_c on 2R and δ uncertain.

(3) The study of KDP in its quantum paraelectric state at 16.5kbars and 10K establishes that the H-atoms are very likely disordered as $T_c \rightarrow$0K and that the separation is $\sim$0.22Å, validating the linear extrapolation of the KDP-DKDP

system, and probably the LHP-LDP and H_2SQ. systems also, to a δ of $\sim$0.2Å as $T_c \rightarrow$0K. The along-bond thermal motion at 16.5kbars and 10K has also been shown to be large enough in comparison to δ to prevent KDP from ordering – providing a structural basis for the loss of the ordered phase.

An explanation for these results, unfortunately, is not possible using the long accepted tunnelling model which fails to account for the relationships between δ, 2R and T_c observed in the present work.

In the light of recent Japanese spectroscopic results (Tominaga *et al.* (1983a,b), Tokunaga and Matsubara (1987)), however, and a very high resolution atmospheric-pressure structural study of DKDP (McMahon *et al.* 1990a) which strongly suggests that the P atom is disordered over two sites, ΔP=0.143(7)Å apart, above T_c and that the transition therefore involves an order-disorder of the entire H_2PO_4 groups such that the symmetric PO_4 group above T_c (Tokunaga (1984)) is a 50:50 average over two distorted ferroelectric configurations, a radically revised theory of the H-ordering transition is being developed by Prof. R. Blinc (1990), the originator of the present tunnelling model, based on a similar interpretation recently proposed for the transition in CsDP (Kojyo and Onodera (1988)).

In essence, a system of two-configurationally disordered PO_4 groups is assumed above T_c, with interactions proportional to the distortion of the groups. The H atoms then play the purely local role of tending to make adjacent PO_4 groups orient the same way via the relative energies of different H_2PO_4 configurations.

This theory has still to be completed and no explanation for the results of the present work is yet available. However, one immediate and crucial outcome of the new theory is that T_c should depend on the magnitude of the PO_4 distortion, which is measured by the magnitude of ΔP. Although there is little hope of making a direct determination of ΔP at high pressures and relating it to the pressure induced reduction in T_c, the magnitude of ΔP may be estimated from the anisotropy of the P-atom thermal motion which would be expected to decrease at high pressures if ΔP decreases. The large reduction in the magnitude of U^{22}(P) in DCsDP (Table 4.6) may be important in this respect (the P atoms will be disordered along the *b*-axis in CsDP-DCsDP) although the very anisotropic nature of the P-atom thermal motion in KDP at 16.5kbars and 10K

(Table 4.8), which might be expected to be very much more isotropic if $\Delta P \rightarrow 0$Å as $T_c \rightarrow 0$K, remains a mystery.

A series of high-pressure structural work focussed on the PO_4 group, especially the thermal motion of the P atom, is now needed, with the Ahsbahs cell, combined with the use of a PSD, uniquely capable of providing the very high quality of data that will be required.

Chapter 5

High-Pressure Structural Studies of High-T_c Superconductors

5.1 Introduction

Compared to the high-pressure structural study of H-ordering materials, the structural study of high-T_c superconductors at high pressure is a very recent field with the first results being published by Kaldis *et al.* in 1989. Sections 3 to 5 of this chapter describe three structural studies of the $La_{1.85}Sr_{0.15}CuO_4$ and $YBa_2Cu_4O_8$ superconductors up to pressures of 46kbars using neutron powder-diffraction and single-crystal x-ray diffraction techniques, and represent a high proportion of the high-pressure structural studies made on high-T_c materials to date. A comparison of the results obtained using the various techniques clearly demonstrates the problems that can arise in high-pressure structural studies, and these are discussed in section 6.

5.2 High-T_c Superconductors

Although the magnitude of dT_c/dP in the high-T_c superconductors, where T_c in this case is the superconducting transition temperature, is only a fraction of the values observed in the H-ordering materials, the range of values from $0Kkbar^{-1}$ in $YBa_2Cu_3O_{7-x}$ to $0.55Kkbar^{-1}$ in $YBa_2Cu_4O_8$ (Griessen (1987), van Eenige *et*

al. (1990)), has created great excitement as this range of values opens up the possibility of finding structural changes that occur in the latter material, but not in the former, and thus identifying a structural basis for the superconducting transition. This possibility is further enhanced by the discovery of a new series of oxide superconductors $L_{2-x}Ce_xCuO_{4-y}$ (L=Pr, Nd, Sm) which have a negative dT_c/dP.

Such a link between dT_c/dP and the crystal structure may be expected to be most evident in materials in which dT_c/dP is large and most interest has therefore been focussed on $La_{1.85}Sr_{0.15}CuO_4$ (T_c =~37K) and $YBa_2Cu_4O_8$ (T_c=80K) which have a dT_c/dP of $0.37Kkbar^{-1}$ and $0.55Kkbar^{-1}$ respectively.

Figures 5.1 and 5.2 show the $La_{1.85}Sr_{0.15}CuO_4$ or 2-1-4 structure and the $YBa_2Cu_4O_8$ or 1-2-4 structure in their room-temperature phases. The 2-1-4 structure (Figure 5.1) is the simpler of the two, and may be viewed as planes of CuO_6 octahedra of the perovskite structure, alternating with a buckled rocksalt La(Sr)-O slab which is rotated in the basal plane by 45°. The crystal is tetragonal with spacegroup I4/mmm at room temperature but undergoes a structural phase transition to an orthorhombic phase, spacegroup Abma, below 180K. The orthorhombic structure is derived from the tetragonal structure by tilting of the CuO_6 octahedra around the orthorhombic *b* axis In the 1-2-4 structure (Figure 5.2), the octahedra of the 2-1-4 structure are replaced by two 'half-octahedra', the CuO_5 square pyramids, which are separated by the Y atoms. These double pyramid slabs are linked through two parallel Cu-O chains (along the *b*-axis), which results in a relative displacement of alternate slabs along the *b*-axis and hence a large *c*-axis repeat of ~27Å.

Recently Cava *et al.* (1988) have shown that in $YBa_2Cu_3O_{7-x}$ the change in T_c on varying x from 0.6 to 0.0 is accompanied by a reduction in the distance from the basal-plane Cu of the pyramids to the apical oxygen (denoted Cu-O2 in the 2-1-4 material and Cu2-O1 in the 1-2-4 structure). Closer examination (Cava *et al.* (1990)) has shown that there is a very close correspondence between the changes in T_c and the Cu-O1 bondlength with x. Kaldis *et al.* (1989) have shown, using high-pressure angle-dispersive neutron-diffraction, that the only notable structural change on compressing polycrystalline $YBa_2Cu_4O_8$ to 10kbars was a substantial decrease in this apical Cu-O bondlength. They associated this

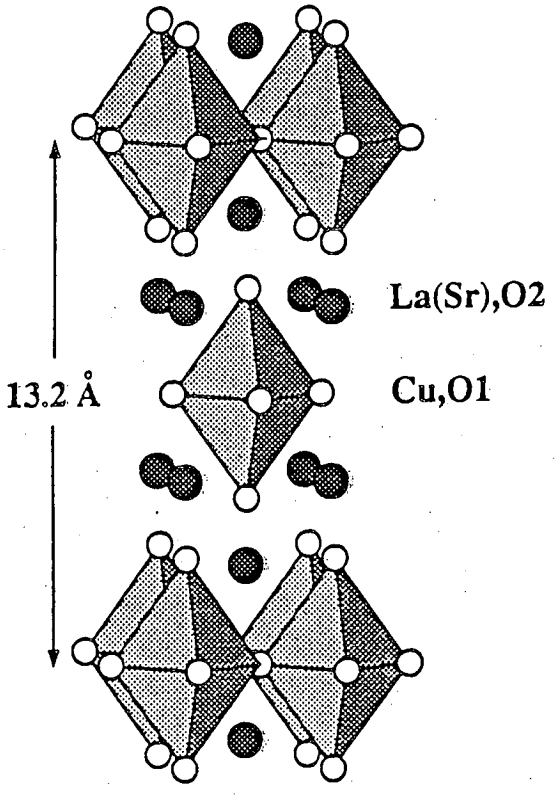

Figure 5.1: The crystal structure of $La_{1.85}Sr_{0.15}CuO_4$ in its room-temperature phase.

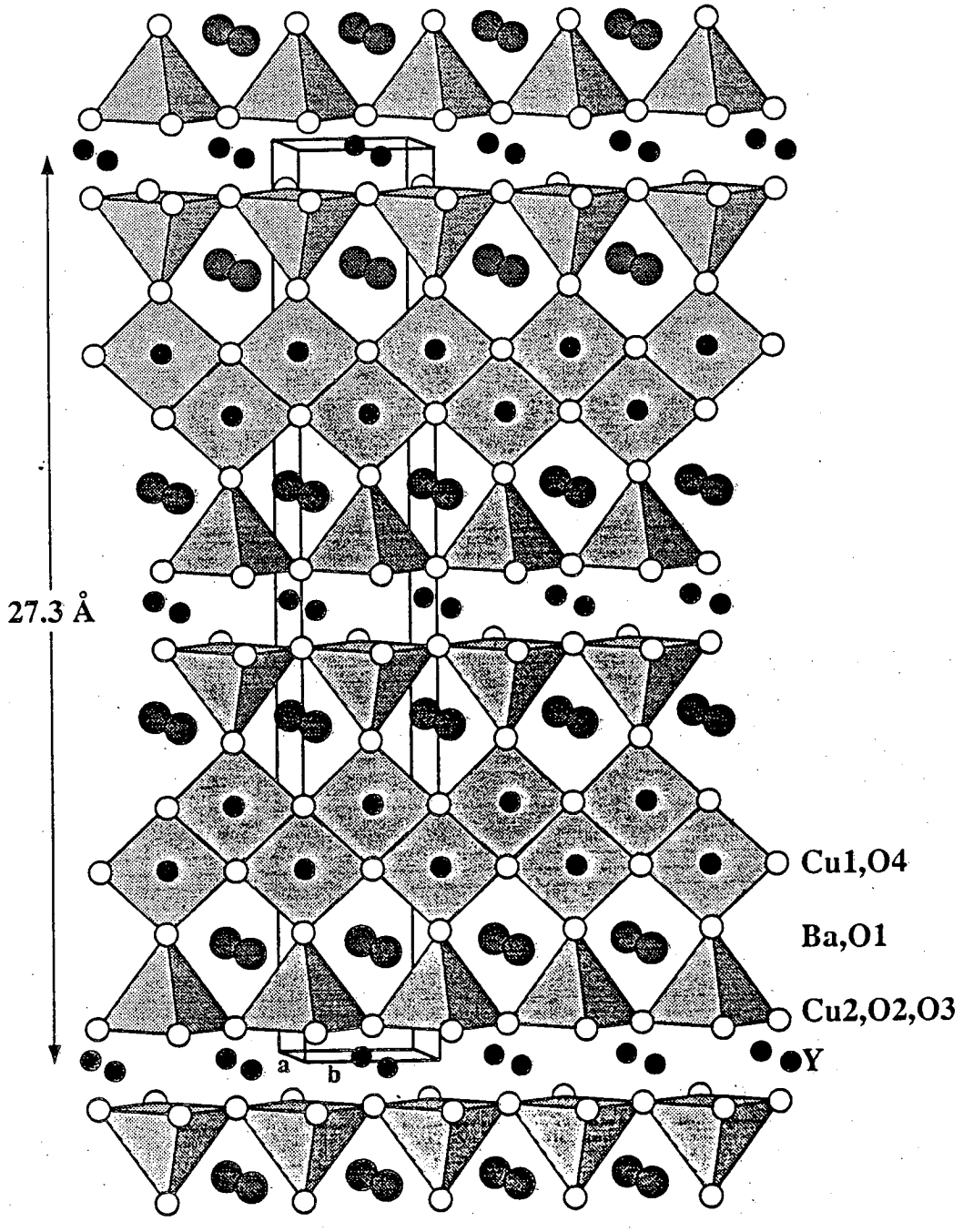

Figure 5.2: The crystal structure of $YBa_2Cu_4O_8$ in its room-temperature phase.

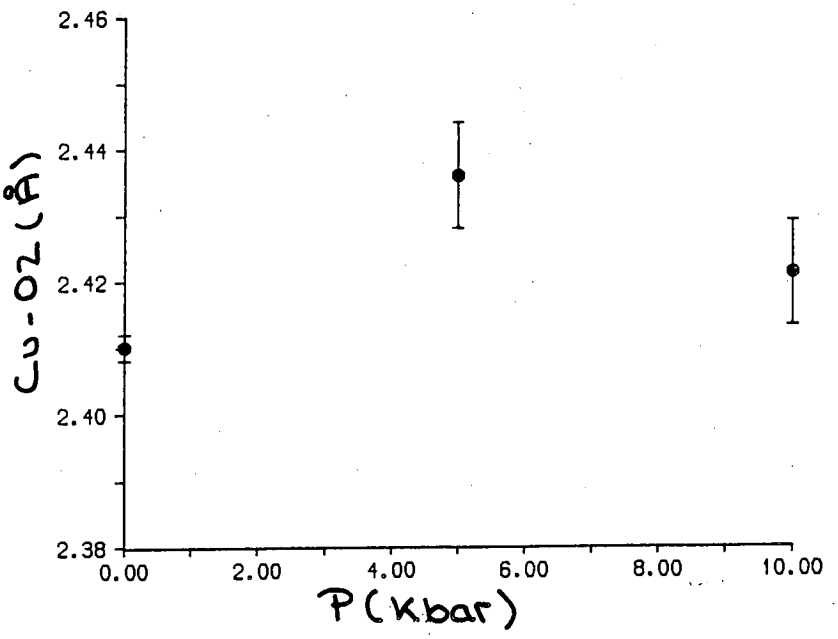

Figure 5.3: The pressure dependence of the apical Cu-O bondlength in La_2CuO_4 at room temperature. (After Howard *et al.* (1989).)

with the simultaneous increase in T_c.

A similar high-pressure neutron-diffraction study of La_2CuO_4 (Howard *et al.* (1989)), however, showed a very different behaviour of the apical Cu-O bondlength which first *increased* in length when the pressure was raised to 5kbars before decreasing again nearly to its atmospheric-pressure value at 10kbars (Figure 5.3). This intriguing result prompted the present structural work on the pressure dependence of the superconducting derivative of La_2CuO_4, $La_{1.85}Sr_{0.15}CuO_4$, with the aim of determining the pressure dependence of the apical Cu-O bondlength.

The determination of the positional parameters of the O atoms amongst the much heavier Y, La, Ba and Sr atoms has led to most structural investigations of high-T_c superconductors being made using neutron-diffraction techniques because of the comparative scattering power of the atoms. This dependence on neutron-diffraction techniques, however, and the fact that most oxide superconductors are only available in powder form, limited the high-pressure structural study of Kaldis *et al.* to 10kbars although T_c has been measured in many cases to much higher pressures (Griessen (1987)). It was therefore hoped in the present work to increase the upper pressure limit at which the materials could

be measured by using single-crystal techniques or powder-based techniques on a spallation neutron source.

5.3 A High-Pressure Structural Study of Tetragonal $La_{1.85}Sr_{0.15}CuO_4$

5.3.1 Introduction

The large difference in the pressure dependence of the apical Cu-O bondlength in (nonsuperconducting) La_2CuO_4 and in (superconducting) $YBa_2Cu_4O_8$ prompted the question as to whether the difference was due to the fact that one material was superconducting while the other was not, or that the difference was due to the different crystal structures. In order to test these possibilities, a high-pressure structural study was made of superconducting $La_{1.85}Sr_{0.15}CuO_4$ using the same pressure cell and pressure fluid as was used by both Kaldis *et al.* and Howard *et al.*

5.3.2 Experiment and Data Analysis

The carefully characterised powder sample of $La_{1.85}Sr_{0.15}CuO_4$ was provided by Dr. B. Raveau of ISMRA, Caen. The pressure cell used was a clamp-type 'dumb-bell' cell made from maraging steel which allowed a sample volume of $\sim 125 mm^3$. This was the same pressure cell used by both Howard *et al.* and Kaldis *et al.* The pressure fluid was Fluorinert – a mixture of fluorocarbons. No pressure calibrant was used in the present study as the resulting powder peaks could not be decoupled from those of the sample by multi-phase refinement and would thus be considered as contaminant peaks. The pressure was measured from a prior calibration of the resulting pressure from a known applied load to the cell which is considered to be known to within 5%.

The diffraction data were collected on the D1A powder diffractometer at the ILL (Hewat and Bailey (1976)) using a calibrated wavelength of 1.909(1)Å. Profiles

were collected at atmospheric pressure (on a sample outside the cell), 6kbars and 10kbars, as well as a single low-temperature data collection at 4K and an estimated pressure of 7kbars. At each pressure great care was taken to ensure that the pressure cell was replaced at the same position on the diffractometer in order to avoid centering errors of the sort discussed in Chapter 2. The vice-type arrangement used to hold the pressure cell at room temperature made this task quite simple and centering errors is this case are regarded as minimal.

In each case the profile patterns were collected from 5° to 156° in 2Θ using a 2Θ step size of 0.05°. The data collection time at each pressure was 12-14 hours. The typical peakwidth was 0.4° FWHM. Very intense and broad peaks were found in the profile arising from the maraging steel of the cell, which although cadmium was used to shield most of the cell from the incident beam, still scatters strongly into the detector. Such peaks were present at angles centred on 56°, 83° and 109° and these regions were estimated visually from the profiles and were excluded from the profile refinement. Exclusion of these areas resulted in a loss of 6 sample peaks from a free-sample total of 31 distinct peaks.

The powder patterns were refined using the PROFIL Rietveld program at the ILL (Cockcroft (1989)). No correction was necessary for pressure cell absorption and the background level for the pattern was determined visually. Isotropic thermal parameters were refined for each atom. In all cases the instrumental zero and asymmetry parameters obtained from the refinements were found to be self consistent. The lattice parameters and final refined positional coordinates and thermal parameters for the three room-temperature studies are given in Table 5.1 along with the calculated apical Cu-O2 bondlength. The results of Howard *et al.* for La_2CuO_4 in its orthorhombic phase are also given for comparison.

Table 5.2 shows the results for the low-temperature study of orthorhombic $La_{1.85}Sr_{0.15}CuO_4$ at the nominal pressure of 7kbars. The thermal parameters had to be fixed in order to refine the data. Values have been calculated for the orthorhombic distortion, $2(a-b)/(a+b)$; for the orthorhombic analogue of the tetragonal c/a ratio, $2\sqrt{2}c/(a+b)$; and for the orthorhombic tilt angle of the octahedra, $\tan^{-1}(x(O2)/z(O2))(a/c)$. The low-temperature results of Francois *et al.* (1987) at atmospheric pressure, transformed to the Abma spacegroup, are also given for comparison.

$La_{1.85}Sr_{0.15}CuO_4$	1bar	6 kbar	10 kbar
a(Å)	3.7743(1)	3.7696(1)	3.7681(1)
b(Å)	13.2193(4)	13.2058(6)	13.2004(5)
z(O2)	0.1823(3)	0.1846(6)	0.1831(5)
z(La,Sr)	0.3604(2)	0.3599(3)	0.3595(3)
B(La,Sr)	0.50(6)	0.99(12)	0.84(13)
B(Cu)	0.42(8)	0.60(16)	0.43(17)
B(O1)	0.57(9)	0.12(13)	0.23(11)
B(O2)	0.49(8)	0.15(11)	0.28(9)
R_{wp}(%)	7.4	9.9	10.1
Cu-O2(Å)	2.410(3)	2.438(8)	2.417(7)
La_2CuO_4	1bar	5 kbar	9 kbar
a(Å)	5.3938(2)	5.3830(4)	5.3736(4)
b(Å)	5.3466(2)	5.3418(4)	5.3378(4)
c(Å)	13.1309(4)	13.120(1)	13.114(1)
z(O1)	−0.0071(2)	−0.006(1)	−0.008(1)
x(O2)	0.0338(4)	0.039(2)	0.029(3)
z(O2)	0.1830(1)	0.1850(6)	0.1842(6)
x(La)	−0.0066(3)	−0.008(2)	−0.004(2)
z(La)	0.3615(1)	0.3612(3)	0.3616(3)
Cu-O2(Å)	2.410(2)	2.436(8)	2.421(8)

Table 5.1: Pressure dependence of the unit cell dimensions and structural parameters in (tetragonal) $La_{1.85}Sr_{0.15}CuO_4$ and (orthorhombic) La_2CuO_4 (from Howard *et al.*) at room temperature. The isotropic thermal parameters for $La_{1.85}Sr_{0.15}CuO_4$ are given in $Å^2$ and R_{wp} is the weighted profile R-factor.

Parameter	1 bar, 7K	7kbars, 4K
a(Å)	5.348(2)	5.3270(7)
b(Å)	5.324(2)	5.3111(6)
c(Å)	13.200(4)	13.167(1)
z(O1)	−0.0049(3)	−0.0045(39)
x(O2)	0.0245(5)	0.0346(30)
z(O2)	0.1821(2)	0.1836(8)
x(La,Sr)	−0.0055(4)	−0.0281(31)
z(La,Sr)	0.3608(1)	0.3595(4)
Cu-O2(Å)	2.407(3)	2.425(11)
2(a−b)/(a+b)%	0.45(6)	0.30(2)
$2\sqrt{2}$c/(a+b)%	3.498(2)	3.501(1)
tilt angle (°)	3.12(7)	4.4(4)
Reference	Francois *et al.*	This work

Table 5.2: Unit cell dimensions and structural parameters at 1bar and at a nominal '7kbars' in the orthorhombic phase of $La_{1.85}Sr_{0.15}CuO_4$ near 4K.

5.3.3 Discussion and Conclusions

Comparison of the precision of the results obtained in the high-pressure studies with that obtained in the atmospheric-pressure study shows the esd's on the lattice parameters to be similar in all cases and that they are very precisely determined. This reemphasises the point raised in Chapter 2 about the very precise lattice parameters available when using Rietveld fitting techniques. Comparison of the estimated errors on the positional coordinates shows the esd's in the high-pressure studies at room temperature to be up to twice those in the atmospheric-pressure study, resulting in a Cu-O2 bondlength with an estimated error 2-3 three times that obtained at atmospheric pressure. Comparison of the *absolute* error on the Cu-O2 bondlength, however, shows it to be four times that obtained for a similar length bond (O-H-O) in the previous chapter, emphasising the higher precision available with single-crystal techniques. Comparison of the present high-pressure results for the low-temperature orthorhombic structure show the esd's on the high-pressure data to be up to 13 times larger than those obtained by Francois *et al.* at atmospheric pressure. The largest errors are for those coordinates characterising the orthorhombic distortion, that is x(O1), x(O2) and x(La,Sr), and result in a Cu-O2 bondlength with an esd almost 4 times that at atmospheric pressure. The refined thermal parameters in this study are not thought to be physically meaningful, in contrast to the results from the previous chapter.

The Cu-O2 bondlengths from the present room-temperature studies are plotted against pressure in Figure 5.4 which shows that although the lattice parameters decrease quite normally in length with pressure (Table 5.1), there is a clear anomaly in the pressure dependence of the Cu-O2 bondlength. In contrast to the previous $YBa_2Cu_4O_8$ results, but in remarkably similar fashion to the La_2CuO_4 results of Howard *et al.* (compare Figures 5.3 and 5.4), the Cu-O bondlength first increases with pressure then decreases – over a pressure range where T_c is linear (Griessen (1987)). The present results, therefore, do not exhibit the same relationship between T_c and the apical Cu-O bondlength as has been seen in $YBa_2Cu_4O_8$. Possible reasons for this may be due to the structural differences between $La_{1.85}Sr_{0.15}CuO_4$ and $YBa_2Cu_4O_8$, especially the lack of the linking Cu1-O4 chains in the 2-1-4 structure. However, the differences are not certain, as the $YBa_2Cu_4O_8$ data were collected at only two pressures, atmospheric pressure

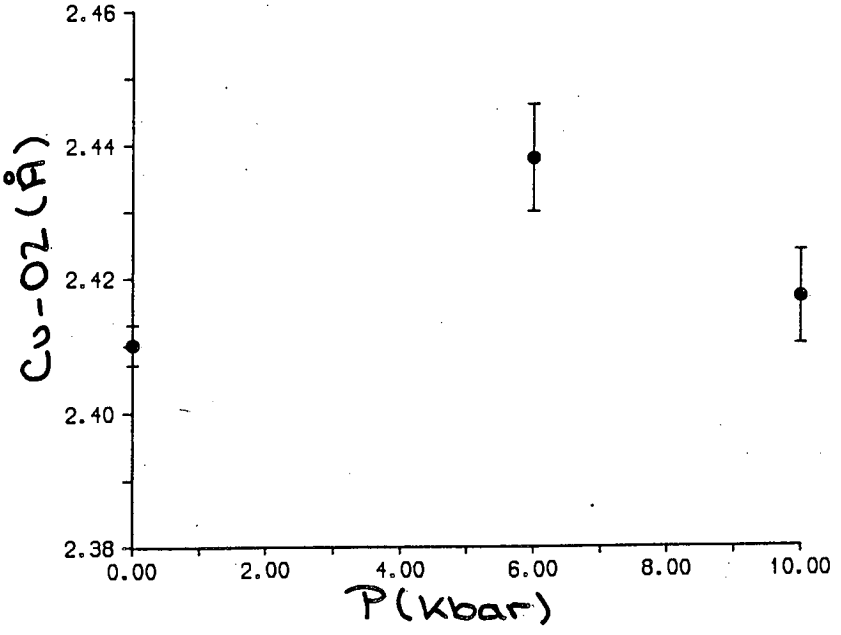

Figure 5.4: The pressure dependence of the apical Cu-O2 bondlength in $La_{1.85}Sr_{0.15}CuO_4$ at room temperature.

and 10kbars, and thus the intermediate behaviour of the Cu-O bondlength is unknown and may well exhibit a similar non-linear behaviour.

The conclusions above between the magnitude of T_c and the Cu-O bondlength are based on the assumption that the structural changes with pressure are the same at room temperature and at T_c. This assumption would seem to be given some justification by the low-temperature results which show, at least, that the Cu-O2 bondlength does indeed increase from its atmospheric-pressure value with pressure, as at room temperature. However, to test this assumption more rigorously it would be necessary to perform a series of experiments in the orthorhombic phase, closer to T_c. Such a series of experiments are discussed in the next section.

5.4 A High-Pressure Structural Study of Orthorhombic $La_{1.85}Sr_{0.15}CuO_4$

5.4.1 Introduction

The results given in the previous section for the structure of $La_{1.85}Sr_{0.15}CuO_4$ in its orthorhombic phase illustrated the poorer quality of results obtained compared to the tetragonal phase due to the poor signal-to-noise combined with the small orthorhombic splitting of the peaks. In order to resolve this problem it was hoped to use the D2B powder diffractometer at the ILL to collect the orthorhombic data as this instrument has considerably higher resolution (narrower peak widths) than D1A. Unfortunately, this instrument was unavailable and the high-pressure data had to be collected on D1A once again. However, in order to overcome the problems of the poorer quality of the refinement in the orthorhombic phase, a Paureau-Vettier gas pressure cell was used, which allowed a much larger sample volume, thus giving a considerable improvement in the signal-to-noise ratio. It was hoped that this improved determination of the powder profile would allow a better refinement of the orthorhombic structure. The upper pressure limit of the gas cell, though, was only 5kbars; however this pressure limit would be sufficient to determine if the apical Cu-O bondlength increased with applied pressure over this range.

5.4.2 Experiment and Data Analysis

The carefully characterised sample of $La_{1.85}Sr_{0.15}CuO_4$ was again provided by Dr. B. Raveau ISMRA, Caen. The pressure cell used was a Paureau-Vettier (1975) gas cell and contained a sample volume of $\sim$4000mm^3. The pressure transmitting medium was He gas and the pressure was measured using a digital pressure gauge which had an accuracy of 50bars. The diffraction data were collected on the D1A diffractometer (Hewat and Bailey (1976)) using a wavelength of 1.909(1)Å.

The pressure cell was loaded into a standard ILL orange cryostat which was

carefully centred on the diffractometer. Although the centering of the pressure cell was more difficult when using the cryostat, any centering errors would not affect the trend of the Cu-O bondlength with pressure as the pressure in the cell was varied *in situ*. The absolute values of the Cu-O bondlength, however, may be affected by any miscentering.

The pressure cell was cooled to 55K and powder profiles were collected at 1bar, 2.5kbars and 5kbars. As for the previous experiments in the tetragonal phase, the profiles were obtained from 5° to 156° in 2Θ with a 2Θ step size of 0.05° and each profile was collected for 12 hours.

Refinements were made while the data collection was still in process using the PROFIL Rietveld program. Although the pressure cell was again shielded from the direct beam using cadmium, very intense powder lines from the aluminium body of the cell were present. These peaks were at 2Θ angles centred on 56°, 84°, 113° and 132°, and these regions were estimated visually and excluded from the profiles used for structure refinement. No absorption correction was necessary for the pressure cell and the background level was determined visually for each profile. Isotropic thermal parameters were refined for each atom at all pressures and the instrument zero and asymmetry parameters were found to be self consistent at all pressures.

Low-temperature data were also collected with a sample in the dumb-bell pressure cell for comparison with the gas cell results. Two data collections were made; one at 1bar and 54K and one at a nominal pressure of 7kbars and 54K. Refinement of the data in this case proceeded as for the low-temperature experiment in the previous section, with the same ranges of the profile being omitted due to powder lines from the pressure cell.

The final refined atomic coordinates and thermal parameters for the gas cell data are given in Table 5.3 which also gives the Cu-O2 bondlength at each pressure and calculated values for for the orthorhombic distortion, $2(a-b)/(a+b)$; for the orthorhombic analogue of the tetragonal c/a ratio, $2\sqrt{2}c/(a+b)$; and for the orthorhombic tilt angle of the octahedra, $\tan^{-1}\,(x(O2)/z(O2))(a/c)$. The final refined parameters for the dumb-bell cell experiments are given in Table 5.4, again with the Cu-O bondlength, orthorhombic distortion and orthorhombic tilt angle. Using the unit-cell dimensions determined in the gas cell experiments

He-gas cell	1bar, 55K	2.5kbars, 55K	5kbars, 55K
a(Å)	5.3422(1)	5.3365(1)	5.3310(1)
b(Å)	5.3193(1)	5.3169(1)	5.3149(1)
c(Å)	13.1810(2)	13.1752(2)	13.1701(2)
z(O1)	0.0025(8)	0.0010(10)	0.0020(10)
x(O2)	0.0320(7)	0.0314(7)	0.0289(8)
z(O2)	0.1827(1)	0.1824(2)	0.1825(1)
x(La,Sr)	−0.0044(8)	−0.0054(9)	−0.0050(1)
z(La,Sr)	0.3607(1)	0.3610(1)	0.3609(1)
B(La,Sr)	0.09(4)	0.04(4)	0.03(4)
B(Cu)	−0.08(5)	0.06(5)	−0.07(5)
B(O1)	0.14(5)	0.16(5)	0.13(6)
B(O2)	0.02(5)	−0.02(6)	0.10(6)
R_{wp}(%)	8.9	9.0	8.0
Cu-O2(Å)	2.414(3)	2.409(3)	2.409(3)
2(a−b)/(a+b)%	0.43(1)	0.37(1)	0.30(1)
$2\sqrt{2}$c/(a+b)%	3.497(1)	3.498(1)	3.499(1)
tilt angle (°)	4.06(2)	3.99(2)	3.68(2)

Table 5.3: The unit-cell dimensions and refined atomic and thermal parameters from data collected in the He-gas cell at 1bar,2.5kbars and 5kbars in the orthorhombic phase of $La_{1.85}Sr_{0.15}CuO_4$ at 55K. The isotropic thermal parameters are given in Å^2. R_{wp} is the weighted profile R-factor.

allowed the pressure in the dumb-bell cell to be calibrated as 5.0(2)kbars.

5.4.3 Discussion and Conclusions

Comparing first the quality of the results obtained from the gas cell with those obtained from the dumb-bell cell, it can be seen that all parameters are considerably better determined in the refinements from the gas-cell data. The reason for this is the far higher signal-to-noise ratio available when using the gas cell due

Dumb-bell cell	1bar, 55K	5kbars, 55K
a(Å)	5.3411(4)	5.3310(6)
b(Å)	5.3174(4)	5.3125(5)
c(Å)	13.1789(6)	13.1694(9)
z(O1)	0.010(1)	0.010(2)
x(O2)	0.032(4)	0.028(6)
z(O2)	0.1834(8)	0.1851(9)
x(La,Sr)	−0.015(5)	−0.030(4)
z(La,Sr)	0.3602(3)	0.3585(4)
B(La,Sr)	0.1(1)	0.2(2)
B(Cu)	0.2(1)	0.7(2)
B(O1)	−0.4(2)	−0.4(2)
B(O2)	0.5(2)	1.0(3)
R_{wp}(%)	10.0	12.4
Cu-O2(Å)	2.423(11)	2.442(13)
2(a−b)/(a+b)%	0.44(4)	0.35(4)
$2\sqrt{2}$c/(a+b)%	3.497(4)	3.450(4)
tilt angle (°)	4.04(3)	3.50(3)

Table 5.4: The unit cell dimensions and refined structural parameters from data collected using the dumb-bell cell at 1bar and at a calibrated pressure of 5kbars in the orthorhombic phase of $La_{1.85}Sr_{0.15}CuO_4$ at 55K. The isotropic thermal parameters are given in Å^2.

to its larger sample volume (~30 times that in the dumb-bell cell) and the lower absorption of the cell itself. This improved signal-to-noise ratio is illustrated in Figure 5.5 which shows the same angular scan range for the atmospheric-pressure profiles using the gas cell (Figure 5.5a) and the dumb-bell cell (Figure 5.5b). The data collection times were similar and the intensities of the peaks can therefore be compared directly, giving a signal-to-noise ratio using the gas cell that is ~10 times that using the dumb-bell cell.

Comparison of the cell parameters obtained in the two atmospheric-pressure studies shows that they differ by ~0.02%, indicating that the pressure cells were probably not at the same position on the diffractometer during the data collections. This difference, though, has no effect on the calculated Cu-O2 bondlength within error.

Figure 5.6 shows the Cu-O2 bondlength plotted against pressure for the gas-cell data (o) and dumb-bell cell data (□) and shows that although the Cu-O2 bondlengths determined at atmospheric pressure are the same within error, the gas-cell results exhibit a slight shortening of the Cu-O2 bondlength with pressure while the dumb-bell cell results suggest that the bondlength increases by 0.019Å on applying a pressure of 5kbars. Comparison of the positional coordinates (Tables 3.3 and 3.4) shows that this is due to large shifts in the z(La/Sr) and z(O2) coordinates in the dumb-bell refinement, neither of which is present in the gas-cell study at the same pressure.

These very different results from the gas cell and the dumb-bell cell may also explain the different behaviour of the Cu-O2 bondlength with pressure in the orthorhombic phase with that determined in the tetragonal phase in the previous section, being, as they were, determined using the different cells. This explanation is strengthened by the results from a very recent determination of the pressure dependence of the structure of tetragonal $La_{1.85}Sr_{0.15}CuO_4$ at room temperature by Pei *et al.* (1990) to 5.3kbars using a He-gas pressure cell and TOF neutron powder-diffraction techniques. They found the Cu-O2 bondlength to exhibit a small monotonic decrease as a function of pressure (Figure 5.7), in disagreement with the results in the previous section, but in good agreement with the slight decrease in the bondlength observed in the present study of the orthorhombic structure using a gas cell. These similarities in the gas cell re-

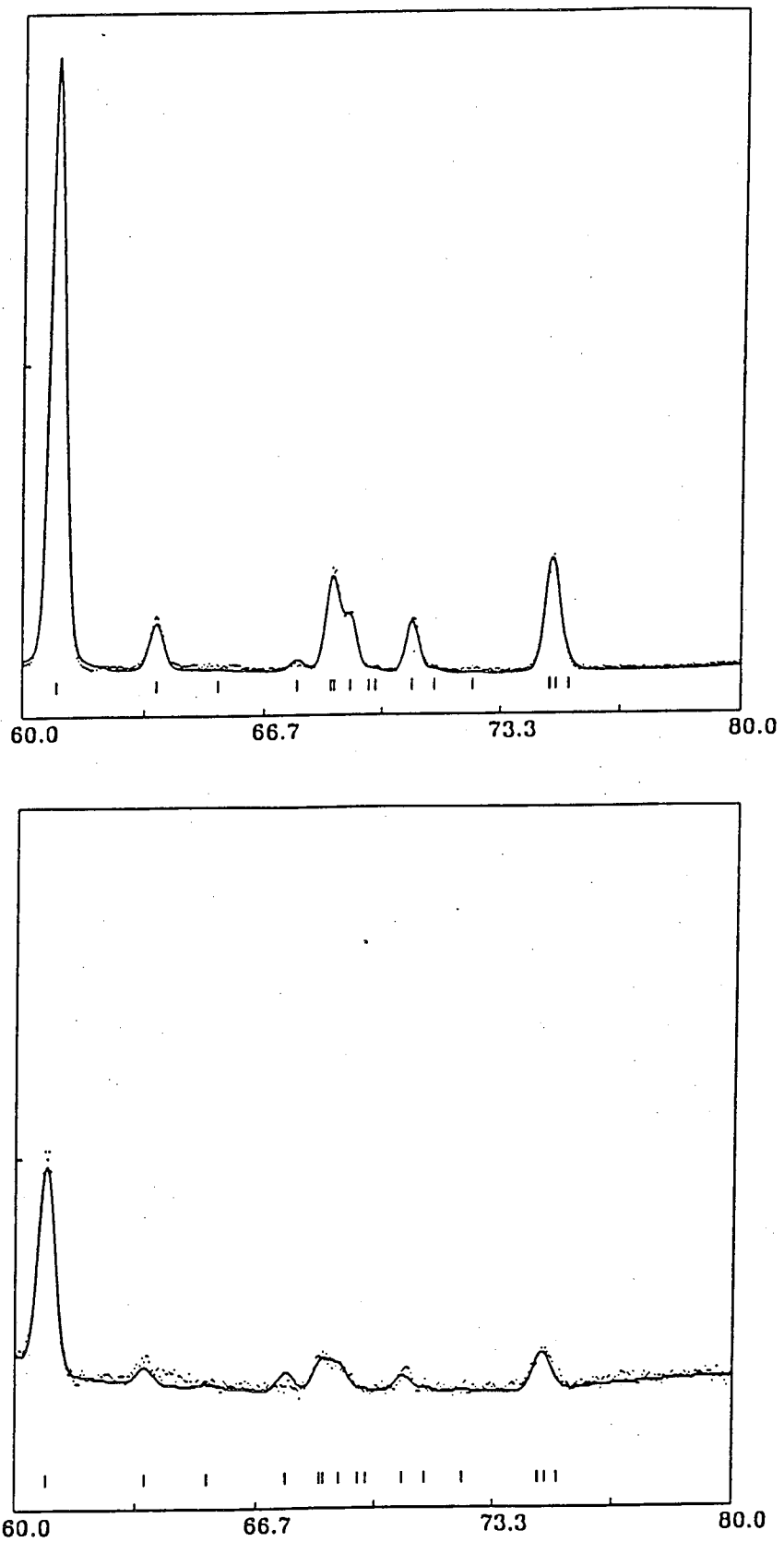

Figure 5.5: A section of the powder profile obtained from $La_{1.85}Sr_{0.15}CuO_4$ at 55K in (a) the gas cell, and (b) the dumb-bell cell.

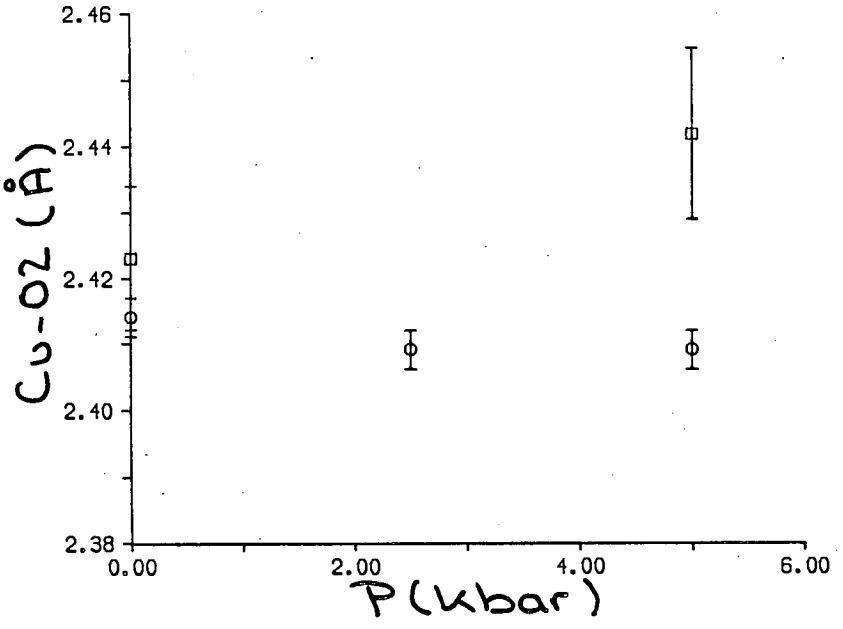

Figure 5.6: The pressure dependence of the apical Cu-O2 bondlength in $La_{1.85}Sr_{0.15}CuO_4$ at 55K from data collected in the gas cell (o) and the dumb-bell cell (□).

sults, and their disagreement with the dumb-bell cell results, may have one of two possible explanations.

(1) That the pressure dependence of the structure is somehow changed by the use of He gas as a pressure transmitting medium compared to fluorocarbons. This may be the case, for example, if the He diffuses into the crystal structure at high pressure.

(2) That the poor signal-to-noise ratio in the studies using the dumb-bell cell and any structured background from the Fluorinert, may result in systematic errors in the refined structure. The results obtained from the dumb-bell cell may therefore be incorrect, resulting from poor quality data. If this is the case, then the results of Kaldis *et al.* and Howard *et al.* must also be called into question as they both employed the same dumb-bell pressure cell and pressure fluid.

In order to decide which of these two explanations was correct, an attempt was made to collect high-pressure diffraction data from $La_{1.85}Sr_{0.15}CuO_4$ using TOF neutron powder-diffraction techniques at the Rutherford Appleton Laboratory.

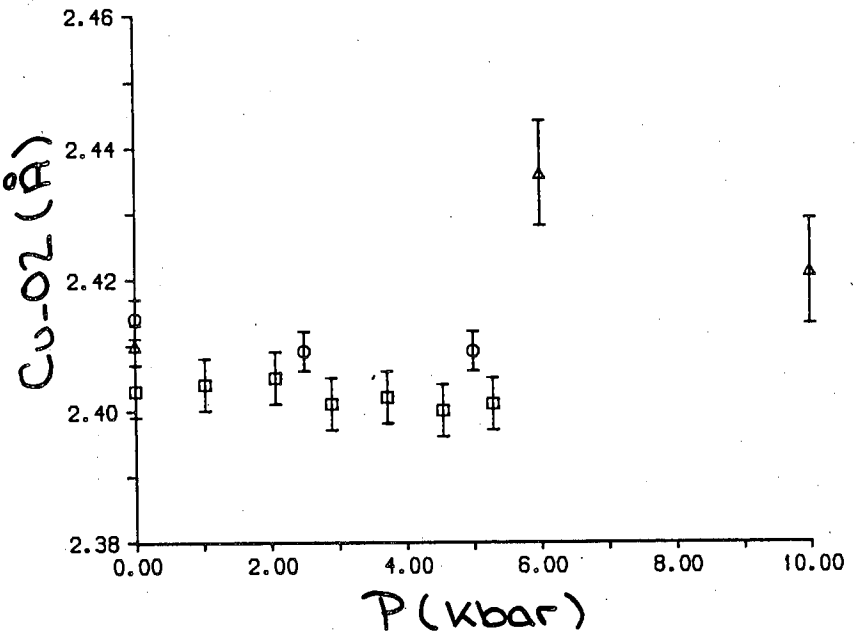

Figure 5.7: The pressure dependence of the apical Cu-O2 bondlength in $La_{1.85}Sr_{0.15}CuO_4$ from data collected in the orthorhombic phase using the gas cell (o), from the room-temperature data of Pei *et al.* (□) and from the data collected at room temperature using the dumb-bell cell (△).

This technique avoided any cell centering errors and the 90° scattering geometry allowed powder lines from the pressure cell to be omitted from the powder profiles. The pressure fluid was again Fluorinert. However, the quality of the data was poor and did not allow the structure to be refined with sufficient accuracy to allow the pressure dependence of the Cu-O2 bondlength to be determined.

This inability to accurately determine the structure of $La_{1.85}Sr_{0.15}CuO_4$ as a function of pressure using neutron powder-diffraction techniques for comparison with the present results, and the inability to obtain pressures of more than 10kbars, prompted the search for another method of determining the pressure dependence of $La_{1.85}Sr_{0.15}CuO_4$. Although it is planned to use the Paris cell for such studies to pressures of 100kbars in the future, the quality of the data is, at present, too poor to allow bondlengths to be determined to the accuracy required.

However, the recent availability of high-quality single-crystal samples of high-T_c superconductors has permitted the use of single-crystal techniques to determine the pressure dependence of the structure of these materials. The first samples obtained were of the $YBa_2Cu_4O_8$ material and were too small to allow them to be used for high-pressure single-crystal neutron-diffraction experiments. The crystals were, though, perfect for single-crystal x-ray diffraction studies offering the ability to determine the pressure dependence of the structure above 50kbars and allow a direct comparison with the results of Kaldis *et al.* However, to determine the position of the Cu and O atoms accurately in the presence of the heavy Y and Ba atoms would require the x-ray diffraction data be of the highest quality. The study of $YBa_2Cu_4O_8$ using AgK_α radiation (to achieve the highest possible resolution and to reduce absorption by the sample) thus represents a perfect test of the newly developed single-crystal x-ray diffraction techniques described in Chapter 3 and is the first high-pressure structural study of a high-T_c superconductor using this technique.

5.5 A High-Pressure Structural Study of $YBa_2Cu_4O_8$

5.5.1 Introduction

With the very recent determination of the pressure dependence of T_c in the 1-2-4 material to 120kbars (van Eenige *et al.* (1990)) it would be of great interest to follow the pressure dependence of the crystal structure of the 1-2-4 compound to higher pressures than have been possible to date using neutron powder-diffraction techniques. This would allow the uncertainty in the pressure dependence of the Cu2-O1 bondlength to be resolved (by determining the Cu2-O1 bondlength to considerably higher pressures, allowing an easier discrimination between the large decrease seen by Kaldis *et al.* (1989) and the smaller decrease estimated by Pei *et al.* (1990)) and the pressure dependence of the Cu2-O1 bondlength to be compared to the pressure dependence of T_c, which shows a dT_c/dP of $0.55 Kkbar^{-1}$ to ~40kbars and then a decrease in the magnitude of dT_c/dP which remains non-zero to 120kbars where T_c is 108K.

This section describes a structural study of $YBa_2Cu_4O_8$, using single-crystal x-ray diffraction techniques, to 46.5kbars, the highest pressure obtained in any structural study of a high-T_c material to date.

5.5.2 Experiment and Data Analysis

The sample crystal of $YBa_2Cu_4O_8$ was $100 \times 120 \times 80 \mu m^3$ and was cut from a larger crystal supplied by Prof. E. Kaldis, ETH, Zurich. The data were collected in a Merrill-Bassett DAC. In the Ammm spacegroup the atoms occupy special positions such that their x and y coordinates are fixed by symmetry. Therefore only the z coordinates have to be determined, in particular the Cu2-O1 bondlength depends only on the z coordinates of the Cu2 and O1 atoms. Due to the angular limits imposed by the DAC, which severly limit the accessible reflections to those lying close to the reciprocal plane parallel to the diamond faces (Merrill and Bassett (1974)), the crystal was mounted with the b-axis (in

the Ammm spacegroup) lying along the cell axis. This allowed access to the high-l reflections.

The DAC was assembled with a tungsten gasket with a 300μm diameter hole and the pressure fluid was 4:1 methanol:ethanol, previously dried using a molecular sieve. The cell was pressurised to 9.0(5) kbars, the pressure being measured using the ruby fluorescence method, and was mounted on a CAD-4 diffractometer and aligned using AgK_α radiation (graphite monochromator).

Initial scans of the sample showed the crystal to be comprised of two slightly misaligned parts, a problem observed in a number of other crystals. However, the misalignment was small enough to enable the intensity from both parts of the crystal to be collected together in the same scan.

All possible reflections were collected, using ω-scans, to a 2Θ limit of approximately 80° ($\sin\Theta/\lambda$=1.15Å^{-1}). These data included reflections to $h = 7$ and $l = 48$ in the ($h0l$) layer, to $h = 7$ and $l = 55$ in the ($h1l$) layer and to $h = 2$ and $l = 38$ in the ($h2l$) layer, giving a total of 339 independent reflections. The data were collected in the fixed-ϕ geometry and each reflection was measured at three positions 0.5° apart around the scattering vector to detect simultaneous diffraction by the diamonds (Chapter 3.2). After correcting the data for both sample and pressure cell absorption, and refining an isotropic extinction correction, the data were refined using the PROMETHEUS suite of crystallographic programs (Zucker *et al.* (1983)). Comparison of the calculated and measured intensities showed a number of reflections to have intensities significantly weaker than their calculated values. Analysis of the crystal size and position in the gasket hole showed these reflections to be affected by partial occlusion of either the incident or diffracted beam by the gasket, and were subsequently removed from the data set.

Before continuing, the lattice parameters were accurately determined using the 8-position method as adapted for the CAD-4.

The pressure was then increased to 31.0(5)kbars and the same procedure was repeated. Comparison of the results with those obtained at 9kbars showed that the structural changes with pressure were slight and increased precision of the atomic coordinates would be desirable, this was achieved through the use of the

'Leverage' program.

The full procedure was repeated with a data collection at 46.5(5)kbars, where the increased precision showed the Cu2-O1 bondlength to have changed by 10σ from its atmospheric-pressure value. In order to follow the pressure dependence of the structure precisely, it was felt that the lower pressure data should be recollected to the same precision. The pressure was therefore carefully reduced to 15.0(5)kbars and exactly the same data set was collected as at 46.5kbars, with the same equivalent reflections, omitting the same occluded reflections and using the same scan times. This procedure was then repeated at pressures of 32.0(5)kbars and then at 2.0(5)kbars – a pressure just sufficient to keep the cell sealed and the sample mounting secure. This latter data was collected to give a low-pressure reference data set to determine if the angular restrictions imposed by the pressure cell, or possible uncertainties in the pressure-cell absorption correction, resulted in any small bias in the refined structural parameters. Finally, the pressure was increased to 45kbars and another data set was collected to check the reproducibility of the results. At each pressure, (i) the unit cell parameters were determined using the eight-position method (ii) the pressure was remeasured after the data collection to ensure in had remained constant.

The five data sets 2, 15 32 45 and 46.5kbars were all corrected for pressure cell and sample absorption and also for (isotropic) extinction. The data were then refined, again using PROMETHEUS, and refined atomic coordinates and unit cell dimensions are given in Table 5.5. Atomic thermal parameters were also refined for all atoms at each pressure and although reasonable values were obtained, the errors were quite large – especially for the O atoms and for all atoms along the direction (b) of the low resolution data – and are therefore not given. Table 5.5 also contains the calculated Cu2-O1 bondlength at each pressure and shows the final R-factor. The number of reflections used in each refinement was almost identical except for the refinement at 15kbars were some 50 reflections were lost due to a hardware fault during data processing.

Table 5.5 also contains the atmospheric-pressure results of Bordet *et al.* (1989) obtained by neutron powder-diffraction techniques, the values obtained by extrapolating the present high-pressure results to atmospheric pressure, and the results of Kaldis *et al.* (1989) at 10kbars.

Pressure	AP	AP	2(1)kbars	10kbars,165K
a(Å)	3.8454(8)		3.8437	3.8394(1)
b(Å)	3.876(1)		3.876	3.871(2)
c(Å)	27.263(5)		27.246	27.2025(14)
z(Ba)	0.13483(1)	0.13483	0.13485(2)	0.1353(3)
z(Cu1)	0.21298(1)	0.21293	0.21293(4)	0.2135(2)
z(Cu2)	0.06153(1)	0.06146	0.06148(3)	0.061(1)
z(O1)	0.14545(5)	0.14512	0.1451(2)	0.1434(3)
z(O2)	0.05228(6)	0.0523	0.0523(2)	0.0534(2)
z(O3)	0.05236(5)	0.0523	0.0525(2)	0.0524(2)
z(O4)	0.21801(6)	0.21762	0.2176(2)	0.2172(2)
Cu2-O1(Å)	2.288(1)	2.281	2.280(5)	2.242(9)
R(%)		–	3.8	
Reference	Bordet *et al.*	This work	This work	Kaldis *et al.*
Pressure	15(1)kbars	32(1)kbars	45(1)kbars	46.5(10)kbars
a(Å)	3.829(1)	3.811(1)	3.795(1)	3.800(1)
b(Å)	3.872(3)	3.865(3)	3.862(3)	3.862(3)
c(Å)	27.137(9)	26.968(9)	26.86(1)	26.882(6)
z(Ba)	0.13502(2)	0.13520(2)	0.13532(2)	0.13530(2)
z(Cu1)	0.21289(4)	0.21286(3)	0.21284(3)	0.21288(4)
z(Cu2)	0.06166(4)	0.06184(3)	0.06198(3)	0.06191(4)
z(O1)	0.1448(2)	0.1446(2)	0.1446(2)	0.1446(2)
z(O2)	0.0527(2)	0.0528(2)	0.0525(2)	0.0527(2)
z(O3)	0.0522(2)	0.0526(2)	0.0526(2)	0.0525(2)
z(O4)	0.2172(2)	0.2170(2)	0.2171(2)	0.2169(2)
Cu2-O1(Å)	2.256(5)	2.232(5)	2.219(5)	2.223(5)
R(%)	4.2	3.9	3.8	4.3
Reference	This work	This work	This work	This Work

Table 5.5: Unit cell dimensions, refined atomic z-coordinates and Cu2-O1 bondlength in $YBa_2Cu_4O_8$ as a function of pressure. The final value of the conventional R-factor is also included. The atmospheric-pressure (AP) results of Bordet *et al.* (1989) and the high-pressure results of Kaldis *et al.* (1989) are given for comparison. The second column gives the values obtained by extrapolating the high-pressure results to AP, as discussed in the text. The x and y coordinates are $(\frac{1}{2},\frac{1}{2})$ for the Ba and for Y (whose z-coordinate is also zero): (0,0) for Cu1, Cu2 and O1: $(\frac{1}{2},0)$ for O2: and $(0,\frac{1}{2})$ for O3 and O4. Esd's are quoted (in parentheses) on the last quoted place; no esd's are quoted for

5.5.3 Discussion and Conclusions

Comparing first the precision of the structural parameters refined at 2kbars with those obtained by Bordet *et al.* at atmospheric pressure, it can be seen that the esd's on the heavy atom (Ba, Cu1, Cu2) positional coordinates in the present work are 2-4 times those obtained at atmospheric pressure. The ratio is also similar, 3-4, for the lighter O atoms showing that accurate diffraction data can now be collected at high pressure using AgK_α radiation, allowing the positions of light atoms to be refined with high precision even in the presence of much heavier atoms.

The high quality of the high-pressure data is also evident on comparing the precision of the refined coordinates at each pressure: in each case the esd's are almost identical with no degradation in the quality of the data as the pressure is increased. It would then seem that the use of tungsten gaskets significantly reduces the problems of a thinning gasket, allowing a precise determination of crystal structures independent of either wavelength or pressure. This is a significant advance in the determination of crystal structures at high pressure.

Table 5.5 also allows a comparison of the precision of the present work with the neutron powder-diffraction study of Kaldis *et al.* at 10kbars. The magnitude of the oxygen-atom esd's are approximately the same in each case, while the esd's on the (heavy) Ba and Cu atoms are considerably smaller in the present study (by a factor of up to 7) resulting in a determination of the Cu2-O1 bondlength with an esd half that of the neutron-diffraction study.

The present results then indicate that using state-of-the-art techniques, which must now include the use of tungsten gaskets and AgK_α radiation to allow significantly higher resolution, it is now possible to determine the crystal structure of high-T_c materials at high pressure, including the O atoms, with a precision that is comparable, or better than, that obtainable using neutron powder-diffraction techniques. This removal of the reliance on neutron-diffraction techniques will allow the pressure dependence of the structures to be followed to considerably higher pressures than have been possible to date, as well as making the high-pressure structural study of such materials more available to researchers, with, as the results indicate here, no loss in precision to the highest pressures.

The variations with pressure of the refined z coordinates are shown in Figures 5.8 and 5.9. In Figure 5.9, the average of the two basal-plane oxygen (O2 and O3) coordinates is plotted to bring out the apparent small change in the average despite the less regular variation in the individual values. Figure 5.10 shows the variation with pressure of the Cu2-O1 and Cu1-O1 bondlengths and the pressure dependence of the separation of the Ba-O1 layers (see Figure 5.2). In Figures 5.8, 5.9 and 5.10, the dot-dash line shows the rates-of-change observed in the previous study of Kaldis *et al.*

Two atmospheric-pressure (AP) values are given for each variable in Figures 5.8, 5.9 and 5.10. The one shown by the solid circle is the value obtained by extrapolating the present high-pressure results to AP, with the results given in column 2 of Table 5.5. The values given by the solid triangles are those obtained by Bordet *et al.* (column 1 of Table 5.5) and comparison with the extrapolated AP values shows that they are some small, but significant, differences, illustrating the need for the low-pressure reference data set. The dot-dash lines show the rates-of-change found in the study of Kaldis *et al.*, starting from the extrapolated values of the present study and do not, necessarily, pass through the actual values obtained in that study.

It can be seen from Figures 5.8, 5.9 and 5.10 that the principal structural changes with pressure are in the z coordinates of the Ba, O4, Cu2 and O1 atoms – the latter two resulting in a reduction in the Cu2-O1 bondlength of 3% at 50kbars compared to a reduction in the c cell dimension of only $\sim$1.5% (Table 5.5). Thus the Cu2-O1 bondlength decreases both in fractional and absolute terms.

Figures 5.8, 5.9 and 5.10 also show that the effects of pressure on the structure are considerably smaller than those reported by Kaldis *et al.* and it is doubtful, given the relatively poor precision of the neutron-diffraction study, that the small structural changes that might be expected to occur at a pressure of 10kbars were large enough to have been seen. It is therefore felt that the results of the previous neutron-diffraction study should now be treated as substantially unreliable, as probably should the results of Howard *et al.* and the present study of the tetragonal phase of $La_{1.85}Sr_{0.15}CuO_4$, although further work is required to check this.

It would seem, therefore, that the pressure dependence of the critical apical

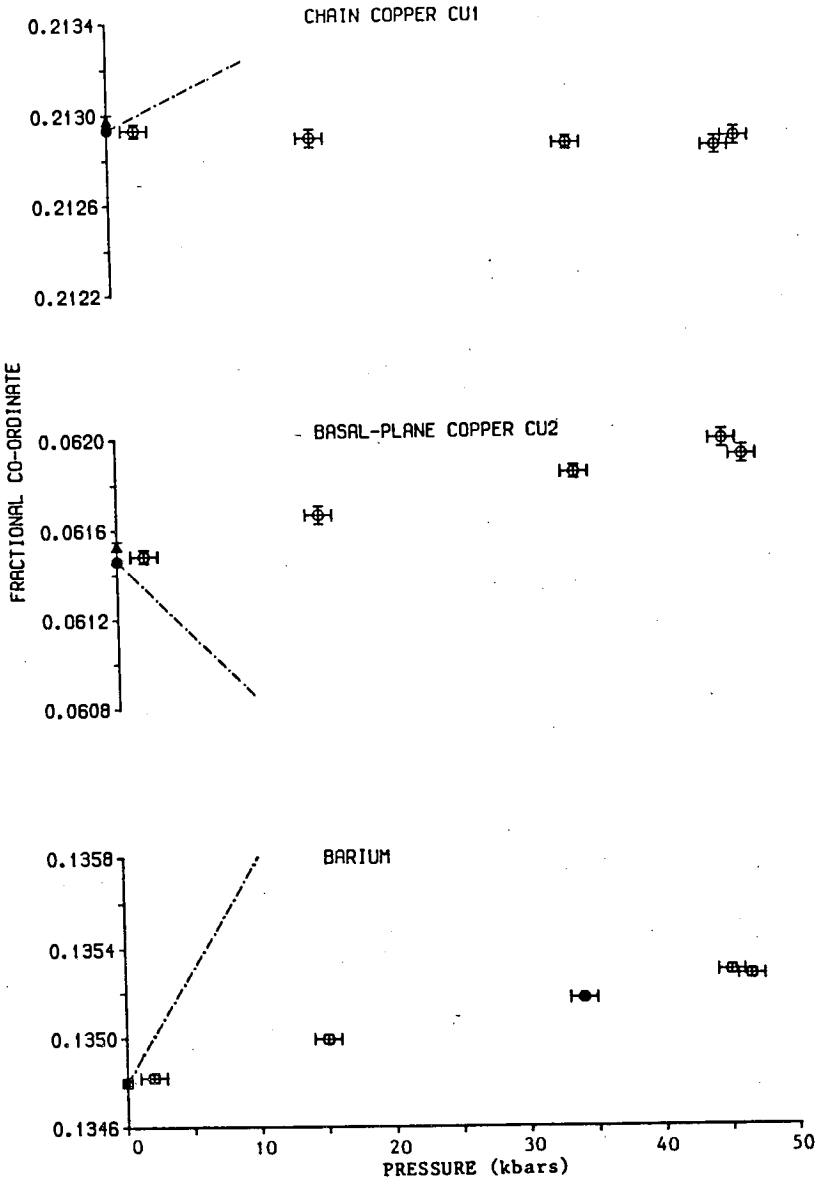

Figure 5.8: The pressure dependence of the c-axis fractional coordinates of the metal atoms in $YBa_2Cu_4O_8$. The dot-dashed line (---) represents the rates of change reported by Kaldis *et al.* and has been transposed vertically to begin at the ambient pressure value obtained in this study. The data point shown as a solid circle (●) is the extrapolation of the results of this study while that plotted as a triangle (▲) is the value obtained by Bordet *et al.* (1989). In the case of Ba, the (●) and (▲) points overlap.

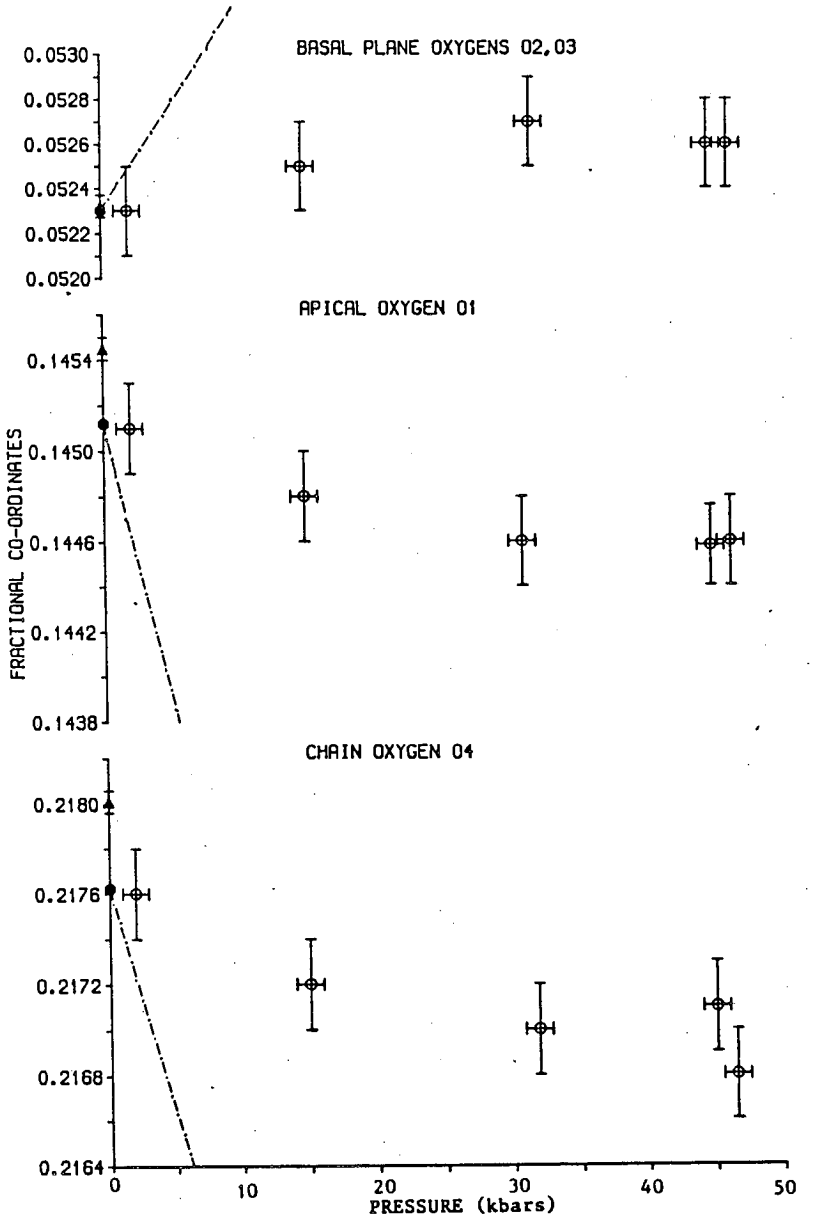

Figure 5.9: The pressure dependence of the c-axis fractional coordinates of the mean value of the basal plane oxygens (O2 and O3), the apical oxygen (O1), and the chain oxygen (O4) in $YBa_2Cu_4O_8$. The dot-dashed line (-·-) represents the rates of change reported by Kaldis *et al.* (1989) and has been transposed vertically to begin at the ambient pressure value obtained in this study. The data point shown as a solid circle (•) is the extrapolation of the results of this study while that plotted as a triangle (▲) is the value obtained by Bordet *et al.* (1989). In the case of O2/O3, the • and ▲ points overlap.

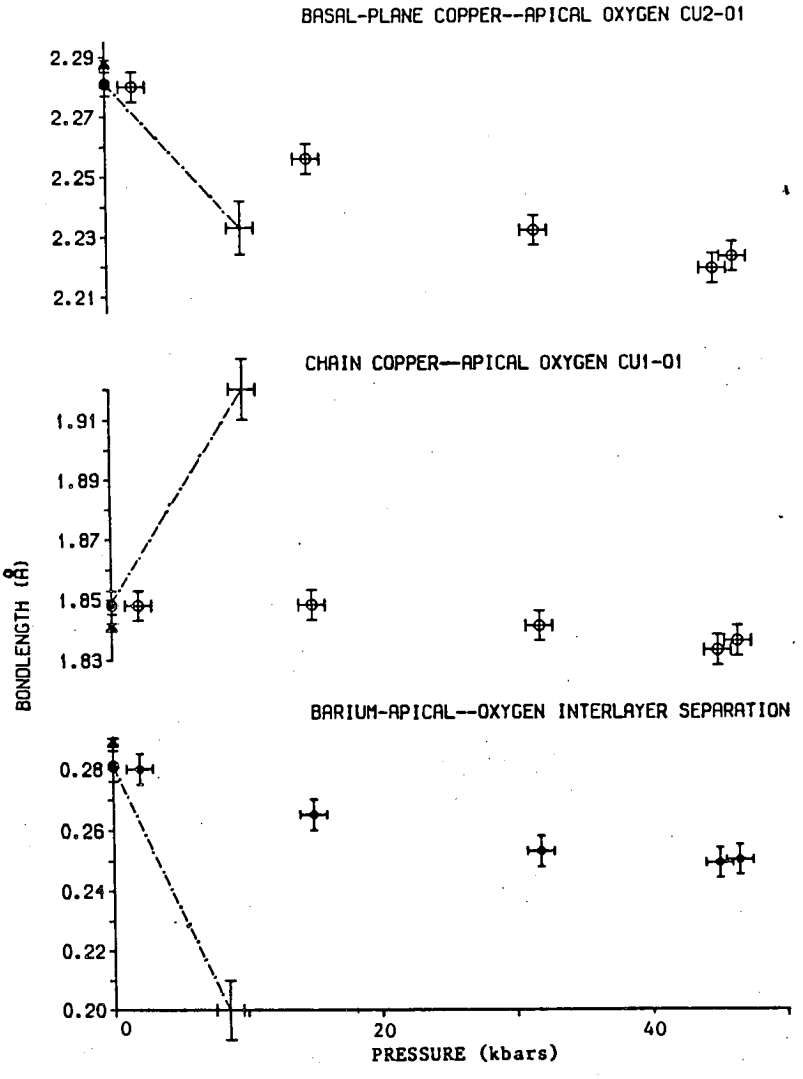

Figure 5.10: The pressure dependence of the bondlengths Cu2-O1, Cu1-O1 and the separation of the Ba and O1 layers (see Figure 5.2) in $YBa_2Cu_4O_8$. The dot-dashed line (-·-) represents the rates-of-change reported by Kaldis *et al.* and has been transposed vertically to begin at the ambient pressure value obtained in this study; the neutron error bars are included to compare the precision with the x-ray results of the present study. The data point shown as a solid circle (•) is the extrapolation of the results of this study while that plotted as a triangle (▲) is the value obtained by Bordet *et al.* (1989).

Cu-O bondlength decreases at a rate that is larger than would be expected from simply the reduction in the unit cell dimensions, but at a rate that is substantially smaller than previously claimed. The compression of the Cu-O bondlength would also seem to be smoothly varying, in contrast to the results of Howard *et al.* and the initial results on tetragonal $La_{1.85}Sr_{0.15}CuO_4$, but in agreement with the gas-cell results of Pei *et al.* and the present results from orthorhombic $La_{1.85}Sr_{0.15}CuO_4$.

Finally, there is the question as to whether the pressure dependence of the Cu2-O1 bondlength in $YBa_2Cu_4O_8$ follows the pressure dependence of T_c in that they show the same curvature above 40kbars, the pressure at which dT_c/dP starts to decrease. Although there some evidence for this may be found in the present results (Figure 5.10), structural studies are required at pressures of ~70kbars to firmly establish any relationship. The lack of any reduction in the data quality at the highest pressures in the present studies will allow similar high-precision studies to be made at these pressures. Such studies are now in progress.

5.6 Conclusions

The single-crystal x-ray diffraction study of $YBa_2Cu_4O_8$ illustrates the high quality of data that can now be expected to be collected using AgK_α radiation combined with tungsten gaskets, and represents the first accurate structural study to have been made using AgK_α. Although work is still required to enable accurate thermal parameters to be refined using these techniques, it is clear that the main problems of using shorter wavelength radiation can now be solved, and that it is now not only possible to collect high-quality data using AgK_α radiation, but also to determine the location of light atoms with a precision that is similar to, or better than, that obtainable using high-pressure neutron powder-diffraction techniques.

The results of the three structural studies strongly suggest that the high-pressure neutron-diffraction studies made using the dumb-bell pressure cell and Fluorinert as a pressure fluid, including the present study of tetragonal $La_{1.85}Sr_{0.15}CuO_4$, are prone to serious systematic errors which cast considerable doubt on the ac-

curacy of the refined structures and calculated bondlengths. The exact cause of these errors is uncertain at present but graphically illustrates the effect that a structured background may have on the data quality. It is probably interesting in this respect to note that the structural studies of Kaldis *et al.* and Howard *et al.* were made by authors unfamiliar with high-pressure diffraction techniques, as was the initial study of $La_{1.85}Sr_{0.15}CuO_4$ presented here, while both the study of orthorhombic $La_{1.85}Sr_{0.15}CuO_4$ and the single-crystal x-ray diffraction measurements were made after over two years experience of high-pressure diffraction techniques, while the study of Pei *et al.* was made at the IPNS neutron source at Argonne, a facility with considerable expertise in high-pressure time-of-flight techniques.

It would then seem that the basal-plane copper to apical oxygen bondlength in both $La_{1.85}Sr_{0.15}CuO_4$ and $YBa_2Cu_4O_8$ varies smoothly with pressure in a way that is both less dramatic and more subtle than has been claimed to date. This slow variation of the Cu-O bondlength with pressure then requires both relatively high pressure and accurate data in order to determine the relationship between the bondlength and the superconducting temperature T_c, a combination that single-crystal x-ray diffraction is, at present, uniquely able to satisfy.

Chapter 6

Conclusions

The principal aim of this thesis was to examine the techniques by which crystal structures could be determined at high pressure and to develop new techniques, or improvements to existing techniques, to enable structures to be determined with increased accuracy. To this end, a detailed review of high-pressure diffraction equipment and techniques has been presented and the limits imposed on the accurate determination of crystal structures at high pressure prior to this thesis have been discussed. An understanding of these limits has allowed several major improvements to have been made using both x-ray and neutron-diffraction techniques on both powder and single-crystal samples.

For single-crystal neutron-diffraction studies, development of an optimised data collection strategy for use with the Ahsbahs sapphire-anvil pressure cell and a position-sensitive detector, has allowed maximum use to have been made of limited experimental time. Combined with the use of 'Leverage' techniques, highly-detailed structural studies have been made on hydrogen-bonded systems with an accuracy considerably higher than that available previously.

Analysis of the diffraction processes when using a diamond-anvil pressure cell for single-crystal x-ray diffraction studies has shown that a previously unsuspected source of error – the removal of intensity from either the incident or diffracted beam by simultaneous diffraction by the diamond anvils – can reduce the intensity of reflection by up to 50%. This process has been studied using MoK_α, AgK_α and synchrotron radiation and a data collection strategy developed to allow detection of those affected reflections.

The use of tungsten gaskets for single-crystal x-ray diffraction studies has also been explored. The very high absorption of tungsten for both MoK_α and AgK_α radiation, even when the gasket is thinned at high pressures, offers a solution to the long-standing problems of poor data quality when using AgK_α radiation, and the reduction in the quality of diffraction data as the pressure is increased.

Development work has been done on powder-based x-ray and neutron-diffraction techniques. The Paris cell for powder diffraction on a pulsed neutron source has reached a pressure of 60kbars – a pressure not achieved since the late 1960's using this technique – and promises the Rietveld refinement of structures at pressures in excess of 100kbars. The development of the Edinburgh Imaging Plate system, a project in which the author hopes to play a principal part in the future, has only very recently begun but promises to be one of the most fruitful areas of high-pressure diffraction of the future, allowing the accurate refinement of crystal structures in excess of 500kbars.

The newly developed single-crystal techniques have been applied to the study of two groups of materials – H-ordering systems and high-T_c superconductors – where several new features have been observed.

$PbDPO_4$ has been shown to have the same δ, within error, as $PbHPO_4$ when they have the same ordering temperature T_c. This lends considerable support to the idea that geometrical effects, especially the magnitude of δ, play an important part in the determination of T_c and cannot be ignored. The results for $PbDPO_4$ have also resolved earlier uncertainties about the high-pressure structure of $PbHPO_4$ and has shown the three very different systems $PbHPO_4$-$PbDPO_4$, KH_2PO_4-KD_2PO_4 and $H_2C_4O_4$ to all linearly extrapolate to a δ of $\sim$0.2Å as $T_c \rightarrow$0K. A structural study of CsD_2PO_4, though, has shown the CsH_2PO_4-CsD_2PO_4 system to behave very differently to those listed above although the unique nature of the phase diagrams of CsH_2PO_4 and CsD_2PO_4 makes extrapolation of the present results uncertain. A study of the quantum-paraelectric state of KH_2PO_4, however, suggests that the H atoms are indeed still disordered as $T_c \rightarrow$0K, contrary to some earlier suggestions, and that the separation is $\sim$0.22Å, validating the linear extrapolation of, at least, the KH_2PO_4-KD_2PO_4 system. These results cannot presently be explained by the long-accepted model for the transition but are playing an important role in a new theory currently

under development.

Initial structural studies of tetragonal $La_{1.85}Sr_{0.15}CuO_4$ to 10kbars suggested that the compression of the apical Cu-O bondlength, postulated to be a possible structural determinant of the superconducting temperature T_c, was very similar to that found previously in La_2CuO_4 but considerably different to that found in $YBa_2Cu_4O_8$. Subsequent studies using a helium-gas pressure cell, however, suggested that the dumb-bell pressure cell used in the initial study may cause serious systematic errors in the refined structures. This was confirmed by a single-crystal x-ray diffraction study of $YBa_2Cu_4O_8$ which demonstrated the high quality of the data that can now be expected when using AgK_α radiation in conjunction with tungsten gaskets, and showed the compressibility of the apical Cu-O bondlength to be considerably lower than previously claimed, casting considerable doubts on the results obtained in the dumb-bell pressure cell.

Finally, although the newly developed techniques described in this thesis have allowed appreciable gains to be made in the field of structural studies at high pressure, it is worth speculating as to what other advances will be made in this field in the near future.

One of the most exciting and promising developments of the future will be the extensive use of synchrotron radiation sources – both the current generation of facility and the new generation of brilliant sources – and indeed high-pressure techniques are currently being developed at NSLS (Brookhaven), at Hasylab (FRG), at SRS (Daresbury) and at the Photon Factory (Japan) (Freund and Reikel (1990)). The obvious advantages of the very intense radiation, the availability of high flux at short wavelengths, and the high collimation of the synchrotron beam will offer substantial gains to be made in the signal-to-background ratio, allowing the precise measurement of very weak reflections from weakly scattering samples (for example H_2 or He), or from very small samples. The latter opens up the exciting prospect of extending single-crystal diffraction into the Megabar region.

Although very few monochromatic x-ray single-crystal studies have been made at atmospheric pressure using synchrotron radiation, the first high-pressure structural study using monochromatic techniques was recently made on a $30\times70\times60\mu m^3$ single-crystal of $AlPO_4$ at 29kbars using a wavelength of $\sim$0.54Å (Sowa

et al. (1990)). Comparison with an identical study made on a laboratory x-ray source showed a gain in signal-to-noise on weak peaks of a factor of 22.

Use of the Laue technique has, as said previously, been used widely in the protein crystallography community and has recently attracted considerable interest in the field of high-pressure diffraction (King *et al.* (1989), Jenkins and Clark (1990)). Initial results, although not yet yielding refined structures, are very encouraging and the use of this technique again opens up the prospect of ultra-high pressure structural studies into the Megabar region. It may also prove possible, with the use of so-called micro-crystals ($\sim 10 \times 10 \times 10 \mu m^3$), to take a small single crystal through a strongly first-order phase transition that would cause larger crystals to shatter, allowing single-crystal studies of phases that would otherwise require powder techniques.

With the advent of evermore intense spallation neutron sources, the future would also seem bright for Laue techniques using neutrons. The considerable neutron flux at short wavelengths that such sources provide offers the prospect of very high resolution ($\sin\Theta/\lambda > 2.0 Å^{-1}$) structural studies. The use of the Paris cell in a $2\Theta=90°$ scattering geometry would allow such studies to be made at pressures in excess of 100kbars, opening up the new fields of high-pressure magnetism and, perhaps, inelastic scattering.

It would then seem that after nearly a decade of relative stagnation that high-pressure crystallography has entered a new and exciting phase, with the determination of the crystal structure of systems such as metallic ice now, perhaps, finally within reach.

References

Ahsbahs H., Revue Phys. Appl. 19, 819 (1984a)

Ahsbahs H., Rev. Sci. Inst. 55, 99 (1984b)

Ahsbahs H., Prog. Cryst. Growth. Charact. 14, 263 (1987)

Alkire R.W., Vergamini P.J., Larson A.C. and Morosin B., Acta Cryst. C40, 1502 (1984)

d'Amour H., Schiferl D., Denner W., Schulz H. and Holzapfel W.B., J. Appl. Phys. 49, 4411 (1978)

d'Amour H., Denner W. and Schulz H., Acta Cryst. B35, 550 (1979)

Andre D., Fourme R. and Renaud M., Acta Cryst. B27, 2371 (1971)

Arndt U.W. and Mathieson A. McL., editors. 'International Meeting on the Accurate Determination of X-ray Intensities and Structure Factors', Acta Cryst. A25 (1969)

Ardnt U.W., Methods Enzymol. 114, 472 (1985)

Bacon G.E., 'Neutron Diffraction' (Clarendon Press:Oxford (1975))

Barnett J.D., Pack J. and Hall H.T., Trans. Amer. Crystallogr. Assoc. 5, 113 (1969)

Barnett J.D., Block S. and Piermarini G.J., Rev. Sci. Inst. 44, 1 (1973)

Bell P.M. and Mao H.K., Carnegie Inst. Washington Yearb. 80, 404 (1981)

Besedin S.P., Makarenko I.N., Stishov S.M., Glazkov V.P., Goncharenko I.N., Irodova A.V., Somenkov V.A. and Shil'stein S.Sh., High Pressure Research 4, 447 (1990)

Besson J.M., Weill G., Hamel G., Nelmes R.J., Loveday J.S. and Hull S., To be Published (1990)

Birch F., J. Geophys. Research 83, 1257 (1978)

Birch F., J. Geophys. Research 91, 4949 (1986)

Blessing R.H., Cryst. Rev. 1, 3 (1987)

Blinc R., J. Phys. Chem. Solids 13, 204 (1960)

Blinc R., Private Communication (1990)

Bloch D., Paureau J., Voiron J. and Parisot G., Rev. Sci. Inst. 47, 296 (1976)

Boehler R. and Kennedy G.C., J. Phys. Chem. Sol. 41, 517 (1980)

Bordet P., Hodeau J.L., Argond R., Muller J., Marezio M., Martinez J.C., Prefean J.J., Karpinski J., Kaldis E., Rusiecki S. and Bucher B., Physica C 162, 524 (1989)

Bridgman P.W., The Physics of High Pressure (Dover Publications:New York (1971))

Brugger R.M., Bennion R.B., Worlton T.G. and Peterson E.G., U.S. Atomic Energy Commision Report IDO-17170 (Wash. D.C.(1966))

Brugger R.M., Bennion R.B., Worlton T.G. and Meyers W.R., Procedings of the Symposium on Crystal Structures at High Pressure (Seattle, American Crystallographic Association (1969)) pp141

Buras B., Gerward L., Glazer A.M., Hidaka M. and Staun Olson J., J. Appl. Cryst. 12, 531 (1979)

Busch G. and Scherrer P., Naturwiss 23, 737 (1935)

Carlile C.J. and Salter D.C., High Temperatures-High Pressures 10, 1 (1978)

Carter W.J., Marsh S.P., Fritz J.N. and McQueen R.G., Nat. Bur. Stand. U.S. Special Publication 326, (1971)

Cava R.J., Batlogg B., Rabe K.M., Rietman E.A., Gallagher P.K. and Rupp L.W., Physica C. 156, 523 (1988)

Cava R.J., Hewat A.W., Hewat E.A., Batlogg B., Marezio M., Rabe K.M., Krajewski J.J., Peck W.F. and Rupp L.W., Physica C 165, 419 (1990)

Chhabildas L.C. and Ruoff A.L., J. Appl. Phys. 47, 4182 (1976)

Cockcroft J.K., PROFIL program, ILL Grenoble (1989)

Convert P. and Forsyth J.B., editors. 'Position Sensitive Detection of Thermal Neutrons' (Academic Press:New York (1983))

Decker D.L., J. Appl. Phys. 36, 157 (1965)

Decker D.L., J. Appl. Phys. 37, 502 (1966)

Decker D.L., J. Appl. Phys. 42, 3239 (1971)

Decker D.L., Bassett W.A., Merrill L., Hall H.T. and Barnett J.D., J. Phys. Chem. Ref. Data 1, 773 (1972)

Decker D.L. and Worlton T.G., J. Appl. Phys. 43, 4799 (1972)

Denner W., d'Amour H., Schulz H. and Stoeger W., J. Appl. Cryst. 10, 177 (1977)

Denner W., Schulz H. and d'Amour H., J. Appl. Cryst. 11, 260 (1978)

van Eenige E.N., Griessen R., Wijngaarden R.J., Karpinski J., Kaldis E., Rusiecki S. and Jilek E. Physica C 168, 482 (1990)

Endo S., Chino T., Shinji T. and Koto K., Nature 340, 452 (1989)

Finger L.W., Hadidiacos C.G. and Ohashi Y., Carnegie Inst. Washington Yearb. 72, 694 (1973)

Finger L.W. and King H.E., American Mineralogist 63, 337 (1978)

Finger L.W. and Hazen R.M., J. Appl. Phys. 49, 5823 (1978)

Finger L.W., Hazen R.M., Zou G., Mao H.K. and Bell P.M., Appl. Phys. Lett. 39, 892 (1981)

Fourme R., J. Appl. Cryst. 1, 23 (1968)

Flack H., Acta Cryst. A30, 569 (1974)

Forman R.A., Piermarini G.J., Barnett J.D. and Block S., Science 176, 284 (1972)

Francois M., Yuan K., Fischer P. and Decroux M., Solid State Commun. 63, 1 (1987)

Freund A.K. and Riekel C., editors 'Procedings of the ESRF workshop on single-crystal diffraction and scattering at high pressure' Held in Munich July 1989.

Fritz J.N., Marsh S.P., Carter W.J. and McQueen R.G., Nat. Bur. Stand. U.S. Special Publication 326, (1971)

Fujishiro I., Piermarini G.J., Block S. and Munro R.G., High Pressure Reasearch and Industry, ediors. Backmann C.M., Johannson T. and Tegner L., Procedings of the 8th AIRAPT Conference, Uppsala, Sweden. Volume II, pp608

Fujii Y., Hase K., Ohishi Y., Fujihisa H., Hamaya N., Takemura K., Shimomura O., Kikegawa T., Amemiya Y. and Matsushita T., Phys. Rev. Lett. 63, 358 (1989)

Gesi K. and Ozawa K., Jap. J. Appl. Phys. 17, 435 (1978)

Glinneman J., Private Communication (1990)

Gomez de Andrez D., Helliwell M., Habash J., Dodson E.J., Helliwell J.R., Bailey P.D. and Gammon R.E., Acta Cryst. B45, 482 (1989)

Griessen R., Phys. Rev. B. 36, 5284 (1987)

Hamilton W.C., International Tables for Crystallography Vol IV pp273 (Kynoch Press:Birmingham (1974))

Harding M.M., Maginn S.J., Campbell J.W., Clifton I. and Machin P., Acta Cryst. B44, 142 (1988)

Hazen R.M., American Mineralogist 61, 266 (1976)

Hazen R.M. and Finger L.W., Carnegie Inst. Washington Yearb. 76, 655 (1977)

Hazen R.M. and Finger L.W., Carnegie Inst. Washington Yearb. 78, 658 (1979)

Hazen R.M. and Finger L.W., Rev. Sci. Inst. 52, 75 (1981a)

Hazen R.M. and Finger L.W., J. Appl. Cryst. 14, 234 (1981b)

Hazen R.M. and Finger L.W., Carnegie Inst. Washington Yearb. 80, 373 (1981c)

Hazen R.M. and Finger L.W., American Mineralogist 74, 352 (1989)

Heinz D.L. and Jeanloz R., J. Appl. Phys. 55, 885 (1984)

Hewat A.W. and Bailey I., Nucl. Inst. and Meth. 137, 463 (1976)

Hewat A.W., Private Communication (1989)

Hochli U.T. and Boatner L.A., Phys. Rev. B 20, 266 (1979)

Hochli U.T., Ferroelectrics 35, 17 (1981)

Holzapfel W.B., 'Simple Molecular Systems at Very High Density' editors Polian A., Loubeyre P. and Boccara N. NATO ANSI series (Plenum Press:New York (1989))

Howard C., Nelmes R.J. and Vettier C., Solid State Commun. 69, 261 (1989)

Huber G., Syassen K. and Holzapfel W.B., Phys. Rev. B 15, 5123 (1977)

Ichikawa M., Acta Cryst. B34, 2074 (1978)

Ichikawa M., Chem. Phys. Lett. 79, 583 (1981)

Ichikawa M., Motida K. and Yamada N., Phys. Rev. B 36, 874 (1987)

Iwata Y., Koyano N. and Shibyu I., J. Phys. Soc. Japan. 49, 304 (1980)

Jauch W., Schulz A.J. and Schneider J.R., J. Appl. Cryst. 21, 975 (1988)

Jeffrey R.N., Barnett J.D., Vanfleet H.B. and Hall H.T., J. Appl. Phys. 37, 3172 (1966)

Jenkins B. and Clark S.M., Daresbury Laboratory Technical Memorandum DL/SCI/TM65E March 1990.

Jorgenson J.D., J. Appl. Phys. 49, 5473 (1978)

Jorgenson J.D., Private Communication (1988)

Jorgenson J.D., Schuttler H.B., Hinks D.G., Capone D.W., Zhang H.K., Brodsky M.B., and Scalapino D.J., Phys. Rev. Lett. 58, 1024 (1987)

Kaldis E., Fischer P., Hewat A.W., Hewat E.H., Karpinski J. and Rusiecki S., Physica C. 159, 668 (1989)

Katrusiak A., High Pressure Research 4, 496 (1990)

Katrusiak A. and Nelmes R.J., J. Phys. C 19, L765 (1986a)

Katrusiak A. and Nelmes R.J., J. Appl. Cryst. 19, 73 (1986b)

Keller R. and Holzapfel W.B., Rev. Sci. Inst. 48, 517 (1977)

Khvostantsev L.G., High Temperature-High Pressure 16, 165 (1984)

King H.E. and Finger L.W., J. Appl. Cryst. 12, 374 (1979)

King H.E., 'High Pressure Crystallography with a CAD4' Instruction Manual, Enraf-Nonius, Delft (1981)

King H.E., Newsam J.M., Jones R.H., Yang C.Z. and Xie D.E., NSLS Annual Report 1989

Koepke J., Dietrich W., Glinneman J. and Schulz H., Rev. Sci. Inst. 56, 2119 (1985)

Kojyo N. and Onodera Y., J. Phys. Soc. Japan 57, 4391 (1988)

Kudoh Y., The 25th High Pressure Conf. of Japan Abstr. pp102 (1984)

Kuhs W.F., Finney J.L., Ahsbahs H. and Londono D., ILL Experimental Reports 1986 pp86 (1986)

Kuhs W.F., Ahsbahs H., Londono D. and Finney J.L., Physica B 156 and 157, 684 (1989)

Kuhs W.F., Private Communication (1989)

Lawrence M.C. and Robertson G.N., Ferroelectrics 25, 179 (1980a)

Lawrence M.C. and Robertson G.N., J. Phys. C 13, L1053 (1980b)

Lawrence M.C. and Robertson G.N., Ferroelectrics 34, 179 (1981)

Lehmann M.S. and Larson F.K., Acta Cryst. A30, 580 (1974)

Lehmann M.S., Kuhs W.F., McIntyre G.J., Wilkinson C. and Allibon J.R., J. Appl. Cryst. 22, 562 (1989)

LeSar R., Ekberg S.A., Jones L.H., Mills R.L., Schwalbe L.A. and Schiferl D., Solid State Commun. 32, 131 (1979)

LeSar R., 'Simple Molecular Systems at Very High Density' editors Polian A., Loubeyre P. and Boccara N. NATO ANSI series (Plenum Press:New York (1989))

Levien L., Prewitt C.T. and Weidner D.J., American Mineralogist 65, 920 (1980)

Litvin D.F. and Ponyatovskii E.G., Sov. Phys.–Crystallog. 11, 322 (1966)

Lynch R.W. and Drickamer H.G., J. Chem. Phys. 45, 1020 (1966)

McMahon M.I., Nelmes R.J., Kuhs W.F. and Piltz R.O., Europhysics Letters 13, 143 (1990a)

McMahon M.I., Piltz R.O. and Nelmes R.J., To be published (1990b)

McWhan D.B., Bloch D. and Parisot G., Rev. Sci. Inst. 45, 643 (1974)

Malinowski M., J. Appl. Cryst. 20, 379 (1987)

Mao H.K. and Bell P.M., Science 191, 851 (1976a)

Mao H.K. and Bell P.M., Carnegie Inst. Washington Yearb. 75, 827 (1976b)

Mao H.K. and Bell P.M., Science 200, 1145 (1978a)

Mao H.K., Bell P.M., Shaner J.W. and Steinberg D.J., J. Appl. Phys. 49, 3276 (1978b)

Mao H.K. and Bell P.M., Carnegie Inst. Washington Yearb. 79, 409 (1980)

Mao H.K., Xu J. and Bell P.M., J. Geophys. Res. 91, 4673 (1986)

Matsushita E. and Matsubara T., Prog. Theor. Phys. 67, 1 (1982)

Menoni C.S. and Spain I.L., High Temperatures-High Pressures 16, 119 (1984)

Merrill L. and Bassett W.A., Rev. Sci. Inst. 45, 290 (1974)

Meyer G.M., Nelmes R.J. and Vettier C., J. Phys. C 13, 4035 (1980)

Ming L.C., Manghnani M.H., Balogh J., Quadri S.B., Skelton E.F. and Jamieson J.C., J. Appl. Phys. 54, 4390 (1983)

Morosin B. and Samara G.A., Ferroelectrics 3, 49 (1971)

Motida K. and Ichikawa M., J. Phys. Soc. Japan 58, 2810 (1989)

Mylov V.P., Shirokov A.M., Shuvalov L.A., Kharitonov V.N., Brzhezina B., Sov. Phys. Crystallogr. 24, 738 (1979)

Negran T.J., Glass A.M., Brickencamp C.S., Rosenstein R.D., Osterheld R.K. and Susott R., Ferroelectrics 6, 179 (1974)

Nelmes R.J. and Choudhary R.N.P., Solid State Commun. 26, 823 (1978)

Nelmes R.J., Meyer G.M. and Tibballs J.E., J. Phys. C 15, 59 (1982)

Nelmes R.J., Tun Z. and Kuhs W.F., Ferroelectrics 71, 125 (1987)

Nelmes R.J., Ferroelectrics 71, 87 (1987)

Nelmes R.J., J. Phys. C 21, L881 (1988)

Ogata K., Takeuchi Y. and Kudoh Y., Zeit fur Krist. 179, 403 (1987)

Okada M. and Iwasaki H., Phys. Status Solidi 58, 623 (1980)

Paureau J. and Vettier C., High Temperatures-High Pressures 7, 529 (1975)

Peercy P.S. and Samara G.A., Phys. Rev. B 8, 2033 (1973)

Pei S., Jorgenson J.D., Hinks D.G., Dabrowski B., Lightfoot P. and Richards D.R., Physica C submitted (1990)

Piermarini G.J., Block S. and Barnett J.D., J. Appl. Phys. 44, 5377 (1973)

Piermarini G.J. and Block S., Rev. Sci. Inst. 46, 973 (1975)

Piermarini G.J., Block S., Barnett J.D. and Forman R.A., J. Appl. Phys. 46, 2774 (1975)

Piltz R.O., McMahon M.I. and Nelmes R.J., ILL Experimental Reports (1988)

Piltz R.O., Nelmes R.J. and McMahon M.I., (1990) To be published

Piltz R.O., McMahon M.I. and Nelmes R.J., Submitted to Zeit. fur Kryst. (1990)

Piltz R.O., and Nelmes R.J., (1990) To be published

Pistorius C.W.F.T., Prog. Solid State Chem. 11, 1 (1976)

Prince E. and Nicholson W.L., 'Structure and Statistics in Crystallography' editor Wilson A.J.C. (Adeline Press:New Ypork (1985)) pp183

Restori R., Tun Z., Nelmes R.J. and McIntyre G.J., J. Phys. C 20, L591 (1987)

Rietveld H.M., J. Appl. Cryst. 2, 65 (1969)

Ritzkallah P.J., Maginn S.J. and Harding M.M., Acta Cryst. B46, 193 (1990)

Robertson J.M. and Ubbelohde A.R., Proc. Royal Soc. A 170, 222 (1939)

Samara G.A., Phys. Rev. Lett. 27, 103 (1971)

Samara G.A., Ferroelectrics 22, 925 (1979)

Samara G.A., Ferroelectrics 71, 161 (1987)

Santoro A., Weir C.E., Block S. and Piermarini G.J., J. Appl. Cryst. 1, 101 (1968)

Schiferl D., Rev. Sci. Inst. 48, 24 (1977a)

Schiferl D., High Temperatures-High Pressures 9, 71 (1977b)

Schiferl D., Jamieson J.C. and Lenko J.E., Rev. Sci. Inst. 49, 359 (1978)

Schiferl D., Johnson S.W. and Zinn A.S., High Pressure Research 4, 393 (1990)

Semmingsen D. and Thomas T., Preprint (1990)

Skelton E.F., Webb A.W., Qadri S.B., Wolf S.A., Lacor R.C., Feldman J.L., Elam W.T., Carpenter E.R. and Huang C.Y., Rev. Sci. Inst. 55, 849 (1984)

Sowa H., Reithmayer K., Macavei J., Rieck W, Schulz H. and Kupak V., To be pulished in J. Appl. Cryst. 23, (1990)

Spetzler H., Sammis C.G. and O'Connell R.J., J. Phys. Chem. Sol. 33, 1727 (1972)

Takeuchi Y., J. Min. Soc. Jpn. 14, 258 (1986)

Tatsuzaki I. and Yamanaka A., Phase Transitions 10, 143 (1987)

Tibballs J.E., Nelmes R.J. and McIntyre G.J., J. Phys. C 15, 37 (1982a)

Tibballs J.E. and Nelmes R.J., J. Phys. C 15, L849 (1982b)

Tokunaga M., Prog. Theor. Phys. 80, 156 (1984)

Tokunaga M. and Matsubara T., Ferroelectrics 72, 175 (1987)

Tominaga Y., Kasahara M., Urabe H. and Tatsuzaki I., Solid State Commun. 47, 835 (1983a)

Tominaga Y., Urabe H. and Tokunaga M.S., Solid State Commun. 48, 265 (1983b)

Tun Z., Nelmes R.J. and McIntyre G.J., J. Phys. C 20, 5667 (1987)

Tun Z., Nelmes R.J., Kuhs W.F. and Stansfield R.F.D., J. Phys. C 21, 245 (1988)

Tun Z., Nelmes R.J. and Kuhs W.F., To be Published (1990)

Vereschagin L.F., Yakovlev E.N. and Timofeev Y.A., Sov. Phys. JETP 21, 304 (1975)

Vohra Y.K. and Ruoff A.L., High Pressure Reasearch 4, 296 (1990)

Weir C.E., Block S. and Piermarini G., J. Res. Nat. Bur. Stand. 69C, 275 (1965)

Weir C.E., Piermarini G. and Block S., Rev. Sci. Inst. 40, 1133 (1969)

Weir S.T., Vohra Y.K., Vanderborgh C.A. and Ruoff A.L., Phys. Rev. B 39, 1280 (1989)

Wilkinson C., Khamis H.W., Stansfield R.F.D. and McIntyre G.J., J. Appl. Cryst. 21, 471 (1988)

Xu J., Mao H.K. and Bell P.M., High Temperatures-High Pressures 16, 495 (1984)

Yagi T., Shimomura O., Yamaoka S., Takemura K. and Akimoto S., 'Solid State Physics under Pressure' editor. Minomura S. (Terra Scientific (1985)) pp363

Yasuda N., Fujimoto F., Okamoto M., Shimizu H., Yoshino Y. and Inuishi Y., Phys. Rev. B 20, 2755 (1979)

Zou G., Mao H.K. and Bell P.M., Carnegie Inst. Washington Yearb. 81, 392 (1982a)

Zou G., Bell P.M. and Mao H.K., Carnegie Inst. Washington Yearb. 81, 436 (1982b)

Zucker U.H., Perenthaler E., Kuhs W.F., Bachmann R. and Schulz H., J. Appl. Cryst. 16, 358 (1983)

Published Work

Physica C 166 (1990) 329–333
North-Holland

PRESSURE DEPENDENCE OF THE STRUCTURE OF La–Sr–Cu–O

R.J. NELMES [a], N.B. WILDING [a], P.D. HATTON [a], V. CAIGNAERT [b], B. RAVEAU [b], M.I. McMAHON [a] and R.O. PILTZ [a]

[a] *Department of Physics, University of Edinburgh, Edinburgh EH9 3JZ, UK*
[b] *ISMRA, Bd Maréchal Juin, 14032 Caen Cédex, France*

Received 7 November 1989
Revised manuscript received 20 January 1990

A high-resolution neutron powder diffraction study has been carried out to study the effect of pressure on the structure of the oxide superconductor $La_{1.85}Sr_{0.15}CuO_4$ in its room-temperature tetragonal phase. The refined atomic coordinates indicate an anomalous behaviour of the bond linking the copper atom to the apical oxygen atom (Cu–O2) of the CuO_6 octahedra. The length of this bond increases significantly when the pressure is raised from its atmospheric value to 6 kbar, before decreasing again when the pressure is increased further to 10 kbar. By contrast, the superconducting transition temperature increases linearly with pressure to well above 10 kbar. This result differs from recent work on other oxide superconductors in which increases in T_c have been attributed to linearly related *decreases* in the corresponding apical Cu–O distance.

1. Introduction

Since the early days of the high-T_c oxide superconductors, it has been known that applied pressure can have a strong effect on the value of the superconducting transition temperature T_c [1]. A knowledge of the effects of pressure on the crystal structure might therefore have an important bearing on an understanding of the superconducting mechanism. With these considerations in mind, a number of groups have been seeking to identify possible correlations between structural changes in oxide superconductors under pressure and the value of T_c. The main focus of this interest has been those classes of superconductors for which the rate of change of T_c with pressure is large, e.g. $La_{2-x}M_xCuO_4$ (M = Sr, Ba, Ca) and $YBa_2Cu_4O_8$ (see table I). By virtue of their large value of dT_c/dP, such compounds offer perhaps the greatest promise for investigations of the effect of pressure-induced structural changes on the value of T_c.

Table I
Examples of high-T_c superconductors with a large dT_c/dP

Compound	T_c [K]	dT_c/dP [K/kbar]	Ref.
$La_{2-x}M_xCuO_4$	~37	0.37	[5]
$YBa_2Cu_4O_8$	80	0.55	[6]

Fig. 1 shows the structures of both the $La_{2-x}Sr_xCuO_4$ or 2–1–4 compound [2], and the $YBa_2Cu_4O_8$ or 1–2–4 compound [3], in their room-temperature phases. The 2–1–4 structure (fig. 1a) is the simpler of the two, and may be viewed as planes of CuO_6 octahedra of the perovskite structure, alternating with a buckled rocksalt La(Sr)–O slab which is rotated in the basal plane by 45°. In the 1–2–4 structure, the octahedra of the 2–1–4 structure are replaced by two "half-octahedra", the CuO_5 square pyramids, which are separated by the Y atoms (see fig. 1b). These double-pyramid slabs are linked through two parallel Cu–O chains (along the *b*-axis), which results in a relative displacement of alternate slabs along the *b*-axis and hence a large *c*-axis repeat of ~27 Å.

Both structures thus have in common the CuO_5 square pyramids, as halves of the CuO_6 octahedra in the 2–1–4 compound and as discrete units in the 1–2–4 case. Recently, evidence for interesting structural changes under pressure in this part of the 1–2–4 structure has been reported by Kaldis et al. [4]. Their neutron powder diffraction study of

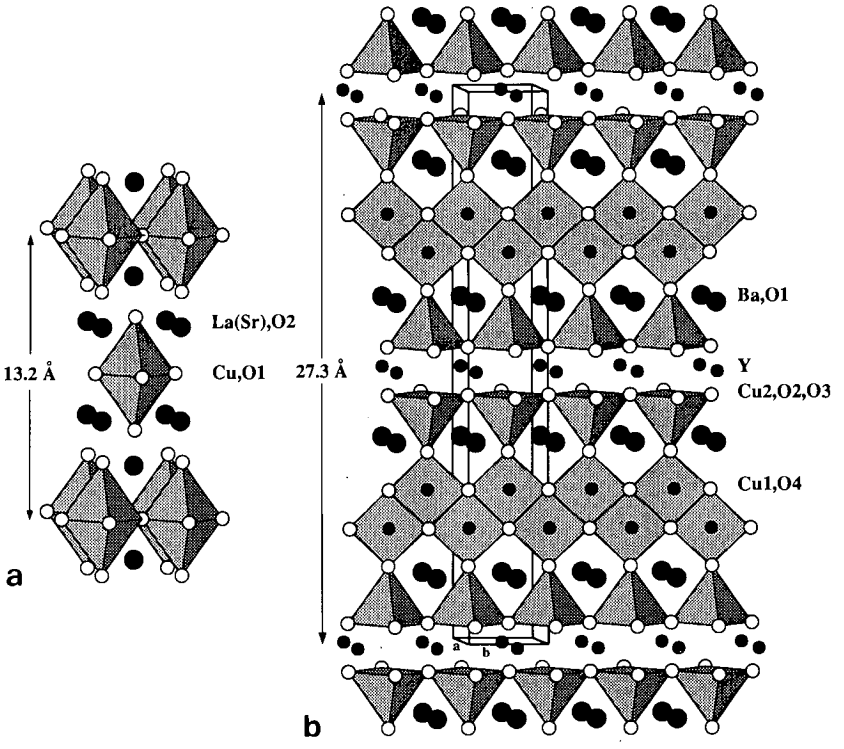

Fig. 1. The structures of (a) $La_{2-x}Sr_xCuO_4$ and (b) $YBa_2Cu_4O_8$ in their room-temperature phases.

$YBa_2Cu_4O_8$ as a function of temperature and pressure revealed a large decrease in the apical Cu–O distance of the CuO_5 pyramids (Cu2–O1 in their notation) of about 0.05 Å, or 2.5%, as the pressure was raised from its atmospheric value to 10 kbar – a range over which T_c increases almost linearly [6]. The authors attributed this effect to a charge transfer to the Cu–O planes (the basal planes of the CuO_5 pyramids) as the pressure was increased, resulting in an increase in T_c. This mechanism involves the linking Cu–O chains, which are absent from the $La_{2-x}Sr_xCuO_4$ structure.

Detailed structural studies of the $La_{2-x}Sr_xCuO_4$ superconductor family under pressure have so far been restricted to the parent compound of the family, La_2CuO_4. This material has the tetragonal structure of K_2NiF_4 (as in fig. 1a) at elevated temperatures (>500 K), while at room temperature and down to 1.5 K it is orthorhombic. The orthorhombic structure is derived from the tetragonal structure by tilting of the CuO_6 octahedra around the orthorhombic b-axis [#1]. A neutron powder diffraction study by Howard et al. [7] has shown that the orthorhombic distortion of the unit cell decreases with increasing pressure at room temperature. However, results for the tilt of the CuO_6 octahedra – which characterises the internal orthorhombic distortion – were less clear.

In the light of the conclusion of Kaldis et al. [4] we have extracted the apical Cu–O distance of the CuO_6 octahedra (Cu–O2 in this case) from the results of Howard et al. [7] for La_2CuO_4. We find that,

[#1] Various workers have employed different space-group settings and different schemes for designating the contents of the asymmetric unit for the orthorhombic structure. Standard crystallographic convention defines $b>a>c$ for orthorhombic unit cells, but it is less confusing to define the 13 Å translation as c, to correspond to the c-axis of the tetragonal phase. We have therefore chosen the Abma setting with $a>b$ which is consistent with the previous paper by Howard et al. [7]. Finally, we have retained the original description of the structure by Grande et al. [8], namely, employing O(1) to designate the equatorial atom with coordinates $\approx (\frac{1}{4}, \frac{1}{4}, 0)$ and O(2) for the apical atom at $\sim (00z)$.

contrary to the result for $YBa_2Cu_4O_8$, this distance *increases* when the pressure is raised to 5 kbar, before decreasing again nearly to its ambient pressure value at 10 kbar. This intriguing result has prompted us to perform a comparative experiment on the substituted superconducting derivative $La_{1.85}Sr_{0.15}CuO_4$, with the aim of measuring the Cu–O2 distance as a function of pressure. Given that the value of dT_c/dP for the 2–1–4 compound is approximately half of the value for the 1–2–4 superconductor, associated structural changes may be expected to be correspondingly smaller over the same pressure range, but still readily measurable with current techniques.

2. Experiment and data analysis

Like its parent compound, $La_{1.85}Sr_{0.15}CuO_4$ exists in two distinct phases [9]. At temperatures above 180 K, the structure is tetragonal (space group I4/mmm, see fig. 1a) while below this temperature the CuO_6 octahedra are tilted and the structure becomes orthorhombic (space group Abma) as described above for La_2CuO_4. Another finding of the work of Kaldis et al. on $YBa_2Cu_4O_8$ [4] was that the change in the apical Cu–O distance with pressure does not vary significantly between 5 K and 165 K. Also, the atmospheric pressure study of $La_{1.85}Sr_{0.15}CuO_4$ itself by Francois et al. [10] showed the apical Cu–O distance changed by only ~ 0.005 Å between room temperature and 7 K. These results suggest that the important structural changes can be detected at room temperature, thus avoiding the experimental difficulties associated with low-temperature measurements at high pressures. On this basis, we have performed most of our experiments at room temperature. However, some additional measurements were also made under pressure at low temperature to check that the transition to the orthorhombic phase does not significantly alter the structural changes observed in the room-temperature (tetragonal) phase.

A carefully characterised powder sample of $La_{1.85}Sr_{0.15}CuO_4$ was prepared. Room-temperature profiles were obtained at atmospheric pressure, 6 kbar and 10 kbar, with a single set of low-temperature measurements at 4 K and an estimated pressure of 7 kbar. For the high-pressure measurements, the sample was loaded into the 6 mm diameter sample chamber of a clamp-type cell made of maraging steel. A measured force was applied to the upper piston, and the pressure estimated with the help of prior calibration. This calibration is considered to be known to within 5%. The clamp-cell used for the low-temperature measurements was subsequently found to have a faulty piston, making the true pressure of the nominal 7 kbar run less certain.

All data were collected using the D1A neutron diffractometer at the Institut Laue-Langevin (ILL) [11]. An incident neutron wavelength of 1.909(1) Å was used, and profile patterns were obtained with a 2θ step size of 0.05°. The sample peaks had a typical FWHM of 0.4° in 2θ. The steel housing of the pressure cell gave rise to diffraction peaks centred at 56°, 83° and 109° of 2θ, and these regions were estimated visually and excluded from the profiles used for structure refinement. These exclusions represented a total loss of 6 peaks from the free-sample total of 31 distinct peaks. The powder patterns were refined using the PROFIL Rietveld program at ILL [12]. In all cases the instrumental zero and asymmetry parameters obtained from the refinements were found to be self consistent.

In table II, we present results for the tetragonal cell dimensions, a and b, for the atomic fractional coordinates z(O2) and z(La, Sr), and for the apical Cu–O distance (Cu–O2). Also given in this table are the room-temperature results of Howard et al. [7] for La_2CuO_4 in its orthorhombic phase. Table III shows the results for the low-temperature study of orthorhombic $La_{1.85}Sr_{0.15}CuO_4$ at the nominal pressure of 7 kbar. Values have been calculated for the orthorhombic distortion, $2(a-b)/(a+b)$; for the orthorhombic analogue of the tetragonal c/a ratio, $2\sqrt{2}c/(a+b)$; and for the orthorhombic tilt angle of the octahedra, $\tan^{-1}(x(\mathrm{O2})/z(\mathrm{O2}))(a/c)$. The low-temperature results of Francois et al. at atmospheric pressure [10], transformed to the Abma space group setting, are also given in the table for comparison.

3. Discussion and conclusions

Although the unit cell dimensions and the majority of the bonds decrease quite normally in length

Table II
Pressure dependence of the unit cell dimensions and structural parameters in (tetragonal) $La_{1.85}Sr_{0.15}CuO_4$ and (orthorhombic) La_2CuO_4 at room temperature

Parameter	Atmospheric pressure	6 kbar	10 kbar
$La_{1.85}Sr_{0.15}CuO_4$			
a [Å]	3.7743(1)	3.7696(1)	3.7681(1)
b [Å]	13.2193(4)	13.2058(6)	13.2004(5)
z(O2)	0.1823(3)	0.1846(6)	0.1831(5)
z(La, Sr)	0.3604(2)	0.3599(3)	0.3595(3)
Cu–O2 [Å]	2.410(3)	2.438(8)	2.417(7)

Parameter	Atmospheric pressure	5 kbar	9 kbar
La_2CuO_4			
a [Å]	5.3938(2)	5.3830(4)	5.3736(4)
b [Å]	5.3466(2)	5.3418(4)	5.3378(4)
c [Å]	13.1309(4)	13.120(1)	13.114(1)
z(O1)	−0.0071(2)	−0.006(1)	−0.008(1)
x(O2)	0.0338(4)	0.039(2)	0.029(3)
z(O2)	0.1830(1)	0.1850(6)	0.1842(6)
x(La)	−0.0066(3)	−0.008(2)	−0.004(2)
z(La)	0.3615(1)	0.3612(3)	0.3616(3)
Cu–O2 [Å]	2.410(2)	2.436(8)	2.421(8)

Table III
Unit cell dimensions and structural parameters at 1 bar and a nominal "7 kbar" in the orthorhombic phase of $La_{1.85}Sr_{0.15}CuO_4$ near 4 K.

Parameter	1 bar, 7 K	"7 kbar", 4 K
a [Å]	5.348(2)	5.3270(7)
b [Å]	5.324(2)	5.3111(6)
c [Å]	13.200(4)	13.167(1)
z(O1)	−0.0049(3)	−0.0045(39)
x(O2)	0.0245(5)	0.0346(30)
z(O2)	0.1821(2)	0.1836(8)
x(La, Sr)	−0.0055(4)	−0.0281(31)
z(La, Sr)	0.3608(1)	0.3595(4)
Cu–O2 [Å]	2.407(3)	2.425(11)
$2(a-b)/(a+b)$ [%]	0.45(6)	0.30(2)
$2\sqrt{2}c/(a+b)$	3.498(2)	3.501(1)
tilt angle [°]	3.12(7)	4.4(4)
Reference	[10]	this work

under pressure, the results in table II show a clear anomaly in the behaviour of the apical Cu–O distance as the pressure is increased. This is illustrated in fig. 2. Evidently, and in sharp contrast to the 1–2–4 compound, the distance at first increases with

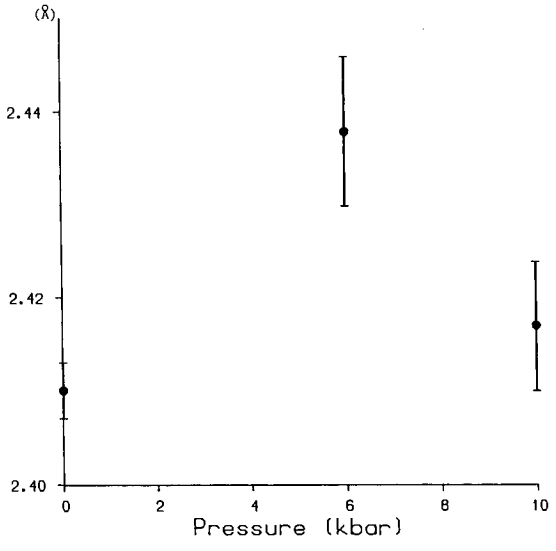

Fig. 2. The pressure dependence of the apical Cu–O2 bondlength in $La_{2-x}Sr_xCuO_4$ at room temperature.

pressure and then decreases – over a pressure range in which T_c increases linearly [5]. Furthermore, the results are remarkably similar to those obtained for La_2CuO_4 in its orthorhombic phase, which are included in table II for comparison. Thus our results do not show the particular relationship between T_c and pressure-induced structural changes proposed by Kaldis et al. [4]. This may reveal an important effect of the structural differences between the two compounds – as already mentioned, the linking Cu1–O4 chains of the 1–2–4 structure are absent from the 2–1–4 structure (see fig. 1). But the contrast in behaviour is not yet entirely clear because the measurements of the apical Cu–O distance in the 1–2–4 compound were made at only two pressures, 1 bar and 10 kbar, so it is possible that an intermediate measurement would reveal the nonlinear behaviour we have found in $La_{1.85}Sr_{0.15}CuO_4$.

Our conclusions are based on the assumption that structural changes with pressure will not differ significantly between room temperature and T_c. Some test of this assumption is afforded by the low-temperature results (table III) which show, at least, that Cu–O2 does indeed *increase* with pressure, as at room temperature. The uncertainty about the true pressure of the low-temperature experiment can be re-

duced by comparing the pressure dependence of the unit-cell volume with the room-temperature value (table II) [#2]: this indicates that the pressure must have been close to the estimated 7 kbar, and the Cu–O2 value agrees within its (quite large) error with the interpolated room-temperature value at this pressure. In addition, the change of only ~ 0.005 Å in the Cu–O2 distance found by Francois et al. [10] on cooling from room temperature to 7 K is small compared to the changes under pressure, and there is no reason to expect this small temperature dependence of the Cu–O2 distance to vary significantly with pressure.

It would certainly be of interest now to make a more detailed comparative study of the pressure dependence of both the $YBa_2Cu_4O_8$ and the $La_{1.85}Sr_{0.15}CuO_4$ compounds near their respective T_cs.

Acknowledgements

We would like to thank Dr. A.W. Hewat, Dr. C. Vettier and Mr. J. Davies of the ILL for their advice and expert assistance in carrying out the experiments. Dr. Hewat also kindly provided us with original drawings for fig. 1. We acknowledge funding support from the Science and Engineering Research Council.

[#2] At room temperature, the cell dimensions obtained by Francois et al. [10] are about 0.1% larger than our values in table II. This is almost certainly attributable to a difference in wavelength calibration. Therefore, in estimating the pressure dependence of the unit-cell volume at low temperature, the cell dimensions measured by Francois et al. (as given in table III) have first been reduced by 0.1%.

References

[1] R. Griessen, Phys. Rev. B 36 (1987) 5284.
[2] N. Nguyen, J. Choisnet, M. Hervieu and B. Raveau, J. Sol. State Chem. 39 (1981) 120.
[3] P. Fischer, J. Karpinski, E. Kaldis, E. Jilek and S. Rusiecki, Sol. State Commun. 69 (1989) 531.
[4] E. Kaldis, P. Fisher, A.W. Hewat, E.A. Hewat, J. Karpinski and S. Rusiecki, Physica C 159 (1989) 668.
[5] S. Yomo, C. Murayama, H. Takahashi, N. Mori, K. Kishio, K. Kitazawa and K. Fueki, Jpn. J. Appl. Phys. 26 (1987) L602.
[6] B. Bucher, J. Karpinski, E. Kaldis and P. Wachter, Physica C 157 (1989) 478.
[7] C. Howard, R.J. Nelmes and C. Vettier, Sol. State Commun. 69 (1989) 261.
[8] Von B. Grande, Hk. Müller-Buschbaum and M. Schweizer, Z. Anorg. Allg. Chem. 428 (1977) 120.
[9] D. McK. Paul, G. Balakrishnan, N. Bernhoeft, W.I.F. David and W.T.A. Harrison, Phys. Rev. Lett. 58 (1987) 1976.
[10] M. Francois, K. Yvon, P. Fischer and M. Decroux, Sol. State Commun. 63 (1987) 1.
[11] A.W. Hewat and I. Bailey, Nucl. Instr. and Meth. 137 (1976) 463.
[12] J.K. Cockcroft, PROFIL program, ILL Grenoble (1989).

Ferroelectrics, 1990, Vol. 108, pp. 277–282
Reprints available directly from the publisher
Photocopying permitted by license only

NEUTRON-DIFFRACTION STUDIES OF THE RELATIONSHIP BETWEEN T_c AND H-BOND DIMENSIONS IN H-ORDERING TRANSITIONS

M.I. McMAHON, R.O. PILTZ AND R.J. NELMES
Department of Physics, University of Edinburgh, Mayfield Road, Edinburgh EH9 3JZ, U.K.

Abstract Neutron-diffraction studies have been carried out on KH_2PO_4, and other H-bonded materials exhibiting a similar H-ordering phase transition, just above the transition temperature T_c, at atmospheric pressure and under applied hydrostatic pressures up to 19 kbar. The results show a systematic relationship between T_c and δ, where δ is the separation between the two sites over which the H atoms are 50:50 disordered above T_c.

INTRODUCTION

KH_2PO_4 (KDP) undergoes an H-ordering transition on cooling through T_c = 122 K to its ferroelectric phase. Above T_c, the H atoms are 50:50 disordered over two off-centre sites in short O—H—O bonds linking the PO_4 groups. Below T_c, the H atoms order onto one of these sites. The deuterated form, KD_2PO_4 (DKDP), exhibits the same behaviour at the substantially higher T_c of 229 K.

The application of hydrostatic pressure decreases T_c in both KDP and DKDP[1]. In KDP, T_c falls to 0 K at 17 kbar; it is estimated that a pressure of ~65 kbar is needed to reduce T_c to 0 K in DKDP. Pressure also reduces the O—H(D)—O bondlength, 2R, and the H-site separation, δ; previous neutron-diffraction studies of KDP and DKDP by us have established that the changes in 2R and δ† under pressure are linearly related to the changes in T_c under pressure, up to at least 12 kbar[2,3,4].

Similar results have been obtained for $H_2C_4O_4$ (squaric acid or H_2SQ) which also has an H-ordering transition. But H_2SQ has a much

†Note that δ is the separation of the maxima of the H (or D) distribution, as determined from diffraction data. This is to be distinguished from the separation, Δ, of the minima of the double-minimum H(D) potential well. Because of the asymmetry of each minimum of the well, δ is less than Δ – more so for H than for D, because the H energy levels are higher in the well.

higher T_c (= 374 K) than KDP, and the ordering below T_c is antiferroelectric[5] (unlike KDP). Furthermore, the structure of H_2SQ is two-dimensionally linked by the H-bonds – forming $H_2C_4O_4$ sheets which are not H-bonded to one another – whereas KDP has a three-dimensionally linked H_2PO_4 framework. Despite these substantial differences, not only do 2R and δ again decrease linearly with T_c under pressure, but the relationship is such that compression of δ in H_2SQ to the same value as in KDP (at atmospheric pressure) removes most of the large difference in T_c[6].

These results suggest that T_c is strongly determined just by the magnitude of δ in any system. To explore this relationship further, we have now made structural studies of two other H-ordering systems – namely, $PbHPO_4$ (LHP) and its deuterated form LDP, and $NH_4H_2PO_4$ (ADP) and its deuterated form DADP. In LHP – for which the atmospheric-pressure results have already been obtained[7] – the PO_4 groups are linked only one-dimensionally by the O–H–O bonds, forming HPO_4 chains; T_c is 310 K for LHP and rises to 452 K for LDP; and the ordering below T_c is ferroelectric. The structure of ADP is isomorphous with KDP above T_c, but the ordering below T_c is antiferroelectric. T_c is 151 K for ADP and rises to 235 K for DADP.

EXPERIMENTS

All the neutron-diffraction data were collected at the Institut Laue-Langevin, Grenoble, using high-resolution single-crystal techniques. As the purpose was to determine the relationship between T_c, 2R and δ, the data had to be collected as nearly as possible <u>at</u> T_c. In practice, they were collected just above T_c, in the range T_c + 3 K to T_c + 16 K. The data for KDP, DKDP, ADP, LHP and H_2SQ under pressure were obtained using a clamp-type pressure cell[8], while a new sapphire-anvil cell[9] was used for the LDP study. In all cases, the sample was surrounded by a pressure-transmitting fluid to achieve hydrostatic conditions. So as to determine the smaller values of δ reliably, data were collected out to $\sin\theta/\lambda \gtrsim 1.1$ Å^{-1}.

RESULTS

Figure 1 shows how T_c varies in relation to 2R for various pressures in all the systems studied except ADP-DADP. The points for ADP (at

atmospheric pressure and at 9 kbar, where T_c = 120 K) and for DADP (at atmospheric pressure) are omitted so as not to overcrowd the Figure. The ADP and DADP points are all ~0.02 Å smaller in 2R than the lines in the Figure would predict for KDP and DKDP, respectively, at the ADP and DADP values of T_c.

Although T_c appears to vary linearly with 2R within each system, as shown by the three points for KDP and for H_2SQ, there is no evident simple relationship between one system and another. But when T_c is plotted against δ instead, as in Figure 2, a striking relationship emerges. In all these different systems, deuterated and undeuterated, T_c extrapolates to 0 K at the same δ of about 0.2 Å – except, perhaps, for LHP (see below). (The ADP and DADP points are again omitted from

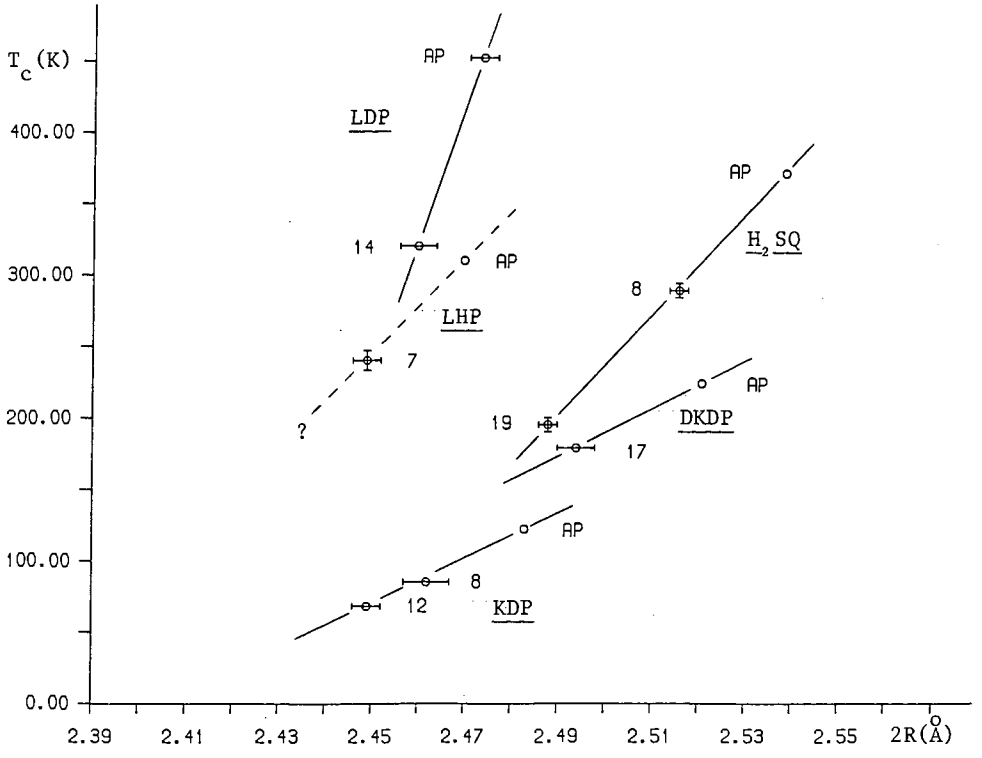

FIGURE 1 The variation of T_c and the O–H(D)–O bondlength, 2R, with pressure in KH_2PO_4 (KDP), KD_2PO_4 (DKDP), $H_2C_4O_4$ (H_2SQ), $PbHPO_4$ (LHP) and $PbDPO_4$ (LDP). The pressure is given against each point as AP (atmospheric pressure) or the number of kbar applied. Where error bars are not shown, the error is less than the size of the symbol used to plot the point. The query about LHP is explained in the text.

the Figure. When plotted in terms of δ, they lie very close to the KDP and DKDP lines – within ~0.01 Å in δ.)

Figure 2 also suggests that the rate of change of T_c with δ increases as the dimensionality of the H-bonding decreases, KDP → H_2SQ → LHP. But this depends on the interpretation of the result for LHP at 7 kbar, which was obtained from a possibly too small and restricted data set for an accurate study of the low symmetry (monoclinic) structure. By contrast, the result for LDP at 14 kbar is based on a nearly full three-dimensional data set, and it seems probable that this establishes the rate of change of T_c with δ in the LHP-LDP system – a rate of change from which the LHP point deviates by only 1.5 e.s.d.'s in any case. However, Figure 1 shows that the 2R value for LHP at 7 kbar also appears lower than expected from the general trends of the other results, and the determination of 2R is less likely to be

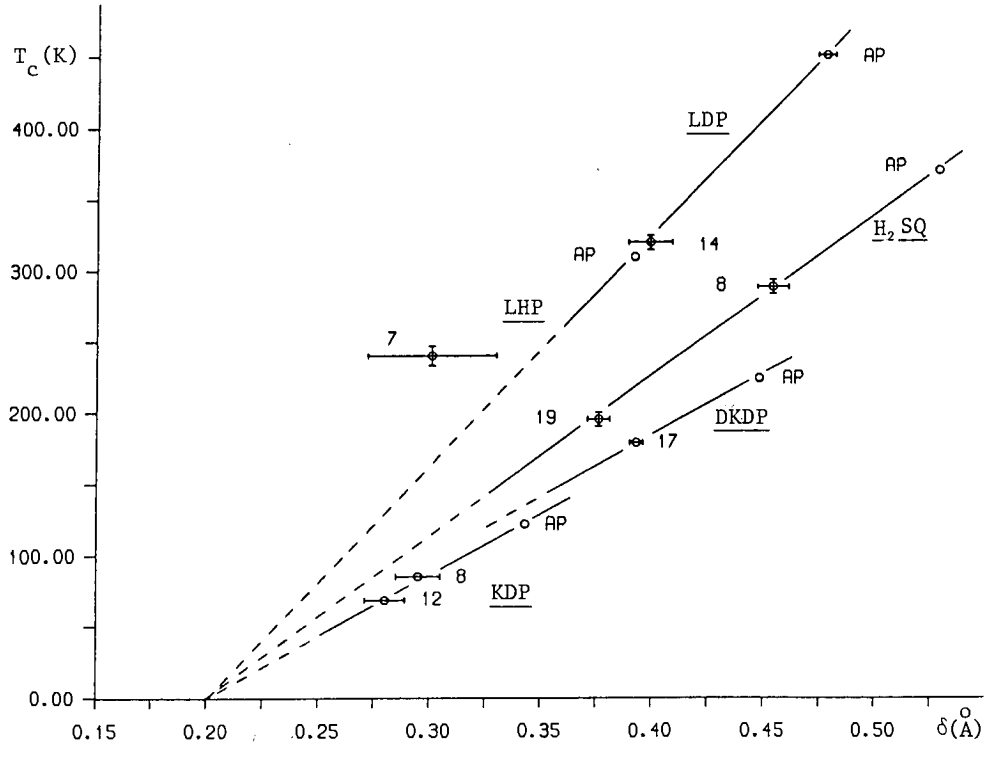

FIGURE 2 The variation of T_c and the H(D)-site separation, δ, with pressure in KDP etc., as in Figure 1. No separate line has been drawn through the two LHP points, at AP and 7 kbar, because of the uncertainty about the 7 kbar result (see the text).

affected by the restrictions of the data set. So a definite conclusion about LHP must await a further study with more data.

The intermediate position of H_2SQ in the sequence, and the fact that the ADP and DADP points lie almost on the KDP and DKDP lines in Figure 2, suggest that the relationship between T_c and δ is not significantly influenced by the nature of the H ordering – ferroelectric or antiferroelectric.

DISCUSSION

The results give strong evidence that δ – rather than 2R – is the structural parameter most directly connected with T_c. In particular, it seems that the δ value of ~0.2 Å has some fundamental significance common to both deuterated and undeuterated systems.

In an accompanying paper on the geometric isotope effect[10], we note that we depend on the KDP point at 12 kbar to exclude the possibility that T_c is proportional to δ^2. The H_2SQ points are also closer to a straight line than a δ^2 variation, but over the range of the H_2SQ measurements the difference is not large enough to be decisive. That said, there is no present reason to doubt the experimental values as they are plotted, and the possible significance of the common δ value for $T_c \to 0$ K (linearly) should be examined.

In the case of KDP, we have previously shown that when δ falls to 0.2 Å the r.m.s. along-bond zero-point motion of the H atom exceeds the half-distance, $\delta/2$, between the H sites[2]. Then the thermal motion is always sufficient to take the H atom from one minimum of the potential well to the other. And this is a plausible explanation for the loss of the ordered phase (i.e. $T_c \to 0$ K). Such an explanation suggests that the H ordering might be generally understood in terms of thermal excitation over the potential barrier between the sites, rather than tunnelling through it – as discussed further in our accompanying paper[10]. But it is not yet clear how these ideas can account for the wide, and apparently systemic, variation in $dT_c/d\delta$ among the different systems studied.

At least – and independently of the query raised above about the relationship between T_c and δ – the results suggest that H(D)-ordering transitions of the KDP type share a common form of dependence on the local H(D) potential, particularly as manifested in the size of δ.

Acknowledgements – we gratefully acknowledge the part played by Dr. W.F. Kuhs of the Institute of Crystallography, University of Karlsruhe, in the $PbDPO_4$ studies, both in the data collection and in preparing (with Dr. H. Ahsbahs) the high-pressure cell for the experiment at 14 kbar; also the participation of Dr. G.J. McIntyre of I.L.L., Grenoble, in the $NH_4H_2PO_4$ high-pressure studies. We are grateful to Dr. H. Arend, Dr. D.J. Lockwood and Dr. D. Semmingsen for kindly providing, respectively, the $PbHPO_4$, the $PbDPO_4$ and the squaric acid crystals. This work is supported by a grant from the Science and Engineering Research Council.

REFERENCES

1. G.A. Samara, Phys. Rev. Lett., 27, 103-6 (1971).
2. J.E. Tibballs, R.J. Nelmes and G.J. McIntyre, J. Phys. C, 15, 37-58 (1982).
3. J.E. Tibballs and R.J. Nelmes, J. Phys. C, 15, L849-53 (1982).
4. R.J. Nelmes, J. Phys. C, 21, L881-6 (1988).
5. D. Semmingsen and J. Feder, Solid State Commun., 15, 1369-72 (1974).
6. Z. Tun, R.J. Nelmes and G.J. McIntyre, J. Phys. C, 20, 5667-75 (1987); Z. Tun, R.J. Nelmes and W.F. Kuhs, in preparation; R. Restori, Z. Tun, R. Ramirez, R.J. Nelmes and G.J. McIntyre, Submitted to J. Phys. C.
7. Z. Tun, R.J. Nelmes and W.F. Kuhs, in preparation.
8. D. Bloch, J. Paureau, J. Voiron and G. Parisot, Rev. Sci. Instrum., 47, 266-8 (1976).
9. H. Ahsbahs, Rev. Phys. Appl., 19, 819 (1984).
10. R.O. Piltz, M.I. McMahon and R.J. Nelmes, Ferroelectrics, Proc. Int. Meeting on Ferroelectricity, Saarbrücken 1989.

Ferroelectrics, 1990, Vol. 108, pp. 271–276
Reprints available directly from the publisher
Photocopying permitted by license only

NEUTRON-DIFFRACTION STUDIES OF THE GEOMETRIC ISOTOPE EFFECT IN H-ORDERING TRANSITIONS

R.O. PILTZ, M.I. McMAHON AND R.J. NELMES
Department of Physics, University of Edinburgh, Mayfield Road, Edinburgh EH9 3JZ, U.K.

Abstract Neutron-diffraction studies have been carried out on $PbHPO_4$ and its deuterated form $PbDPO_4$ just above their respective H(D)-ordering phase transition temperatures, T_c, at atmospheric pressure. For $PbDPO_4$, data have also been collected under pressure. The results are compared with a similar study of KH_2PO_4 and KD_2PO_4. In both systems, the large change in T_c on deuteration at atmospheric pressure appears to be attributable simply to the accompanying increase in δ, where δ is the separation between the two sites over which the H(D) atoms are disordered above T_c.

INTRODUCTION

KH_2PO_4 (KDP) undergoes an H-ordering transition on cooling through T_c = 122 K to its ferroelectric phase. Above T_c, the H atoms are 50:50 disordered over two off-centre sites in short O–H–O bonds linking the PO_4 groups. Below T_c, the H atoms order onto one of these sites. The deuterated form, KD_2PO_4 (DKDP), exhibits the same behaviour at the substantially higher T_c of 229 K.

To account for the large isotope effect on T_c, the proton tunnelling model was introduced[1] and soon became the established basis for models of phase transitions of this kind[2]. But the change in T_c on deuteration is accompanied by significant increases in the O–H–O bondlength, 2R, and the H-site separation, δ; these changes are not explicitly incorporated into the tunnelling model. Neutron-diffraction studies show that 2R and $\delta^\dagger$ both reduce with pressure[3,4], as does T_c[5]. This invites the question as to whether the isotope effect on T_c may be

---

†Note that δ is the separation of the maxima of the H (or D) distribution, as determined from diffraction data. This is to be distinguished from the separation, Δ, of the minima of the double-minimum H(D) potential well. Because of the asymmetry of each minimum of the well, δ is less than Δ – more so for H than for D, because the H energy levels are higher in the well.

partly, or even wholly, attributable to the accompanying geometrical changes. Ichikawa[6,7] has shown that for a number of KDP isomorphs and their deuterated forms there is an approximately linear relationship between T_c and 2R. He concluded that the increase in T_c on deuteration arises from the increase in 2R alone, and termed this the 'geometric istotope effect'. However, a more precise examination of the variation of T_c with 2R in KDP and DKDP shows that although the difference in T_c is much reduced when KDP and DKDP are compared at the same 2R, it is still 40 K[8]. Moreover, it was shown that if the comparison is made instead at the same δ, then the difference in T_c is reduced to only 15 K or less, suggesting that δ is the more important geometrical determinant of T_c.

We have now made a comparative study of KDP-DKDP with the related but substantially different system $PbHPO_4$ (LHP) – $PbDPO_4$ (LDP), to examine how much of the isotope effect on T_c can be explained by geometrical factors in each case. LHP – for which the atmospheric-pressure results have already been obtained[9] – has an H-ordering transition to a ferroelectric phase at T_c = 310 K, much higher than the value of T_c in KDP. Also, the PO_4 groups are only one-dimensionally linked by O–H–O bonds in LHP, forming HPO_4 chains that are not cross-linked to one another, whereas the O–H-O bonds in KDP form a three-dimensionally linked H_2PO_4 framework. The isotope effect on T_c is similar in both systems, with T_c rising to 452 K in LDP.

EXPERIMENTS

All the neutron-diffraction data were collected at the Institut Laue-Langevin, Grenoble, using high-resolution, single-crystal techniques. As the purpose was to determine the relationship between T_c, 2R and δ, the data had to be collected as nearly as possible <u>at</u> T_c. In practice, they were collected just above T_c, in the range T_c + 3 K to T_c + 16 K. The data for KDP and DKDP under pressure were obtained using a clamp-type pressure cell[10], while a new sapphire-anvil cell[11] was used for the LDP study. In all cases, the sample was surrounded by a pressure-transmitting fluid to achieve hydrostatic conditions. So as to determine the smaller values of δ reliably, data were collected out to $\sin\theta/\lambda \gtrsim 1.1$ Å^{-1}.

RESULTS

Figure 1(a) shows how T_c varies in relation to 2R under pressure for KDP and DKDP. It can be seen that, as already stated, compression of 2R in DKDP to the value in KDP at atmospheric pressure (2.483 Å) reduces the difference in T_c, ΔT_c, to 40 K. If, instead, the T_c variation is plotted against δ, as in Figure 1(b), then ΔT_c for KDP and DKDP compared at the same δ can be seen to be only 15 K, and might even be zero within the uncertainties of the results.

Figures 2(a) and 2(b) present the equivalent results for the LHP-LDP system. In this case, ΔT_c (=105 K) at constant 2R is much larger than for KDP-DKDP, though ΔT_c at constant δ is comparable (zero within ~10 K).

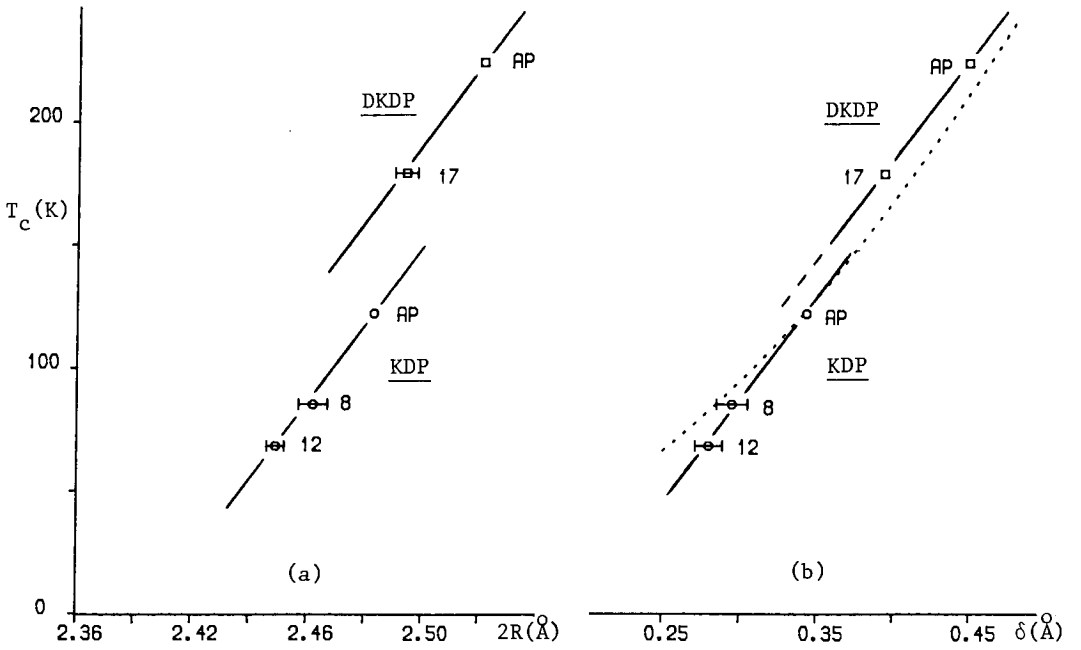

FIGURE 1 (a) The variation of T_c and the O—H—O bondlength, 2R, and (b) the variation of T_c and the H-site separation, δ, under pressure in KH_2PO_4 (KDP) and KD_2PO_4 (DKDP). The KDP points are represented by circles, and the DKDP points by squares. The pressure is given against each point as AP (atmospheric pressure) or the number of kbar applied. Where error bars are not shown, the errors are less than the size of the symbol used to plot the point. The curve in (b) shows $T_c \propto \delta^2$ through the AP point of KDP.

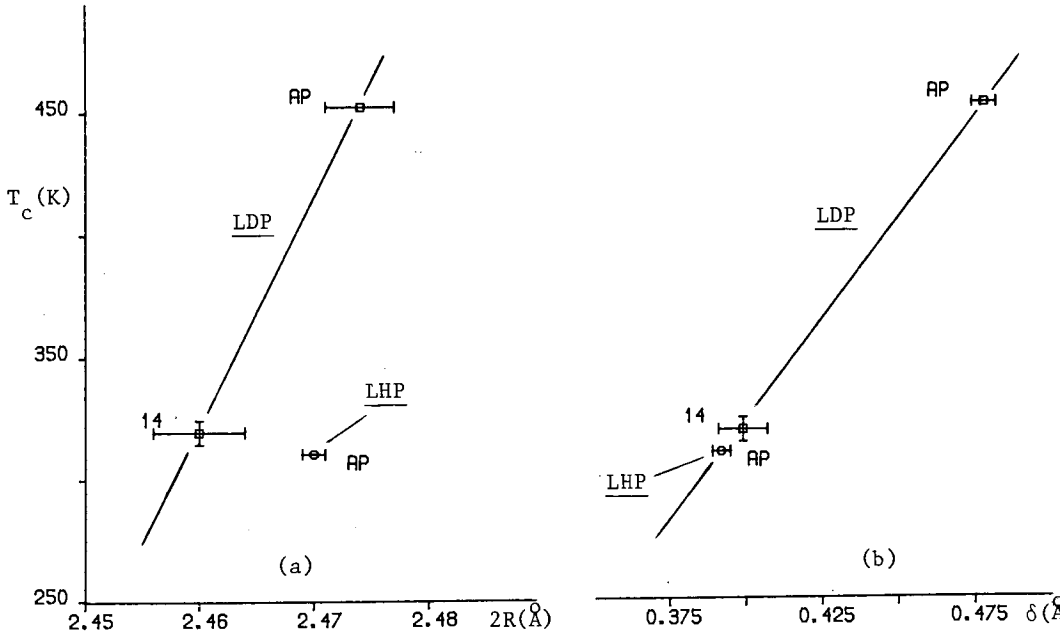

FIGURE 2 (a) The variation of T_c and the O–H–O bondlength, 2R, and (b) the variation of T_c and the H-site separation, δ, under pressure in $PbHPO_4$ (LHP) and $PbDPO_4$ (LDP), as for KDP and DKDP in Figure 1. A circle is used to represent the one LHP point (at AP), and squares are used for the LDP points.

It is clear that in both systems the deuteration effect on T_c is completely, or almost completely, suppressed when δ is kept constant. By contrast, the change in T_c on deuteration at constant 2R is certainly not zero, and also the magnitude of ΔT_c appears to vary widely with the system studied.

DISCUSSION

It seems reasonable to expect that, for a given system, the H(D) potential remains unaltered if 2R is kept constant[12], and hence that the value of ΔT_c at constant 2R estimates the direct isotope effect on T_c. However, caution must be exercised because there are a number of other significant structural changes on deuteration, even if 2R is kept constant, and these may either reduce or amplify the apparent effect of

the mass change alone[8]. This point is underlined by the new results for LHP-LDP, where the large ΔT_c (at constant 2R) of 105 K will significantly affect the thermal fluctuations of the H(D) potential[13].

The fact that ΔT_c at constant δ is close to zero in both systems, despite the large difference in ΔT_c at constant 2R, is a persuasive argument for focussing on δ as the crucial variable, and attributing the isotope effect on T_c entirely, or almost entirely, to the accompanying increase in δ.

A possible interpretation is that T_c has a simple classical dependence on the proton – proton dipole interaction[14], giving $T_c \propto \delta^2$. For KDP-DKDP, the T_c ratio at atmospheric pressure is 1.84 and the δ^2 ratio (at T_c) is 1.71: the small difference reflects the gap of 0.02 Å in δ between the KDP and DKDP lines in Figure 1(b). For LHP-LDP, the T_c and δ^2 ratios are 1.46 and 1.47, respectively – the same within error. But, of course, $T_c \propto \delta^2$ is at variance with the linear relationships drawn in Figures 1(b) and 2(b). The curve of $T_c \propto \delta^2$ is shown for KDP in Figure 1(b), taking the well-determined atmospheric pressure result as the reference point. The curve is well away from the measured δ value at T_c = 68 K (12 kbar) – though possible uncertainties in the measurement of T_c make it difficult to entirely exclude $T_c \propto \delta^2$ on the basis of this one measurement. Results for $H_2C_4O_4$ in our accompanying paper[15] also appear to show a clearly linear relationship, but the points lie within two esd's of a δ^2 variation. On balance, the weight of the present structural evidence is against T_c varying as δ^2, but not conclusively so.

Alternatively, it may be possible to understand T_c simply as the temperature at which the along-bond H(D) thermal motion becomes small enough in relation to δ for the H(D) atoms to be confined to one site. However, T_c is not necessarily expected to be the same at precisely the same δ in that case, because the pressure required to get the same δ will make 2R smaller in the deuterated form (see Figures 1 and 2). This difference in 2R, and any dependence of thermal motion on particle mass, mean that the along-bond thermal motion of H and D will generally differ at the same δ and temperature. The evidence that ΔT_c (at the same δ) is larger in KDP-DKDP than it is at higher temperature in LHP-LDP (compare Figures 1(b) and 2(b)) may be significant in this context.

If T_c does, by whatever mechanism, depend most directly on δ, the

changes in T_c on deuteration at constant 2R are readily understood. At constant 2R, the double-minimum H(D) potential remains unaltered as H is replaced by D, but the D energy levels are lower in the potential minima[12]. Due to the asymmetry of the minima, δ is then larger for D than for H at the same 2R (i.e. the O–D distance is shorter than O–H), giving rise to the difference in T_c. However, the fact that the change in T_c at constant 2R is so much greater for LHP-LDP than for KDP-DKDP remains to be explained.

There is clearly much that now needs to be better understood. At the very least, the results presented here strongly suggest that any direct tunnelling effect on T_c is very small, or even zero – though, of course, tunnelling may be implicated in the geometrical changes[16]. The theory of KDP-type transitions now needs to be revised to take explicit account of geometrical effects.

Acknowledgements – we gratefully acknowledge the part played by Dr. W.F. Kuhs of the Institute of Crystallography, University of Karlsruhe, in the $PbDPO_4$ studies, both in the data collection and in preparing (with Dr. H. Ahsbahs) the high-pressure cell for the experiment at 14 kbar. We are grateful to Dr. H. Arend and Dr. D.J. Lockwood for kindly providing the $PbHPO_4$ and the $PbDPO_4$ crystals, respectively. This work is supported by a grant from the Science and Engineering Research Council.

REFERENCES

1. R. Blinc, J. Phys. Chem. Solids, 13, 204-11 (1960).
2. R. Blinc and B. Zeks, in Soft Modes in Ferroelectrics and Antiferroelectrics (North-Holland, Amsterdam, 1974).
3. J.E. Tibballs, R.J. Nelmes and G.J. McIntyre, J. Phys. C, 15, 37-58 (1982).
4. J.E. Tibballs and R.J. Nelmes, J. Phys. C, 15, L849-53 (1982).
5. G.A. Samara, Phys. Rev. Lett., 27, 103-6 (1971).
6. M. Ichikawa, Chem. Phys. Lett., 79, 583-7 (1981).
7. M. Ichikawa, Phys. Rev. B, 36, 874-6 (1987).
8. R.J. Nelmes, J. Phys. C, 21, L881-6 (1988).
9. Z. Tun, R.J. Nelmes and W.F. Kuhs, in preparation.
10. D. Bloch, J. Paureau, J. Voiron and G. Parisot, Rev. Sci. Instrum., 47, 266-8 (1976).
11. H. Ahsbahs, Rev. Phys. Appl., 19, 819 (1984).
12. M.C. Lawrence and G.N. Robertson, J. Phys. C, 13, L1053-9 (1980); also Ferroelectrics, 34, 179-86 (1981).
13. Z. Tun, R.J. Nelmes, W.F. Kuhs and R.F.D. Stansfield, J. Phys. C, 21, 245-58 (1988).
14. See M. Tokunaga and T. Matsubara, Ferroelectrics, 72, 175-91 (1987).
15. M.I. McMahon, R.O. Piltz and R.J. Nelmes, Ferroelectrics, Proc. Int. Meeting on Ferroelectricity, Saarbrücken 1989.
16. T. Matsubara and E. Matsushita, Prog. Theor. Phys., 71, 209 (1984).

EUROPHYSICS LETTERS 15 September 1990

Europhys. Lett., **13** (2), pp. 143-148 (1990)

Possible Disorder of the P Atom in KD_2PO_4 (§).

M. I. McMAHON (*), R. J. NELMES (*), R. O. PILTZ (*) and W. F. KUHS (**)

(*) *Department of Physics, University of Edinburgh*
Mayfield Road, Edinburgh EH9 3JZ
(**) *Institut für Kristallographie, Universität Karlsruhe*
Kaiserstrasse 12, 7500 Karlsruhe, FRG

(received 1 June 1990; accepted 23 July 1990)

PACS. 61.50K – Crystallographic aspects of polymorphic and order-disorder transformations.
PACS. 61.60 – Specific structures of inorganic compounds.
PACS. 77.80B – Transitions and Curie point.

Abstract. – Very high-resolution neutron diffraction data have been collected from KD_2PO_4 (DKPD) at $T_c + 5$ K. Analysis of these data shows that the P-atom distribution is highly anharmonic, so much so that it can be modelled as disorder over three sites—a central site at the mean position, and two others displaced symmetrically along $\pm z$, where z is the direction that becomes the polar axis of the low-temperature ferroelectric (FE) phase below T_c. The displaced sites correspond to the two FE configurations of the PO_4 groups. It is concluded that the population of these sites is $\geqslant 40\%$ in each, leaving only $\leqslant 20\%$ at the central site. This indicates a much greater preponderance of the FE configurations just above T_c than predicted by the standard model of phase transitions of this type.

KH_2PO_4 (KDP) has a well-known H-ordering phase-transition on cooling through $T_c = 122$ K from a paraelectric to ferroelectric phase. Above T_c the H-atoms in the O—H—O bonds linking the PO_4 groups are 50 : 50 disordered over two sites, while below T_c the H-atoms are fully ordered onto one of these sites. The ordering of the H-atoms below T_c is accompanied by relative displacements of the heavy atoms (K, P and O) along the ferroelectric z-axis. Deuteration to KD_2PO_4 (DKDP) increases T_c to 229 K.

The long accepted theory of the phase transition in KDP is in terms of the ordering H-atoms «driving» a displacive transition in the heavy-atom structure, and this has been the basis for explanations of the dramatic change in T_c with deuteration. However, recent Raman studies have indicated that the site symmetry of the PO_4 group remains the same on going through T_c [1-3] suggesting that the entire H_2PO_4 group, and not just the H-atoms, may be disordered over the two ferroelectric configurations above T_c, ordering onto one of them below T_c. But NQR and other well-established measurements support the standard model [4], in which all six possible configurations of the H_2PO_4 group are present above T_c—the two ferroelectric (FE) configurations, with the protons attached to either the two

(§) The neutron-diffraction data were collected at the Institute Laue-Langevin, Grenoble.

«upper» or the two «lower» oxygens (along z), *and* the four different antiferroelectric (AFE) configurations, with the protons attached to one «upper» and one «lower» oxygen of the PO_4 group. It is possible that the Raman measurements are detecting short-range, dynamic correlations dominated by the FE configurations.

The two-configuration interpretation of the Raman work implies that each of the heavy atoms is disordered over two sites, displaced from each other along z, above T_c. The site separations can be estimated from neutron and X-ray scattering studies of the ferroelectric fluctuations [5-7] which yield the amplitudes of atomic motion between the FE configurations. The P atom has the largest amplitude, and it is greater (at 0.08 Å) in DKDP than in KDP. A P-sites separation, ΔP, of ~ 0.16 Å (twice the amplitude) is large enough to resolve by diffraction techniques, unlike any possible two-site distribution for the K and O atoms where the separation would be < 0.02 Å [5-7]. In the case of the Slater model, there are also the four AFE configurations which do not involve displacement of the P atom along z. The AFE configurations, being less energetically favourable, have half the population of the FE configurations just above T_c [8], so that on a simple multi-site description the P atom distribution along z will be 1:2:1—that is to say, 25% in each of the FE configurations, again ~ 0.16 Å apart, and 50% at the undisplaced mid-point (summing over the four AFE configurations). In the same notation, the two-configuration model predicts a 1:0:1 distribution.

To attempt to discriminate between these two substantially different P-atom distributions—and indeed to establish whether there is any detectable departure at all from a harmonic distribution—we have made a very high-resolution neutron diffraction study of DKDP just above T_c, using a well-characterized, 95%-deuterated sample. All data were collected on the D9 diffractometer at the Institut Laue-Langevin, Grenoble.

The sample was a single crystal of volume 20 mm^3. T_c was determined from the splitting of the 060 reflection and data were collected at $T_c + 5$ K, using a calibrated wavelength of 0.4602(1) Å. The unit cell parameters were determined to be $a = b = 7.457(2)$ Å and $c = 6.955(2)$ Å.

4222 reflections were measured to a $\sin\theta/\lambda$ limit of 1.89 Å^{-1}, well above the range of our previous studies of KDP and DKDP [9]. At low θ, all possible reflections were measured to allow the refinement of an anisotropic extinction correction. At higher θ, preference was given to reflections having high l indices to maximise spatial resolution along z. Trial refinements were made during the data collection using one-site and two-site models for the P-atom distribution; this allowed reflections sensitive to the fine details of the distribution to be identified and measured more carefully. A small 2D position-sensitive detector was used to improve the precision with which the weak peaks could be measured.

After correcting for sample absorption and extinction, the data were averaged to yield 1328 independent reflections. The internal and statistical R-factors on averaging were 3.3% and 4.7%, respectively. All corrections averaging and least-squares refinements were carried out with the Prometheus suite of crystallographic programs [10]. No correction was made for TDS, except as estimated in table II (below).

Initial refinement of the data revealed a strongly anharmonic distribution of the P atom along the z-axis, as shown in fig. 1. No similar anharmonicity was found for the O and K atoms. Also, as previously noted [7], the harmonic component of the thermal motion of the P atom along z, U^{33}(P), is much higher than would be expected by scaling the value of U^{33}(P) in the fully-ordered structure in proportion to the absolute temperature. Such a behaviour can be indicative of multi-site disorder and a two-site model was therefore tested for the P atom, with the two half-occupied sites each displaced ~ 0.08 Å from the (0, 0, 0) position along the $\pm z$-directions. This model refined well. The high quality and high resolution of the data allowed the z-coordinate of the sites, z(P), and the z-axis thermal motion about the displaced

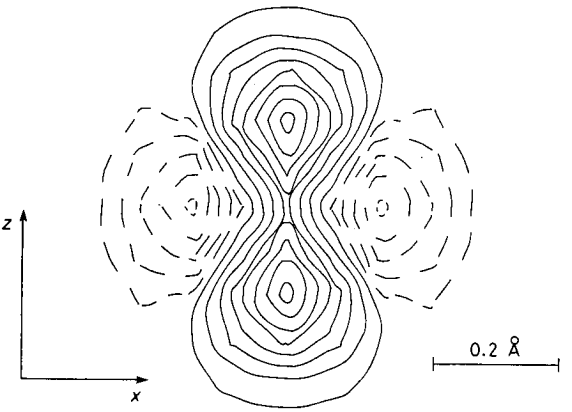

Fig. 1.

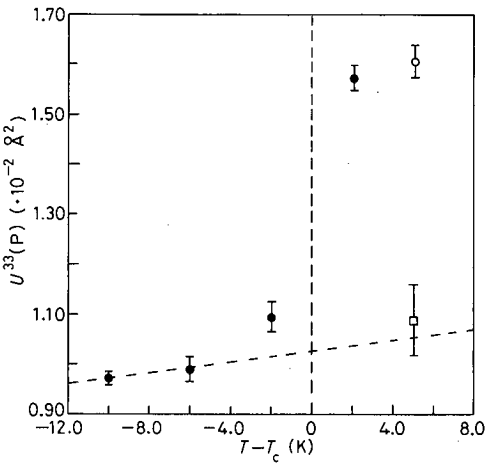

Fig. 2.

Fig. 1. – The anharmonic deformation of the P atom in a (010) section: the x and z axes are indicated. The map shows the deviations from a purely harmonic probability distribution and is calculated from the refined fourth-order anharmonic terms. The full and dashed lines represent, respectively, positive and negative density.

Fig. 2. – The variation of the U^{33}(P) thermal parameter *vs.* temperature near T_c. The filled circles are from previous structural studies in which the data were corrected for TDS and refined with a single-site model. The open symbols show the values obtained in the present study for, respectively, U^{33}(P) in the single-site model (○) and U_m^{33}(P) in the two-site, or **1**:0:1, model (□). The line is an extrapolation from the U^{33}(P) values well below T_c in proportion to T(K).

TABLE I. – *Refined structural parameters for the* P *atom at* $T_c + 5$ K *for the single-site anharmonic model and the two-site harmonic model in terms of fractional coordinates, harmonic parameters* U^{ij} *(in* 10^{-2} Å^2*) and fourth-order anharmonic terms* D^{ijkl} *(in* 10^{-4} Å^4*). The thermal parameters are uncorrected for* TDS. The unit cell parameters (*a*, *b*, *c*), *derived* P-*atom site separation* (ΔP), *weighted R-factors* (ωR) *and number of refined parameters are also given. The estimated standard deviations are given, in brackets, on the last quoted place. Values without* e.s.d.'s *are fixed by symmetry.*

		Anharmonic	Two-site
P	x	0	0
	y	0	0
	z	0	0.0103(5)
	U^{11}	0.986(14)	0.98(4)
	U^{22}	$= U^{11}$	0.94(4)
	U^{33}/U_m^{33}	1.46(3)	0.98(6)
	U^{12}	0	0.10(5)
	D^{1122}	0.00011(3)	0
	D^{3333}	− 0.00040(8)	0
	$a = b$ (Å)	7.457(2)	7.457(2)
	c(Å)	6.955(2)	6.955(2)
	ΔP (Å)	0	0.143(7)
	ωR (%)	3.601	3.589
	no. of parameters	33	34

sites, $U_m^{33}(P)$, both to be varied: despite the high correlation between $z(P)$ and $U_m^{33}(P)$, th refinement was very stable. (The subscript m distinguishes the z-axis thermal motion in th multi-site model from that in the single-site model.) The refined P-atom parameter obtained for the (single-site) anharmonic model and the two-site model are given in table I along with the weighted R factors and number of parameters varied overall. The refined sit separation ΔP of the P atom in the two-site model is 0.143(7) Å, in good agreement with th value of 0.160(12) Å obtained from the X-ray and neutron scattering studies of the soft-mod just above T_c [5-7]. Also, as shown in fig. 2, the refined $U_m^{33}(P)$ value for each half-site is th same, within error, as that predicted by extrapolating the thermal parameters obtaine below T_c in proportion to $T(K)$. Use of Hamilton's R-factor test [11] shows the two-sit model to give a better fit to the data than the single-site, anharmonic model at the 99 confidence level.

In order to test other possible disorder models for the P atom, we have also refined th data using multi-site models having distributions of 1:2:1, 1:1:1 and 2:1:2. (Th distribution $a:b:a$ means $(a/2a+b)\%$ of the P atom is displaced from the (0, 0, 0) positio along the $+z$-axis, the same along $-z$, and $(b/2a+b)\%$ remains at the (0, 0, 0) position.) Th 1:2:1 distribution is that predicted just above T_c for the Slater model of the KDP transitio as already discussed. The 1:1:1 and 2:1:2 distributions have no specific theoretical bas and were chosen to provide intermediate distributions between the 1:0:1 and 1:2: models. To extend any trends beyond the 1:0:1 distribution, in the direction of increasin population of the FE configurations, it was also useful to refine a $2:-1:2$ model despite it unphysical character. For each distribution, the anisotropic thermal motion of the P ato was constrained to be the same about all three sites.

The refined separation ΔP of the outer (FE) sites, the refined $U_m^{33}(P)$ thermal paramete and the weighted R-factor are given in table II for each of the different models. All yie identical fits to the data, but the results as plotted in fig. 3*a*) and *b*) show that only the simp 1:0:1 two-site distribution or the 2:1:2 three-site distribution refine to a site-separatio and a $U_m^{33}(P)$ thermal parameter which are both in accord with physically plausible estimat of their values (as indicated by arrows in the figures). The discrimination against the 1:1: distribution is perhaps marginal. But it seems clear that the 1:2:1 distribution predicte from the Slater model, although yielding the same goodness of fit to the data as the oth models, can be excluded: it corresponds to a P-atom separation between the two F

TABLE II. – *The refined* P-*atom site separation,* ΔP, *and* $U_m^{33}(P)$ *thermal parameters at* $T_c + 5$ K *f various multisite* P-*atom distributions. To allow comparison of the present thermal parameters wi those of previous studies of* DKDP, *for all of which the data were* TDS *corrected, a scaling of* 1.11 *h been applied to give the* TDS «*corrected*» *values shown in column* 4. *The scaling factor was chos such that the termal parameters of the other heavy atoms* (K *and* O) *in the present study were scaled to the values obtained in a previous,* TDS *corrected, study at* $T_c + 5$ K [9]. *The weighted R-factors f each model are given in column* 5.

Relative distribution	Occupation of off-centre site (%)	ΔP (Å)	$U_m^{33}(P)$ (10^{-2} Å^2)	ωR (%
1:2:1	25	0.257(13)	0.73(12)	3.589
1:1:1	33	0.191(9)	0.98(8)	3.589
2:1:2	40	0.166(8)	1.05(7)	3.589
1:0:1	50	0.143(7)	1.09(7) [a]	3.589
2:−1:2	66	0.128(6)	1.11(7)	3.589

(*a*) As plotted (open square) in fig. 2. Compare the uncorrected value of 0.98(6) in table I.

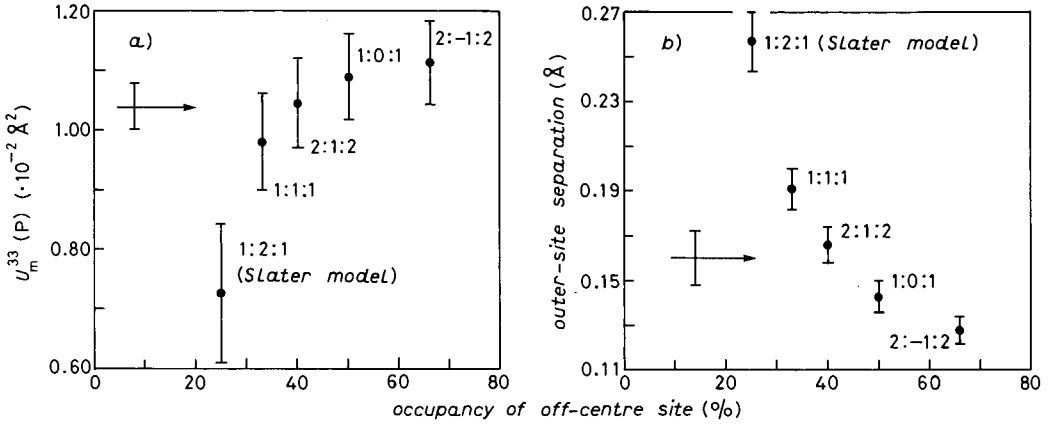

Fig. 3. – *a*) The refined U_m^{33}(P) thermal parameter, and *b*) the refined outer-site separation, ΔP, as a function of the occupancy of the outer sites at $T_c + 5$ K, as tabulated in table II. The arrows show *a*) the estimated value of U_m^{33}(P) at $T_c + 5$ K, obtained from extrapolation of the previous studies below T_c (fig. 2) and *b*) the site separation obtained from the X-ray and neutron scattering studies of the ferroelectric fluctuation just above T_c. Error bars show the e.s.d.'s on all values, including those represented by the arrows.

configurations about 50% larger than the saturated displacements of the ferroelectric phase, and to thermal motion about each site that is 30% smaller than found below T_c, both of which are physically unreasonable discrepancies.

In summary, although it is not possible to distinguish completely between multi-site disorder and thermal anharmonicity in this study(1), we can conclude i) that the P-atom distribution is highly anharmonic, with a form corresponding to increased density displaced along $\pm z$ from the mean P-atom position, and ii) that the distribution implied by the standard Slater model is not consistent with our results. Interpreted in terms of disorder over the FE and AFE configurations of the H_2PO_4 group, our results indicate a much greater preponderance of the FE configurations than predicted by the Slater model at $T_c + 5$ K, possibly corresponding even to the simple two-configuration interpretation of the Raman studies. In fact, a complete absence of the AFE configurations is improbable, and it is doubtful if the Raman measurements are sufficiently sensitive to exclude at least a 2:1:2 distribution. This could also be consistent with the NQR studies, taking account of the fact that the NQR timescale probes only the average over the H_2PO_4 configurations.

---

(1) Itoh [12] has claimed to demonstrate two-site disorder of the P atom from Mo$K\alpha$ X-ray diffraction data using a «split-atom method». Full details have not been published, but the only plausible interpretation is that the P atom distribution was fitted with two off-centre «half atoms» constrained to be isotropic. If the actual distribution is anisotropic, this procedure is bound to yield a nonzero site separation, even if the distribution is completely harmonic—that being the only way such a model can represent the anisotropy. There is no basis for attributing all anisotropy to multi-site disorder, as this method does. What is precisely at issue is the *distinction* between anisotropy and multi-site disorder. Making this distinction requires data of sufficiently high resolution, which involves reaching $\sin\theta/\lambda > 1.5$ Å^{-1} in the present case—well beyond what is attainable by X-ray diffraction using Mo $K\alpha$. As we have shown, even with neutron diffraction techniques (which give better data than X-ray diffraction at high $\sin\theta/\lambda$ due to the absence of a form factor) extended to $\sin\theta/\lambda = 1.9$ Å^{-1}, it is not possible to distinguish decisively between a number of descriptions of the P-atom distribution, only one of which is a simple two-site disorder.

On balance, the evidence appears to favour an interpretation of the transition based o or at least involving, order-disorder behaviour of the PO_4 groups, as has previously bee proposed for KDP [13] and developed in detail for the KDP-type transition in CsH_2PO_4 [14

* * *

We should like to thank Prof. R. BLINC and Prof. V. H. SCHMIDT for helpful discussion This work has been supported by the UK Science and Engineering Research Coun through research grants and access to the neutron-beam facilities at the Institut Lau Langevin, Grenoble.

REFERENCES

[1] TOMINAGA Y., KASAHARA M., URABE H. and TATSUZAKI I., *Solid State Commun.*, 47 (198 835.
[2] TOMINAGA Y., URABE H. and TOKUNAGA M., *Solid State Commun.*, 48 (1983) 265.
[3] TOKUNAGA M. and MATSUBARA T., *Ferroelectrics*, 72 (1987) 175.
[4] BLINC R. and ZEKS B., *Ferroelectrics*, 72 (1987) 193.
[5] BLEIF H.-J., COWLEY R. A. and NELMES R. J., *J. Phys. C*, 15 (1982) L-201.
[6] COWLEY R. A., BLEIF H.-J., ANDREWS S. R. and NELMES R. J., *Physica B*, 120 (1983) 26
[7] NELMES R. J., KUHS W. F., HOWARD C. J., TIBBALLS J. E. and RYAN T. W., *J. Phys. C*, (1985) L-1023.
[8] SCHMIDT V. H., WANG J. T. and SCHNACKENBERG P., *Jpn. J. Appl. Phys.*, 24, Suppl. 24 (1983) 944.
[9] NELMES R. J., *Ferroelectrics*, 71 (1987) 87.
[10] ZUCKER U. H., PERENTHALER R., KUHS W. F., BACHMANN R. and SCHULZ H., *J. Ap Cryst.*, 16 (1983) 358.
[11] HAMILTON W. C., *Acta Cryst.*, 18 (1965) 502.
[12] ITOH K., IMAOKA H. and NAKAMURA E., *Proc. Meeet. Phys. Soc. Jpn.*, 2 (1985) 117.
[13] TOKUNAGA M., *Prog. Theor. Phys. Suppl.*, 80 (1984) 156.
[14] KOJYO N. and ONODERA Y., *J. Phys. Soc. Jpn.*, 57 (1988) 4391.

High Pressure Research, 1990, Vol. 4, pp. 444–446
Reprints available directly from the publisher
Photocopying permitted by license only

HIGH-PRESSURE NEUTRON DIFFRACTION STUDIES OF KH_2PO_4-TYPE PHASE TRANSITIONS

M.I. McMAHON, R.J. NELMES and R.O. PILTZ

Department of Physics, University of Edinburgh,
Edinburgh EH9 3JZ, U.K.

High-pressure neutron-diffraction studies have been carried out on KH_2PO_4, KD_2PO_4, $H_2C_4O_4$ and $PbHPO_4$, using single-crystal samples. The results show that changes in the H-ordering temperature, T_c, with pressure (or deuteration) in these systems can be largely attributed to the variation of the H-site separation, δ, with pressure (or deuteration).

KEY WORDS: Hydrogen-ordering transitions, crystal structure determination, neutron diffraction

In KH_2PO_4 (KDP) at room temperature, the H atoms are disordered over two sites in the short hydrogen bonds that link the PO_4 groups. On cooling through the H-ordering ferroelectric transition at T_c = 122 K, the H atoms all order onto one of the two sites, forming asymmetric O–H····O bonds. Replacement of H by D dramatically increases T_c, which rises to 229 K in KD_2PO_4 (DKDP). In the accepted theory of the KDP-type of transition, this effect is attributed solely to the mass dependence of quantum tunnelling (Blinc 1960). There are many other H-ordering systems exhibiting similar behaviour. Here we consider two examples for comparison with (D)KDP, namely $H_2C_4O_4$ (squaric acid, or H_2SQ) and $PbHPO_4$ (LHP). H_2SQ has an H-ordering transition at T_c = 374 K and its deuterated form, D_2SQ, has T_c = 516 K. LHP has T_c = 310 K and this rises to 452 K in the deuterated form, LDP.

The H (or D) ordering temperature is also altered by pressure. In KDP, T_c falls by ~5 K kbar^{-1}, and more rapidly with increasing pressure until $T_c \to 0$ K at 17 kbar (Samara 1971). In H_2SQ and LHP, the rate of decrease of T_c is larger, at ~11 K kbar^{-1} (Samara and Semmingsen 1979, Mylov *et al* 1979). In the corresponding deuterated forms dT_c/dP is similar, but a little smaller in magnitude.

From a series of neutron diffraction experiments on KDP and DKDP at pressures up to ~20 kbar, we have shown (i) that deuteration increases not only T_c but also the overall O····O bondlength, 2R, and the H(D) site separation, δ, and (ii) that the effect of pressure on DKDP is to reduce 2R and δ, as well as T_c. At the pressure for which δ(DKDP) is reduced to its value in KDP at atmospheric pressure, T_c(DKDP) is about 135 K (see Figure 1). This strongly suggests that almost all the change in T_c on deuteration is attributable to the accompanying increase

in δ (Nelmes 1988) and, hence, that it is not necessary to invoke quantum tunnelling to account for the deuteration effect.

If changes in T_c with deuteration are attributable to geometrical factors, it is possible that differences in T_c between different H-ordering systems are also geometrical in origin.

On this basis we have undertaken a systematic study of KDP, H_2SQ, LHP and their deuterated forms to investigate the relationship between T_c and the H-bond geometry as both are varied under pressure in different systems. The crystal structure determinations have been carried out by neutron diffraction, using single-crystal samples held in a clamp-type pressure cell (Bloch *et al* 1976) with 'Fluorinert' as the pressure-transmitting medium. The data were collected on the D15 diffractometer at the Institut Laue-Langevin, Grenoble. All the measurements were made just above T_c, in the range T_c + 2 K to T_c + 5 K.

The results, including those obtained at atmospheric pressure (labelled AP), are shown in Figure 1 in terms of δ plotted against T_c at various pressures. The sample pressure is

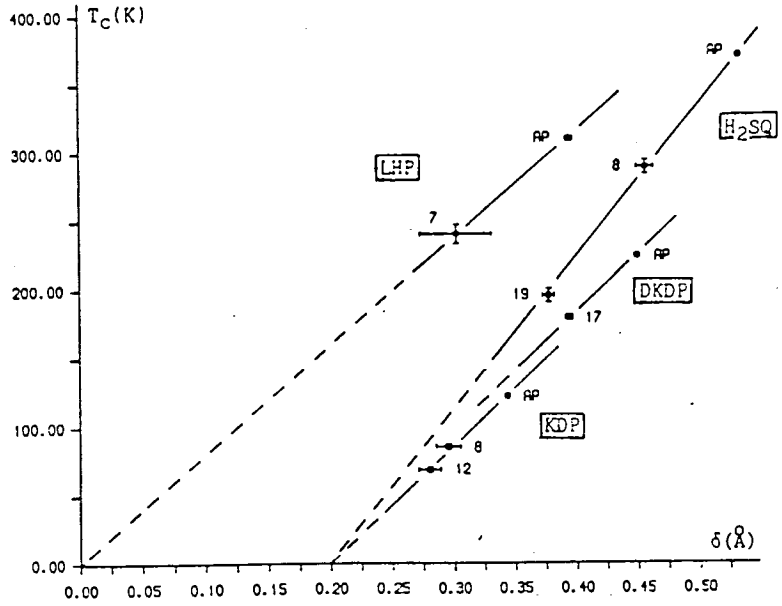

Figure 1. The variation of T_c and δ with pressure.

shown against each point in kbar. The results for KDP and DKDP are from Nelmes (1988) and references therein; those for H_2SQ are from Tun et al (1989) and Restori et al (1989); and that for LHP at atmospheric pressure is from Tun et al (1989). The results for LHP at 7 kbar are from a recent attempt to obtain more reliable H coordinates than in the earlier work of Restori et al (1987) – and closer to T_c. A full account of this new study of LHP will be published separately.

Figure 1 illustrates the geometric isotope effect (Ichikawa 1978) relating KDP and DKDP (see above). Turning to KDP and H_2SQ, it can be seen that in this case, also, the large difference of 250 K in T_c at atmospheric pressure can be mostly attributed to the difference in δ. And, in both systems, extrapolation to T_c = 0 K corresponds to a value of ~0.2 Å for δ. It is clear that, despite the substantial differences in structure between KDP and H_2SQ, these two systems share a remarkably common relationship between T_c and δ, which strongly suggests that the local H potential (i.e. δ) is the principal determinant of the H-ordering temperature.

Figure 1 shows that LHP is different: in particular, δ extrapolates to zero at T_c = 0 K. This is of considerable interest in relation to other evidence that LHP remains slightly acentric above T_c (Lockwood et al 1985). This bias would be expected to favour a relatively high H-ordering temperature for any given value of δ – as observed.

Further work is now in hand to check these conclusions, and to obtain results for D_2SQ and LDP.

Acknowledgements

This work is supported by a research grant from the Science and Engineering Research Council.

References

R. Blinc (1960) J. Phys. Chem. Solids 13, 204.
D. Bloch, J. Paureau, J. Voiron and G. Parisot (1976) Rev. Sci. Instr. 47, 266.
M. Ichikawa (1978) Acta Cryst. B34, 2074.
D.J. Lockwood, N. Ohno, R.J. Nelmes and H. Arend (1985) J. Phys. C18, L559.
V.P. Mylov, A.M. Shirokov, L.A. Shuvalov, V.N. Kharitonov and B. Brzhezina (1979) Sov. Phys. Cryst. 24, 738.
R.J. Nelmes (1988) J. Phys. C21, L881.
R. Restori, Z. Tun, R.J. Nelmes and G.J. McIntyre (1987) J. Phys. C20, L591.
R. Restori, Z. Tun, R. Ramirez, R.J. Nelmes and G.J. McIntyre (1989). Submitted to J. Phys. C.
G.A. Samara (1971) Phys. Rev. Lett. 27, 103.
G.A. Samara and D. Semmingsen (1979) J. Chem. Phys. 71, 1401.
Z. Tun, R.J. Nelmes and W.F. Kuhs (1989). In preparation.

High Pressure Research, 1990, Vol. 4, pp. 402–404
Reprints available directly from the publisher
Photocopying permitted by license only

HIGH RESOLUTION X-RAY DIFFRACTION STUDIES AT HIGH PRESSURES

J.S. LOVEDAY, R.J. NELMES AND M.I. McMAHON

Department of Physics, University of Edinburgh
Mayfield Road, Edinburgh EH9 3JZ, U.K.

The principal sources of systematic error in high-pressure x-ray structure determination with a diamond anvil cell have been studied in detail. The results of these studies have been used to develop techniques to minimise or correct for these effects.

KEY WORDS: X-ray, single crystal, structure determination, diamond anvil cell

The accuracy of single-crystal high-pressure x-ray structural studies using diamond anvil cells (DACs) has always been significantly poorer than that obtainable under ambient conditions: for example, it has proved difficult to obtain accurate thermal parameters and to perform high-resolution studies using short wavelength radiation. Such accuracy is essential for studies of structural phase transitions and small structural changes affecting physical properties. So we have made a detailed study of the effect of a Merrill-Bassett DAC on measured sample reflection intensities. The principal contributions are:

a) The overlapping of sample reflections and reflections from the diamonds. This can be a considerable effect as the diamonds reflect up to 30% of the direct beam. However, as diamond has relatively few reflections, overlaps are rare and easily calculable and so do not present a serious problem in practice.

b) The structured background arising from the powder patterns of the gaskets and the beryllium backing discs. Standard data collection procedures allow for this by using ω scans, at the expense of poorer signal-to-background ratios implying increased count times and/or reduced precision. The level of the background depends on both the orientation of the cell and the degree of penetration of the beam through the gasket, and is hence dependent on the x-ray wavelength and the gasket material. This suggests a reason for the poorer results usually obtained with AgKα radiation as the signal-to-background value is typically 10 times lower than for MoKα.

c) The effect of simultaneous diffraction by the diamonds and the sample. As has been stated, the diamonds scatter radiation strongly and so, by diffracting either the beam incident on the

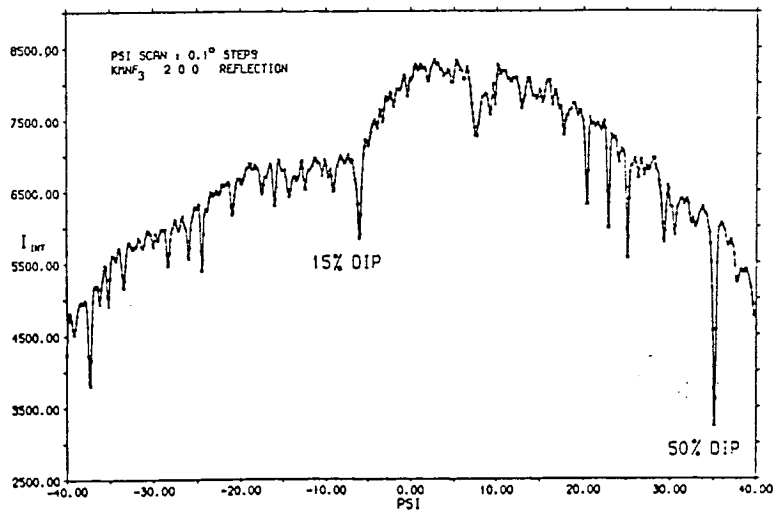

Figure 1. A typical psi scan of a sample reflection showing the numerous dips in intensity due to simultaneous diffraction.

sample or that diffracted from it, they can substantially reduce the measured sample intensity. Examples of this are shown in Figure 1. Such events are much more common than overlapping reflections (as under (a) above) and hence present a more serious problem.

d) Absorption by the cell. The standard method of determining this is to measure the variation in intensity of the direct beam as the ungasketted cell is rotated in the beam. This technique has one major drawback in that the direct beam is usually much larger than the typical size of a sample crystal. The procedure does not then correct properly for some features of the cell absorption – for example, the effect of the hole in the beryllium backing disc, as Figure 2 shows.

As a result of these studies a number of changes have been incorporated into our data collection strategies:

a) To detect the effects of (i) dips due to simultaneous diffraction (as in Figure 1) and (ii) overlapping diamond reflections, data are collected at several values of psi close to the standard measuring position (ψ = 0°).

b) It is clearly desirable to use θ-2θ type scans if possible, as these result in a better signal-to-background ratio. But it is then necessary to account for the contribution of the powder background. This can be measured by offsetting the cell about its axis at each measuring position and repeating the scan.

c) The inadequacies of the standard absorption correction can be addressed by use of a better collimated beam. The best way of achieving this appears to be to use psi scans of the reflections from a sample-sized crystal placed on a half cell. If these scans are corrected for sample absorption their shape can be used to derive the true absorption curve for the cell.

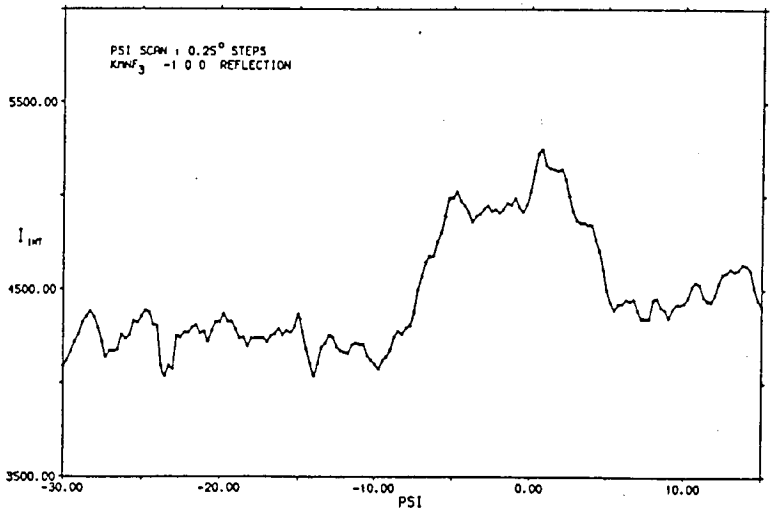

Figure 2. A psi scan corrected for both sample and cell absorption. The feature in the middle results from the diffracted beam passing up the hole in the beryllium backing disc.

High Pressure Research, 1990, Vol. 4, pp. 450–452
Reprints available directly from the publisher
Photocopying permitted by license only

THE APPLICATION OF NEUTRON POWDER DIFFRACTION TECHNIQUES FOR CRYSTALLOGRAPHIC STUDIES AT HIGH PRESSURES

P.D. HATTON, C.J. HOWARD, M. McMAHON, R.J. NELMES and N. WILDING

Department of Physics, University of Edinburgh,
Mayfield Road, Edinburgh EH9 3JZ, U.K.

For phase transition studies, neutron powder diffraction offers a number of important advantages over x-ray based techniques, for example ab-initio structural determination. There are two distinct methods using either monochromatic angular dispersive geometry on a reactor cold source or time-of-flight energy-dispersive techniques requiring a pulsed neutron source. Both techniques offer comparable resolution but have differing advantages for high pressure studies. Recent studies illustrate the benefits of the two methods and the application of these to solve unknown crystal structures.

KEY WORDS: Neutrons, structure determination, powder diffraction.

For phase transition studies the use of single-crystal diffraction is limited since many structural transitions, particularly those involving a volume collapse, cause single crystals to shatter. Such considerations suggest recourse to powder-based techniques, albeit with an unavoidable loss of detail. For x-ray diffraction, rapid developments in the use of synchrotron radiation have made energy-dispersive x-ray diffraction (EDXRD) the primary quantitative technique for high pressure studies. The relatively poor resolution and unreliable intensity information have however restricted the use of EDXRD to the determination of unit cell dimensions of high symmetry materials.

To obtain structural information concerning the atomic positional parameters we have to use neutron diffraction. For neutron diffraction, the small scattering cross section requires a sample volume of several mm^3 (up to a few cm^3!) resulting in both relatively massive pressure cells and severe restrictions on the maximum pressure (~25 kbar). Nevertheless, the larger sample size required for neutron diffraction does permit accurate intensity measurements and the use of Rietveld refinement techniques to derive atomic positional parameters.

There are two distinct methods of obtaining a neutron powder pattern. The first is a conventional angle (2θ) scan employing a monochromatic neutron beam (e.g. the D1A or D2B instruments at ILL). The disadvantage of this method for high pressure studies is the obscuration of parts of the pattern by diffraction from the cell housing. However, with a good structural model and enough information in the diffraction pattern away from the cell

peaks, it is possible to obtain accurate positional parameters and hence to study the structural changes under pressure. In collaboration with B. Raveau, V. Caignaert (Caen), A. Hewat and C. Vettier (ILL) we have studied both La_2CuO_4 [1] and the substituted superconductor $La_{1.85}Sr_{0.15}CuO_4$. The superconductor $YBa_2Cu_4O_8$ has a high pressure dependence of T_c (0.55 K/kbar) and in a recent study a clear relationship between structure and T_c was observed [2]. With increasing pressure, T_c increases, and the distance from Cu in the plane to the apex oxygen bridging to the chain was reduced by as much as 0.05 Å at 10 kbar. It was therefore of interest to see if such effects are observed in La_2CuO_4 and $La_{1.85}Sr_{0.15}CuO_4$ where T_c = 37 K and dT_c/dp = 0.32 K/kbar (for $La_{1.8}Sr_{0.2}CuO_4$). The results are shown in Table 1. Clearly the Cu-O(2) bond increases in length with increasing pressure. All other bond lengths behave normally, as do the lattice parameters. The results therefore do not support the particular relationship between T_c and structural changes under pressure proposed by Kaldis *et al* [2].

Table 1

La_2CuO_4(Abma)	1 bar	5 kbar	9 kbar
a(Å)	5.3938(2)	5.3830(4)	5.3736(4)
b(Å)	5.3466(2)	5.3418(4)	5.3373(4)
c(Å)	13.1309(4)	13.120(1)	13.114(1)
La x	-0.0066(3)	-0.008(2)	-0.004(2)
z	0.3615(1)	0.3612(3)	0.3616(3)
01 z	-0.0071(2)	-0.006(1)	-0.008(1)
02 x	0.0338(4)	0.039(2)	0.029(3)
z	0.1830(1)	0.1850(6)	0.1842(6)
Cu-02(Å)	2.410(2)	2.436(8)	2.421(8)

$La_{1.85}Sr_{0.15}CuO_4$(Immm)	1 bar	6 kbar	10 kbar
a(Å)	3.7743(1)	3.7696(1)	3.7681(1)
c(Å)	13.2193(4)	13.2058(6)	13.2004(5)
La/Sr z	0.3604(2)	0.3599(3)	0.3595(3)
02 z	0.1823(3)	0.1846(6)	0.1831(5)
Cu-02(Å)	2.409(3)	2.437(8)	2.417(7)

The second technique for obtaining neutron powder patterns is to use a pulsed neutron spallation source. The diffraction pattern is obtained by measuring the time-of-flight (TOF) of each scattered neutron. The principal advantages of such an arrangement is the fixed geometry, leading to easier designs of high pressure cells, and the ability to obtain a diffraction

pattern free from any scattering from the cell housing. This is achieved by employing a 90° detector and collimating both the incident and scattered beams. In collaboration with J.D. Jorgensen (Argonne) we have studied the high pressure phase transition in dirhenium dodecacarbonyl ($Re_2(CO)_{10}$). Earlier Raman studies have suggested, via group theoretical analysis, that the transition involves a molecular rearrangement from staggered to eclipsed geometry at 5 kbar (Figure 1) [3]. The low symmetry and large unit cell of this material make it important to observe a complete diffraction profile. Diffraction profiles from both phases were obtained which clearly display the transition. To solve the structure of the new phase, stable only under high pressure, it is first necessary to determine an accurate unit cell so that the reflections can be assigned Miller indices. Unfortunately such an exercise requires the highest d-spacings and these are not observable using a 90° detector. Indeed in ambient $Re_2(CO)_{10}$ there are ~10 lines with d-spacings larger than 4Å.

Such considerations suggest that the optimal path to solving new structures under pressure involves both monochromatic and TOF techniques. Initial patterns obtained with long wavelength (~3 Å) radiation should be used to determine an accurate cell followed by TOF methods to obtain the most extensive set of Bragg intensities using the method developed by Pawley [4].

Figure 1 Proposed phase transition in $Re_2(CO)_{10}$

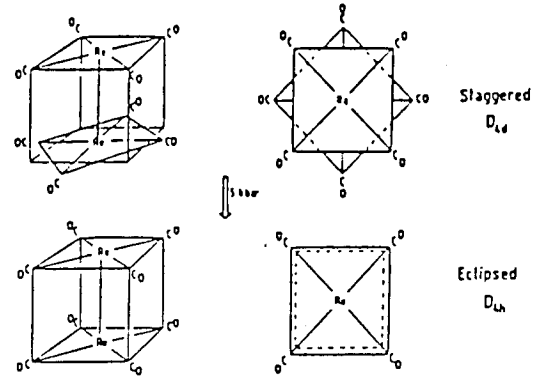

[1] Howard C.J., Nelmes R.J. and Vettier C. (1989) Solid State Communications 69, 261.
[2] Kaldis E., Fischer P., Hewat A.W., Hewat E.A., Karpinski J. and Rusiecki, S. (1989) Physica C to be published.
[3] Adams D.M., Hatton P.D., Shaw A.C. and Tan, T-K. (1981) J. Chem. Soc. Chem. Comm. 226.
[4] Pawley G.S. (1981) J. Appl. Cryst. 14 357.

J. Appl. Cryst. (1990). 23, 392–396

The Effect of Diffraction by the Diamonds of a Diamond-Anvil Cell on Single-Crystal Sample Intensities

BY J. S. LOVEDAY, M. I. MCMAHON AND R. J. NELMES

Physics Department, University of Edinburgh, Mayfield Road, Edinburgh EH9 3JZ, Scotland

(*Received* 10 *April* 1990; *accepted* 21 *May* 1990)

Abstract

The integrated intensities measured in X-ray single-crystal high-pressure structural studies using a diamond-anvil cell are shown to be reduced substantially when the diamonds diffract at the same setting as the sample – by as much as 50% in some cases. The pressure and wavelength dependence of this process have been studied and also the effect of changing the beam divergence by the use of a synchrotron beam. The consequences for the accuracy of structural information derived from data sets collected at high pressure are considered and a data-collection strategy for detecting and avoiding the effects of diamond diffraction is proposed.

Introduction

The accuracy of the structural information obtained from high-pressure X-ray diffraction studies using single-crystal samples in diamond-anvil cells (DAC's) is critically dependent on the extent to which accurate corrections can be made for the effects of the cell on the measured intensities of sample reflections. The most significant of these effects are the scattering by the gasket, diamonds and beryllium backing plates and the reduction of intensity due to cell absorption. Most of these effects have long been recognized (Ahsbahs, 1987; Finger & King, 1978; Denner, Schulz & d'Amour, 1978) and procedures exist to correct for or to avoid them.

A phenomenon that appears not to have been studied for single-crystal data collection, though, is the possible removal of a significant amount of intensity from either the beam incident on, or diffracted by, the sample due to simultaneous diffraction by either or both of the diamond anvils. The equivalent effect has been observed in energy-dispersive powder diffraction and also in studies of the pseudo-Kossel pattern produced when fluorescence from a powder sample inside a DAC passes through one of the diamonds (Okada & Iwasaki, 1980). In this paper, we show that 'simultaneous diffraction' processes can produce remarkably large effects in single-crystal diffraction.

Measurements and discussion

Initial evidence for significant simultaneous diffraction effects was encountered in some measurements of the variation of integrated intensity with rotation about the scattering vector of a sample in a DAC (ψ scans), as illustrated in Fig. 1. These measurements were made on a crystal of the cubic perovskite $KMnF_3$, mounted in a Merrill–Bassett DAC (Merrill & Bassett, 1974), using a CAD-4 four-circle diffractometer and Mo $K\alpha$ radiation (graphite monochromator). The integrated intensity of the 200 reflection was obtained from θ–2θ scans performed at successive steps of 0·1° in ψ. The numerous sharp dips of up to −50% in the measured intensity were tentatively attributed to the effect of diamond reflections, in view of the form and distribution of the dips – although their size was difficult to explain since preliminary studies on single diamond anvils had shown the maximum intensity scattered to be only about 1% of the primary beam. (The gradual overall variation in integrated intensity in Fig. 1, peaking near $\psi = 5°$, is due to the dependence of the cell absorption on the orientation of the cell as this changes with ψ.)

Fig. 2 shows that there are clearly two possible types of simultaneous diffraction process that could reduce the intensity of sample reflections: either part of the beam incident on the sample can be diffracted by the diamond between the sample and the X-ray source (the 'incident-beam event' shown in Fig. 2), or part of the beam diffracted by the sample can be further diffracted by the diamond between the sample and the detector (the 'diffracted-beam event' in Fig. 2). To examine the hypothesis that such events are the cause of the observed dips, a number of tests were made.

First, it was necessary to investigate whether the diamonds in the loaded pressure cell (as used to obtain the results in Fig. 1) reflected a larger amount of an incident beam than the isolated diamonds used in the preliminary studies. The CAD-4 detector was set to monitor the primary beam, with appropriate attenuation, and measurements were made as the diamond on the detector side of the gasket of the

0021-8898/90/050392-05$03.00

loaded DAC was stepped (on ω) through its 220 reflection. The result is shown in Fig. 3. The modest applied pressure of 0·25 GPa can be seen to have dramatically increased the effective scattering power of the diamond, causing a 10% reduction of the primary-beam intensity. This was confirmed by moving the detector to measure the intensity of the diamond reflection as shown by the dashed line and circular symbols in Fig. 3: clearly there is close correspondence in both position (in ω) and size between the diamond reflection and the dip in the primary beam. The same technique was used to measure the scattering power (the percentage of the primary beam scattered) of different classes of diamond reflection under the same conditions, and it was found that only the five strongest classes of reflection affect the primary beam significantly – the 111 class by 20–30%, the 220 class by 10–15% as in Fig. 3, the 311 class by about 7%, and the 400 and 440 classes by about 4%. Effects of this magnitude represent about a 30-fold increase over the scattering power of an unstressed diamond.

Having demonstrated that diffraction by the diamonds can scatter a significant fraction of the primary beam, it was necessary to show that this can account for all of the dips observed in the ψ scans. To this end the orientation matrices of the sample and the diamonds were used to predict both the value of ψ at which significant events would occur and also the propagation direction of the beams diffracted by the diamonds. The marks shown below the ψ scan in Fig. 4 are at the predicted values of ψ for incident- and diffracted-beam events involving the five strongest classes of reflection listed above, the relative strengths of which are represented by the lengths of the marks. There can be seen to be generally good agreement between the predicted events and the observed dips, in terms of both position and relative magnitude. All the obvious dips correspond to predicted events, and often to a near coincidence of two or more of them: for example, the dip labelled 1 in Fig. 4 can be seen to arise from the superposition of a 220 incident-beam event and a 220 diffracted-beam event; dip 4 is from two 311 incident-beam events, separated just enough to show up as a broadening of the dip. [The large (50%) dip in Fig. 1 can be attributed to 111 incident- and diffracted-beam events coinciding.] Discrepancies of up to 2–3° (in ψ) b]etween calculated and observed positions are often found, as for dip 3 in Fig. 4, and are attributable to small errors in the orientation matrices, to which the calculations are quite sensitive. Variations in the relative magnitudes of dips away from the predictions – as for dip 2 in Fig. 4, which is predicted to be stronger than dip 1 — are believed to arise from the anisotropic stresses on the diamonds. More detailed checks, on this and other ψ scans, confirm (i) that there are no dips that cannot be accounted for and (ii) that all predicted events give rise to dips.

As final confirmation, a search was made for direct evidence to connect simultaneous diffraction and the dips. In the case of incident-beam events, the best method was to monitor the primary-beam intensity as the sample ψ scan passed through a dip – employing the technique illustrated in Fig. 3 to detect diamond-anvil reflections. In all cases studied, the primary-beam intensity showed a reduction whose

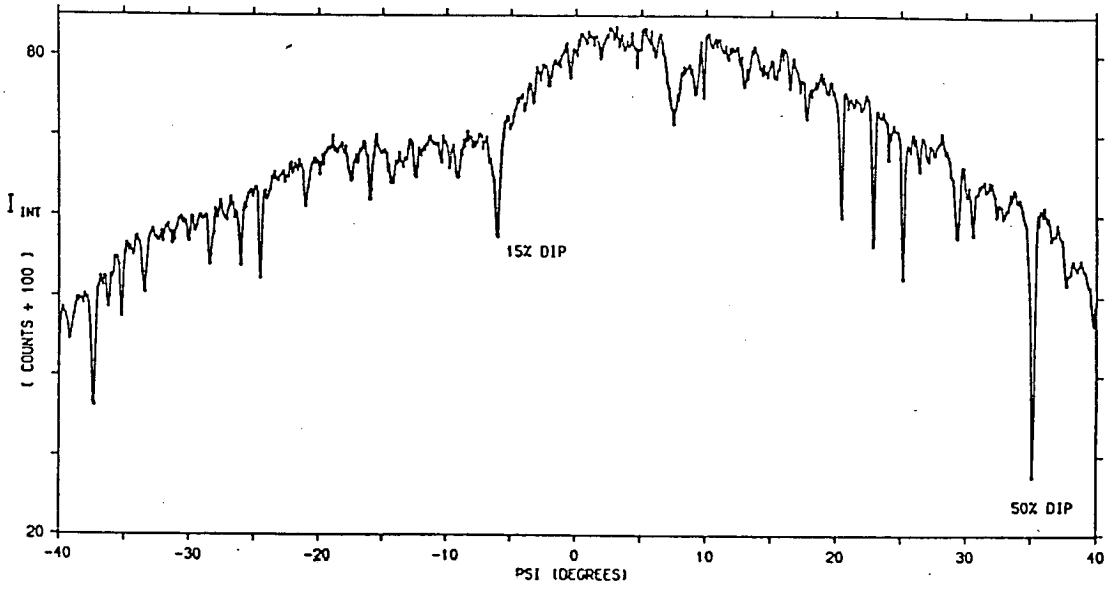

Fig. 1. Integrated intensity, I_{INT}, *versus* ψ for the 200 reflection of a $KMnF_3$ sample under pressure in a Merrill–Bassett diamond-anvil cell (DAC). I_{INT} is the total integrated counts at each point, divided by 100.

magnitude was consistent with the measured scattering power of the class of diamond reflection predicted to be involved. Furthermore, the magnitude of the dip in the measured sample reflection intensity was simply the percentage* reduction of the primary-beam intensity. The procedure used to seek direct evidence for diffracted-beam events was more complicated because these events do not affect the primary beam (see Fig. 2), and it is not possible in general to intercept the reflected beam from the diamond with the CAD-4 detector (which is confined to measurements in the horizontal plane). Hence it was necessary to calculate the path of the reflected beam for the predicted event and place a second detector to intercept it. To put the intensities of the diamond and sample reflections on a common scale, the second detector was also used to measure the sample intensity. Fig. 5 shows a diffracted-beam event due to a diamond 220 reflection, successfully recorded at the predicted position of the detector. Furthermore, taking into account the uncertainty of the diffractometer setting (0·1° in ψ) and the differences in absorption for the diamond and sample reflections, there is close agreement between the diamond reflection and the dip in the sample intensity in terms of both size* and ψ setting.

To summarize, in all cases studied, a dip in the sample intensity is accompanied by evidence of a simultaneous diffraction event or events consistent with the measured scattering power of the class or classes of diamond-anvil reflections predicted by calculations. And there appears to be no difference in

* The *absolute* transfer of intensity from the sample reflection to an incident-beam event cannot be checked directly because (unlike a diffracted-beam event) the diamond intercepts a much larger incident beam than does the sample.

* See the preceding footnote.

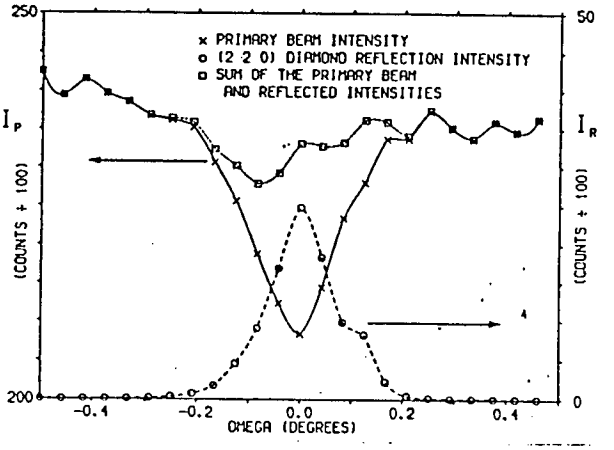

Fig. 3. An ω scan through a 220 diamond reflection from a DAC under pressure (○), setting $\omega = 0$ at the peak, and the intensity of the primary beam (×) measured for each step through the reflection. The sum of the primary-beam intensity (I_P) and the intensity in the reflection (I_R) is also shown (□). I_P and I_R are the recorded counts at each point, divided by 10.

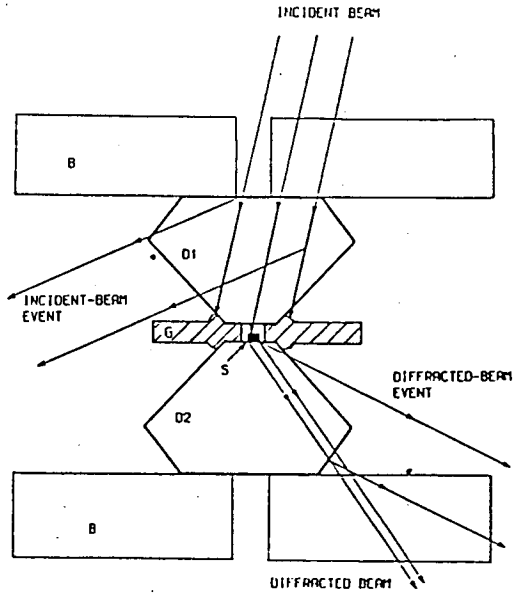

Fig. 2. A cross section through part of a Merrill–Bassett cell showing the ray paths for simultaneous diffraction (i) by the diamond ($D1$) in the beam incident on the sample (S) and (ii) by the diamond ($D2$) in the beam diffracted by the sample. The sample is enclosed, with a hydrostatic medium, in a hole in the metal gasket (G) between the diamonds. The diamonds are supported on beryllium backing discs (B) which are seated into the steel body of the pressure cell (not shown).

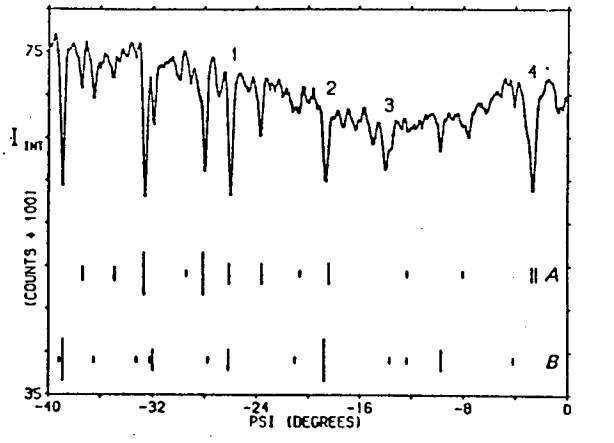

Fig. 4. Integrated intensity, I_{INT}, *versus* ψ for the 110 KMnF$_3$ reflection, at a pressure of 0·25 GPa. The vertical marks show the predicted positions of incident-beam events (labelled A) and diffracted-beam events (B). The lengths of the marks represent the relative scattering powers of the diamond reflections involved, as given in the text – the longest is for 111-type reflections, the next for 220, the next for 311 and the shortest for both 400 and 440. I_{INT} is the total integrated counts at each point, divided by 100. The dips labelled 1, 2, 3, and 4 are discussed in the text.

the magnitude of incident- and diffracted-beam events involving diamond-anvil reflections of the same class. Because the dips are usually only $\lesssim 0{\cdot}5°$ wide in ψ they would not be recognized in a conventional ψ scan, with a step size of 2° or more – there would simply be an occasional low-intensity value, not obviously outside statistical fluctuations.

In view of the marked difference between the scattering power of an unstressed diamond and of the diamond anvils of a cell at the low pressure used in the studies described above, it is important to know whether the effects of simultaneous diffraction become even greater at higher pressures. To study this, measurements were made of the diamond-anvil scattering power with the DAC at pressures of 3 GPa and ambient pressure, in addition to the 0·25 GPa of the initial studies above. While the cell was at 3 GPa, measurements were also made using Ag $K\alpha$ (instead of Mo $K\alpha$) to look for evidence of wavelength dependence. The results confirmed the very much smaller scattering power of the diamonds at ambient pressure, and showed that the (greater) scattering power at 3 GPa is the same as at 0·25 GPa. Hence, the dramatic effect of pressure is brought about within the first 0·1 or 0·2 GPa of applied load. The scattering power is also unaffected by changing the wavelength from Mo $K\alpha$ (0·71 Å) to Ag $K\alpha$ (0·56 Å), and since only the same five classes of reflection give rise to significant effects, the typical density of dips does not change either.

There is a great deal of interest at present in developing high-pressure crystallographic techniques using synchrotron sources, so the effect of the different characteristics of a synchrotron beam, such as the reduced divergence, has been investigated. Integrated-intensity ψ scans were collected on beamline 10A at the Photon Factory, Tsukuba, using the same $KMnF_3$ sample and DAC as for the laboratory-source measurements. Fig. 6(*a*) shows one such scan and Fig. 6(*b*) shows the same scan collected using the CAD-4 diffractometer, as already described. The dips in the scan obtained with the synchrotron beam are much deeper, and they are also narrow in ψ. The narrowness is further illustrated by the synchrotron measurements in Fig. 6(*c*) which resolve the laboratory-source dip in Fig. 6(*d*) into two dips only 0·1° apart. These differences in depth and width may be attributable to the absence of a $K\alpha$ doublet in the synchrotron beam as well as the reduced beam divergence. Further work is required to check this using a laboratory source and a silicon monochromator.

We have shown that simultaneous diffraction can have a considerable effect on the intensities of sample reflections, but it has not yet been shown how

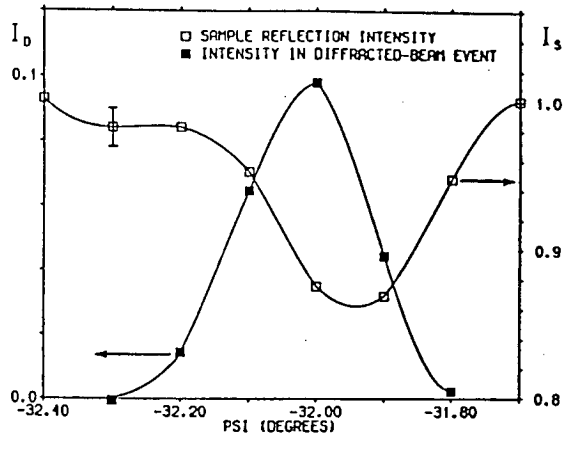

Fig. 5. The peak intensity of a 200 $KMnF_3$ sample reflection, I_S, and the peak intensity of a diffracted-beam event involving a 220 diamond reflection, I_D, as a function of ψ at a pressure of 0·25 GPa. I_S and I_D were measured with the same detector and have been put on a common scale normalized to 1·00 at the maximum sample intensity. A typical error bar is shown for one of the points. *Note* the ψ scale is much expanded compared with Figs. 1 and 4.

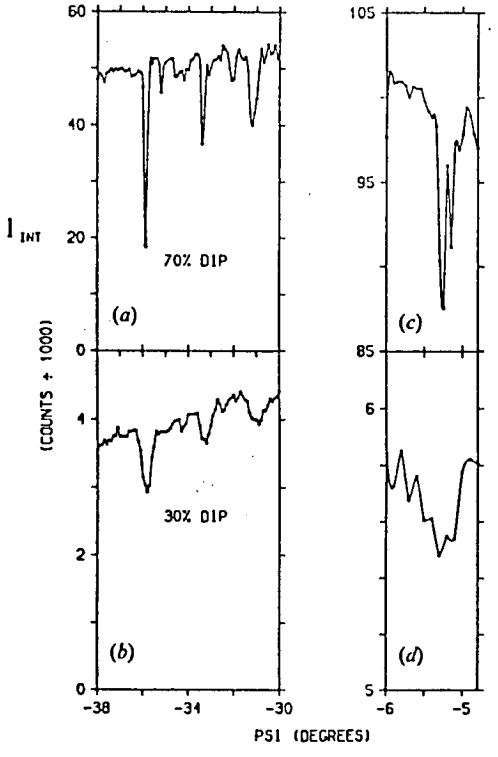

Fig. 6. Integrated intensity, I_{INT}, *versus* ψ for the 110 $KMnF_3$ reflection in a DAC at a pressure of 1·3 GPa (*a*) measured on a synchrotron beam at the Photon Factory, and (*b*) measured on a laboratory source, with (*c*) the detail of two resolved dips in the synchrotron measurements and (*d*) the corresponding unresolved dip in the laboratory-source measurements. I_{INT} is the total integrated counts at each point, divided by 1000. *Note* the difference in ψ scale between the two parts of the figure.

many reflections in a data set will be affected at ψ_m, the value of ψ where they are measured (generally that which minimizes the cell absorption). To investigate this and to develop a data-collection strategy to avoid simultaneous diffraction, a full data set was collected on the CAD-4 diffractometer with each reflection being measured at three values of ψ at 0·5° intervals about ψ_m. This three-point scan provided a method for detecting affected reflections and showed the integrated intensity of about 20% of all reflections to be reduced by more than two standard deviations at the measuring position, in a data set generally collected with a $\sigma(I)/I$ of 3%. Since the average separation of dips as a function of ψ is determined by the unit-cell dimensions of diamond, a similar result may be expected for any sample irrespective of its own unit-cell dimensions.

The points at which the dips occur in a ψ scan appear to be pseudo-randomly distributed and so the main consequence of ignoring the effect may be simply to reduce the precision of the derived information. However, there is evidence that higher-angle sample reflections are less affected. This is attributable to the larger angular separation of the $K\alpha_1$ and $K\alpha_2$ reflections at high 2θ (sample), which prevents them both being affected by the same strong (and, thus, low-2θ) diamond reflection. To the extent that the average magnitude of dips decreases with increasing 2θ, the thermal parameters of the sample will be underestimated. (A full account of 2θ dependence also involves consideration of the way the diamond reflections pass through the reflection condition. But this will not alter the general trend.)

Concluding remarks

It appears that simultaneous diffraction by the diamonds of a DAC can introduce significant errors into the measured sample intensities for 20% or more of the reflections in a data set. However, the use of a small ψ scan in the data collection makes it possible to detect and hence eliminate contaminated data. The synchrotron experiments suggest that while the dips are of larger magnitude their reduced width may make it easier to avoid them. However, further work is required to test this fully. In addition, the consequences of simultaneous diffraction need to be investigated for other techniques such as energy-dispersive powder diffraction and structure solution by the Laue method.

We are most grateful to Professor H. Iwasaki and Dr S. Sasaki for assistance in arranging and carrying out the measurements at the Photon Factory, to the National Laboratory for High-Energy Physics, KEK, for access to the Photon Factory facilities, to the Royal Society for funding a study visit to Japan by one of us (RJN) and to Dr Ross Piltz for valuable assistance with computer programming and analysis. This overall programme of work on diamond-anvil-cell techniques is supported by a grant from the Science and Engineering Research Council, including a research associateship for one of us (JSL). Part of the work has been performed under the approval of the Photon Factory Program Advisory Committee (Proposal no. 89–104).

References

AHSBAHS, H. (1987). *Prog. Cryst. Growth Charact.* **14**, 263–302.

DENNER, W., SCHULZ, H. & D'AMOUR, H. (1978). *J. Appl. Cryst.* **11**, 260–264.

FINGER, L. W. & KING, H. E. (1978). *Am. Mineral.* **63**, 337–342.

MERRILL, L. & BASSETT, W. A. (1974). *Rev. Sci. Instrum.* **45**, 290–294.

OKADA, M. & IWASAKI, H. (1980). *Phys. Status Solidi*, **58**, 623–628.